Dipl.-Ing. Manuel Christian Maier, BSc

From Chemistry to Plant: Advanced Designed Micro Reactor Systems for Continuous Multiphase Reactions Utilizing Additive Manufacturing

DOCTORAL THESIS

to achieve the university degree of
Doktor der technischen Wissenschaften

submitted to

Graz University of Technology

Supervisor

Assoc.Prof. Dipl.-Ing. Dr.techn. Heidrun Gruber-Wölfler
Institute of Process and Particle Engineering

Graz, Austria, September 2021

Abstract

In recent years, the pharmaceutical industry is slowly adapting from a batch-wise to a continuous production. This is due to the well-known advantages shown by a continuous production of a more stable product quality, decreased foot prints of industrial plants and greener approaches of chemical synthesis. Continuous manufacturing of Active Pharmaceutical Ingredients (*APIs*) also provides the possibility to locally fulfill sudden spike demands in times of shortages as seen by the current COVID-19 pandemic.

This work targets such demands by contributing to an interdisciplinary work flow approach called Chemistry to Plant (*C2P*), which targets to provide fast an industrial chemical plant for an *API* synthesis. The plant design concept is based on additive manufacturing to produce a chemical milli- or micro reactor adapted to a specific chemical task. The reactor is assembled from a developed structure element database by a simple click-and-drop like procedure. Elements can be chosen based on their fluid mechanical characteristics and simply scaled to obtain the desired process properties. Characterization of several elements from this database in terms of micro- and macro mixing was experimentally investigated in this work. The Bourne reaction, a system of competing consecutive and parallel reactions, was used to obtained characteristics on the micro mixing level. Macro mixing was investigated by simple residence time experiments with the aid of an optical measurement of a varying liquid tracer.

Detailed knowledge of thermal and kinetic parameters is essential to design a reactor. These data are most of the time not available for newly developed syntheses. To provide the needed data for the above mentioned work flow, two measurement reactor concepts were developed within this work. The first developed reactor concept is a micro Continuous Stirred Tank Reactor (*CSTR*) cascade. It allows to integrate sensors and monitor a reaction progress between the vessels in the cascade. The concept allows to achieve high mixing performances even at low flow rates by adjusting the rotation speed of incorporated magnetic stirrers. This reactor concept was used to estimate reaction time scales of a direct oxidation of Grignard reagents with oxygen. The gained insight into the

mixing limited reaction from these investigations led to advanced additively manufactured reactors designed from the structure database. The second measurement reactor concept presents an isothermal flow calorimeter to investigate the thermal and kinetic behavior of organic syntheses in continuous flow. The device combines commercial and additive manufactured components into a modular and extendable measurement system for chemical reactions. A direct heat flux is measured with the aid of Seebeck elements of each reactor segment and provides local information of a reaction progress. The calorimeter is internally calibrated with integrated heating foils and operated at isothermal conditions. True isothermal operation is achieved of each segment separately by a *PID* based temperature control by means of a micro controller. Performance of the designed calorimeter was validated with the above mentioned characterization techniques and by measuring acid-base neutralization with a mean error of 1.75% from the literature value. Overall, the presented reactor concepts and the developed *C2P* work flow of this work have the potential to reduce the time to market for novel chemical syntheses.

Kurzfassung

In den letzten Jahren stellte sich die pharmazeutische Industrie langsam von einer chargenweisen auf eine kontinuierliche Produktion um. Dies liegt an den bekannten Vorteilen einer kontinuierlichen Produktion durch stabilere Produktqualität, geringere ökologischen Fußabdrücke von Industrieanlagen und umweltfreundlichere Ansätze von chemischen Synthesen. Die kontinuierliche Herstellung von pharmazeutischen Wirkstoffen (*APIs*) bietet auch die Möglichkeit in Zeiten von Produktionsengpässen, wie sie in der aktuellen COVID-19-Pandemie aufgetreten sind, diese örtlich und spontan zu erfüllen.

Diese Arbeit zielt auf solche Anforderungen ab, indem sie zu einem interdisziplinären Workflow-Ansatz namens Chemistry to Plant (*C2P*) beiträgt, der darauf abzielt, innerhalb kürzester Zeit eine industrielle chemische Anlage für die *API*-Synthese bereitzustellen. Das Anlagenkonzept basiert auf der additiven Fertigung, um einen Milli- oder Mikroreaktor herzustellen, der an eine spezifische chemische Aufgabe angepasst ist. Der Reaktor wird aus einer entwickelten Strukturelementdatenbank durch ein einfaches Click-and-Drop-Verfahren zusammengesetzt. Elemente können basierend auf ihren strömungsmechanischen Eigenschaften ausgewählt und einfach skaliert werden, um die gewünschten Prozesseigenschaften zu erhalten. In dieser Arbeit wurde die Charakterisierung mehrerer Elemente aus dieser Datenbank in ihrer Mikro- und Makromischleistung experimentell untersucht. Die Bourne-Reaktion, ein System konkurrierender aufeinanderfolgender und paralleler Reaktionen, wurde verwendet, um Eigenschaften auf der Mikromischungsebene zu erhalten. Die Makromischeigenschaften wurden durch einfache Sprungversuche mit Hilfe einer optischen Verweilzeitmessung eines variierenden flüssigen Tracers untersucht.

Für die Auslegung eines Reaktors sind detaillierte Kenntnisse der thermischen und kinetischen Parameter erforderlich. Diese Daten stehen für neu entwickelte Synthesen meist nicht zur Verfügung. Um die benötigten Daten für den oben genannten Workflow bereitzustellen, wurden im Rahmen dieser Arbeit zwei Messreaktorkonzepte entwickelt. Das erste entwickelte Reaktorkonzept ist eine kontinuierliche Mikrorührkesselkaskade

(*CSTR*). Sie ermöglicht die Integration von Sensoren und die Überwachung eines Reaktionsverlaufs zwischen den Kesseln in der Kaskade. Das Konzept ermöglicht durch Anpassung der Drehzahl der eingebauten Magnetrührer auch bei geringen Durchflussmengen hohe Mischleistungen zu erreichen. Dieses Reaktorkonzept wurde verwendet, um Reaktionszeitskalen einer direkten Oxidation von Grignard-Reagenzien mit Sauerstoff abzuschätzen. Die aus diesen Untersuchungen gewonnenen Erkenntnisse über die mischungslimitierte Reaktion führten zu fortschrittlichen additiv gefertigten Reaktoren, die aus der Strukturdatenbank entworfen wurden. Das zweite Messreaktorkonzept präsentiert ein isothermes Durchflusskalorimeter zur Untersuchung des thermischen und kinetischen Verhaltens einer organischen Synthese im kontinuierlichen Durchfluss. Das Gerät kombiniert kommerzielle und additiv gefertigte Komponenten zu einem modularen und erweiterbaren Messsystem für chemische Reaktionen. Ein direkter Wärmestrom wird mit Hilfe von Seebeck-Elementen jedes einzelnen Reaktorsegments gemessen und gibt einen lokalen Hinweis auf einen Reaktionsverlauf. Das Kalorimeter wird intern mit integrierten Heizfolien kalibriert und kann unter isothermen Bedingungen betrieben werden. Ein wahrer isothermer Betrieb wird für jedes Segment separat durch eine *PID*-basierte Temperaturregelung mittels eines Mikrocontrollers erreicht. Die Performanz des entworfenen Kalorimeters wurde mit den oben genannten Charakterisierungstechniken und durch die Messung einer Säure-Base-Neutralisation mit einem mittleren Fehler von 1,75% vom Literaturwert validiert. Zusammenfassend haben beide Reaktorkonzepte und der entwickelten *C2P* Workflow dieser Arbeit das Potential zu einer verkürzten Markteinführungszeit für neuartige chemische Synthesen zu führen.

Affidavit

I declare that I have authored this thesis independently, that I have not used other than the declared sources/resources, and that I have explicitly indicated all material which has been quoted either literally or by content from the sources used.

The text document uploaded to TUGRAZonline is identical to the present doctoral thesis.

Date

Signature

Acknowledgments

First of all, I would like to thank my girlfriend Marlies for supporting and encouraging me during the ups and downs of my PhD studies. I am looking forward to the exiting years to come. I am thankful for all the discussion and time spend with my brother Oliver. As his younger sibling, he definitely was a role model who kept the bar high to follow. To my parents I also have to express my gratitude for their efforts and time spent for helping me become the person I am. Then I would like to thank all of my friends for spending entertaining hours at and off university during day and (mainly) night.

A special thank goes to the CoSy Pro group from the IPPE. It was a pleasure to work in such a highly entertaining and joyful working group with so many talented scientists. I express my sincere gratitude to Heidi for enabling this and previous works in her group. One could not think of a better and caring supervisor in terms of scientific knowledge and gin culture. I would also like to thank the CCFLOW project team as well as all industrial partners and the numerous students I was allowed to supervise and work with. And finally, I would like to thank all of the IPPE employees for being simply the best.

Contents

List of Figures

List of Supporting Figures

List of Tables

List of Supporting Tables

CHAPTER 1

Introduction

Contents

In recent years, interest of pharmaceutical companies in continuous manufacturing of Active Pharmaceutical Ingredients (*APIs*) and final dosage forms increased. [2, 3] This is mainly attributed to the constant product quality, less energy demanding and greener processing compared to batch manufacturing. [4] The current *API* production in a batch-wise manner also limits pharmaceutical companies in their possibility to react swiftly to market demands as batch production sites are scattered all around the globe. Consequently, lead times of up to 12 months need to be considered during the production and well planning ahead is required to not run out of materials. [5] Here continuous manufacturing and especially flow chemistry can centralize again the point of *API* production closer to the final preparation of the pharmaceutical dosage form at the point of need. For such a flexible production using flow chemistry, also a flexible and modular plant and reactor design approach is needed to account for the demanding multistep processing found in the *API* production. [6] Additive manufacturing can be seen as one solution to provide such aspects by producing on-demand the needed reaction hardware. [7] This work takes on a similar approach by utilizing additive manufacturing as key technology to produce chemical reactors tailor-made for their application. The current work is part of an inter-

disciplinary work flow which aims to design and run a chemical production plant in a few months, see Sec. 1.5.

1.1 Outline of the Thesis

An introduction to continuous manufacturing is given in Chap. 1 with a special focus on the pharmaceutical industry. Current trends in this context are presented and general advantages of continuous manufacturing are compared to batch-wise manufacturing as well as limitations are given for both manufacturing routes. Flow chemistry, as part of continuous manufacturing, is discussed with a focus on micro reactor technology. Micro reactor design guidelines from literature used for the produced reactors in this work are presented. Then reactor characterization and evaluation methods on the macro- and micromixing level are shown. An general introduction to additive manufacturing is given with a detailed presentation of the two used manufacturing techniques, Selective Laser Melting (*SLM*) and Digital Light Processing (*DLP*), utilized in this work. The next part of Chap. 1 deals with reaction calorimetry, first showing state of the art batch techniques and principles and later on focusing on current trends of continuous flow calorimetry. Finally, an overview of the Chemistry to Plant (*C2P*) approach is given in this chapter.

A development to *3D* printed and customized reactors for the oxidation of Grignard reagents is the shown in Chap. 2. This chapter is taken from the journal publication in *Reaction Chemistry and Engineering* by Maier *et al.*: Manuel C. Maier, René Lebl, Philipp Sulzer, Josef Lechner, Torsten Mayr, Matej Zadravec, Eyke Slama, Stefan Pfanner, Christoph Schmölzer, Peter Pöchlauer, C. Oliver Kappe, and Heidrun Gruber-Woelfler. "Development of customized 3D printed stainless steel reactors with inline oxygen sensors for aerobic oxidation of Grignard reagents in continuous flow". In: *Reaction Chemistry and Engineering* 4.2 (2019), pp. 393–401. ISSN: 20589883. DOI: 10.1039/C8RE00278A. URL: http://xlink.rsc.org/?DOI=C8RE00278A. The approach of using a modular structure database for the fast design of additive manufactured reactors was developed within this work. This approach allows to select reactor components as required by the process conditions, *e.g.* mixing properties, to be chosen and scaled properly to the remaining reactor components.

The above mentioned reactor design procedure requires knowledge of kinetic as well as thermodynamic properties of the desired reaction. These values are most of the time not available in the initial research phase of novel flow chemistry. The usage of batch equipment, like batch calorimeter, is limited for most continuous flow applications as process conditions are fundamentally different. Because of that, a continuous flow calorimeter was developed to generate the needed properties for the reactor design. This device is presented in Chap. 3, which is taken from the journal publication in *Reaction Chemistry and Engineering* by Maier *et al.*: Manuel C. Maier, Michael Leitner, C. Oliver Kappe, and Heidrun Gruber-Woelfler. "A modular 3D printed isothermal heat flow calorimeter for reaction calorimetry in continuous flow". In: *Reaction Chemistry and En-*

gineering 5.8 (2020), pp. 1410–1420. ISSN: 20589883. DOI: 10.1039/d0re00122h. URL: http://xlink.rsc.org/?DOI=D0RE00122H. The presented flow calorimeter combines *3D* printing with commercial available electronics into a modular and customizable measurement device. Its reactor segments are temperature controlled independently at isothermal conditions. The developed calorimeter allows to measure fast (ms range) reaction under steady state conditions.

The last Chap. 4 is also taken from the journal article published in *Organic Process Research & Development* by Maier *et al.*: Manuel C. Maier, Alessia Valotta, Katharina Hiebler, Sebastian Soritz, Kristian Gavric, Bianca Grabner, and Heidrun Gruber-Woelfler. "3D Printed Reactors for Synthesis of Active Pharmaceutical Ingredients in Continuous Flow". In: *Organic Process Research and Development* (2020). ISSN: 1520586X. DOI: 10.1021/acs.oprd.0c00228. This work presents three different cases for the synthesis of *APIs* with contributions of *3D* printed reactors. The first case shows advances of the reactor design approach presented in Chap. 2 for the direct oxidation of Grignard reagents. Next, another *3D* printed reactor was utilized for achieving fast mixing in a synthesis cascade leading to a valsartan precursor. In the third and final case, a Continuous Stirred Tank Reactor (*CSTR*) is shown for the production of resveratrol derivatives. This reactor was made of a *UV*-curable resin and used for the first step of a multiphase enzymatic decarboxylation followed by a Heck cross-coupling reaction.

Chap. 5 summarizes this thesis and discusses possible further extensions of the presented work. Especially the combination of *3D* printed reaction ware and continuous flow processing seems to be a promising match. On-demand reaction ware will most likely contribute to a more localized production of *APIs*.

1.2 Comparison of continuous and batch manufacturing

The pharmaceutical industry is mainly relying on batch manufacturing due to complex multi-step processes and easy traceability of final products. The approach to use batch manufacturing has the advantages that various operations can be carried out in the same equipment at reduced instrumentation costs, which provides a needed flexibility especially when only small product quantities are produced. For the production of larger product quantities, batch manufacturing becomes cost intensive since high labor and handling costs, shut down times and varying product quality over several batches can be seen. A continuous production mode could overcome these problems and actions are taken to promote it for the continuous production of drug products. [2, 3] However, continuous processing is only slowly established in the pharmaceutical industry mainly because of the lack of flexibility and robustness of the used processes. Additional hurdles are strict regulations with respect to product quality similar as in the batch production, additional investment costs for a switch from existing batch to continuous equipment and the low amounts of produced goods. [2, 11, 12] A continuous production furthermore needs a higher degree of process design compared to batch manufacturing. [13, 11] Critical process

attributes need to be defined, measured and monitored to ensure a product quality within defined limits. This can be done by real time inline measurements, which allow real time and feedback control. As a consequence, better process quality and control is gained.

1.3 Microreactor technology in flow chemistry

In the publication of Roberge *et al.* [14] they suggest that 50% of reactions in the fine and pharmaceutical industry would benefit from a continuous production based mainly on micro reactors, often referred to as flow chemistry. They identified the frequently handling of solids as one of the main hurdles, which needs to be overcome for an industrial implementation. But a possibility of safer and more efficient reactions at scale as well as reduced time during the R&D process in small scale outweighs this limitation.

A micro reactor is defined in this work as a reactor with internal channel geometries below one millimeter. Above this value and if it could hold only a few milliliters, one would define such a reactor as a milli reactor. Safer processes and enhanced process conditions are possible in milli- and micro reactors due to the high surface-to-volume ratio. At these small dimension, enhanced mixing and heat transfer characteristics can be seen. [15] A surface-to-volume ratio of a few thousand to ten thousand square meter per cubic meter can be found in micro reactors compared to a values below one hundred for batch equipment. [16] This allows a precise control of the reaction at isothermal conditions. Operations are possible at greener and more efficient reaction conditions at higher concentrations with less or even no solvent. [17] Additionally, the small internal volumes of these reactors require less energy to heat up the system and allow to use less raw material during a process development of new synthetic routes. Less material in the process also reduces the risk of possible fatalities. Operations at currently forbidden conditions are enabled in micro reactors at high pressures and temperatures well above boiling points or even at super critical conditions. All these possibilities are summarized in a concept called Novel Process Window (*NPW*). [18, 19, 20]

Flow chemistry carried out in micro reactors focuses on rapid or hazardous chemistry including unstable intermediates. Requirements for a flow reaction are soluble starting materials in the working fluid without or limited formation of solid material. This requirement is given by above mentioned small channel dimensions to prevent blockage of a reactor. To be able to assess the benefits of flow chemistry for different kinds of reactions, Roberge *et al.* [14] introduced four classes of reaction types.

- Type A reactions have a half life time frame below one second and are usually mixing controlled. Therefore, a slow dosing procedure needs to be used in a batch operation to prevent a run-away scenario. The reaction mainly takes place in the mixing zone whereby flow chemistry in micro structured reactors can provide the needed fast mixing and removal of reaction heat. These type of reactions include reaction species like halogens, amides as well as organometallic reagents.

- Type B reactions are rapid, in the range of then seconds to several minutes and are controlled by their kinetics. These reactions would benefit from isothermal conditions and proper control of stoichiometry, which can be provided in micro reactors and might lead to higher yields. Here mixing is not so critical anymore and a continuous reactor can be optimized by its residence time with a minimized pressure drop.

- Type C reactions include slow and hazardous reactions in the range of more than ten minutes, which are normally carried out at batch conditions. Here flow chemistry could increase product quality and provides a safer possibility through the used low internal volumes.

- Type D reactions include all other reactions not belonging to the above types. These reactions are normally carried out highly diluted in batches.

Application of micro reactor technology to the above mentioned type A and B reactions would be beneficial mainly because of the proper local temperature control. Type C reactions are normally more suitable for batch-wise processing. Micro reactor technology is only needed for type C reactions that require a short exposure to high temperatures or pressures as well as to increase safety of auto-catalytic processes. Type D reaction can be accelerated under *NPW* conditions in a micro reactor to provide an enhanced reaction activation or alternative other highly active reagents can be used.

Another aspect to consider whether to use a continuous process in a micro reactor is the number of present phases. As mentioned above, micro reactors can handle solids only poorly. In more then 60% of the reactions studied by Roberge *et al.*, [21] solids are present whether as reactant, catalyst or product. Thus, the multipurpose usage of micro reactors is currently limited to homogeneous and to gas-liquid or liquid-liquid reactions.

1.3.1 Microreactor design guidelines

A guideline to design micro reactors in five steps was published by Hessel *et al.* [22] This approach is described below and used in this work in combination with additional design guidelines from literature. [23, 24, 25] These guidelines compare respective time scales with each other in the form of dimensionless numbers and suggests their limitations for desired reactor characteristics.

A characteristic internal length scale, most of the time defined as hydraulic diameter d_h, is chosen in **step 1**. This diameter defines the heat and mass transfer characteristics of a reactor and is the most critical parameter for milli- and micro reactors. A smaller diameter generally reduces the mixing length scale and therefore reduces the needed mixing time. A general trend can be seen with respect to kinetic and heat generation of a reaction. The more energy needs to be transferred out of the system, the smaller a diameter should be. There are different paths to calculate a needed hydraulic diameter. One possibility is to use

an energy balance like approach to prevent a hot spot formation. [26] Another approach utilizes given reaction kinetics of a tubular reactor, [27] which leads to a characteristic diameter to prevent hot spot formation and can be calculated with the following equations:

Heat production potential S' defined as

$$S' = \frac{\Delta T_{ad}}{T_w}\gamma \tag{1.1}$$

showing the adiabatic temperature rise ΔT_{ad} (K), wall temperature T_w (K) and dimensionless Arrhenius number γ.

$$\gamma = \frac{E_a}{RT_w} \tag{1.2}$$

with Arrhenius activation energy E_a (J mol)$^{-1}$ and general gas constant R (J mol^{-1} K^{-1}).

Adiabatic temperature rise ΔT_{ad} is defined as

$$\Delta T_{ad} = \frac{c_{1,0}(-\Delta H_R)}{\rho c_p} \tag{1.3}$$

showing the limiting component c_1 at time 0 (mol m^{-3}), reaction enthalpy ΔH_R (J mol^{-1}), mixture density ρ (kg m^{-3}) and heap capacity of the reactor content c_p (J kg^{-1} K^{-1}).

The ratio of the characteristic reaction time t_r to the cooling time t_c is expressed as

$$N = \frac{t_r}{t_c} = \frac{1}{k(T_w)c_{1.0}^{m-1}}\frac{4\alpha}{d_h \rho c_p} \tag{1.4}$$

with a reaction rate coefficient $k(T_w)$ (mol$^{1\text{-(m)}}$ L$^{(m)\text{-}1}$ s^{-1}) calculated at the wall temperature T_w with a reaction order m and heat transfer coefficient α (W m^{-2} K^{-1}).

The reaction time scale can be estimated by

$$t_r \propto \frac{1}{k(T_w)c_{1.0}^{m-1}} \tag{1.5}$$

and the Arrhenius correlation in the form of

$$k(T_w) = k_0 e^{-\frac{E_a}{RT_w}} \tag{1.6}$$

including the pre-exponential factor k_0 (mol$^{1\text{-(m)}}$ L$^{(m)\text{-}1}$ s^{-1}).

The heat transfer coefficient α in Equ. 1.4 can be calculated with the dimensionless Nusselt number

$$Nu = \frac{\alpha d_h}{\lambda_W} = \frac{convective\ heat\ flux}{conductive\ heat\ flux} \tag{1.7}$$

with the wall heat conductivity λ_W (W m^{-1} K^{-1}). A value for the Nu number is

depending on the flow regime inside the micro reactor, *e.g.* $Nu = 3.66$ for a tubular and laminar flow in a pipe. [28]

An empirical relation for N_{min} of Equ. 1.4 can be used to estimate d_h as a function of the heat production potential S'. [29] In this correlation the parameter B is depending on the reaction order m.

$$\begin{gathered} N_{min} = (\frac{t_r}{t_c})_{min} = 2.72S' - B\sqrt{S'} \\ B = 0 \; for \; (m = 0) \\ B = 2.6 \; for \; (m = 0.5) \\ B = 3.37 \; for \; (m = 1) \\ B = 4.57 \; for \; (m = 2) \end{gathered} \tag{1.8}$$

Another possibility to calculate the diameter d_h to prevent a hot spot formation is given by the fourth Damköhler number.

$$DaIV = \frac{\rho k_w c_{1.0}^m \Delta H_R {d_h}^2}{\lambda_W \Delta T_W} = \frac{heat\,of\,reaction}{heat\,removed\,by\,heat\,transfer} < 0.2 \tag{1.9}$$

including the temperature increase ΔT_W (K) of the reaction media with respect to the wall temperature.

After taking thermal effects into account for a defined diameter d_h, its influence needs to be investigated on the mixing performance. A too narrow channel in combination with a long channel length induces a higher pressure drop and increases the energy demand and pumping costs. This pressure drop can be used to estimate a mixing time scale together with an energy dissipation rate. It also needs to be noted, that not all dissipated energy will be used for mixing. A completely mix flow before a reaction starts is desired and shown by the second Damköhler number.

$$DaII = \frac{t_m}{t_r} = \frac{mixing\,time}{reaction\,time} < 1 \tag{1.10}$$

whereby the reaction time is defined in Equ, 1.5 and a mixing time can be calculated with

$$t_m = 17.3 \left(\frac{\nu}{\epsilon}\right)^{(1/2)} \tag{1.11}$$

with the kinematic viscosity ν ($m^2\ s^{-1}$) and the energy dissipation rate ϵ ($m^2\ s^{-3}$ or $W\ kg^{-1}$). The energy dissipation rate can be described as

$$\epsilon = \frac{\Delta p u}{\Delta l \rho} \tag{1.12}$$

including the pressure loss per unit length of the reactor $\Delta p / \Delta l$ ($Pa\ m^{-1}$) and flow velocity u ($m\ s^{-1}$). A pressure drop can be calculated with

$$\Delta p = \lambda_f \frac{l\rho}{2d_h} u^2 \tag{1.13}$$

with a reactor length l (m) and a friction factor λ_f for laminar flow in a circular channel

$$\lambda_f = \frac{C_f}{Re} = \frac{64}{Re} \tag{1.14}$$

including the dimensionless Reynolds number

$$Re = \frac{ud_h}{\nu} = \frac{ud_h\rho}{\eta} = \frac{inertial\ forces}{viscous\ forces} \tag{1.15}$$

with a flow velocity u calculated by the cross sectional area A (m^2) and volumetric flow rate Q ($m^3\ s^{-1}$)

$$u = \frac{Q}{A} = \frac{4Q}{d^2\pi} \tag{1.16}$$

Step 2 includes the setting of a channel length. As mentioned above, this length also contributes to the mixing performance by influencing the pressure drop. A compromise between a desired narrow Residence Time Distribution (*RTD*) and a low pressure drop needs to be done. [24] The following consideration of a complete reaction within a reactor is given by the first Damköhler number. This number should be greater than one but is normally set between five to ten for practical reasons.

$$DaI = \frac{\tau}{t_r} = \frac{mean\ residence\ time}{reaction\ time} > 1 \tag{1.17}$$

whereby τ can be determined as

$$\tau = \frac{l}{u} = \frac{V_r}{Q} \tag{1.18}$$

with the reactor volume V_r (m^3).

In **step 3** the channel walls are defined. They play an important role for the heat management in a reactor, especially for high endo- or exothermic reactions. Here the time scale for heat conduction in the channel walls has to be lower than the residence time of the fluid. This isothermal operation is represented by the third Damköhler number:

$$DaIII = \frac{k_r c^m \Delta H_R l}{c_p \Delta T_z u} = \frac{heat\ of\ reaction}{down\ stream\ temperature\ increase} \approx 1 \tag{1.19}$$

with the down stream temperature increase ΔT_z (K).

Step 4 deals with increasing process throughput by dimensioning of the number of micro channels. The number of channels a process fluid needs to be distributed to and the channel diameter determine the velocity through the device and influence the yield. There are basically two approaches taken by internal and external numbering up. By internal

numbering up, the functional reactor elements are replicated and placed in the initial reaction environment, *e.g.* one thermostat used for all reactor elements. While in the external numbering up approach all functional elements of a reaction setup are multiplied.

The final **step 5** deals with the design of a fluid distribution system to the numbered up reactors. Different ways can be taken by successively splitting a stream while reducing its cross-sectional area. [30] Here nature inspired approaches or mathematical based approaches can be found. [31, 32]

1.3.2 Evaluation of reactor performance

Very fast reactions, as commonly found in flow chemistry, require a sufficient mixing for homogeneous and heterogeneous reactions. A basic reactor characterization can be carried out at the micro and macro mixing level as described in the following.

1.3.2.1 Macromixing

Experimental evaluation to determine a *RTD* of a reactor allows to get insight into the flow pattern and mixing on the macro scale. [33] Deviations from the ideal reactor models used in reaction engineering can be investigated with this well established investigation method to identify axial dispersion and back mixing effects. In this evaluation, a non-dimensional Bodenstein number Bo is defined as the ratio of convective mass transfer over axial dispersion:

$$Bo = \frac{uL_{char}}{D_{ax}} = \frac{convective\ mass\ transfer}{axial\ dispersion} \tag{1.20}$$

where u is the flow velocity, L_{char} (m) is a characteristic length of the device and D_{ax} ($m^2\ s^{-1}$) is the axial dispersion coefficient. A high Bo number, normally above 100, represents an ideal plug flow-like behavior of the reactor. Values below 100 represent a higher back mixing and the reactor is best represented by a *CSTR*. Different models can be used to convert the obtained experimental data from the *RTD* experiment and are reported in literature. [33]

The distribution of respective times needed of different fluid elements to pass through a reactor is called the exit age distribution E, or *RTD* of a fluid. A simple way to obtain this E curve for a given reactor is experimentally done by using step or pulse input signals to it with the aid of a nonreactive tracer. The tracer concentration at the reactor's in- and outlet is followed over time. A dimensionless form of the cumulative tracer concentration, the so called F curve, can be obtained with this information. [33] In this work, mainly step experiments were carried out to evaluate reactor performance because of the simpler experimental procedure.

1.3.2.2 Micromixing

An estimation of the mixing time on the micro scale can be obtained by mixing sensitive reactions. [1, 34] This work focused on the Bourne reaction, which has a proposed time frame for the half-life time of 727 ms. [35] A re-calculation of the proposed value gave a half-live time of approximately 30 ms for only considering the rate limiting 2p step and neglecting the o-R path, see detailed reaction scheme in Chap. 2 and 4. This makes the rate limiting and product forming step of the Bourne reaction by a factor of 6 slower than the 2,2-dimethoxypropane (*DMP*) hydrolysis. [35] This seems to be an appropriate value by comparing their published data. Mixing sensitive reactions always yield a combination of the chosen elements for the first contacting mixing point and following reactor elements used to provide a certain residence time. With carried out experiments and obtained yields, only a rough estimation of mixing performance is possible. For almost no product formation, a mixing time below the half-life time can be assumed for the used Bourne reaction.

1.3.3 Microfabrication techniques

Additive manufacturing, also know as *3D* printing, is commonly used for rapid prototyping of small product quantities, production of customized objects and readily used for the production of milli- and microfluidic reactors. [36, 37, 38, 39] Additive manufacturing got this attention because of the automated and assembly-free nature of production, reduced costs and fast-improving resolution of the final produced reactors. The unique characteristics of additive manufacturing lead to the following benefits: [40]

- No additional tools are needed during manufacturing, which significantly reduces production ramp-up time and expenses
- Production of small product amounts are feasible and economical
- Designs can be quickly adapted
- A product's function can be optimized (for example optimized cooling channels)
- Economical custom products are feasible (one part at a time)
- Reduced waste since only the object's material is needed
- A potential simplification of supply chains, shorter lead times, lower inventories is possible
- Designs can be customized for a specific case

While there are various manufacturing techniques with a broad range of available materials currently used for additive manufacturing, they all follow a similar production

sequence. [41] First, a conceptional design as Computer Aided Design (*CAD*) is made and mainly converted to an Standard Triangle Language (*STL*) file. This file is then manipulated, arranged in space and transferred to the additive manufacturing machine. After an initial machine setup and definition of manufacturing parameters, the additive manufacturing is started. A general additive manufacturing procedure includes the selective application of material according to a cross-sectional area of the desired geometry by tracing a two dimensional layer in the form of a contour and then an infill. Once the single layer is completed, the build platform or printer head will move a short distance from the building plate. If needed, a new layer of raw material is distributed and the whole procedure is repeated until the final layer is completed. The produced part is most of the time attached to a building plate and needs to be removed and probably cleaned from excess building material. Post-processing is followed by removing supporting materials and modifying the part for its final application. Some features of three popular additive manufacturing techniques, *DLP*, Fused Deposition Modeling (*FDM*) and *SLM*, are shown in Tab. 1.1

Feature	*DLP*	*FDM*	*SLM*
3D-capability	Very little topological restriction in *3D* architecture. Only dimensional limits. High optical absorption is required to create micro channel roof	Limited to circular channel cross-sections and orthogonal junctions	Very little topological restriction in *3D* architecture. Only dimensional limits. Powder bed gives additional support – less support structures needed
Resolution	Current: ∼100 μm channels with opaquing agent	Current: ∼350 μm	Current: ∼300 μm Min. feature size 40-200 μm [42]
Solvent compatibility	Commercial resins are water-resistant. Varying resistance to organic solvents (Somos 5530HT, 9920 is resistant to most solvents, Watershed is not resistant to ethanol). Higher *MW* hydrogel resins are not water or solvent resistant	Thermoplastics are water resistant. Varying chemical resistance	Similar to properties of the bulk material
Gas permeability	Most *SLA* resins are hard plastics with poor gas permeability; commercial elastomeric *SLA* resins are typically sold uncharacterized	Most *FDM* thermoplastics are hard plastics with poor gas permeability	Gas tight built
Mechanical strength	Young's modulus vary with material – Ormocer (1–4 GPa), WaterShed (2.7 GPa) Minimal anisotropy in mechanical properties	Young's modulus (*ABS*, *PC*, *PPS*, *COC*: ∼2–3 GPa) Anisotropy in strength – inter-layer bonding weak	Similar to properties of the bulk material [43] e.g. ∼200 GPa for Stainless Steel
Bio compatibility	Many resins are cytotoxic and not biocompatible. WaterShed and Visijet *SLA* Clear are USP Class VI plastic. PEG-DA is biocompatible	Many biocompatible thermoplastics available – *ABS*, *PLA*, *ABS*, *COC*, *PP*	Different metals used for implants TiAl6V4 and CoCrMo [43]

Table 1.1: Features of some additive manufacturing techniques. Column entries taken from Bhattacharjee *et al.* [36] and additional information added.

1.3.3.1 Selective Laser Melting - SLM

Selective Laser Melting (*SLM*) is a powder-based additive manufacturing technique. In contrast to Selective Laser Sintering (*SLS*), a *SLM* process completely melts the used powder rather than partially melting it. A high-density solid body is created from several possible materials such as polymers, metals, ceramics and composites. [44, 45] The printing process consists of a successive selective and layer-wise melting of a powder bed by means of a high intensity laser beam under an inert gas atmosphere. A basic *SLM* setup is shown in Fig. 1.1.

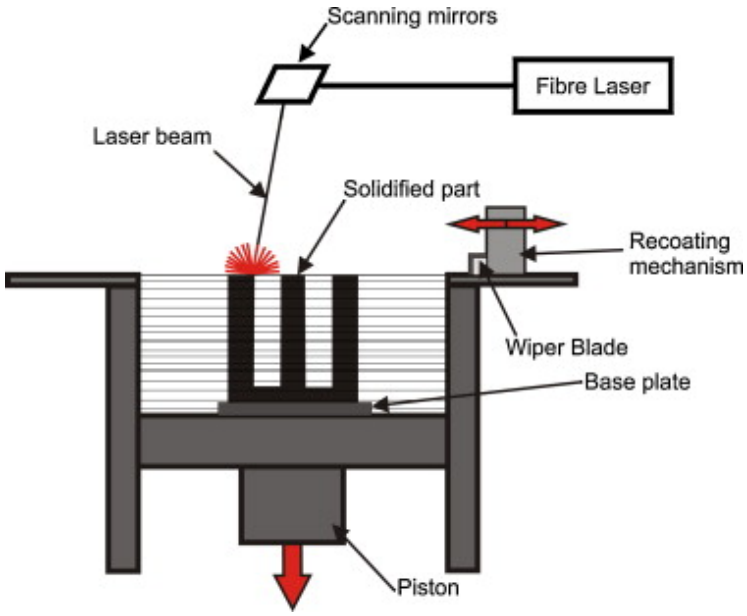

Figure 1.1: Principle structure of a *SLM* process. Reprinted from reference [46] with permission from Elsevier

A powder bed is applied to a building platform and smoothed with a scraper or roller blade. Then a laser is guided by mirrors according to a desired cross sectional printing area, according to the sliced *CAD*-design, to melt and combine the powder bed to the previous layer. Next, the platform is lowered, a new powder layer is applied and the next cycle started. After the printing, the part is freed from unused powder, which is recycled after a sieving step, and post-processed by means of surface treatments and stress relief annealing. Drawbacks of *SLM* include the formation of internal cracks as a result of local overheated areas during the printing and relatively high surface roughness. [45]

SLM was used in this work to manufacture reactors made of stainless steel. With this manufacturing technique, it was possible to produce reactor geometries with material characteristics similar to the bulk substance. This allowed to use a thin wall thickness between the reaction media and coolant and consequently increased the heat transfer. Furthermore, the used 316L steel showed a good solvent compatibility as well as compatibility

with most of the frequently occurring materials used in organic synthesis. Another advantage is that metal printed reactor geometries can be processed with standard machines and tools.

1.3.3.2 Digital Light Processing - DLP

Digital Light Processing (*DLP*) is an additive manufacturing technique very similar to Stereo Lithography (*SLA*). Both procedures use photo-polymerization of a liquid resin in a layer-wise procedure as shown in Fig. 1.2. Generally, it is possible for both procedures to use a bottom-up or top-down approach, whereby the top-down approach has the advantage that the illuminated layer is not exposed to the atmosphere and the amount of polymer in the storage vat is reduced. [36] The main difference of the techniques is the possibility of *DLP* to cure a respective layer all at once. While in *SLA* a laser beam is guided across a layer, *DLP* projects the layer with a dedicated mirror guidance of a light beam or by simply a high resolution *LCD* display. [47] This results in a curing time per layer which is independent on the amount of cross-sectional area to cure.

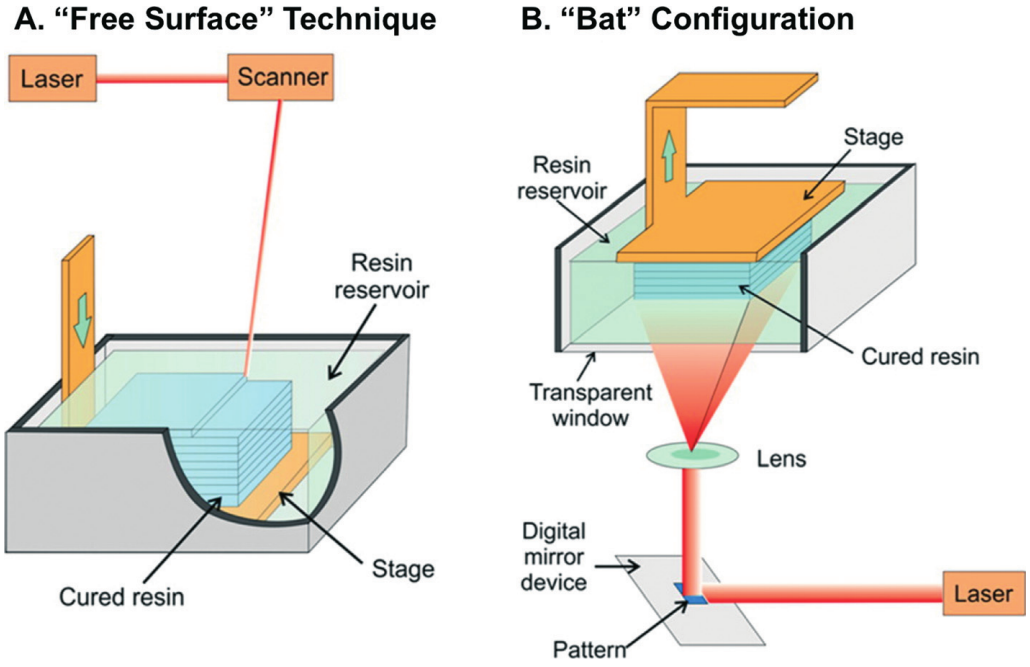

Figure 1.2: Stereo Lithography (*SLA*) configurations. (A) shows a free surface or bottom-up technique in which a laser cures material close to the surface of a vat. (B) shows the simultaneously curing of a whole cross section in the so called bat or top-down configuration commonly found in *DLP*. Reprinted from reference [36] with permission from Royal Society of Chemistry

The printing procedure for *DLP* consists of an initial binding step to the stage platform followed by a layer-wise manufacturing. A sectional layer is projected through the bottom of the resin vat and solidifies to the previous one. In a next step, the stage is moved upwards to rip off polymer from the transparent bottom of the vat and new resin is

allowed to enter the gap. This ripping applies stress on the unfinished part and may cause failures during printing. The next layer is then started slightly above the previous one in a height between 25 to 100 μm. This height needs to be chosen depending on the curing parameters of a resin in a way, that the maximum step length is slightly smaller than the achievable curing depth of a layer. The curing depth is depending on the used polymer, intensity of the light source and curing time. [48]

DLP was used in this work mainly to produce casing elements for the calorimeter shown in Chap. 3. It showed to be a cheap manufacturing possibility of highly detailed parts especially useful during design iterations. Most of the commonly used polymers for this manufacturing technique are not compatible with organic solvents, thus limiting the application of *DLP* for the production of reactors. Nevertheless, a *CSTR* applied at mild reaction conditions is shown in Chap. 4

1.4 Reaction Calorimetry

To carry out a chemical process in a safe and controlled manner, it is of utmost importance to know the risks related to toxicity and reactivity of the involved chemicals. [49] Especially thermal risks associated with the reactivity of a reaction are a major concern in the process design phase. To keep a reaction under controlled conditions, the heat production of exothermic reactions has to be considered in the design of process and safety relevant equipment. This heat production can be characterized by a combination of both kinetic and thermodynamic effects of a chemical reaction. Both effects can be monitored by reaction calorimetry by following the heat flow rate of a reaction, making calorimetry a differential kinetic analysis method. [33] The heat flow rate is proportional to the rate of conversion and can be expressed as:

$$\dot{q}_{Reaction}(t) \sim r(t) V_r \tag{1.21}$$

where $\dot{q}_{Reaction}$ is the reaction heat flow rate (W), r the rate of reaction (mol m^{-3} s^{-1}) and V_r the reactor volume (m^3). These quantities change with time and reaction progress. In contrast to reaction calorimetry, other analytical methods applied to kinetic analysis, such as online concentration measurements of reaction spectra (*UV*-*VIS*, *NIR*, Raman), can be seen as integral kinetic methods. [33] Here a direct correlation is shown between concentration and measurement signal:

$$s_i(t) \sim c_i(t) \tag{1.22}$$

with s_i as value of the ith reaction component measured by the analytical sensor of the above mentioned spectra techniques with the concentration c_i (mol m^{-3}). A combination of both differential and integral analysis methods showed great improvement of kinetic analysis. [50, 51, 52]

The following sections first present the risks generally related to chemical processing

and gives information about key parameters to characterize them. Secondly, a short overview about the fundamentals of batch calorimetry are given. Then the focus will be on current trends in continuous flow calorimetry with an overview of currently available measuring methods and devices.

1.4.1 Risks assessment of a chemical processing

A general risk of thermal reactions can be characterized by a risk assessment in three steps: search and identification of possible dangers and hazards, risk analysis and establishing risk reducing measures. [53] To carry out this risk analysis, the behavior of a chemical process is normally evaluated by constructing a run-away scenario. [49] In such a scenario the loss of a critical temperature control unit during the process is assumed, leading to a quasi-adiabatic operation mode. As a consequence, the reaction content's temperature increases with a change in reaction rate, potential activation of secondary reactions and pressure increase due to solvent evaporation or decompositions. This scenario is depicted in Fig. 1.3.

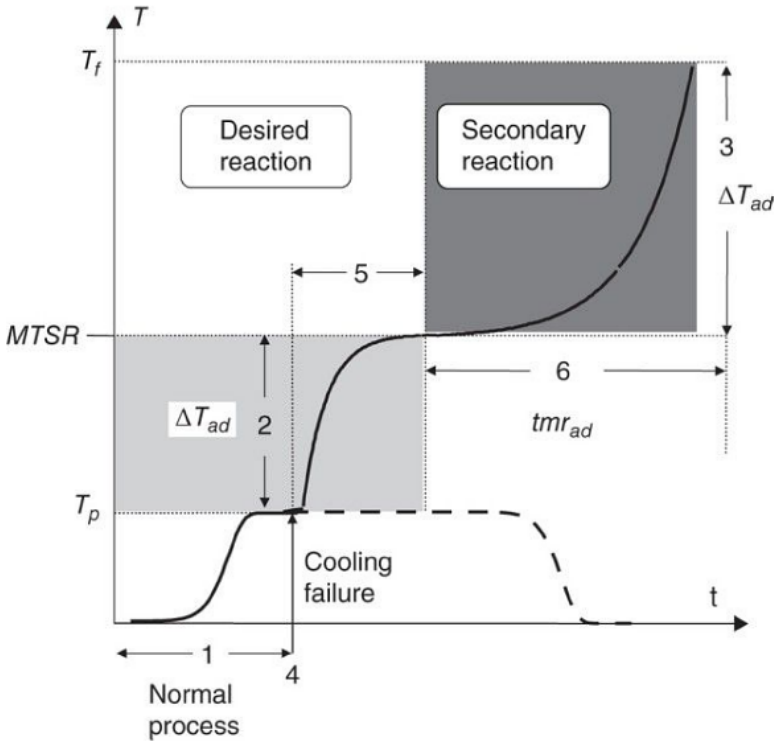

Figure 1.3: Runaway scenario of an exothermic batch reaction after a cooling failure. Reprinted from reference [53] with permission from John Wiley and Sons

The maximum achievable temperature T_f of the reaction content shown in Fig. 1.3 as well as the time to a possible thermal explosion are important safety aspects in the risk assessment. Consequently, the related thermal and kinetic parameters of the desired and

secondary reactions need to be analyzed. In a practical manner, the number of needed properties is reduced to obtain an educated estimate on quantities characterizing the potential runaway.

Kinetics of a desired reaction are crucial for the reactor design as well as for the safety assessment. If the above mentioned cooling failure occurs, a desired exothermic reaction continues to heat up the reactor content from the desired reaction temperature T_p based on the temperature depending kinetics. If no heat is transferred to the surrounding, an adiabatic temperature increase with ΔT_{ad} can be seen. Whereby the maximum temperature of the synthesis reaction $MTSR$ achievable by solely the desired reaction is defined as

$$MTSR = T_p + (1 - X)\Delta T_{ad} \; with \; \Delta T_{ad} = \frac{c_{a0}\Delta H_R}{\rho c_p} \tag{1.23}$$

with the desired reaction temperature T_p (K), chemical conversion X, concentration of the main and limiting component c_a at time 0 (mol m^{-3}), reaction enthalpy ΔH_R (J mol^{-1}), mixture density ρ (kg m^{-3}) and heap capacity of the reactor content c_p (J kg^{-1} K^{-1}).

In the worst case, the reactor content's temperature increases further until additional secondary reactions occur. The higher temperature can cause decomposition or evaporation of reaction components, leading to a pressure increase and possible explosions. The time needed for this thermal explosion to occur gets critical when the time to reach a maximum rate under adiabatic conditions becomes shorter than a chosen limit, *e.g.* 10-24 hours for industrial applications [54]. The estimated time to reach a maximum rate under adiabatic conditions tmr_{ad} is defined for a zero order reaction as

$$tmr_{ad} = \frac{c_p R {T_0}^2}{\dot{q}_0 E_a} \tag{1.24}$$

with the heat capacity of the reactor content c_p (J kg^{-1} K^{-1}), general gas constant R (J mol^{-1} K^{-1}), initial temperature T_0 (K), heat release rate $\dot{q}_0$ (W) and Arrhenius activation energy E_a (J $mol)^{-1}$. A more accurate method of estimating tmr_{ad} is to perform an adiabatic experiment and using the following equation: [55]

$$tmr_{ad} = \int_T^{T_m} \frac{dT}{k\left(\frac{T_f - T}{\Delta T_{ad}}\right)^n \Delta T_{ad} c_{a0}^{n-1}} \tag{1.25}$$

with the temperature at maximum rate T_m (K), rate constant k ((mol $m^{-3})^{1-m}$ s^{-1}), reaction order m (-), maximum achievable temperature T_f (K), adiabatic temperature increase ΔT_{ad} (K) and concentration of the main limiting component c_a at time 0 (mol m^{-3}).

1.4.2 Batch Reaction Calorimetry

Batch reaction calorimeter generally consists of a reaction vessel equipped with a stirrer and surrounded by a temperature controlled jacket containing a thermal fluid, see Fig. 1.4. A classification of batch calorimeters is possible based on their measurement and control principles as well as operation modes. [56]

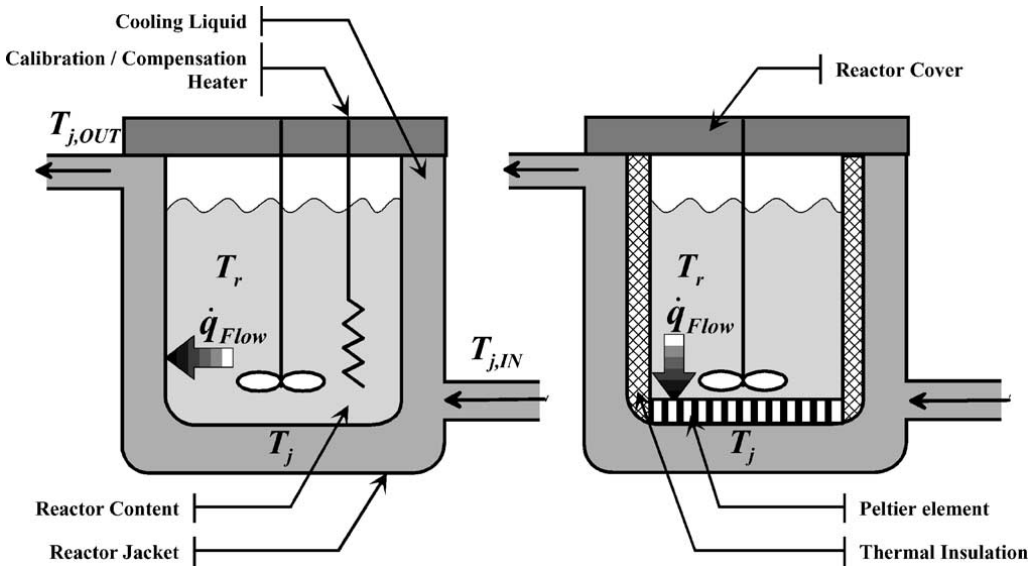

Figure 1.4: Basic set-up of batch calorimeter and their operation modes. (Left) heat flow, heat-balance and power compensation calorimeters. (Right) electric effect or Peltier based calorimeter. Reprinted from reference [56] with permission from Elsevier.

1.4.2.1 Measurement and control principles

Heat flow reaction calorimeters measure the required cooling heat flux $\dot{q}_{Flow}$ by the temperature difference of the reactor content T_r and the cooling liquid T_j while keeping T_r constant. Operation conditions with the corresponding heat transfer coefficient need to be calibrated to convert this temperature difference into a heat flow signal. This calibration is done by an integrated electrical heater. A precise temperature control of the reactor content requires high flow rates of the cooling fluid through the jacket. This measurement principle was first developed by Regenass [57, 58] and is used by most of the commercial reaction calorimeters.

Power compensation reaction calorimeters control the temperature of the reactor content by varying the power supply of a compensation heating. This allows to indirectly monitor the heat flow $\dot{q}_{Flow}$ from the reactor content to the cooling liquid as a correlation to the power consumption. As a consequence, such a measurement principle does not provide active cooling of the reactor content and requires a constant temperature T_j of the cooling fluid in the outer jacket. The power compensation principle was first shown

by Anderson [59].

A heat balance reaction calorimeter controls the reactor content temperature T_r directly with the provided cooling liquid. The transferred heat flux $\dot{q}_{Flow}$ can be calculated with an energy balance of the cooling liquid. To close this equation, it is required to know the heat capacity of the cooling liquid, accurately measure the temperature of inlet $T_{j,IN}$ and outlet $T_{j,OUT}$ of the cooling jacket as well as the mass flow of the liquid. The measurement principle does not need a calibration and was first implemented by Meeks [60].

Peltier reaction calorimeters allow to both actively heat and cool the reaction content with an Peltier element. The heat flow $\dot{q}_{Flow}$ is calculated based on the needed power consumption of the Peltier element and the measured temperature gradient between the cooling liquid and reactor content. Heat transfer is mainly allowed through the Peltier element as indicated by an additional insulation in Fig. 1.4 on the right side. This design was first shown by Becker [61].

1.4.2.2 Operation modes

A calorimetric measurement can be further distinguished between the control strategy for the temperature of the reaction content: [56]

- Isothermal mode with a controlled reaction content temperature T_r at a constant value
- Adiabatic mode whereby the cooling liquid temperature T_j is controlled to avoid heat losses from the reactor content
- Isoperibole mode by holding the cooling liquid temperature T_j at a constant level and leaving the reaction temperature T_r uncontrolled
- Temperature programmed or scanning mode of the user defined temperature profile of the reactor content's temperature T_r

The isothermal operation mode is the most applicable operation mode since no accumulation of heat needs to be considered. This eliminates the dependency of heat capacities on the reaction temperature T_r as well as dependencies of reactor internals like stirrers and sensors. Non-ideal behavior needs to be considered if the isothermal operation can not be granted. In real world applications this can be caused by dynamic events correlated to dosing and circuit control. If this deviation gets significant, it also needs to be considered during the evaluation. The isothermal operation mode will be discussed in more detail in the following section.

1.4.2.3 General isothermal heat flow balance

Steady state balance of a general isothermal heat flow reaction calorimeter is shown in Fig. 1.5 and described in the following. [56]

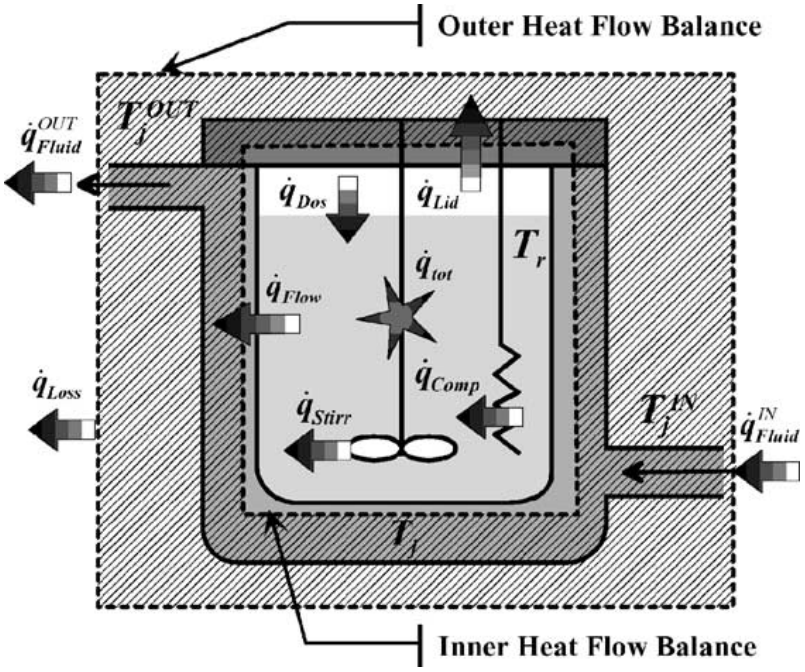

Figure 1.5: Heat flow rates of a general batch calorimeter case under isothermal conditions. Depicted heat fluxes show a positive heat flow rate in the arrow direction. Reprinted from reference [56] with permission from Elsevier.

During calorimetric measurements, the total heat flow rate during a chemical reaction is measured. This total heat flow rate also includes all other kinds of heat producing processes in which heat is released or absorbed. These additional heat sources can be written as:

$$\dot{q}_{tot} = \dot{q}_{React} + \dot{q}_{Mix} + \dot{q}_{Phase} \tag{1.26}$$

with $\dot{q}_{React}$ as reaction heat flow rate (W), $\dot{q}_{Mix}$ as mixing heat flow rate arising from mixing enthalpies while combining different fluids (W) and $\dot{q}_{Phase}$ as heat flow rate during phase changes (W). Assuming a reaction under constant pressure, the reaction heat flow rate is further defines as:

$$\dot{q}_{React} = -\sum_{j=1...N_R} \Delta H_{R,j} r_j V_r \tag{1.27}$$

where $\Delta H_{R,j}$ is the reaction enthalpy of the jth reaction (J mol^{-1}), r_j the jth reaction rate (mol m^{-3} s^{-1}), V_R the reaction volume of the mixture, and N_R as number of chemical reactions. The negative sign in equations 1.27 arises from the general definition in reaction calorimetry that exothermic events have a positive reaction heat flux $\dot{q}_{React}$ with a negative reaction enthalpy ΔH_R. The heat introduced to the reaction mass by stirring can be described by [62]

$$\dot{q}_{Stirr} = Ne\rho_r n_S^3 d_R^5 \tag{1.28}$$

with the Newton number Ne, the density of the reaction mixture ρ_r (kg m^{-3}), the stirrer frequency n_S (Hz) and the stirrer diameter d_R (m). By dosing of reactants, a heat flux $\dot{q}_{Dos}$ is defined as:

$$\dot{q}_{Dos} = \dot{V}_R c_{p,Dos}(T_{Dos} - T_r) \tag{1.29}$$

where $\dot{V}_R$ is the reactant flow rate (mol s^{-1}), $c_{p,Dos}$ the specific heat capacity of the dosing fluid (J mol^{-1} K^{-1}) and T_{Dos} is the temperature of the added fluid.

The measurable heat flow during operation $\dot{q}_{Flow}$ depicted in Fig. 1.4 and 1.5 can be defined under steady state conditions as:

$$\dot{q}_{Flow} = UA(T_r - T_j) \tag{1.30}$$

representing U as the overall heat transfer coefficient (W m^{-2} K^{-1}) and A as the total heat transfer area (m^2). Main contributions of U are a steady state heat transfer coefficient of the reactor h_r (W m^{-2} K^{-1}) and a device specific heat transfer coefficient φ (W m^{-2} K^{-1}) shown in equation 1.31.

$$\frac{1}{U} = \frac{1}{h_r} + \frac{1}{\varphi} \tag{1.31}$$

The device specific coefficient φ can be further shown by:

$$\frac{1}{\varphi} = \frac{L}{\lambda_W} + \frac{1}{h_j} \tag{1.32}$$

with the reactor wall thickness L (m), the material specific heat conductivity of the reactor wall λ_W (W m^{-1} K^{-1}) and a jacked sided steady state heat transfer coefficient h_j (W m^{-2} K^{-1}). Additional resistances of elements implemented to the reactor wall, e.g. Peltier elements, need to be added to equation 1.32.

During a measurement, the above mentioned device specific properties h_r and h_j change depending on reaction progress and operation conditions. h_r is influenced by physical properties of the reaction mixture such as viscosity and h_j is depending on the physical properties of the coolant. Additionally, the contact area A of equation 1.30 can very with reaction progress due to gas formation, dosing and density changes. These influences as well as small heat accumulation inside the reactor are normally neglected during measurement and the steady state equation 1.30 is used. The exact solutions for each specific operation mode can be found in literature. [56]

1.4.3 Continuous flow calorimetry

As shown above in section 1.3, flow chemistry is carried out in micro reactors under assumed isothermal conditions due to their high surface-to-volume ratio. [22] As a result, flow chemistry provides an especially interesting possibility to carry out fast and highly exothermic reactions since a tight temperature control, a safe operation at elevated pressures and a controlled mixing state are provided. A safety analysis as described in section 1.4.1 of such highly exothermic reactions commonly found in flow chemistry is most of the time limited in batch calorimeters. Batch calorimeter have a fundamental different mode of operation by lacking the possibility to operate under steady state conditions. Adaptions of the continuous flow reaction conditions have to be made to still be able to carry out a batch calorimetry measurement of such reactions. Normally, a limited dosing procedure of a reactant is used to prevent an uncontrolled runaway reaction. Depending on the carried out reaction, these dosing limitations of chemicals can lead to different products of mixing limited reactions and consequently to falsified data which is then used for the process design and risk analysis. Therefore, it makes sense to carry out calorimetric measurements under similar continuous conditions as later on used in the desired process.

Continuous flow calorimetry is an emerging field for developing flow chemistry processes. By using micro reactor technology in flow calorimeter, a so called Novel Process Window (*NPW*) is accessible by more extreme conditions like temperature, pressure and concentrations of reactants. [19] The small dimensions of the used micro structures also allow super-critical or solvent free processing carried out safely in laboratory environments. These conditions allow a more efficient and greener processing of chemicals and present an opportunity for flow calorimetry to precisely study thermodynamic and kinetic properties. Common limitations of micro reactor technology can also be applied to flow calorimetry such as handling of solids and problematic long residence times of slow reactions.

1.4.3.1 Types of flow calorimeter

Several types of flow calorimeter are presented in literature and a summary of some available continuous flow calorimeter is given in table 1.2. Their operation mode is mainly isothermal or isoperibole. A general heat balance for such an operation is given later on in Chap. 3. There are four approaches taken for the design of continuous flow calorimeters:

The first one is based on modifying existing batch calorimeter with inserted continuous flow equipment, *e.g.* reactor coils and chips submerged in the temperature controlled coolant in the inner vessel [63] or replacing a crucible, which is normally inserted with a measurement sample, with a micro chip like reactor [64]. Both approaches have advantages of using an already existing calorimeter system with known performance characteristics and calibration possibilities while requiring slight adaptions of the system. On the other side, there might be some connectivity issues with the continuous equipment and modifications on the software side are hardly possible.

Secondly, there is the possibility to use a combination of a transparent chip-like micro

reactor with an infrared thermography heat measurement [65]. This method requires optical access and an expensive infrared camera with a high resolution. The presented system showed an isoperibole mode of operation and was calibrated by Joule heating.

The third approach utilizes a chip-like micro reactor in combination with thermoelectric Seebeck elements. This direct heat flux measurement correlates the transferred heat, from a reactor through a Seebeck element to a heat sink, with a generated voltage signal. These thermoelectric elements can be prepared directly on a micro reactor chip [66, 67] or bigger and commercial Peltier element can be used [68, 69, 70]. Calibrations of the systems can be carried out by a direct Joule heating approach or by externally characterizing the performance of Seebeck elements at a reference temperature. One of the main advantages of this approach is the possibility to use several Seebeck elements distributed over the length of a reactor. Such an approach allows to gain additional insight into the kinetics of a chemical reaction.

Fourthly, several temperature measurements to create a spacial temperature profile downstream of a reactor in combination with a well defined reactor system can be used. [71] This approach solves the energy balance of the well-characterized reactor in combination with a process modeling software to calculate substance and mixture properties. A calibration at process conditions can be carried out without one of the reaction species. The temperature is controlled in an isoperibole mode by a heat transfer through the reactor wall to the coolant in the outer shell.

Some isothermal calorimeter may not be isothermal per definition and behave more like the isoperibole mode by keeping the outer cooling liquid or heating block at a constant value. The local hot spot formation of highly exo- or endothermic reactions is not controlled. Nevertheless, the isothermal operation assumption is valid for reactions with low reaction enthalpies and for low feed rates.

Type	Temperature Range	Max. Pressure	Volume/Reactor	Shown mode of operation
Modified Setline 120 Ref. [64]	-25°C to 120 °C	not stated;	250 x 100 μm 0.07 - 1.1 μL	Isothermal
Modified ChemiSens CPA202 Ref. [63]	-50 to 200 °C	20 bar for ChemiSens CPA202; depending on inserted reaction hardware	250 μL - 2.61 ml Comm. capillaries (0.8 mm *ID*) and micro reactor 250 μL used	Isothermal/ isoperibole
Chip reactor; thermoelec. heat flux measurement Ref. [69, 70]	up to 150 °C	shown until 16 bar	PVDF Foil 0.66 mm d_h & comm. glass chip 1 mm d_h with 0.1 ml	Isothermal/ isoperibole
Chip reactor thermoelec. heat flux measurement Ref. [68, 72]	up to 200 °C	up to 100 bar	0.49 - 8 ml	Isothermal/ isoperibole
Tube-in-tube reactor segment wise temp. measurement [71]	shown at -25 °C	not stated	l = 51 cm *ID* 7.8 mm 17 ml fluid volume static mixer	Isothermal/ isoperibole
Chip reactor thermoelec. heat flux measurement Chap. 3	-25 to 50 °C	up to 100 bar	*ID* 0.8 mm 220 μL	Isothermal

Table 1.2: Comparison of some recently published continuous flow calorimeter setups

1.5 Chemistry to plant approach - C2P

The *C2P* approach is a work flow guided approach for continuous manufacturing, as shown in Sec. 1.2. A desired chemical compound is produced in an organic synthesis which is carried out efficiently in a fast designed and constructed chemical plant. This is possible by a combination of Micro- and Milli Reactor Systems (*MRS*), see Sec. 1.3 and design possibilities enabled by additive manufacturing, [73, 74, 37] Sec. 1.3.3. Compared to commercially available *MRS*, *3D* printed reactors are almost not limited by the design complexity needed for multiphase and multistep applications. By assembling commercial *MRS*, often complex interconnections between the parts have to be made and may limit productivity by influencing the flow regime. [75] This regime is defined by the input conditions and may change throughout a reaction, leading to bad mixing as well as poor mass and heat transfer. A uniquely designed reactor can be manufactured by additive manufacturing adapted to these changes caused by a reaction. This reduces the construction process compared to the conventional approach of searching and adapting commercially available parts of a *MRS* until a desired combination is found. A *3D* printed *MRS* can be designed in a more compact and efficient way by already considering peripheral equipment such as pumps, sensors and valves in the design phase.

Fig. 1.6 shows the developed *C2P* work flow. First, a chemical reaction with an industrial interest for production is defined and initially investigated in terms feasibility. If a suitable approach is found, the reaction conditions are saved in a cloud database. This database is the central knowledge exchange point between the involved project partners. After defining changeable and system parameters needed for the work of each individual partner, the desired reactor is further analyzed by computational simulations of the reaction system including substance data and laboratory based reaction analysis. The developed continuous flow calorimeter, see Chap. 3 plays a central part to provide thermodynamic and kinetic data of the planned reaction. An additional tool during the reaction investigation at various operation conditions is the developed *CSTR* cascade, shown in Chap. 2 and later on in an advanced version in Chap. 4. Its design allows to have multiple fluid ports and implemented process sensors to follow a reaction from vessel to vessel.

In a next step, a *CAD* file of the planned reactor is created. This design is based on existing guidelines [22, 23, 76] as discussed in detail in Sec. 1.3.1. The *CAD* design of a first reactor iteration is assembled from a structure element database first proposed in Chap. 2 and advanced in Chap. 4. This database is parameter depending and used in a click-and-drop like procedure to exchange and automatically adapt structure elements based only on three design parameters. The reactor design is then virtually verified by Computational Fluid Dynamics (*CFD*) simulations and adapted if needed. The final design is then modified from project partners by adding the needed structure support for additive manufacturing and produced in the desired chemical resistant material.

The produced reactors are then characterized according to the mentioned procedures in Sec. 1.3.2. The next step includes the implementation of the reactor in the desired

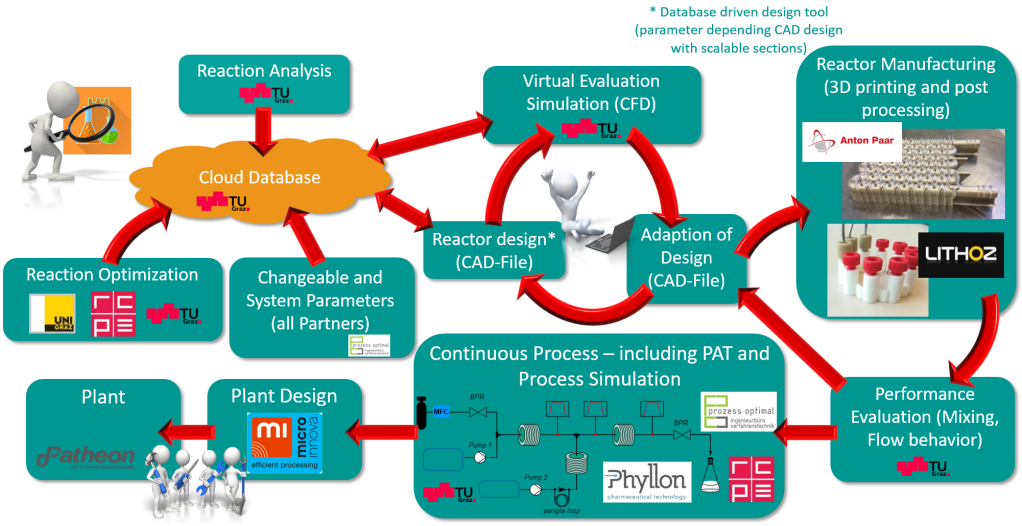

Figure 1.6: Visualization of the *C2P* work flow and involved project partners. After choosing a desired reaction, process parameters are screened and a first reactor model is proposed. A virtual and *3D* printing iteration loop is carried out next to ensure optimized reaction conditions. The next steps are a first lab scale investigation of the process including Process Analytical Technology (*PAT*) and process simulation with a following detailed engineering and final operation in an industrial environment.

plant, for a first validation in a laboratory scale. In this stage process conditions are screened already with the later on used Process Analytical Technology (*PAT*) tools as well as simulated on a process basis. The obtained results are then used in the following detail engineering. Process simulation, decision of adequate *PAT* solutions as well as detail engineering were started and included already during the reactor design phase. All gathered information are then used to bring the desired production plant to scale, either by scaling-out or numbering up approaches. This strong collaboration based work flow with a constant data exchange between project partners aims to reduce the time to a final producing plant from years to 2 – 3 months.

The aerobic oxidation of a Grignard reagent shown in Chap. 2 and Chap. 4 was used to develop the above mentioned work flow. In Chap. 2, a focus is held on the reaction itself and the reactor design concept leading to the structure element database. The continuous flow calorimeter shown in Chap. 3 was developed then to have a reaction analysis tool available within the *C2P* work flow for fast continuous flow syntheses. Chap. 4 then focuses on the implementation and process control of various reactor designs created with the structure element database. These reactors were used to successfully show the mixing and temperature dependent oxidation of a Grignard reagent.

Bibliography

[1] John R. Bourne, Oemer M. Kut, Joachim Lenzner, and Horst Maire. "Kinetics of the diazo coupling between 1-naphthol and diazotized sulfanilic acid". In: *Industrial & Engineering Chemistry Research* 29.9 (Sept. 1990), pp. 1761–1765. ISSN: 0888-5885. DOI: 10.1021/ie00105a004. URL: http://pubs.acs.org/doi/abs/10.1021/ie00105a004%20https://pubs.acs.org/doi/abs/10.1021/ie00105a004.

[2] Peter Poechlauer, Julie Manley, Rinus Broxterman, Björn Gregertsen, and Mats Ridemark. "Continuous processing in the manufacture of active pharmaceutical ingredients and finished dosage forms: An industry perspective". In: *Organic Process Research and Development* (2012). ISSN: 10836160. DOI: 10.1021/op300159y.

[3] Peter Poechlauer, Juan Colberg, Elizabeth Fisher, Michael Jansen, Martin D. Johnson, Stefan G. Koenig, Michael Lawler, Thomas Laporte, Julie Manley, Benjamin Martin, and Anne O'Kearney-Mcmullan. "Pharmaceutical Roundtable Study Demonstrates the Value of Continuous Manufacturing in the Design of Greener Processes". In: *Organic Process Research and Development* 17.12 (2013), pp. 1472–1478. ISSN: 10836160. DOI: 10.1021/op400245s.

[4] Stephen G. Newman and Klavs F. Jensen. "The role of flow in green chemistry and engineering". In: *Green Chemistry* 15.6 (2013), pp. 1456–1472. ISSN: 14639270. DOI: 10.1039/c3gc40374b. URL: http://dx.doi.org/10.1039/C3GC40374B.

[5] David J. am Ende and Mary T. am Ende. *Chemical Engineering in the Pharmaceutical Industry*. Ed. by David J. Ende and Mary T. Ende. Second Edi. John Wiley & Sons, Inc., Mar. 2019. ISBN: 9781119285496. DOI: 10.1002/9781119600800. URL: https://onlinelibrary.wiley.com/doi/book/10.1002/9781119600800.

[6] Gerard Capellades, Clemence Neurohr, Naomi Briggs, Kersten Rapp, Gregory Hammersmith, David Brancazio, Bridget Derksen, and Allan S. Myerson. " On-Demand Continuous Manufacturing of Ciprofloxacin in Portable Plug-and-Play Factories: Implementation and In Situ Control of Downstream Production ". In: *Organic Process Research & Development* (2021). ISSN: 1083-6160. DOI: 10.1021/acs.oprd.1c00117.

[7] Philip J. Kitson, Guillaume Marie, Jean-Patrick Francoia, Sergey S. Zalesskiy, Ralph C. Sigerson, Jennifer S. Mathieson, and Leroy Cronin. "Digitization of multistep organic synthesis in reactionware for on-demand pharmaceuticals". In: *Science* 359.6373 (Jan. 2018), pp. 314–319. ISSN: 0036-8075. DOI: 10.1126/science.aao3466. URL: http://www.sciencemag.org/lookup/doi/10.1126/science.aao3466%20http://www.ncbi.nlm.nih.gov/pubmed/29348235%20https://www.sciencemag.org/lookup/doi/10.1126/science.aao3466.

[8] Manuel C. Maier, René Lebl, Philipp Sulzer, Josef Lechner, Torsten Mayr, Matej Zadravec, Eyke Slama, Stefan Pfanner, Christoph Schmölzer, Peter Pöchlauer, C. Oliver Kappe, and Heidrun Gruber-Woelfler. "Development of customized 3D printed stainless steel reactors with inline oxygen sensors for aerobic oxidation of Grignard reagents in continuous flow". In: *Reaction Chemistry and Engineering* 4.2 (2019), pp. 393–401. ISSN: 20589883. DOI: 10.1039/C8RE00278A. URL: http://xlink.rsc.org/?DOI=C8RE00278A.

[9] Manuel C. Maier, Michael Leitner, C. Oliver Kappe, and Heidrun Gruber-Woelfler. "A modular 3D printed isothermal heat flow calorimeter for reaction calorimetry in continuous flow". In: *Reaction Chemistry and Engineering* 5.8 (2020), pp. 1410–1420. ISSN: 20589883. DOI: 10.1039/d0re00122h. URL: http://xlink.rsc.org/?DOI=D0RE00122H.

[10] Manuel C. Maier, Alessia Valotta, Katharina Hiebler, Sebastian Soritz, Kristian Gavric, Bianca Grabner, and Heidrun Gruber-Woelfler. "3D Printed Reactors for Synthesis of Active Pharmaceutical Ingredients in Continuous Flow". In: *Organic Process Research and Development* (2020). ISSN: 1520586X. DOI: 10.1021/acs.oprd.0c00228.

[11] Sau L. Lee, Thomas F. O'Connor, Xiaochuan Yang, Celia N. Cruz, Sharmista Chatterjee, Rapti D. Madurawe, Christine M. V. Moore, Lawrence X. Yu, and Janet Woodcock. "Modernizing Pharmaceutical Manufacturing: from Batch to Continuous Production". In: *Journal of Pharmaceutical Innovation* 10.3 (Sept. 2015), pp. 191–199. ISSN: 1872-5120. DOI: 10.1007/s12247-015-9215-8. URL: http://link.springer.com/10.1007/s12247-015-9215-8.

[12] Hans Leuenberger. "New trends in the production of pharmaceutical granules: batch versus continuous processing". In: *European Journal of Pharmaceutics and Biopharmaceutics* 52.3 (Nov. 2001), pp. 289–296. ISSN: 09396411. DOI: 10.1016/

S0939-6411(01)00199-0. URL: https://www.sciencedirect.com/science/article/pii/S0939641101001990%20https://linkinghub.elsevier.com/retrieve/pii/S0939641101001990.

[13] Lawrence X. Yu. "Pharmaceutical Quality by Design: Product and Process Development, Understanding, and Control". In: *Pharmaceutical Research* 25.4 (Apr. 2008), pp. 781–791. ISSN: 0724-8741. DOI: 10.1007/s11095-007-9511-1. URL: https://doi.org/10.1007/s11095-007-9511-1%20http://link.springer.com/10.1007/s11095-007-9511-1.

[14] Dominique M. Roberge, Laurent Ducry, Nikolaus Bieler, Philippe Cretton, and Bertin Zimmermann. "Microreactor technology: A revolution for the fine chemical and pharmaceutical industries?" In: *Chemical Engineering and Technology* 28.3 (2005), pp. 318–323. ISSN: 09307516. DOI: 10.1002/ceat.200407128. URL: https://onlinelibrary.wiley.com/doi/abs/10.1002/ceat.200407128.

[15] Norbert Kockmann. *Process Engineering Methods and Microsystem Technology*. Vol. 5. 2008, pp. 1–45. ISBN: 9783527616749. DOI: 10.1002/9783527616749.ch1. URL: http://dx.doi.org/10.1002/9783527616749.ch1.

[16] Matthew B. Plutschack, Bartholomäus Pieber, Kerry Gilmore, and Peter H. Seeberger. "The Hitchhiker's Guide to Flow Chemistry". In: *Chemical Reviews* 117.18 (Sept. 2017), pp. 11796–11893. ISSN: 0009-2665. DOI: 10.1021/acs.chemrev.7b00183. URL: http://pubs.acs.org/doi/10.1021/acs.chemrev.7b00183.

[17] Charlotte Wiles and Paul Watts. "Continuous flow reactors: a perspective". In: *Green Chem.* 14.1 (2012), pp. 38–54. ISSN: 1463-9262. DOI: 10.1039/C1GC16022B. URL: http://dx.doi.org/10.1039/C1GC16022B%20http://xlink.rsc.org/?DOI=C1GC16022B.

[18] Volker Hessel, Dana Kralisch, Norbert Kockmann, Timothy Noël, and Qi Wang. "Novel Process Windows for Enabling, Accelerating, and Uplifting Flow Chemistry". In: *ChemSusChem* 6.5 (May 2013), pp. 746–789. ISSN: 18645631. DOI: 10.1002/cssc.201200766. URL: https://chemistry-europe.onlinelibrary.wiley.com/doi/abs/10.1002/cssc.201200766%20https://onlinelibrary.wiley.com/doi/10.1002/cssc.201200766.

[19] Volker Hessel, Dana Kralisch, and Norbert Kockmann. *Novel Process Windows*. Ed. by Volker Hessel, Dana Kralisch, and Norbert Kockmann. Weinheim, Germany: Wiley-VCH Verlag GmbH & Co. KGaA, Nov. 2014, pp. 1–314. ISBN: 9783527654826. DOI: 10.1002/9783527654826. URL: http://doi.wiley.com/10.1002/9783527654826.

[20] Volker Hessel, Dana Kralisch, and Norbert Kockmann. "Novel Process Windows". In: *Novel Process Windows*. Weinheim, Germany: Wiley-VCH Verlag GmbH & Co. KGaA, Jan. 2015, pp. 15–24. ISBN: 9783527654840. DOI: 10.1002/9783527654826.ch2.

[21] Dominique M. Roberge. "An integrated approach combining reaction engineering and design of experiments for optimizing reactions". In: *Organic Process Research and Development* 8.6 (2004), pp. 1049–1053. ISSN: 10836160. DOI: 10.1021/op0400160.

[22] V Hessel, S Hardt, and H Löwe. *Chemical Micro Process Engineering: Fundamentals, Modelling and Reactions*. Weinheim: Wiley-VCH, 2004. ISBN: 9783527307418. DOI: 10.1002/3527603042.

[23] Norbert Kockmann. "Pressure loss and transfer rates in microstructured devices with chemical reactions". In: *Chemical Engineering and Technology* 31.8 (2008), pp. 1188–1195. ISSN: 09307516. DOI: 10.1002/ceat.200800065.

[24] Norbert Kockmann, Michael Gottsponer, Bertin Zimmermann, and Dominique M. Roberge. "Enabling continuous-flow chemistry in microstructured devices for pharmaceutical and fine-chemical production". In: *Chemistry - A European Journal* 14.25 (2008), pp. 7470–7477. ISSN: 09476539. DOI: 10.1002/chem.200800707.

[25] Norbert Kockmann, Michael Gottsponer, and Dominique M. Roberge. "Scale-up concept of single-channel microreactors from process development to industrial production". In: *Chemical Engineering Journal* 167.2-3 (2011), pp. 718–726. ISSN: 13858947. DOI: 10.1016/j.cej.2010.08.089. URL: http://dx.doi.org/10.1016/j.cej.2010.08.089.

[26] Thomas Westermann and Leslaw Mleczko. "Heat Management in Microreactors for Fast Exothermic Organic Syntheses—First Design Principles". In: *Organic Process Research & Development* 20.2 (Feb. 2016), pp. 487–494. ISSN: 1083-6160. DOI: 10.1021/acs.oprd.5b00205. URL: https://pubs.acs.org/doi/10.1021/acs.oprd.5b00205.

[27] Albert Renken and Lioubov Kiwi-Minsker. "Chemical Reactions in Continuous –flow Microstructured Reactors". In: Feb. 2006, pp. 173–201. DOI: 10.1002/9783527616749.ch6. URL: https://onlinelibrary.wiley.com/doi/abs/10.1002/9783527616749.ch6.

[28] Frank P Incropera and David P DeWitt. *Fundamentals of Heat and Mass Transfer*. John Wiley & Sons, 1996, p. 890. ISBN: 0471304603. DOI: 10.1016/j.applthermaleng.2011.03.022. arXiv: 1105-.

[29] Jens Weitkamp and Roger Gläser. "Chemische Technik: Prozesse und Produkte". In: *Wiley-VCH: Weinheim.* (2004), 645 ff.

[30] Stephen A. Solovitz and Jeffrey Mainka. "Manifold Design for Micro-Channel Cooling With Uniform Flow Distribution". In: *Journal of Fluids Engineering* 133.5 (May 2011). ISSN: 0098-2202. DOI: 10.1115/1.4004089. URL: https://asmedigitalcollection.asme.org/fluidsengineering/article/doi/10.1115/1.4004089/450502/Manifold-Design-for-MicroChannel-Cooling-With.

[31] V.A. Antonets, M.A. Antonets, and I.A. Shereshevsky. "The statistical cluster dynamics in the dendroid transfer sys- tems". In: *Fractals in the Fundamental and Applied Sciences* (1991), pp. 59–71.

[32] Yongping Chen and Ping Cheng. "Heat transfer and pressure drop in fractal tree-like microchannel nets". In: *International Journal of Heat and Mass Transfer* 45.13 (2002), pp. 2643–2648. ISSN: 00179310. DOI: 10.1016/S0017-9310(02)00013-3.

[33] Octave Levenspiel. *Chemical Reaction Engineering*. 3rd Ed. New York: Wiley, 1999, pp. 293–320. ISBN: 0-471-25424-X.

[34] M.-C. Fournier, L. Falk, and J. Villermaux. "A new parallel competing reaction system for assessing micromixing efficiency—Experimental approach". In: *Chemical Engineering Science* 51.22 (Nov. 1996), pp. 5053–5064. ISSN: 00092509. DOI: 10.1016/0009-2509(96)00270-9. URL: https://linkinghub.elsevier.com/retrieve/pii/0009250996002709.

[35] Sebastian Schwolow, Jutta Hollmann, Berthold Schenkel, and Thorsten Röder. "Application-Oriented Analysis of Mixing Performance in Microreactors". In: *Organic Process Research & Development* 16.9 (Sept. 2012), pp. 1513–1522. ISSN: 1083-6160. DOI: 10.1021/op300107z. URL: http://pubs.acs.org/doi/10.1021/op300107z.

[36] Nirveek Bhattacharjee, Arturo Urrios, Shawn Kang, and Albert Folch. "The upcoming 3D-printing revolution in microfluidics". In: *Lab on a Chip* 16.10 (2016), pp. 1720–1742. ISSN: 1473-0197. DOI: 10.1039/C6LC00163G. arXiv: 15334406. URL: http://xlink.rsc.org/?DOI=C6LC00163G%20http://www.ncbi.nlm.nih.gov/pubmed/27101171%20http://www.pubmedcentral.nih.gov/articlerender.fcgi?artid=PMC4862901.

[37] Anthony K. Au, Wilson Huynh, Lisa F. Horowitz, and Albert Folch. "3D-Printed Microfluidics". In: *Angewandte Chemie International Edition* 55.12 (Mar. 2016), pp. 3862–3881. ISSN: 14337851. DOI: 10.1002/anie.201504382. URL: http://doi.wiley.com/10.1002/anie.201504382%20http://www.ncbi.nlm.nih.gov/pubmed/26854878%20https://onlinelibrary.wiley.com/doi/10.1002/anie.201504382.

[38] Andrew J. Capel, Andrew Wright, Matthew J. Harding, George W. Weaver, Yuqi Li, Russell A. Harris, Steve Edmondson, Ruth D. Goodridge, and Steven D.R. R Christie. "3D printed fluidics with embedded analytic functionality for automated reaction optimisation". In: *Beilstein Journal of Organic Chemistry*

13 (Jan. 2017), pp. 111–119. ISSN: 18605397. DOI: 10.3762/bjoc.13.14. URL: http://www.beilstein-journals.org/bjoc/content/13/1/14.

[39] Sergio Rossi, Alessandra Puglisi, and Maurizio Benaglia. "Additive Manufacturing Technologies: 3D Printing in Organic Synthesis". In: *ChemCatChem* 10.7 (Apr. 2018), pp. 1512–1525. ISSN: 18673880. DOI: 10.1002/cctc.201701619. URL: https://onlinelibrary.wiley.com/doi/10.1002/cctc.201701619%20https://chemistry-europe.onlinelibrary.wiley.com/doi/abs/10.1002/cctc.201701619%20http://doi.wiley.com/10.1002/cctc.201701619.

[40] Jan Holmström, Jouni Partanen, Jukka Tuomi, and Manfred Walter. "Rapid manufacturing in the spare parts supply chain: Alternative approaches to capacity deployment". In: *Journal of Manufacturing Technology Management* 21.6 (2010), pp. 687–697. ISSN: 1741038X. DOI: 10.1108/17410381011063996.

[41] Ian Gibson, David W Rosen, and Brent Stucker. "Design for Additive Manufacturing". In: *Additive Manufacturing Technologies*. Boston, MA: Springer US, 2010, pp. 299–332. ISBN: 978-1-4419-1120-9. DOI: 10.1007/978-1-4419-1120-9_11. URL: https://doi.org/10.1007/978-1-4419-1120-9_11%20http://link.springer.com/10.1007/978-1-4419-1120-9_11.

[42] André De Vries. "3D-Printed Metal Flow Reactors and Mixers". In: *RSC Symposium Chemspec*. München, Germany, 2017. URL: https://www.chemspeceurope.com/2019/assets/CSE18_RSCArchive_2017_7b.pdf.

[43] Ben Vandenbroucke and Jean Pierre Kruth. "Selective laser melting of biocompatible metals for rapid manufacturing of medical parts". In: *Rapid Prototyping Journal* 13.4 (Jan. 2007), pp. 196–203. ISSN: 13552546. DOI: 10.1108/13552540710776142. URL: https://doi.org/10.1108/13552540710776142.

[44] Vojislav Petrovic, Juan Vicente Haro Gonzalez, Olga Jordá Ferrando, Javier Delgado Gordillo, Jose Ramón Blasco Puchades, and Luis Portolés Griñan. "Additive layered manufacturing: sectors of industrial application shown through case studies". In: *International Journal of Production Research* 49.4 (Feb. 2011), pp. 1061–1079. ISSN: 0020-7543. DOI: 10.1080/00207540903479786. URL: https://doi.org/10.1080/00207540903479786%20https://www.tandfonline.com/doi/full/10.1080/00207540903479786.

[45] J.-P. Kruth, G Levy, F Klocke, and T.H.C. Childs. "Consolidation phenomena in laser and powder-bed based layered manufacturing". In: *CIRP Annals* 56.2 (2007), pp. 730–759. ISSN: 00078506. DOI: 10.1016/j.cirp.2007.10.004. URL: https://www.sciencedirect.com/science/article/pii/S0007850607001540%20https://linkinghub.elsevier.com/retrieve/pii/S0007850607001540.

[46] Eleftherios Louvis, Peter Fox, and Christopher J. Sutcliffe. "Selective laser melting of aluminium components". In: *Journal of Materials Processing Technology* 211.2 (Feb. 2011), pp. 275–284. ISSN: 09240136. DOI: 10.1016/j.jmatprotec.2010.09.019. URL: https://www.sciencedirect.com/science/article/pii/S0924013610003018%20https://linkinghub.elsevier.com/retrieve/pii/S0924013610003018.

[47] A. Bertsch, S. Zissi, J. Y. Jézéquel, S. Corbel, and J. C. André. "Microstereophotolithography using a liquid crystal display as dynamic mask-generator". In: *Microsystem Technologies* 3.2 (Feb. 1997), pp. 42–47. ISSN: 0946-7076. DOI: 10.1007/s005420050053. URL: https://doi.org/10.1007/s005420050053%20http://link.springer.com/10.1007/s005420050053.

[48] Ferry P.W. Melchels, Jan Feijen, and Dirk W. Grijpma. "A review on stereolithography and its applications in biomedical engineering". In: *Biomaterials* 31.24 (Aug. 2010), pp. 6121–6130. ISSN: 01429612. DOI: 10.1016/j.biomaterials.2010.04.050. URL: https://www.sciencedirect.com/science/article/pii/S0142961210005661%20https://linkinghub.elsevier.com/retrieve/pii/S0142961210005661.

[49] R. Gygax. "Chemical reaction engineering for safety". In: *Chemical Engineering Science* 43.8 (1988), pp. 1759–1771. ISSN: 00092509. DOI: 10.1016/0009-2509(88)87040-4. URL: https://linkinghub.elsevier.com/retrieve/pii/0009250988870404.

[50] Zogg Andreas. *Calorimetry Kinetic and Approach using IR-ATR Spectroscopy Reaction Parameters for the Determination of Thermodynamic*. 15086. ETH Zurich, 2003, pp. 30–35. ISBN: 3906734331.

[51] Vinicius Kartnaller, Danielly C.O. Mariano, and João Cajaiba. "Application of In-Line Mid-Infrared (MIR) Spectroscopy Coupled with Calorimetry for the Determination of the Molar Enthalpy of Reaction between Ammonium Chloride and Sodium Nitrite". In: *Applied Spectroscopy* 70.3 (2016), pp. 531–538. ISSN: 19433530. DOI: 10.1177/0003702815626682. URL: https://doi.org/10.1177/0003702815626682.

[52] Agnieszka Ładosz, Christina Kuhnle, and Klavs F. Jensen. "Characterization of reaction enthalpy and kinetics in a microscale flow platform". In: *Reaction Chemistry and Engineering* 5.11 (2020), pp. 2115–2122. ISSN: 20589883. DOI: 10.1039/d0re00304b. URL: http://xlink.rsc.org/?DOI=D0RE00304B.

[53] Francis Stoessel. *Thermal Safety of Chemical Processes: Risk Assessment and Process Design*. Wiley, Feb. 2008, pp. 1–374. ISBN: 9783527317127. DOI: 10.1002/9783527621606. URL: https://onlinelibrary.wiley.com/doi/book/10.1002/9783527621606.

[54] Andreas Keller, Daniel Stark, Hans Fierz, Elmar Heinzle, and Konrad Hungerbühler. "Estimation of the time to maximum rate using dynamic DSC experiments". In: *Journal of Loss Prevention in the Process Industries* 10.1 (1997), pp. 31–41. ISSN: 09504230. DOI: 10.1016/S0950-4230(96)00037-X.

[55] D. I. Townsend and J. C. Tou. "Thermal hazard evaluation by an accelerating rate calorimeter". In: *Thermochimica Acta* 37.1 (1980), pp. 1–30. ISSN: 00406031. DOI: 10.1016/0040-6031(80)85001-5.

[56] Andreas Zogg, Francis Stoessel, Ulrich Fischer, and Konrad Hungerbühler. "Isothermal reaction calorimetry as a tool for kinetic analysis". In: *Thermochimica Acta* 419.1-2 (Sept. 2004), pp. 1–17. ISSN: 00406031. DOI: 10.1016/j.tca.2004.01.015. URL: https://linkinghub.elsevier.com/retrieve/pii/S0040603104000486.

[57] W. Regenass. "Thermoanalytische Methoden in der Chemischen Verfahrenentwicklung". In: *Thermochim. Acta*. Vol. 20. 1. Elsevier, 1976, pp. 65–79.

[58] Hans Martin. *Waermefiusskalorimetrie unter praeparativen Bedingungen und ihre Anwendung zur Verfolgung der Isomerisierungskinetik von Trimethylphosphit*. Basel: Ph.D. Thesis, University of Basel, 1975.

[59] H M Andersen. "Isothermal kinetic calorimeter applied to emulsion polymerization". In: *Journal of Polymer Science Part A-1: Polymer Chemistry* 4.4 (1966), pp. 783–791.

[60] M R Meeks. "An analog computer study of polymerization rates in vinyl chloride suspensions". In: *Polymer Engineering & Science* 9.2 (1969), pp. 141–151.

[61] F Becker. "Thermokinetische Messmethoden". In: *Chemie Ingenieur Technik* 40.19 (1968), pp. 933–947.

[62] Martin Zogg. *Einführung in die mechanische Verfahrenstechnik mit 29 Tabellen und 32 Berechnungsbeispielen*. Teubner, 1993. ISBN: 3519163195.

[63] Gabriel Glotz, Donald J. Knoechel, Philip Podmore, Heidrun Gruber-Woelfler, and C. Oliver Kappe. "Reaction Calorimetry in Microreactor Environments - Measuring Heat of Reaction by Isothermal Heat Flux Calorimetry". In: *Organic Process Research and Development* 21.5 (2017), pp. 763–770. ISSN: 1520586X. DOI: 10.1021/acs.oprd.7b00092.

[64] M. A. Schneider and F. Stoessel. "Determination of the kinetic parameters of fast exothermal reactions using a novel microreactor-based calorimeter". In: *Chemical Engineering Journal* 115.1-2 (2005), pp. 73–83. ISSN: 13858947. DOI: 10.1016/j.cej.2005.09.019.

[65] Cindy Hany, Christophe Pradere, Jean Toutain, and Jean-Christophe Batsale. "A millifluidic calorimeter with infrared thermography for the measurement of chemical reaction enthalpy and kinetics". In: *Quantitative InfraRed Thermography Journal* 5.2 (Dec. 2008), pp. 211–229. ISSN: 1768-6733. DOI: 10.3166/qirt.5.211-229. URL: http://www.tandfonline.com/doi/abs/10.3166/qirt.5.211-229.

[66] J.Michael Köhler and Martin Zieren. "Chip reactor for microfluid calorimetry". In: *Thermochimica Acta* 310.1-2 (Feb. 1998), pp. 25–35. ISSN: 00406031. DOI: 10.1016/S0040-6031(97)00381-X. URL: https://linkinghub.elsevier.com/retrieve/pii/S004060319700381X.

[67] Yuyan Zhang and Srinivas Tadigadapa. "Calorimetric biosensors with integrated microfluidic channels". In: *Biosensors and Bioelectronics* 19.12 (July 2004), pp. 1733–1743. ISSN: 09565663. DOI: 10.1016/j.bios.2004.01.009. URL: https://linkinghub.elsevier.com/retrieve/pii/S0956566304000260.

[68] S Loebbecke, J Antes, W Ferstl, D Boskovic, T Tuercke, M Schwarzer, and H Krause. "Microreactors for processing of hazardous and explosible reactions". In: *Institution of Chemical Engineers Symposium Series* 153 (2007), pp. 1–6. URL: https://www.mendeley.com/catalogue/microreactors-processing-hazardous-explosive-reactions/.

[69] Felix Reichmann, Stefan Millhoff, Yannick Jirmann, and Norbert Kockmann. "Reaction Calorimetry for Exothermic Reactions in Plate-Type Microreactors Using Seebeck Elements". In: *Chemical Engineering & Technology* 40.11 (Nov. 2017), pp. 2144–2154. ISSN: 09307516. DOI: 10.1002/ceat.201700419. URL: http://doi.wiley.com/10.1002/ceat.201700419.

[70] Timothy Aljoscha Frede, Marlene Dietz, and Norbert Kockmann. "Software-guided microscale flow calorimeter for efficient acquisition of thermokinetic data". In: *Journal of Flow Chemistry* (2021). ISSN: 20630212. DOI: 10.1007/s41981-021-00145-6.

[71] Frederik Mortzfeld, Jutta Polenk, Bertrand Guelat, Francesco Venturoni, Berthold Schenkel, and Paolo Filipponi. "Reaction Calorimetry in Continuous Flow Mode: A New Approach for the Thermal Characterization of High Energetic and Fast Reactions". In: *Organic Process Research and Development* 24.10 (Oct. 2020), pp. 2004–2016. ISSN: 1520586X. DOI: 10.1021/acs.oprd.0c00117. URL: https://doi.org/10.1021/acs.oprd.0c00117%20https://pubs.acs.org/doi/10.1021/acs.oprd.0c00117.

[72] Jürgen Antes. *Fraunhofer Institute for Chemical Technology Ict Reaction Calorimetry in Microreactors*. URL: https://www.ict.fraunhofer.de/content/dam/ict/en/documents/media/em/EM_Reaktionskalorimetrie_V05_en.pdf (visited on 06/22/2021).

[73] Andrew J. Capel, Steve Edmondson, Steven D.R. R. R Christie, Ruth D. Goodridge, Richard J. Bibb, and Matthew Thurstans. "Design and additive manufacture for flow chemistry." In: *Lab on a chip* 13.23 (Dec. 2013), pp. 4583–4590. ISSN: 1473-0189. DOI: 10.1039/c3lc50844g. URL: http://xlink.rsc.org/?DOI=c3lc50844g%20http://www.ncbi.nlm.nih.gov/pubmed/24100659.

[74] Ian Gibson, David Rosen, and Brent Stucker. *Additive manufacturing technologies: 3D printing, rapid prototyping, and direct digital manufacturing, second edition*. 2015, pp. 1–498. ISBN: 9781493921133. DOI: 10.1007/978-1-4939-2113-3. URL: http://www.scopus.com/inward/record.url?eid=2-s2.0-84944216444%7B%5C&%7DpartnerID=40%7B%5C&%7Dmd5=5823d88f66cd6827200a60b798005d95.

[75] Axel Günther and Klavs F. Jensen. "Multiphase microfluidics: from flow characteristics to chemical and materials synthesis". In: *Lab Chip* 6.12 (Dec. 2006), pp. 1487–1503. ISSN: 1473-0197. DOI: 10.1039/B609851G. URL: http://xlink.rsc.org/?DOI=B609851G%20http://www.ncbi.nlm.nih.gov/pubmed/17203152.

[76] Madhvanand N. Kashid, Albert Renken, and Lioubov Kiwi-Minsker. "Gas-liquid and liquid-liquid mass transfer in microstructured reactors". In: *Chemical Engineering Science* 66.17 (2011), pp. 3876–3897. ISSN: 00092509. DOI: 10.1016/j.ces.2011.05.015. URL: http://dx.doi.org/10.1016/j.ces.2011.05.015.

CHAPTER 2

Development of customized 3D printed stainless steel reactors with inline oxygen sensors for aerobic oxidation of Grignard reagents in continuous flow

The following chapter is taken from the same-titled journal article published in *Reaction Chemistry and Engineering* by Maier *et al.*:

Manuel C. Maier[1,2], René Lebl[1,3], Philipp Sulzer[1,4], Josef Lechner[1,2], Torsten Mayr[1,4], Matej Zadravec[1], Eyke Slama[1], Stefan Pfanner[5], Christoph Schmölzer[6], Peter Pöchlauer[6], C. Oliver Kappe[1,3], and Heidrun Gruber-Woelfler[1,2]

Reaction Chemistry and Engineering, 12/2018, DOI: 10.1039/c8re00278a

[1]Center for Continuous Flow Synthesis and Processing (CCFLOW), Research Center Pharmaceutical Engineering GmbH (RCPE), Graz, Austria

[2]Institute of Process and Particle Engineering, Graz University of Technology, Graz, Austria

[3]Institute of Chemistry, University of Graz, Graz, Austria

[4]Institute of Analytical Chemistry and Food Chemistry, Graz University of Technology, Graz, Austria

[5]Anton Paar GmbH, Graz, Austria

[6]Patheon Austria GmbH & Co KG, part of Thermo Fisher Scientific, Linz, Austria

Contents

2.1 Abstract

Additive manufacturing has gained a lot of interest in recent years to create customized reactors and equipment for milli- and micro flow applications. This work presents the development of *3D* printed stain- less steel reactors for the oxidation of Grignard reagents in flow. In our first approach a *3D* printed micro *CSTR* cascade was designed as a tool to get more insight in the reaction kinetics. Novel optical sensors were integrated inline in the cascade to monitor the oxygen consumption in real time. Based on the obtained experimental data and *CFD* simulations, a customized *3D* printed Split-and-Recombine Reactor (*SaRR*) was designed especially for the needs of the reaction.

2.2 Introduction

Organic flow chemistry has developed an increasing interest in performing syntheses in milli- and microreactors. [16, 77, 78] These reactors offer the potential for intensified process conditions through high mass and heat transfer rates due to high surface-to-volume ratios. [20, 79] Milli- and microreactors enable novel reactions to be developed at conditions not easily realized in conventional batch processing. While there are straightforward and cheap ways to set up micro flow processes with standardised tubings as reactors, their mixing properties lack the possibility to be optimized to the predefined process conditions. This missing optimization of- ten results in low product yields with unwanted side product formation. [35, 80] Therefore, a trend has emerged to manufacture chip-like microreactors for these predefined mixing operations. These *2D* chip-like reactors are often made of glass or poly-dimethylsiloxane (*PDMS*), fabricated by etching and micromolding through expensive manual labour. Subsequent adaption or expansion of these reactors is difficult to achieve due to the lack of robust chip-to-chip interconnections. [75]

Rapid developments in the field of *3D* printing show a successful production of milli- and microreactors especially designed for the needs of the process. [36, 37, 81, 82, 83, 84, 85, 86, 87] The lack of robust interconnections can be eliminated through compact design of system parts and thus compacter production lines can be achieved. [7] However, most of these *3D* printed reactors are made of plastics which are unsuitable for most organic solvents. Another drawback of the frequently used polymers is the poor heat transfer characteristics, leading to the formation of possible hot spots during the reaction. Selective Laser Melting (*SLM*) of stainless steel is a suitable *3D* printing technique to

overcome these limitations. [73, 38, 88, 89, 90, 91, 92, 93] *SLM* printed micro reactors show high thermal conductivity, mechanical strength and thermal resistance over a broad range of temperatures. Stainless steel can be easily post processed after the printing in the mechanical workshop, enabling the connection to standard *HPLC* equipment.

This work reports the development of customized *SLM* printed stainless steel reactors for the continuous aerobic oxidation of Grignard reagents. To investigate the intrinsic reaction kinetics, the problem of the coupled mass transfer and proceeding reaction was eliminated by absorbing oxygen beforehand in the solvent. This absorption reduces the reaction to a one phase mixing dependant case. The reactor design for the resulting one phase system was guided by monitoring the oxygen consumption rate during oxidation of the Grignard reagent through implemented novel optical inline oxygen sensors. These sensors show high resistance against the used organic solvent, are able to measure high oxygen concentrations, and respond quickly to changes in the system, thus making them especially useful for fast reactions.

For the reactor design approach, a *3D* printed micro *CSTR* cascade (AP01) was designed as a tool to measure the reaction rate. With this cascade it was possible to estimate the dependency of the oxidation reaction on the degree of mixing by monitoring the oxygen consumption rate with the integrated novel oxygen sensors in the *CSTR* vessels. An estimation of the intrinsic reaction time scale was possible and was used in combination with computational simulations and preliminary knowledge in advanced manufacturing technologies to manufacture another *3D* printed reactor (AP02). This reactor is designed and adapted exactly to the requirements of the one phase Grignard reagent oxidation and utilizes novel *3D* printed three-dimensional structures.

2.2.1 Model reaction – aerobic oxidation of Grignard reagents

Aerobic oxidation of Grignard reagents to the corresponding phenols was selected as a model reaction for the evaluation of both, oxygen sensor performance and mixing efficiency of the *3D* printed reactors. This reaction was developed to provide an efficient green approach towards functionalized phenols using oxygen as an inexpensive and sustainable oxidant. [94] It serves as an alternative for conventional reactions, such as nucleophilic aromatic substitution, [95] oxidations using boronic acids, [96] or cost intensive, toxic, transition metal catalysis based hydroxylation. [97]

Due to the reactive nature of Grignard reagents, their direct oxidation by oxygen is highly demanding in terms of heat and mass transfer. Based on the proposed mechanism of this reaction (Fig. 2.1), fast and efficient mixing is crucial to prevent stoichiometric imbalances, which may cause the formation of side products. Such limitations can be overcome by performing the reaction in a continuous flow regime, as both control over temperature and mixing performance can be enhanced. [98] Furthermore, establishing a continuous flow process allows for an easier and safer execution of the reaction on larger scale, compared to conventional batch methods. [99, 100]

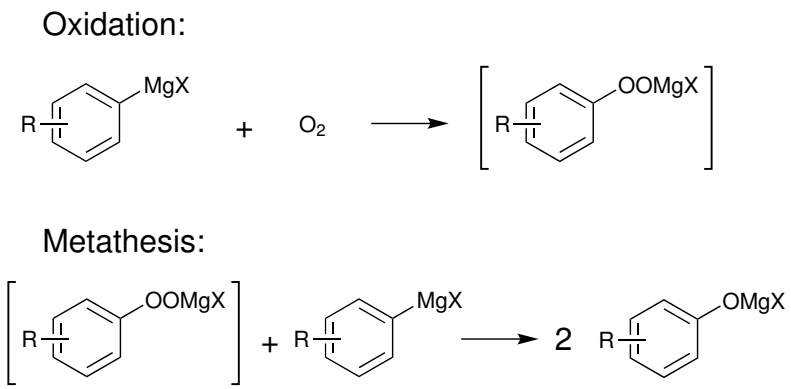

Figure 2.1: Proposed mechanism for the oxidation of Grignard reagents by oxygen via a peroxide intermediate. The initial step is expected to proceed via an electron transfer step between the Grignard reagent and oxygen. [101]

Therefore, this aerobic oxidation of Grignard reagents provides an interesting model reaction for further investigations towards reactor design from many points of view, especially considering its biphasic nature. Successful execution of this oxidation in a customised *3D* printed reactor requires broad chemical resistance, good thermal conductivity, concise mixing and optional implementation of suitable Process Analytical Technology (*PAT*).

Since oxygen is used as a reagent in stoichiometric amounts, accurate control over its dosing and effective concentration is highly desired for any kind of optimization or upscaling. Exact dosing of gases can be easily accomplished in a continuous flow setup using calibrated Mass Flow Controllers (*MFC*).

Inline measurement of the oxygen concentration by novel optical sensors within the flow reactor is a powerful tool to monitor the progress of reaction in real-time. In this work, the simultaneous use of multiple sensors at different stages of the reaction are used to provide further mechanistic insights.

2.3 Results and discussion

2.3.1 Reactor design

To operate a multiphase reactor at its optimum, it is important to characterize the rate limiting time scale. If the mass transfer time scale is significantly slower compared to the intrinsic reaction time scale, undesired by-product formation can occur. To investigate the intrinsic reaction time scale, the oxidation of the Grignard reagents is reduced to a homogeneous reaction system by absorbing oxygen in the solvent beforehand. This reduces the problem to a mixing rate limiting case of a homogeneous reaction system, which is well understood even for fast reactions. [102] In passive mixing elements the degree of mixing of homogeneous reaction systems are predefined by the structures themselves and the operation conditions, *i.e.* inlet flow rates. To investigate a desired reaction with defined

operation conditions, active mixing principles need to be applied. With active mixing, the degree of mixing can be controlled by parameters applied externally to the reactor. However, active mixing elements have the disadvantage that their correct operation has to be monitored. Once the desired process is known, it is economically advantageous to use static mixing elements designed for the prevailing conditions.

The designed micro *CSTR* cascade (Fig. 2.2) has all of the above needed features to characterize a homogeneous reaction. It consists of 10 vessels with an internal diameter of 3 mm, stirred by a magnetic stirring spheroid of 2.4 mm wide and 2.7 mm long, powered and controlled by the magnetic field of a laboratory magnetic stirrer. Each vessel can be configured for different purposes by installing standard *HPLC* fittings/plugs to open or block its upper part. The vessels are connected to each other through 800 μm channels attached tangentially to the spherical bottom part of the vessel. The ring shaped cascade is blocked at a marked position, indicating the in-/outlet of the vessels. With the stirrers inside and fittings connected, the total reactor volume is 275.6 μL. By installing the developed novel optical fibre sensors with standard *HPLC* fittings, the oxygen consumption during the reaction can be monitored in the vessels. The effect of stirring on the rate of oxygen consumption can be influenced through adjusting the stirrer speed. When an increasing *RPM* does not lead to an increasing reaction rate, the operation point for the intrinsic reaction rate can be found.

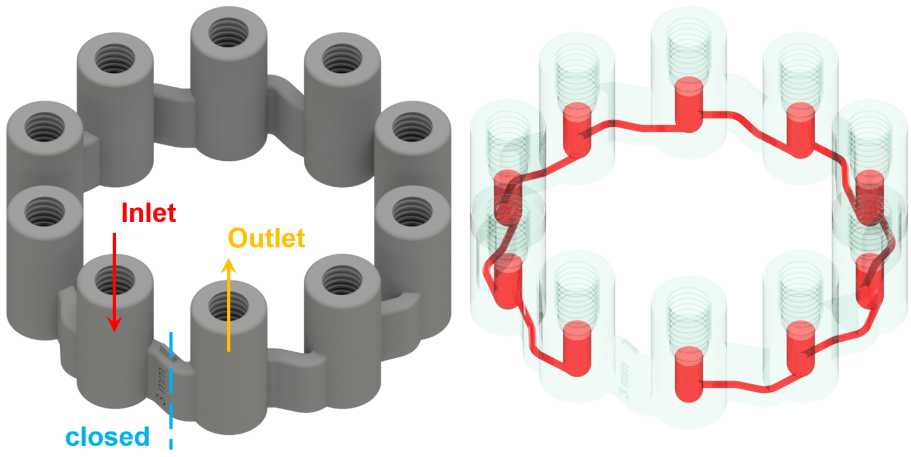

Figure 2.2: *CAD* drawing of the micro *CSTR* cascade (AP01). (Left) View from outside with indication of the blocked parts and resulting in-/outlet vessels. (Right) Exposed channels and vessels of the cascade.

For the homogeneous reaction case of the Grignard reagent oxidation, a customized reactor (AP02, Fig. 2.3) was designed based on the experimentally obtained data from the

CSTR cascade (AP01) and *CFD* simulations of an adapted split and recombine mixing structure (as shown below). The new reactor features fully scalable sections through a parameter depending *CAD* design, which enables numbering up approaches to reach higher throughputs. This scalability is possible since the basic setup of a flow reactor consists always of a precooling, mixing and reaction sections. The parameter dependency allows an arbitrarily scaling of each section by varying only three parameters while noticing the placing of each *CAD* drawing's origin at the point of mixing. This allows the fast interchange of section elements in the design phase of the reactor. The used parameters for the scaling of the sections are d, Le and n, the internal diameter, cubical element length scale and number of elements, respectively. This design allows to calculate the size of each reactor section by multiplying the element length with the number of elements. Through simple spreadsheet calculations it is possible to vary these parameters and directly update the design regarding the needs of the reaction. For the new Split-and-Recombine Reactor (*SaRR*), an internal diameter of 800 μm and an element length scale of 3.5 mm was chosen leading to a reactor volume of 0.565 ml for the mixing elements.

After the basic design of the reactor, the reaction channel was placed inside a cooling shell and openings were added at critical positions to ensure adequate cleaning of the delicate mixing structure. These openings were set to be easily accessible for welding from the outside of the cooling shell. For the layerwise printing, a support was needed to connect the reaction channel with its cooling shell. The support on the inside of the cooling shell was generated by Materialise's Magics software and adapted with a Boolean operation to fit the reaction channel. This operation subtracted the *CAD* drawing of the filled reaction channel body from the generated support, allowing to insert the hollow reaction channel into the final *CAD* file as the last step before printing.

2.3.2 Simulation

Computational Fluid Dynamics (*CFD*) simulation was used to evaluate the mixing geometry of the *SaRR*. The set of governing equations (*i.e.* Navier–Stokes equations) was solved using the Ansys-CFX software package. The geometry of the reactor has been discretized with a hexahedral cell dominated mesh (Fig. 2.4), which consisted of approx. 12 million cells and nodes.

The *CFD* simulation was performed at steady-state. Boundary conditions were set to match the anticipated experimental conditions (shown later). Thus, a flow rate of 1230 μL min^{-1} was chosen for inlet A and two different flowrates, 126 μL min^{-1} (case 1) and 84 μL min^{-1} (case 2), were chosen for inlet B (Fig. 2.5). For quick mixing, it is desirable to bring the flow tendency to a "helical" flow pattern. This pattern can be represented by the velocity helicity, a parameter indicating counter current helical flow behaviour in different sections of the reactor. [103] Helicity is a scalar quantity defined as an inner (dot) product of velocity and vorticity vectors. Fig. 2.5 shows the contour plots for the flow velocity helicity (bottom) at different cross-sections in the reactor. Two main counter current

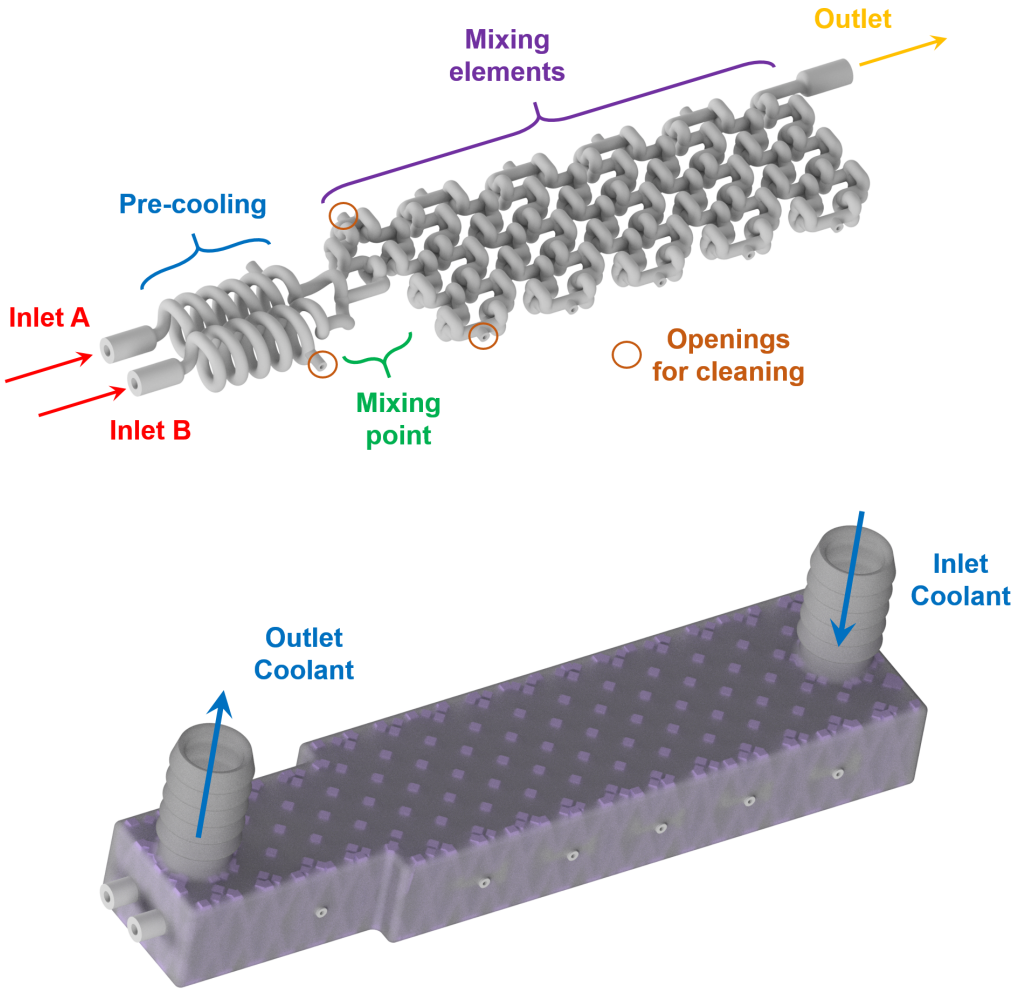

Figure 2.3: *CAD* drawings of the *SaRR* (AP02). (Top) Overview of the reactor sections. By repeating the structure elements, the reactor can be scaled arbitrarily. (Bottom) A *3D* printing support was generated through a Boolean operation to incorporate the reaction channel into the cooling shell.

helical flow patterns can be observed on each cut plane, which change the circumferential position along the reactor. This changing position causes good mixing perpendicular to the main stream direction along the reaction channel.

Another measure of mixing performance is the uniformity index. [104] It was calculated by applying a tracer at inlet A as a passive scalar through tracking the concentration at each cut plane along the reactor length. From the graph in Fig. 2.5 (top right) it can be seen that the tracer uniformity index across different cut planes is increased and reaches a maximum value in the middle of the cut plane section 3, indicating the tracer is fully

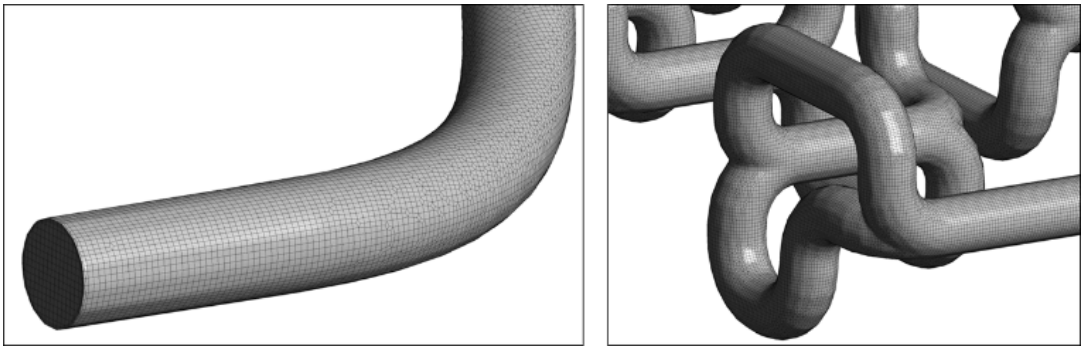

Figure 2.4: Details of numerical mesh at the beginning of the calculated domain of inlet A (left figure) and at the region of mixing elements (right figure).

premixed. With the tracer uniformity index, it was possible to conclude that there are no major differences between the two simulation cases. The obtained simulation results have shown that the designed mixer geometry will lead to very efficient mixing already at a very early stage in the mixing elements section.

2.3.3 3D printing

3D printing of the reactors was done by Selective Laser Melting (*SLM*) to manufacture the stainless steel reactors shown in Fig. 2.6 and 2.7. As presented in a previous work, [93] *SLM* printed reactors are well applicable for organic flow synthesis. Similar to other *3D* printing techniques, the *CAD* drawing needs to be sliced first to generate cross-sectional layers (Fig. S2.1), which were printed layer by layer through fusion of a metal powder bed. This sintering of the layers was done by an *SLM* system from EOS utilizing an ytterbium fibre laser with 400 Watt maximum power input, scanning through a 316 L stainless steel powder bed with a d_{50} of 35.9 μm. For the selected layer height of 40 μm, the laser melted the current layer and the prevailing one to generate well-bonded, gas-tight, high density builds.

After the printing process, the building platform was disassembled from the printer and the unused metal powder was collected for re-use. Inner parts of the prints were freed from the powder with compressed air, ultrasound treatment and dried again with compressed air. Afterwards, stress relief annealing of the printed parts was carried out in a vacuum oven. Next, the reactors were cut from the building platform by means of a band saw, and their surface was refined by sandblasting. Cleaning openings were closed by laser welding and the connection to standard equipment was enabled with 1/16″ stainless steel capillaries welded to the in- and outlets. Finally, the prints were blasted with micro glass beads, and once again, brought into the ultrasonic bath followed by drying with compressed air. Due to the design of the *CSTR* cascade, welding to close the cleaning ports was not necessary, however, the 10–32 UNF printed threads were refined with a thread cutter.

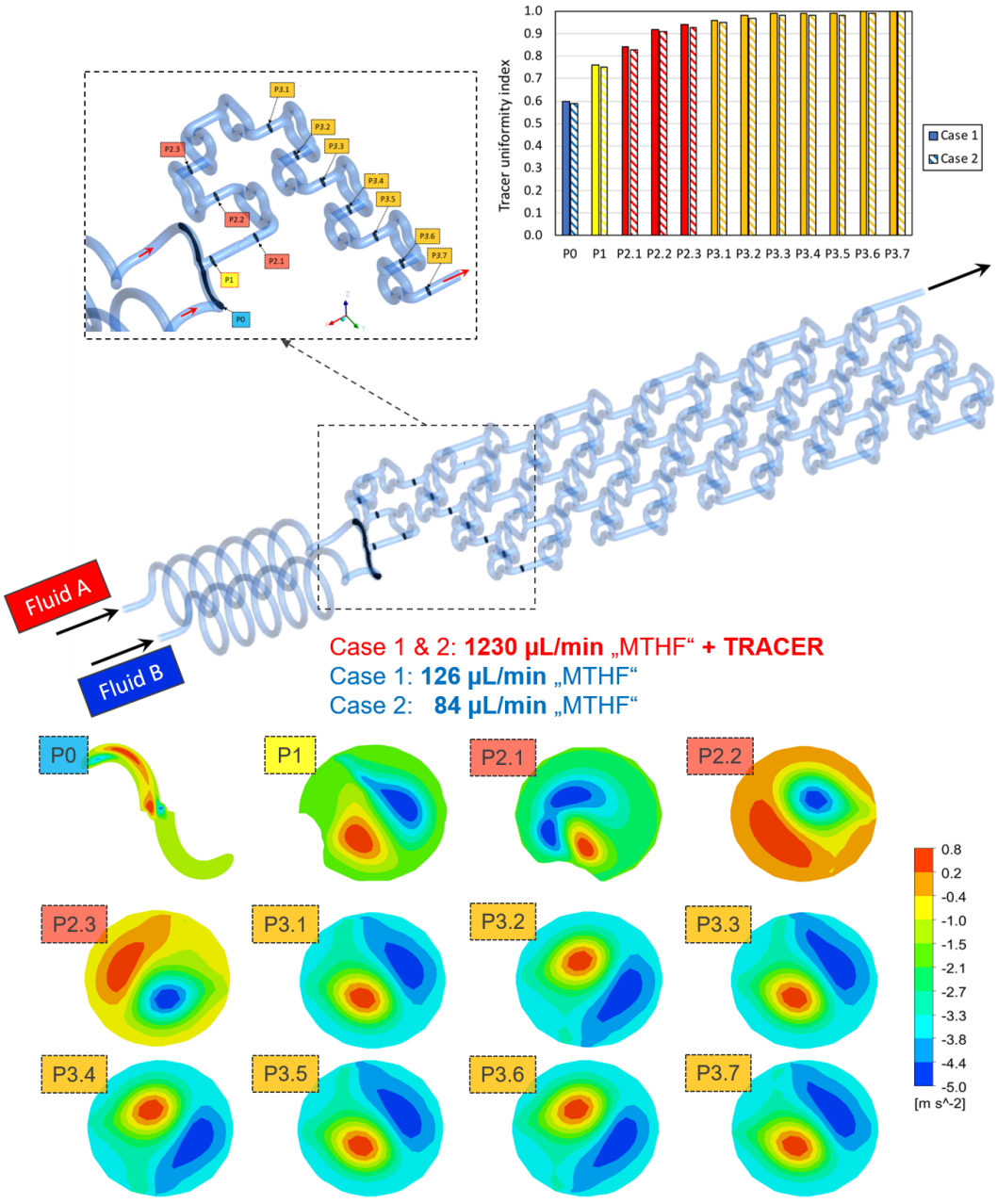

Figure 2.5: Tracer uniformity index for two different cases of mass flow rates with inlet A used as tracer (top). Velocity helicity contour plots on different cut planes along the AP02 reactor geometry (bottom).

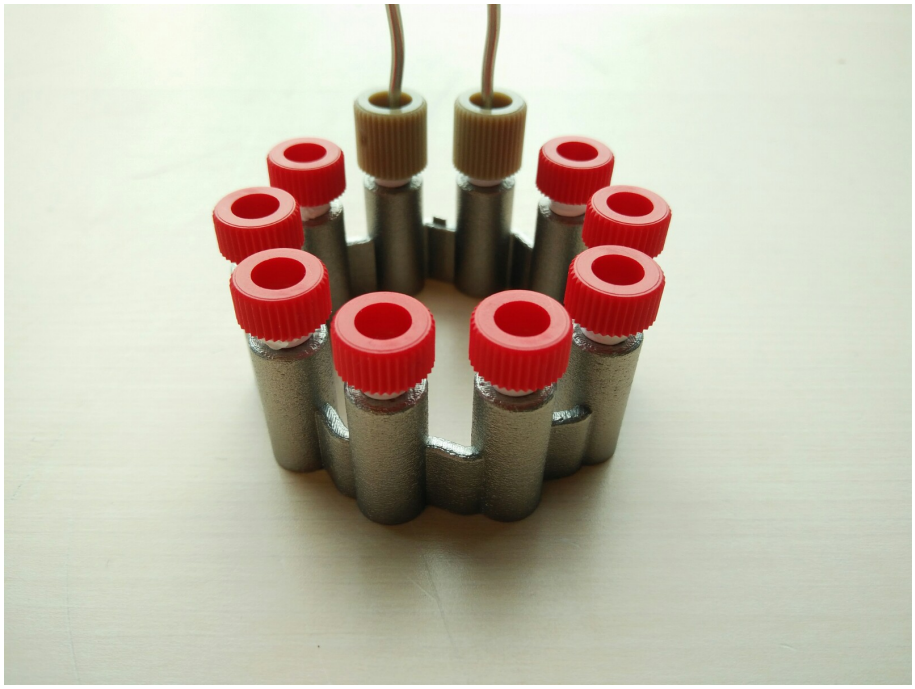

Figure 2.6: *3D* printed *CSTR* cascade (AP01) closed with standard *HPLC* fittings. The *3D* printed 10–32 UNF thread had to be refined after the printing.

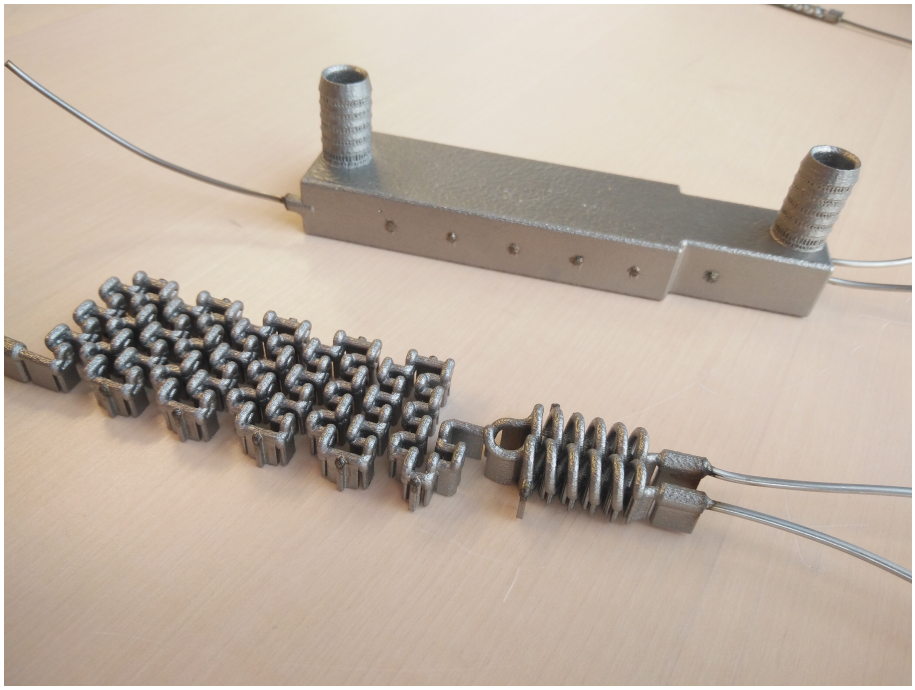

Figure 2.7: *3D* printed *SaRR* (AP02) for the oxidation of Grignard reagents with and without cooling shell. After post processing, 1/16″ capillaries were welded to the in- and outlets for connection with standard *HPLC* equipment.

2.3.4 Characterization of the 3D printed reactors

Due to the low Reynolds number in milli- and microreactors, laminar flow is predominant. As a result, mixing in these reactors must rely solely on diffusive mixing between the fluid elements, leading to long channels to achieve sufficient mixing. [105] However, enhanced laminar mixing can be achieved through chaotic flows. [106] This means large intermaterial contact areas are generated by stretching and folding of the fluid elements. The generation of chaotic flows in microreactors can be achieved through two mixing principles: passive and active. [107] Passive mixing elements are an integral part of the fluid channel and are incorporated during the fabrication. Their efficiency depends on the prevailing process conditions. By applying active mixing elements, the degree of mixing can be controlled by user demands, however, the proper working of the mixing element needs to be monitored.

In this work, the degree of mixing was characterized experimentally by monitoring the product distribution of the diazo coupling between 1-naphthol and diazotized sulphanilic acid, [108] a system of competitive and consecutive reactions (Fig. S2.2). Two isomeric monoazo dyes are formed via primary coupling – o-R and p-R. In a secondary coupling, both monoazo dyes react again with diazotized sulphanilic acid to form the bisazo dye (S). Because primary coupling is much faster compared to the secondary coupling, the yield of bisazo product S (eqn 2.1) is related to the mixing performance, *i.e.* the less product S is formed, the better the mixing. An initial solution of diazonium salt was prepared by diazotization of 10 mmol L^{-1} sulphanilic acid with sodium nitrite and hydrochloric acid. This solution was diluted to 1 mmol L^{-1} for the experiments. The second solution contained 1.2 mmol L^{-1} 1-naphthol dissolved in a buffer solution with 222.2 mmol L^{-1} of sodium carbonate and sodium bicarbonate, respectively. Both solutions combined lead to a pH of 9.9 and ionic strength of 444.4 mmol L^{-1} for the coupling reaction. The experiments were carried out at 25 °C and equal volumetric flow rates. Samples were collected after flushing the reactor for three residence times to reach steady state. Concentration of each component was determined by light absorption measurement for several wavelengths and multiparameter-linear-regression of the absorption spectra. This regression used molar extinction coefficients for each substance based on literature [1] (Tab. S2.1). Due to the overlapping spectra of the monoazo dyes only their sum can be determined correctly. To check for experimental errors, the mass balance of each sample was calculated based on reagent B, which was in depletion. Using this procedure, the experimental error was found to be higher at lower flow rates.

$$Y_S = \frac{2c_S}{c_{p-R} + c_{o-R} + 2c_S} \tag{2.1}$$

The obtained mixing behaviour of the printed reactors in Fig. 2.8 indicates far better performance of both reactors compared to a simple T-mixer. The especially high mixing rates achieved at low flow rates with stirring in the *CSTR* cascade indicate its applicability for measurements of relatively fast reactions. At high flow rates, a changing *RPM* has

shown no effect on the mixing performance of the reactor (Fig. S2.3 and S2.3). The set *RPMs* are not controlled within the cascade and only refer to set values of the laboratory magnetic stirrer. Inertial forces at higher flow rate might influence the small stirring spheroids *RPM* until their rotation is only induced by the flowing fluid.

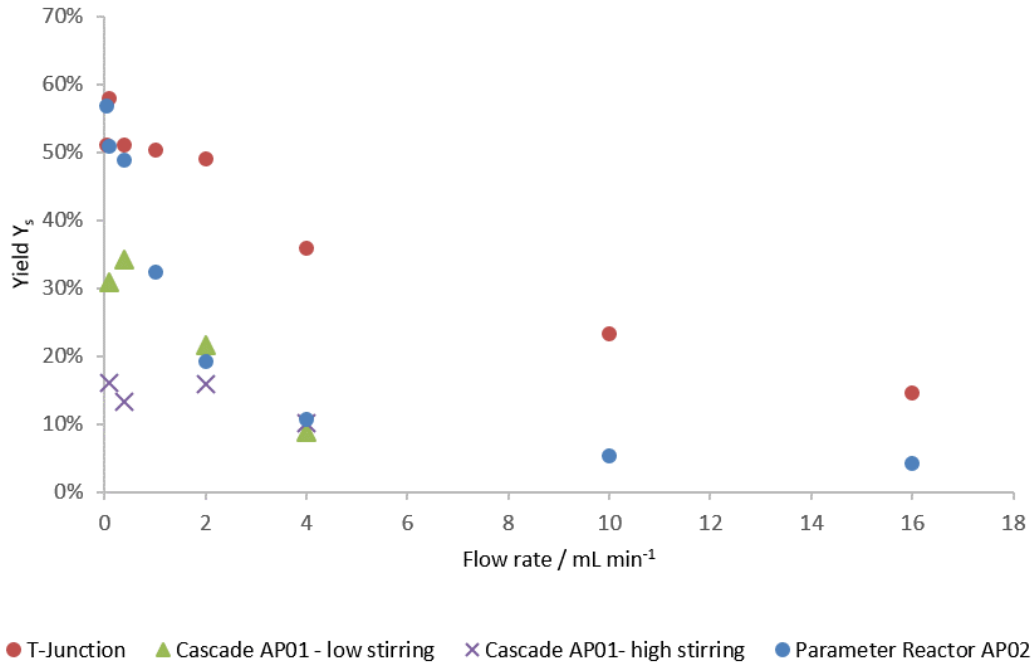

Figure 2.8: Mixing performance evaluated at process conditions in the *3D* printed reactors (AP02 = *SaRR*, AP01 = cascade) and compared to a standard *HPLC* T-junction.

In addition to the mixing evaluation, the Residence Time Distribution (*RTD*) of both printed reactors was investigated. *RTD* experiments were performed with fibre optic probes for the detection of a tracer solution within an inline *UV*/*VIS* flow cell. An instantaneous step change from solvent (12 w% ethanol in water) to tracer solution (0.006 v% anisole in previously mentioned solvent mixture) was possible by using a manual 6-way valve. The *RTD* was evaluated for equal Reynolds numbers as at process conditions for both printed reactors (Fig. S2.5 and S2.6). The *SaRR* AP02 showed plug flow like behaviour at approximately 1.8 ml min^{-1} indicated by a calculated Bodenstein number close to 100. For the cascade AP01, a Bodenstein number close to 20 was obtained at process conditions, indicating a *CSTR* like behaviour. Large deviations from plug flow can be assumed at Bodenstein numbers below 100 leading to higher axial dispersion. [33]

2.3.5 Implementation of novel optical oxygen sensors in the set-up

To follow the chemical transformation, inline oxygen monitoring was implemented into the reactors. The novel oxygen sensors are based on a phase fluorimetry readout sys-

tem. [109] They are applicable for pressurized systems in the presence of organic solvents and high oxygen concentrations by utilizing tailored fibre based optical sensors. Compared to commonly employed sensor materials like sol–gels and polymerswith high oxygen diffusivity, [109] the developed sensors use more robust materials. A *NIR*-emitting Pt-tetraIJ4-fluorophenyl)tetrabenzoporphyrin (PtTPTBPF) [110] dye was immobilized in polyphenylenesulfide (*PPS*) and coated with a CYTOP® protection coating. By affixing the sensor fibre into a standard *HPLC* fitting, it was ready to be implemented into the reactors (Fig. S2.7 and S2.8).

The sensor data is read out with a commercial miniaturized USB phase fluorimeter (FireStingO2) using a custom made Python based evaluation software. The calibration of the sensor can be performed within the reaction environment by controlling the oxygen concentration *via* syringe pumps and mass flow controller. Thorough investigations revealed that the sensor operates according to a linear Stern–Volmer equation, [111] which allows a two-point calibration of oxygen concentration (Fig. 2.9). This two-point calibration allows fast initializing of the sensors at process conditions within the reactor itself.

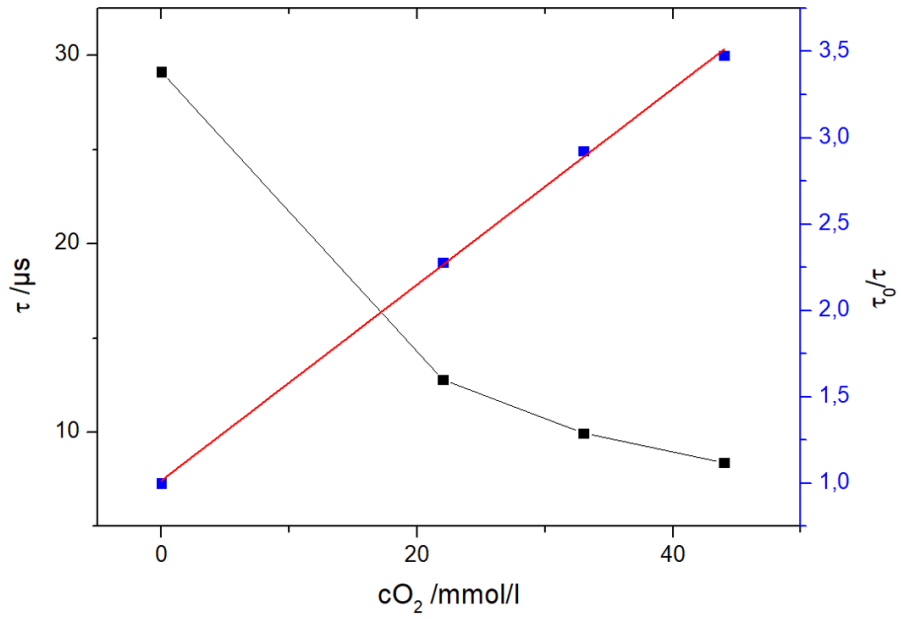

Figure 2.9: Evaluation of the oxygen calibration with the fibre sensor in *THF* at 0 °C and oxygen concentrations up to 42 mmol L^{-1}.

Fig. 2.10 (top) shows positions of the sensors in the reactor setup. Two sensors were introduced before and after the reactor for reference measurements, whereas two sensors were directly implemented into the *CSTR* cascade (first and last chamber). Sensor 1 is used as a reference for determination of the actual oxygen concentration that is inserted before addition of the reagent. The reference is also used to correct the data of pump related fluctuations (Fig. S2.9).

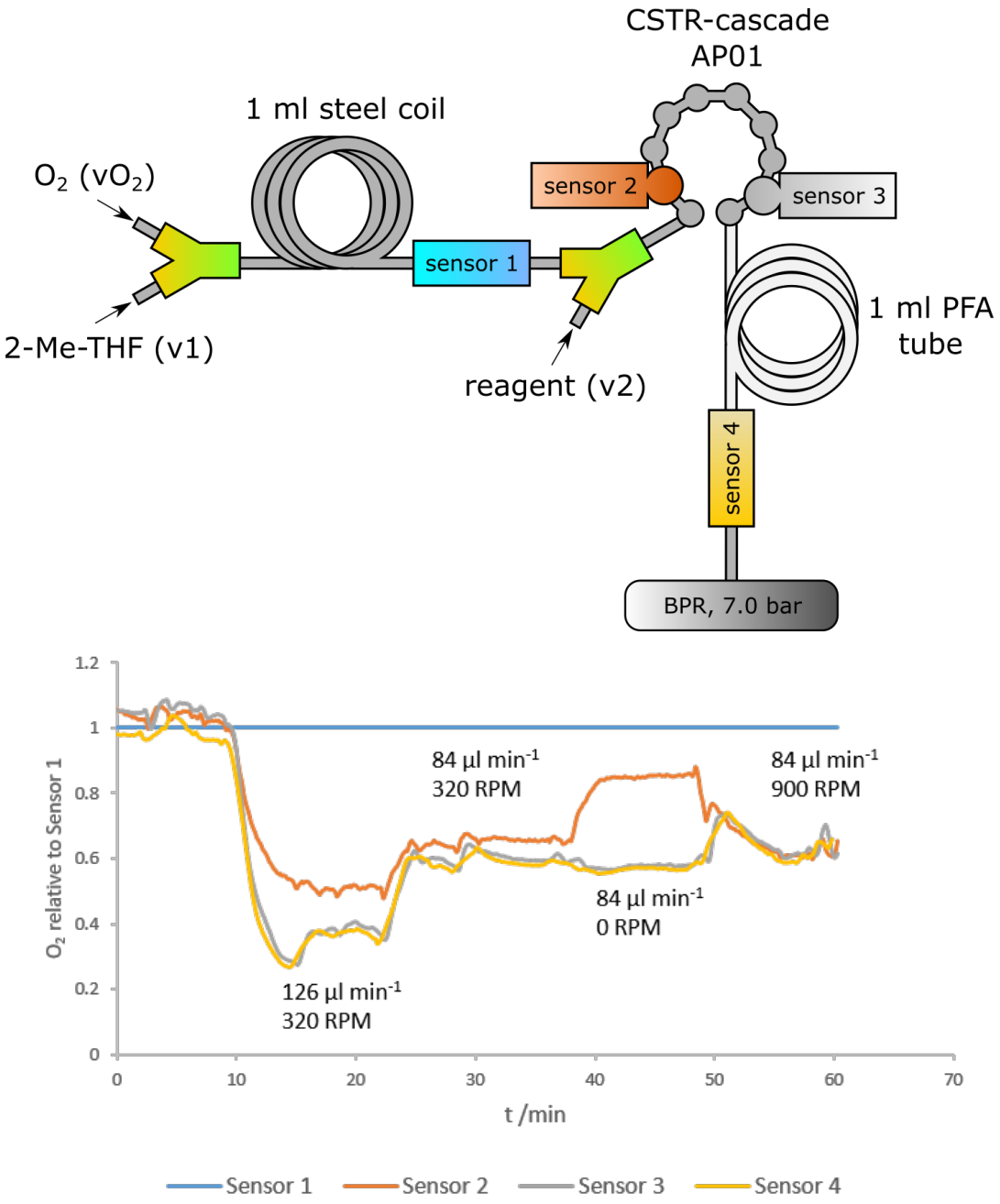

Figure 2.10: Flow setup with sensor arrangement in the reactor (top); relative oxygen content in the reactor at varying reagent flow rate v2 (1 M 4-methoxyphenylmagnesium bromide). vO2: 1500 μl min^{-1} , v1: 1000 μl min^{-1} (bottom).

The data show clearly: the concentration of starting material (4-methoxyphenylmagnesium bromide) correlates with oxygen consumption and the reaction rate depends on stirrer speed (Fig. 2.10, bottom). Whereas 0 *RPM* leads to a significantly decreased conversion in compartment 1 of the cascade, the last section of the measurement (minute 50–60) shows that at 900 *RPM* the reaction is already completely finished at sensor 2 (no further oxygen decrease between sensor 2 and 3). Additionally, the data obtained from the inline measurements with the oxygen sensors indicated a rapid intrinsic chemical reaction, as no further oxygen consumption was observed after an additional residence time coil.

2.3.6 Oxidation of Grignard reagents in the novel reactors

The aerobic oxidation of Grignard reagents was chosen as a model reaction to evaluate the *3D* printed reactors. This evaluation was supported by inline measurements of oxygen concentrations with the novel optical sensors. The reaction outcome was compared for the aerobic oxidation of 4-chlorophenylmagnesium bromide 1 (Fig. 2.11) utilizing the two *3D* printed reactors (AP01 and AP02) and a standard flow reactor made of *PFA* tubing (0.8 mm *ID*).

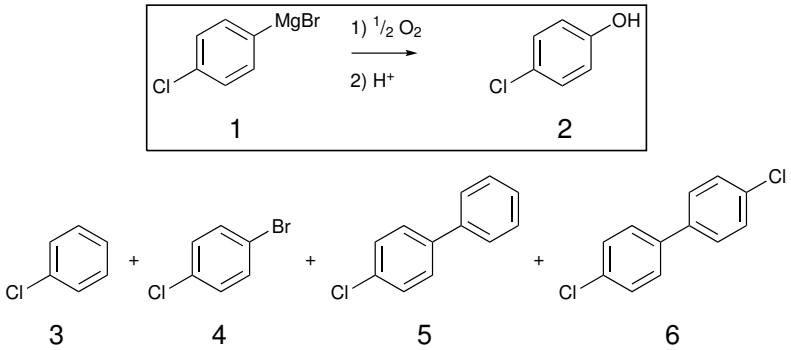

Figure 2.11: Aerobic oxidation of 4-chlorophenylmagnesium bromide **1** including the desired product **2**, quenched starting material **3** and the side products **4**, **5** and **6**.

Fig. 2.12 shows a flow chart for the reaction with the first feed to the reactor containing 1 equiv. of oxygen predissolved in 2-methyltetrahydrofuran (*2-Me-THF*) and the second feed consisting of a 1 M solution of substrate 1 in *2-Me-THF*. For the reactions using *PFA* coil and *CSTR* cascade, those two feeds were combined by a Y-mixer (Fig. S2.8). To ensure the inline measurement of a stable oxygen concentration by the optical sensors, absorption of oxygen (added by a mass-flow controller) in *2-Me-THF* (degassed by purging it with argon prior to the reaction) was done using a stainless steel coil. Before mixing the oxygen solution with the precooled reagent, a reference oxygen sensor was added to all three setups (Sa in Fig. 2.12). All sensors were calibrated prior to the experiments, and are capable of measuring actual oxygen concentrations within the organic solvent. Oxygen

concentration for reactions conducted in the *SaRR* AP02 could only be measured at its outlet, whereby the *CSTR* cascade AP01 allowed for direct implementation of sensors at different intermediate positions. A final oxygen sensor (Sb in Fig. 2.12) was included as a second reference directly before the Back Pressure Regulator (*BPR*) in all setups. A *BPR* was used to ensure a constant pressure of 7 bar in the system.

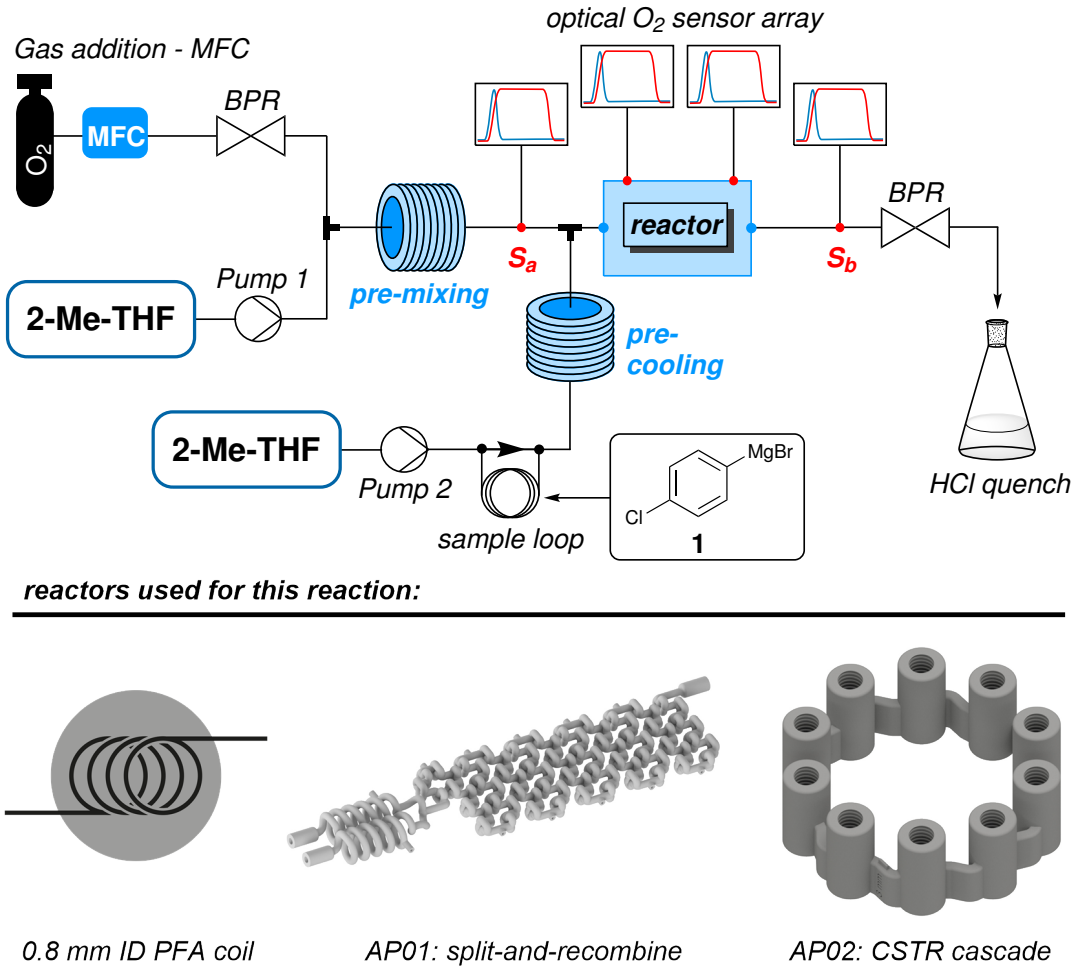

Figure 2.12: General scheme of the reaction set-up to carry out the aerobic oxidation of 1 in three different reactors including the positioning of the optical oxygen sensors.

The reactions were carried out at 0 °C with flow rates of 1000 μl min^{-1} *2-Me-THF*, 1500 μl min^{-1} oxygen (at norm conditions) and 126 μl min^{-1} of the Grignard reagent 1 using a stoichiometric ratio of 1:1 between oxygen and reagent. Complete absorption of oxygen in the solvent at 7 bar was checked prior to mixing with the reagent with transparent tubes. The exiting stream was immediately quenched at the reactor outlet by 0.5 M aqueous *HCl*. Notably, small gas segments were observed at the outlet after the *BPR*, pointing to the presence of unconsumed O_2 in the resulting solution. Crude reaction mixtures were

then analysed by *GC-MS* and *GC-FID* chromatography. The samples were prepared by extraction of the quenched reaction mixture with CH_2Cl_2.

Along with the desired product, 4-chlorophenol **2**, four different species could be identified by *GC-MS* analysis (Fig. 2.11): chlorobenzene **3**, which resulted from the reaction quench and three side products **4**, **5**, and **6** which were presumably formed from radical intermediates. Especially the dichloro-biphenyl product **6** implies the recombination of two chlorophenyl radicals, which might have resulted from stoichiometric imbalances (high local concentrations) due to lower mixing performance. The identities of the two major products **2** and **3** were additionally confirmed by reference substances using *GC-FID*.

As illustrated by the product distribution in Fig. 2.13, considerable reduction of the major side-product **6** could be observed in the printed reactors. This side-product content started at 11.5% in the *PFA* coil experiment and was reduced to 5.5% in the *CSTR* cascade AP01, and to 2.5% in the *SaRR* AP02. Increased selectivity can be ascribed mainly to a better mixing efficiency which limits the rapid chemical transformation as shown in the *CSTR* experiment (Fig. 2.10, bottom). The higher selectivity in reactor AP02 can be explained by a more efficient design of the mixing point in contrast to the used Y-junction as first contact point in the other set ups. Therefore, the cascade AP01 performed worse as might be predicted by the mixing sensitive experiments in Fig. 2.8, where the reaction was started directly in the cascade's second vessel. Additionally, selectivity might also be influenced by the employed reactor material as a better heat management in the reactors was possible through higher thermal conductivity of stainless steel compared to regular *PFA*.

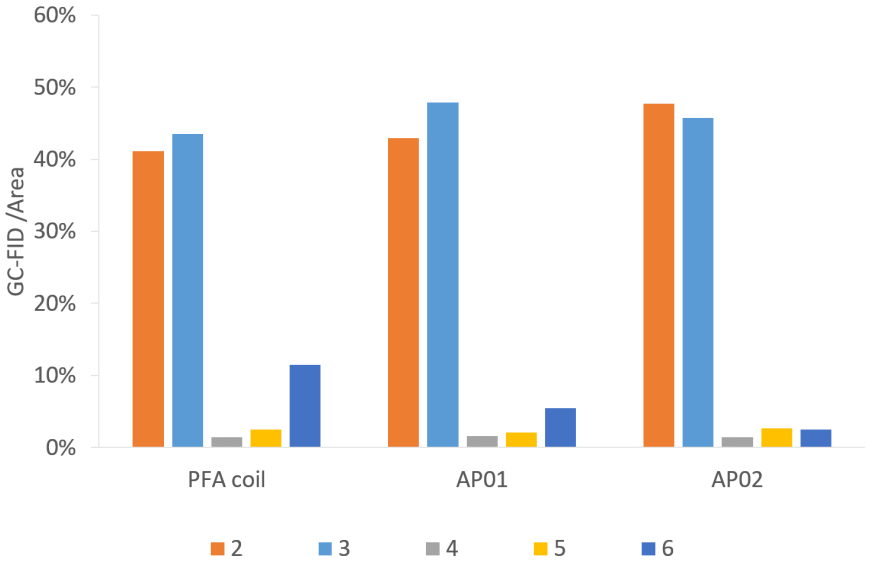

Figure 2.13: Distribution between the desired product **2**, quenched starting material **3** and the side products **4**, **5** and **6** according to *GC-FID* obtained from reactions at 0 °C in three different reactors (AP01 = cascade, AP02 = *SaRR*).

2.4 Conclusions

In this work, a combination of *SLM* *3D* printing of stainless steel and the implementation of novel oxygen sensors for the inline measurement was shown to be a promising combination for investigating the oxidation of Grignard reagents in flow. *3D* printing is a favourable tool for the creation of adaptable reactors and implementation of sensors. With the parameter dependency, the *CAD* files used for the printing can be quickly adapted to the desired process conditions and directly used for *CFD* simulations to predict the flow behaviour and mixing quality. This developed reactor design concept can be used later on for up-scaling approaches to reach higher throughputs. To monitor the processes inside the reactor, sensor ports can be easily implemented into the *3D* designs utilizing standard *HPLC* equipment for the connection. The sensors developed within this work are applicable for high oxygen concentration measurements in pressurised flow systems in the presence of organic solvents. They can be initialized by two-point calibration within the reactor in a short amount of time. By combining the possibilities of *3D* printing with the novel sensors, it was possible to *3D* print a micro *CSTR* cascade as a tool for the reaction investigation incorporating these novel sensors. A fast progress of the reaction was confirmed in the cascade by varying the degree of mixing while monitoring the oxygen consumption with the novel sensors. The obtained insights on the reaction time scale served as basis for the design of a static mixing *SaRR*, which was adapted to the predefined operation conditions. The experimental characterization of both *3D* printed reactors was done by mixing dependant reactions, *RTD* analysis and the aerobic oxidation of 4-chlorophenylmagnesium bromide. Both printed reactors showed high mixing rates and increased selectivity compared to the reaction in a conventional reaction setup consisting of a *PFA* coil and a Y-junction as mixer.

Future work will focus on the influence of surface roughness on the mixing efficiency as well as on a more detailed investigation of the influence of reactor geometry on the reaction outcome.

2.5 Conflicts of interest

There are no conflicts to declare.

2.6 Acknowledgements

The CCFLOW project (Austrian Research Promotion Agency FFG No. 862766) is funded through the Austrian COMET Program by the Austrian Federal Ministry of Transport, Innovation and Technology (BMVIT), the Austrian Federal Ministry of Science, Research and Economy (BMWFW) and by the State of Styria (Styrian Funding Agency SFG).

Appendices

2.A 3D Printing

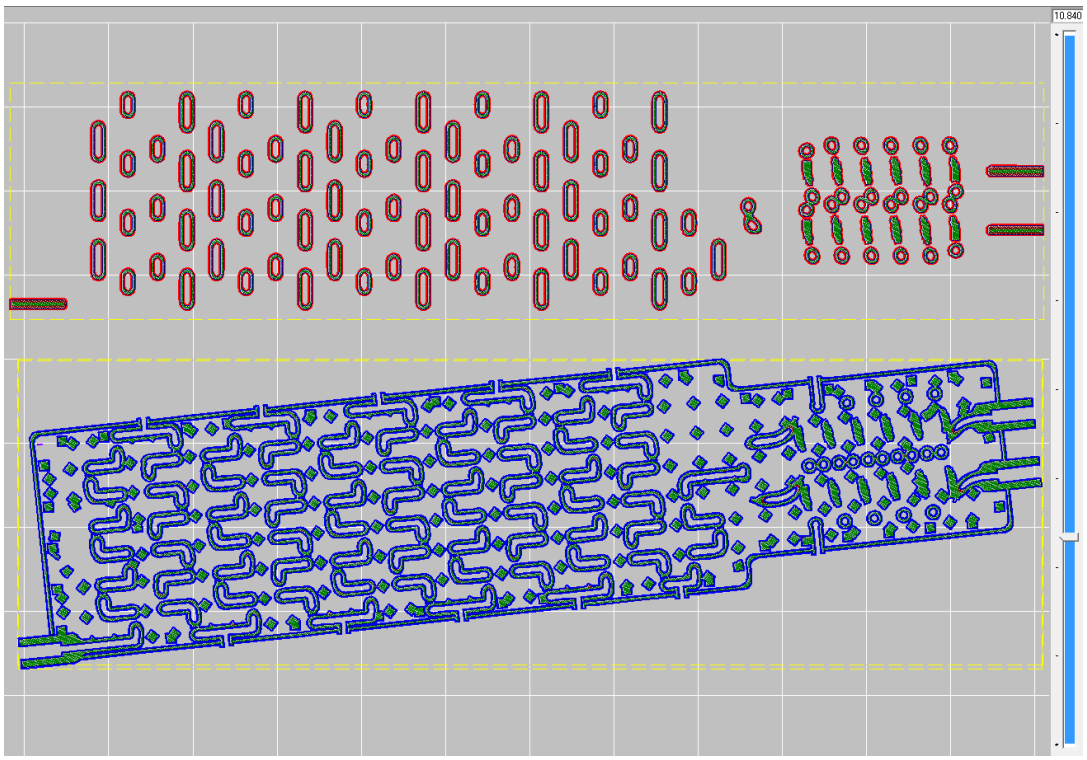

Supporting Information Figure S2.1: Example of a sliced layer of the *SaRR*. For the *3D* printing of the reactors, a building layer thickness of 40 μm was chosen and resulted in a total number of 1050 layers. The printing job was done by an *SLM* system from EOS utilizing an Ytterbium fibre laser with 400 Watt maximum power input. This laser spot scanned through a 316L stainless steel powder bed with a d 50 of 35.9 μm according to the coloured sliced cross-section areas.

2.B Characterization of the 3D printed reactors

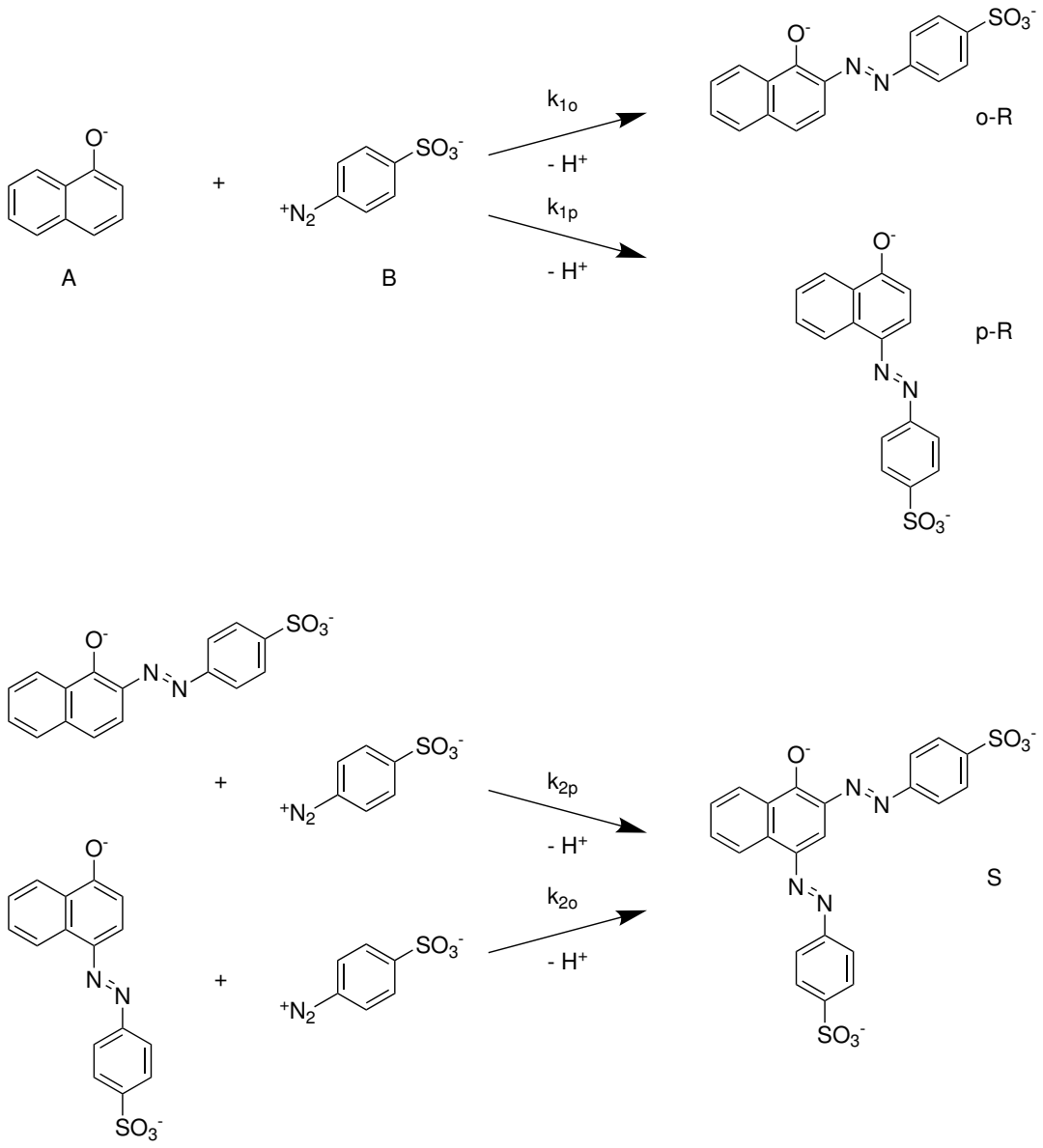

Supporting Information Figure S2.2: Reaction scheme [1] - diazo coupling of 1-naphthol A and diazotized sulphanilic acid B. The ortho monoazo dye o-R and para monoazo dye p-R can further react to the bisazo dye S. Influence on the degree of mixing can be seen by the product distribution of this reaction.

Supporting Information Table S2.1: Molar extinction coefficients of the three dyes published by Bourne *et al.* [1] at the standard conditions T=25 °C, pH 9.9 and I=444.4 mmol L^{-1}. These values were used in the multi-parameter-linear-regression to obtain concentrations of the dyes. Determining separately the concentration of the monoazo dyes was not possible due to overlapping spectra.

Wavelength [nm]	Extinction coefficient [m^2 mol^{-1}]		
	p-R	o-R	S
390	277.6	400.6	465.7
400	411.2	395.5	761.3
410	588.7	463.6	972.2
420	794.2	576.6	1246.9
430	1009.6	722.5	1544.1
440	1227.8	901.8	1830.4
450	1456.9	1110.6	2074.9
460	1717.1	1345.8	2245.5
470	2025.7	1611.5	2318.7
480	2382.1	1892.3	2311.7
490	2728.4	2140.4	2246.2
500	3009.6	2317.9	2157.5
510	3158.5	2381.6	2116.9
520	3140.3	2308	2175
530	2959.1	2108.3	2311.4
540	2618.4	1809.4	2467.4
550	2133.5	1431.3	2590.4
560	1583.6	1018.4	2647.4
570	1057.6	638.6	2618.8
580	609.6	343.8	2486.1
590	302.7	166.1	2259.7
600	130.2	74.8	1964.2
610	54.1	35.3	1618.4
620	23.2	15.7	1265.7
630	11.6	8.7	936.1
640	7.9	6.6	652.1
650	4.7	4.2	428.7
660	4.4	4.2	271.9
670	4.1	4.4	161.2
680	2.5	2.7	89.1
690	2.2	2.8	48.9
700	1.6	2.1	28.3

Mixing performance of the *CSTR* cascade with clockwise and counter clockwise stirrer rotation will be shown in the following. The influence of stirrer *RPM* and channel flow rate can be seen by the product distribution of the diazo coupling between 1-naphthol and diazotized sulphanilic acid. The reaction was started in the cascade's second vessel. Lower yield of product S indicates better mixing. The used stirrer Reynolds numbers Re(stirrer) is calculated with a stirrer diameter of 2.4 mm and the set *RPM* values of the laboratory magnetic stirrer. Channel Reynolds number Re(channel) is based on the channel diameter of 0.8 mm between the vessels. Experimental errors were checked by calculating a mass

balance based on reagent B, which was in depletion. A higher yield of product S led in general to higher experimental errors, whereby a maximum experimental error of 15.5% was found at the lowest flow rate. The mean experimental error of all experiments was close to 4%.

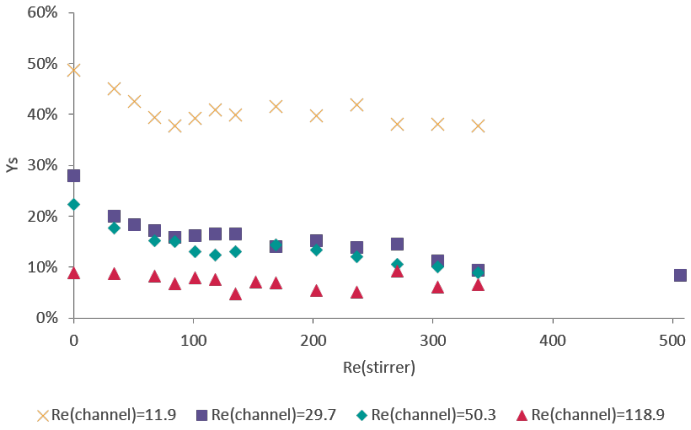

Supporting Information Figure S2.3: Clockwise stirrer rotation led to a local minimum in the S product yield, indicating a local mixing maximum. This maximum vanishes at higher flow rates. A general trend at higher *RPM* leading to better mixing can be observed. The influence of *RPM* on the mixing performance is reduced at higher flow rates.

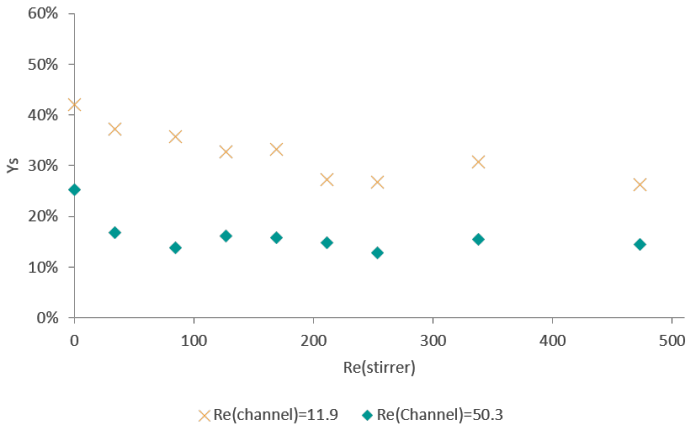

Supporting Information Figure S2.4: In the counter clockwise operation the local minimum is not present. The general performance of the counter clockwise operation is slightly worse compared to the clockwise operation. Again, the influence of *RPM* on the mixing performance is reduced at higher flow rates.

Experiments to determine residence time distributions were carried out by an instantaneous step change from solvent (12 w% ethanol in water) to tracer solution (0.006 v% anisole in previously mentioned solvent mixture) while detecting the response of the reactors by an *UV*/*VIS* flow cell (10 mm optical path length).

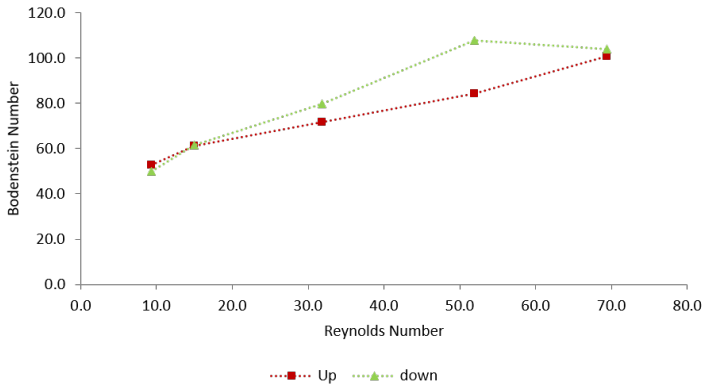

Supporting Information Figure S2.5: Bodenstein Number for different flow rates in the *SaRR* AP02. The steps were performed through one of the reactor feeds while the other one was blocked. A step up means the instantaneous change from solvent to tracer solution and step down the change from tracer solution to solvent. The Reynolds number was calculated with a channel diameter of 0.8 mm and prevailing flow conditions

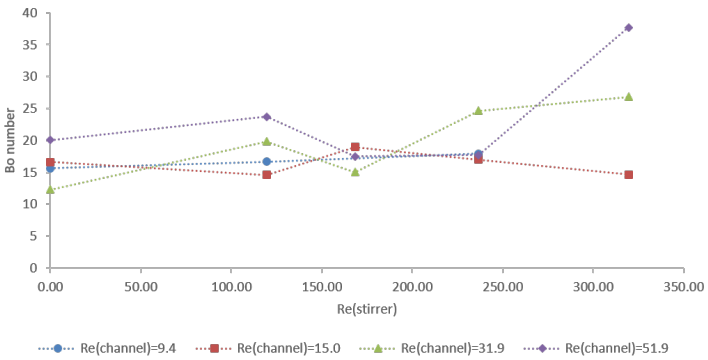

Supporting Information Figure S2.6: Bodenstein Number for different flow and stirring ratesin the *CSTR* cascade AP01. This experimental data was obtained for steps up experiment from solvent to tracer solution fed to the first vessel. The Reynolds numbers were calculated with a channel diameter of 0.8 mm for Re(channel), the set *RPM* value of the magnetic stirrer with a stirrer diameter of 2.4 mm Re(stirrer) and prevailing flow conditions.

2.C Implementation of novel optical oxygen sensors in the set-up

Supporting Information Figure S2.7: Assembled sensors ready to be implemented into the reactors. A two component epoxy resin was used to attach glass fibres in 1/16″ stainless steel tubes which were further glued into *HPLC* fittings. The sensors were ready to use within the reactor after application of indicator and protection coating.

Supporting Information Figure S2.8: Oxygen sensors integrated in the *CSTR* cascade AP01. The sensors were carefully screwed into the reactor compartments to prevent breaking of the glass fibre and then connected to the phase fluorimeter readout system. *PTFE* tape was used to aid proper sealing of the fittings within the pressurized system.

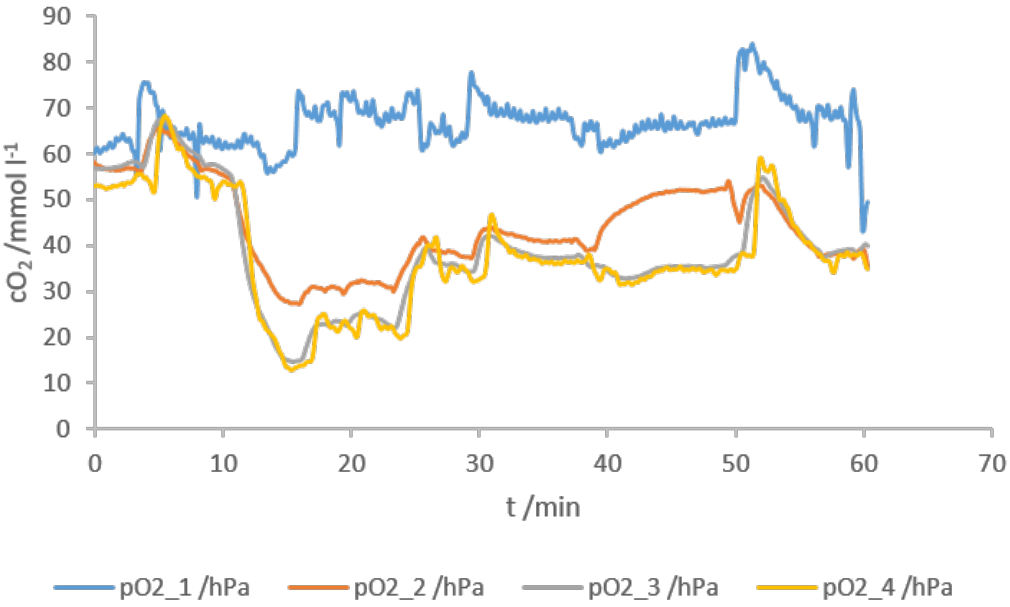

Supporting Information Figure S2.9: Raw data measured by the oxygen sensors 1 to 4 in the *CSTR* cascade. This data was collected every six seconds and flattened by calculating the mean value of the last 20 samples. A time correction was done to account for time delays due to different residence times between the sensors. After this correction, it was possible to calculate a relative oxygen concentration as shown in the bottom of Fig. 2.10.

2.D Oxidation of Grignard reagents in the novel reactors

Solvents and chemicals were obtained from commercial suppliers and were used without any further purification nless otherwise noted. *GC-FID* analysis was performed on a ThermoFisher Focus *GC* with a flame ionization detector, using a TR-5MS column (30 m × 0.25 mm *ID* × 0.25 μm) and helium as carrier gas (1 mL min^{-1} constant flow). The injector temperature was set to 280 °C. After 1 min at 50 °C, the temperature was increased by 25 °C min^{-1} to 300 °C and kept constant at 300 °C for 4 min. The detector gases for flame ionization were hydrogen and synthetic air (5.0 quality). *GC-MS* spectra were recorded using a ThermoFisher Focus *GC* coupled with a DSQ II (EI, 70 eV). A TR-5MS column (30 m × 0.25 mm × 0.25 μm) was used, with helium as carrier gas (1 mL min^{-1} constant flow). The injector temperature was set to 280 °C. After 1 min at 50 °C, the temperature was increased by 25 °C min^{-1} to 300 °C and kept at 300 °C for 3 min.

Bibliography

[1] John R. Bourne, Oemer M. Kut, Joachim Lenzner, and Horst Maire. "Kinetics of the diazo coupling between 1-naphthol and diazotized sulfanilic acid". In: *Industrial & Engineering Chemistry Research* 29.9 (Sept. 1990), pp. 1761–1765. ISSN: 0888-5885. DOI: 10.1021/ie00105a004. URL: http://pubs.acs.org/doi/abs/10.1021/ie00105a004%20https://pubs.acs.org/doi/abs/10.1021/ie00105a004.

[7] Philip J. Kitson, Guillaume Marie, Jean-Patrick Francoia, Sergey S. Zalesskiy, Ralph C. Sigerson, Jennifer S. Mathieson, and Leroy Cronin. "Digitization of multistep organic synthesis in reactionware for on-demand pharmaceuticals". In: *Science* 359.6373 (Jan. 2018), pp. 314–319. ISSN: 0036-8075. DOI: 10.1126/science.aao3466. URL: http://www.sciencemag.org/lookup/doi/10.1126/science.aao3466%20http://www.ncbi.nlm.nih.gov/pubmed/29348235%20https://www.sciencemag.org/lookup/doi/10.1126/science.aao3466.

[16] Matthew B. Plutschack, Bartholomäus Pieber, Kerry Gilmore, and Peter H. Seeberger. "The Hitchhiker's Guide to Flow Chemistry". In: *Chemical Reviews* 117.18 (Sept. 2017), pp. 11796–11893. ISSN: 0009-2665. DOI: 10.1021/acs.chemrev.7b00183. URL: http://pubs.acs.org/doi/10.1021/acs.chemrev.7b00183.

[20] Volker Hessel, Dana Kralisch, and Norbert Kockmann. "Novel Process Windows". In: *Novel Process Windows*. Weinheim, Germany: Wiley-VCH Verlag GmbH & Co. KGaA, Jan. 2015, pp. 15–24. ISBN: 9783527654840. DOI: 10.1002/9783527654826.ch2.

[33] Octave Levenspiel. *Chemical Reaction Engineering*. 3rd Ed. New York: Wiley, 1999, pp. 293–320. ISBN: 0-471-25424-X.

[35] Sebastian Schwolow, Jutta Hollmann, Berthold Schenkel, and Thorsten Röder. "Application-Oriented Analysis of Mixing Performance in Microreactors". In: *Organic Process Research & Development* 16.9 (Sept. 2012), pp. 1513–1522. ISSN: 1083-6160. DOI: 10.1021/op300107z. URL: http://pubs.acs.org/doi/10.1021/op300107z.

[36] Nirveek Bhattacharjee, Arturo Urrios, Shawn Kang, and Albert Folch. "The upcoming 3D-printing revolution in microfluidics". In: *Lab on a Chip* 16.10 (2016), pp. 1720–1742. ISSN: 1473-0197. DOI: 10.1039/C6LC00163G. arXiv: 15334406. URL: http://xlink.rsc.org/?DOI=C6LC00163G%20http://www.ncbi.nlm.nih.gov/pubmed/27101171%20http://www.pubmedcentral.nih.gov/articlerender.fcgi?artid=PMC4862901.

[37] Anthony K. Au, Wilson Huynh, Lisa F. Horowitz, and Albert Folch. "3D-Printed Microfluidics". In: *Angewandte Chemie International Edition* 55.12 (Mar. 2016), pp. 3862–3881. ISSN: 14337851. DOI: 10.1002/anie.201504382. URL: http://doi.wiley.com/10.1002/anie.201504382%20http://www.ncbi.nlm.nih.gov/pubmed/26854878%20https://onlinelibrary.wiley.com/doi/10.1002/anie.201504382.

[38] Andrew J. Capel, Andrew Wright, Matthew J. Harding, George W. Weaver, Yuqi Li, Russell A. Harris, Steve Edmondson, Ruth D. Goodridge, and Steven D.R. R Christie. "3D printed fluidics with embedded analytic functionality for automated reaction optimisation". In: *Beilstein Journal of Organic Chemistry* 13 (Jan. 2017), pp. 111–119. ISSN: 18605397. DOI: 10.3762/bjoc.13.14. URL: http://www.beilstein-journals.org/bjoc/content/13/1/14.

[73] Andrew J. Capel, Steve Edmondson, Steven D.R. R. R Christie, Ruth D. Goodridge, Richard J. Bibb, and Matthew Thurstans. "Design and additive manufacture for flow chemistry." In: *Lab on a chip* 13.23 (Dec. 2013), pp. 4583–4590. ISSN: 1473-0189. DOI: 10.1039/c3lc50844g. URL: http://xlink.rsc.org/?DOI=c3lc50844g%20http://www.ncbi.nlm.nih.gov/pubmed/24100659.

[75] Axel Günther and Klavs F. Jensen. "Multiphase microfluidics: from flow characteristics to chemical and materials synthesis". In: *Lab Chip* 6.12 (Dec. 2006), pp. 1487–1503. ISSN: 1473-0197. DOI: 10.1039/B609851G. URL: http://xlink.rsc.org/?DOI=B609851G%20http://www.ncbi.nlm.nih.gov/pubmed/17203152.

[77] M. Movsisyan, E. I. P. Delbeke, J. K. E. T. Berton, C. Battilocchio, S. V. Ley, and C. V. Stevens. "Taming hazardous chemistry by continuous flow technology". In: *Chemical Society Reviews* 45.18 (2016), pp. 4892–4928. ISSN: 0306-0012. DOI: 10.1039/C5CS00902B. URL: http://xlink.rsc.org/?DOI=C5CS00902B.

[78] Bernhard Gutmann, David Cantillo, and C. Oliver Kappe. "Continuous-flow technology—a tool for the safe manufacturing of active pharmaceutical ingredients." In: *Angewandte Chemie (International ed. in English)* 54.23 (June 2015),

pp. 6688–6728. ISSN: 1521-3773. DOI: 10.1002/anie.201409318. URL: http://doi.wiley.com/10.1002/anie.201409318%20http://www.ncbi.nlm.nih.gov/pubmed/25989203.

[79] Norbert Kockmann, Philipp Thenée, Christoph Fleischer-Trebes, Gabriele Laudadio, and Timothy Noël. "Safety assessment in development and operation of modular continuous-flow processes". In: *Reaction Chemistry & Engineering* 2.3 (2017), pp. 258–280. ISSN: 2058-9883. DOI: 10.1039/C7RE00021A. URL: http://xlink.rsc.org/?DOI=C7RE00021A.

[80] Joseph M. Reckamp, Ashira Bindels, Sophie Duffield, Yangmu Chloe Liu, Eric Bradford, Eric Ricci, Flavien Susanne, and Andrew Rutter. "Mixing Performance Evaluation for Commercially Available Micromixers Using Villermaux–Dushman Reaction Scheme with the Interaction by Exchange with the Mean Model". In: *Organic Process Research & Development* 21.6 (June 2017), pp. 816–820. ISSN: 1083-6160. DOI: 10.1021/acs.oprd.6b00332. URL: http://pubs.acs.org/doi/10.1021/acs.oprd.6b00332.

[81] Reza Amin, Stephanie Knowlton, Alexander Hart, Bekir Yenilmez, Fariba Ghaderinezhad, Sara Katebifar, Michael Messina, Ali Khademhosseini, and Savas Tasoglu. "3D-printed microfluidic devices". In: *Biofabrication* 8.2 (June 2016), p. 022001. ISSN: 1758-5090. DOI: 10.1088/1758-5090/8/2/022001. URL: http://stacks.iop.org/1758-5090/8/i=2/a=022001?key=crossref.42b00d58e7924bfe38fd579dcd1cb84e%20http://www.ncbi.nlm.nih.gov/pubmed/27321137%20https://iopscience.iop.org/article/10.1088/1758-5090/8/2/022001.

[82] Bethany C. Gross, Jayda L. Erkal, Sarah Y. Lockwood, Chengpeng Chen, and Dana M. Spence. "Evaluation of 3D Printing and Its Potential Impact on Biotechnology and the Chemical Sciences". In: *Analytical Chemistry* 86.7 (Apr. 2014), pp. 3240–3253. ISSN: 0003-2700. DOI: 10.1021/ac403397r. URL: http://pubs.acs.org/doi/10.1021/ac403397r%20http://www.ncbi.nlm.nih.gov/pubmed/24432804.

[83] Yong He, Yan Wu, Jian-zhong Fu, Qing Gao, and Jing-jiang Qiu. "Developments of 3D Printing Microfluidics and Applications in Chemistry and Biology: a Review". In: *Electroanalysis* 28.8 (Aug. 2016), pp. 1658–1678. ISSN: 10400397. DOI: 10.1002/elan.201600043. URL: http://doi.wiley.com/10.1002/elan.201600043.

[84] Bethany Gross, Sarah Y. Lockwood, and Dana M. Spence. "Recent Advances in Analytical Chemistry by 3D Printing." In: *Analytical chemistry* 89.1 (Jan. 2017), pp. 57–70. ISSN: 1520-6882. DOI: 10.1021/acs.analchem.6b04344. URL: http://pubs.acs.org/doi/10.1021/acs.analchem.6b04344%20http://www.ncbi.nlm.nih.gov/pubmed/28105825.

[85] Cesar Parra-Cabrera, Clement Achille, Simon Kuhn, and Rob Ameloot. "3D printing in chemical engineering and catalytic technology: structured catalysts, mixers and reactors." In: *Chemical Society reviews* 47.1 (Jan. 2018), pp. 209–230. ISSN: 1460-4744. DOI: 10.1039/c7cs00631d. URL: http://xlink.rsc.org/?DOI=C7CS00631D%20http://www.ncbi.nlm.nih.gov/pubmed/29131228.

[86] Philip J. Kitson, Stefan Glatzel, Wei Chen, Chang-Gen Lin, Yu-Fei Song, and Leroy Cronin. "3D printing of versatile reactionware for chemical synthesis". In: *Nature Protocols* 11.5 (May 2016), pp. 920–936. ISSN: 1754-2189. DOI: 10.1038/nprot.2016.041. URL: http://www.nature.com/articles/nprot.2016.041%20http://www.ncbi.nlm.nih.gov/pubmed/27077333.

[87] Andrew J. Capel, Rowan P. Rimington, Mark P. Lewis, and Steven D. R. Christie. "3D printing for chemical, pharmaceutical and biological applications". In: *Nature Reviews Chemistry* (Nov. 2018), pp. 2397–3358. ISSN: 2397-3358. DOI: 10.1038/s41570-018-0058-y. URL: http://www.nature.com/articles/s41570-018-0058-y.

[88] Raf Reintjens, David J. Ager, and Andr?? H M Andr?? H M André H.M. De Vries. "Flow chemistry, how to bring it to industrial scale?" In: *Chimica Oggi/Chemistry Today* 33.4 (2015), pp. 21–24. ISSN: 19738250. URL: https://www.teknoscienze.com/Contents/Riviste/PDF/CO4_2015_LOW_23-27.pdf.

[89] Gianmario Scotti, Ville Matilainen, Petri Kanninen, Heidi Piili, Antti Salminen, Tanja Kallio, and Sami Franssila. "Laser additive manufacturing of stainless steel micro fuel cells". In: *Journal of Power Sources* 272 (Dec. 2014), pp. 356–361. ISSN: 03787753. DOI: 10.1016/j.jpowsour.2014.08.096. URL: http://dx.doi.org/10.1016/j.jpowsour.2014.08.096%20https://linkinghub.elsevier.com/retrieve/pii/S0378775314013615.

[90] Gianmario Scotti, Petri Kanninen, Ville-Pekka Matilainen, Antti Salminen, and Tanja Kallio. "Stainless steel micro fuel cells with enclosed channels by laser additive manufacturing". In: *Energy* 106 (July 2016), pp. 475–481. ISSN: 03605442. DOI: 10.1016/j.energy.2016.03.086. URL: http://dx.doi.org/10.1016/j.energy.2016.03.086%20https://linkinghub.elsevier.com/retrieve/pii/S0360544216303309.

[91] S. Sandron, B. Heery, V. Gupta, D. A. Collins, E P Nesterenko, P. N. Nesterenko, M. Talebi, S. Beirne, F. Thompson, G. G. Wallace, D. Brabazon, F. Regan, and B. Paull. "3D printed metal columns for capillary liquid chromatography." In: *The Analyst* 139.24 (Dec. 2014), pp. 6343–6347. ISSN: 1364-5528. DOI: 10.1039/c4an01476f. URL: http://xlink.rsc.org/?DOI=C4AN01476F%20http://www.ncbi.nlm.nih.gov/pubmed/25285334.

[92] Vipul Gupta, Mohammad Talebi, Jeremy Deverell, Sara Sandron, Pavel N. Nesterenko, Brendan Heery, Fletcher Thompson, Stephen Beirne, Gordon G. Wallace, and Brett Paull. "3D printed titanium micro-bore columns containing polymer monoliths for reversed-phase liquid chromatography." In: *Analytica chimica acta* 910 (Mar. 2016), pp. 84–94. ISSN: 1873-4324. DOI: 10.1016/j.aca.2016.01.012. URL: http://dx.doi.org/10.1016/j.aca.2016.01.012%20https://linkinghub.elsevier.com/retrieve/pii/S0003267016300617%20http://www.ncbi.nlm.nih.gov/pubmed/26873472.

[93] Bernhard Gutmann, Manuel Köckinger, Gabriel Glotz, Tania Ciaglia, Eyke Slama, Matej Zadravec, Stefan Pfanner, Manuel C. Maier, Heidrun Gruber-Wölfler, and C. Oliver Kappe. "Design and 3D printing of a stainless steel reactor for continuous difluoromethylations using fluoroform". In: *Reaction Chemistry & Engineering* 2.6 (2017), pp. 919–927. ISSN: 2058-9883. DOI: 10.1039/C7RE00176B. URL: http://xlink.rsc.org/?DOI=C7RE00176B.

[94] Zhi He and Timothy F. Jamison. "Continuous-Flow Synthesis of Functionalized Phenols by Aerobic Oxidation of Grignard Reagents". In: *Angewandte Chemie International Edition* 53.13 (Mar. 2014), pp. 3353–3357. ISSN: 14337851. DOI: 10.1002/anie.201310572. URL: http://doi.wiley.com/10.1002/anie.201310572%20http://www.ncbi.nlm.nih.gov/pubmed/24554581.

[95] C. A. Fyfe. *The Hydroxyl Group (1971)*. Ed. by Saul Patai. Chichester, UK: John Wiley & Sons, Ltd., Jan. 1971, pp. 83–127. ISBN: 9780470771259. DOI: 10.1002/9780470771259. URL: http://doi.wiley.com/10.1002/9780470771259.

[96] D. G. Hall. *Boronic Acids*. Ed. by Dennis G. Hall. Weinheim, Germany: Wiley-VCH Verlag GmbH & Co. KGaA, Oct. 2011. ISBN: 9783527639328. DOI: 10.1002/9783527639328. URL: http://doi.wiley.com/10.1002/9783527639328.

[97] Stephan Enthaler and Anna Company. "Palladium-catalysed hydroxylation and alkoxylation." In: *Chemical Society reviews* 40.10 (Oct. 2011), pp. 4912–4924. ISSN: 1460-4744. DOI: 10.1039/c1cs15085e. URL: http://xlink.rsc.org/?DOI=c1cs15085e%20http://www.ncbi.nlm.nih.gov/pubmed/21643619.

[98] Wladimir Reschetilowski, ed. *Microreactors in Preparative Chemistry*. Weinheim, Germany: Wiley-VCH Verlag GmbH & Co. KGaA, Aug. 2013. ISBN: 9783527652891. DOI: 10.1002/9783527652891. URL: http://doi.wiley.com/10.1002/9783527652891.

[99] Ivana Dencic, Volker Hessel, and Wladimir Reschetilowski. *Microreactors in Organic Chemistry and Catalysis*. Ed. by Thomas Wirth. Weinheim, Germany: Wiley-VCH Verlag GmbH & Co. KGaA, Apr. 2013, pp. 373–446. ISBN: 9783527659722. DOI: 10.1002/9783527659722. URL: http://doi.wiley.com/10.1002/9783527659722%20https://doi.org/10.1002/9783527659722.ch11.

[100] Bartholomäus Pieber and C. Oliver Kappe. *Aerobic Oxidations in Continuous Flow*. Vol. 57. Springer, 2015, pp. 97–136. ISBN: 978-3-642-04728-2. DOI: 10.1007/3418_2015_133. URL: http://link.springer.com/10.1007/3418_2015_133.

[101] John F. Garst, Calvin D. Smith, and Alice Chandler Farrar. "Radical intermediates in the oxygenation of phenylmagnesium bromide. Evidence from aromatic phenylation". In: *Journal of the American Chemical Society* 94.22 (Nov. 1972), pp. 7707–7710. ISSN: 0002-7863. DOI: 10.1021/ja00777a016. URL: http://pubs.acs.org/doi/abs/10.1021/ja00777a016.

[102] Magdalena Jasińska. "Test Reactions to Study Efficiency of Mixing". In: *Chemical and Process Engineering* 36.2 (June 2015), pp. 171–208. ISSN: 2300-1925. DOI: 10.1515/cpe-2015-0013. URL: http://content.sciendo.com/view/journals/cpe/36/2/article-p171.xml.

[103] Alex Povitsky. "Three-dimensional flow with elevated helicity in driven cavity by parallel walls moving in perpendicular directions". In: *Physics of Fluids* 29.8 (Aug. 2017), p. 083601. ISSN: 1070-6631. DOI: 10.1063/1.4996179. URL: http://aip.scitation.org/doi/10.1063/1.4996179.

[104] Boštjan Rajh, Chungen Yin, Niko Samec, Matjaž Hriberšek, Filip Kokalj, and Matej Zadravec. "Advanced CFD modelling of air and recycled flue gas staging in a waste wood-fired grate boiler for higher combustion efficiency and greater environmental benefits". In: *Journal of Environmental Management* 218 (July 2018), pp. 200–208. ISSN: 03014797. DOI: 10.1016/j.jenvman.2018.04.030. URL: https://linkinghub.elsevier.com/retrieve/pii/S0301479718304122.

[105] Chia-Yen Lee, Chin-Lung Chang, Yao-Nan Wang, and Lung-Ming Fu. "Microfluidic Mixing: A Review". In: *International Journal of Molecular Sciences* 12.5 (May 2011), pp. 3263–3287. ISSN: 1422-0067. DOI: 10.3390/ijms12053263. URL: https://www.mdpi.com/1422-0067/12/5/3263%20http://www.mdpi.com/1422-0067/12/5/3263.

[106] Edward L. Paul, Victor A. Atiemo-Obeng, and Suzanne M. Kresta. *Handbook of Industrial Mixing*. Ed. by Edward L Paul, Victor A Atiemo-Obeng, and Suzanne M Kresta. Hoboken, NJ, USA: John Wiley & Sons, Inc., Nov. 2003, pp. 1140–1149. ISBN: 0471269190. URL: http://doi.wiley.com/10.1002/0471451452.

[107] Kevin Ward and Z. Hugh Fan. "Mixing in microfluidic devices and enhancement methods". In: *Journal of Micromechanics and Microengineering* 25.9 (Sept. 2015), p. 094001. ISSN: 0960-1317. DOI: 10.1088/0960-1317/25/9/094001. URL: http://stacks.iop.org/0960-1317/25/i=9/a=094001?key=crossref.76c24b2dae65e0dfc89a9f04c8d4462b%20http://www.ncbi.nlm.nih.gov/pubmed/26549938%20http://www.pubmedcentral.nih.gov/articlerender.fcgi?artid=PMC4634658.

[108] J. Bałdyga, J.R. Bourne, and S.J. Hearn. "Interaction between chemical reactions and mixing on various scales". In: *Chemical Engineering Science* 52.4 (Feb. 1997), pp. 457–466. ISSN: 00092509. DOI: 10.1016/S0009-2509(96)00430-7. URL: http://linkinghub.elsevier.com/retrieve/pii/S0009250996004307.

[109] Xu-dong Wang and Otto S. Wolfbeis. "Optical methods for sensing and imaging oxygen: materials, spectroscopies and applications". In: *Chem. Soc. Rev.* 43.10 (May 2014), pp. 3666–3761. ISSN: 0306-0012. DOI: 10.1039/C4CS00039K. URL: http://xlink.rsc.org/?DOI=C4CS00039K%20http://www.ncbi.nlm.nih.gov/pubmed/24638858.

[110] S.M. M Borisov, G. Nuss, W. Haas, R. Saf, M. Schmuck, and I. Klimant. "New NIR-emitting complexes of platinum(II) and palladium(II) with fluorinated benzoporphyrins". In: *Journal of Photochemistry and Photobiology A: Chemistry* 201.2-3 (Jan. 2009), pp. 128–135. ISSN: 10106030. DOI: 10.1016/j.jphotochem.2008.10.003. URL: http://linkinghub.elsevier.com/retrieve/pii/S1010603008004292.

[111] Chris D Geddes and Joseph R Lakowicz. *Reviews in fluorescence 2006*. Springer, 2005. URL: https://scholar.google.at/scholar?hl=de%7B%5C&%7Das_sdt=0%7B%5C%%7D2C5%7B%5C&%7Dq=Reviews+in+fluorescence+2006+geddes%7B%5C&%7DbtnG=.

CHAPTER 3

A modular 3D printed isothermal heat flow calorimeter for reaction calorimetry in continuous flow

The following chapter is taken from the same-titled journal article published in *Reaction Chemistry and Engineering* by Maier *et al.*:

Manuel C. Maier[1,2], Michael Leitner[1,2], C. Oliver Kappe[2,3], and Heidrun Gruber-Woelfler[1,2]

Reaction Chemistry and Engineering, 05/2020, DOI: 10.1039/d0re00122h

[1]Institute of Process and Particle Engineering, Graz University of Technology, Graz, Austria

[2]Center for Continuous Flow Synthesis and Processing (CCFLOW), Research Center Pharmaceutical Engineering GmbH (RCPE), Graz, Austria

[3]Institute of Chemistry, University of Graz, Graz, Austria

Contents

3.1 Abstract

Utilization of highly reactive compounds in novel flow syntheses requires new tools for process development. This work presents such a tool in the form of a modular calorimeter designed for direct heat flux measurements in continuous flow applications. The calorimeter consists mainly of *3D* printed parts, which can be adapted and reassembled easily to meet user-defined applications. By utilizing Selective Laser Melting (*SLM*) of stainless steel and Digital Light Processing (*DLP*) of a *UV*-curable resin, a device is produced to meet the requirements of handling highly reactive organic compounds. Calorimeter segments are temperature-regulated independently of each other by a microcontroller, allowing isothermal operation conditions. Direct heat flux measurements are possible in the device through Seebeck elements which are calibrated internally at prevailing process conditions with the aid of heating foils. Functionality of the designed calorimeter is shown by good agreement of conducted heat flux measurements with literature.

3.2 Introduction

New synthetic pathways are enabled in flow chemistry by utilizing highly reactive compounds in milli and micro fluidic devices. [77, 16] During development of these syntheses, thermodynamic, fluid dynamic, and kinetic investigations are rarely included, but are obligatory for a safe and efficient industrial application. Development is mainly carried out in milli and micro fluidic devices, whereby isothermal conditions are often assumed due to high surface-to-volume ratios and the resulting high heat transfer rates. [22] Based on this assumption, possible hot spot formation is not checked and misinterpretation of reaction data can occur. [26] By trying to achieve higher productivities of the used milli and micro devices by scale-out, underestimation of the length scale change can affect reactor performance and therefore the reaction outcome. [23] In this context, scale-out is defined as a slight change of a length scale to increase productivity, while preserving characteristics of the reactor, such as flow regime or surface phenomena. In addition, reaction and mixture data for these new syntheses are most of the time not easily available since a variety of different substances can be formed at slightly different reaction conditions. However, these data are required for safety evaluations as well as for an efficient process. [79]

Reaction calorimetrical investigations with their different modes of operation [56] play a crucial role to provide fundamental data like enthalpy of reaction, activation energy, heat capacity of a reaction mixture as well as reaction rate. A key parameter for reactor design and safety evaluation is the reaction enthalpy. Standard equipment for reaction enthalpy measurements like batch calorimeters, *e.g.* the RC1 from Mettler Toledo, [112] can only be used to a certain extent for novel reactions under extreme reaction conditions as seen today in flow chemistry. While there exist batch calorimeters with relatively small volumes, [113, 114, 115] their mode of operation is different compared to flow chemical setups, *i.e.* they cannot provide the conditions required to gather meaningful thermodynamic and kinetic

data for continuous flow applications in harsh reaction environments.

Modifying batch calorimeters to meet flow applications is possible through standard *HPLC* equipment, [63] nevertheless, this approach has some drawbacks. It does not provide optimal connectivity of parts to the calorimeter, leads very often to poor mixing performance caused by standard laboratory tubing and connectors, and requires existing software to be adaptable. Another possibility to use existing technology for heat flux measurements is infrared thermography. [65] Disadvantages of this method are a required optical access to the ongoing reaction as well as an expensive camera providing necessary resolution of the small channels.

Flow calorimeters recently developed use thermoelectric principles to directly detect heat fluxes through the Seebeck effect. [66, 67, 64, 68, 69, 116] Their general setup consists of a chip-like reactor separated from a heat sink by Seebeck elements which generate voltage signals proportional to the transferred heat flux. These elements can be manufactured directly on the reactor chip [66, 67] or bigger and cheaper commercially available Seebeck elements can be used. [69] By miniaturization of Seebeck elements, spatially resolved measurements are shown and additional information about reaction time scales are obtained by some designs. [68, 69] Calibration of the Seebeck elements can be done externally or internally by integrated heating in the assembled device, which accounts for heat losses of the system. [68, 116]

All of the mentioned designs lack the possibility to react locally to changing temperature caused by a reaction in the corresponding section of the reactor. Heat fluxes from each section are transferred through a Seebeck element uniformly to one heat sink, with its temperature being regulated by a thermostat set to the desired reaction temperature. Sufficient heat transfer from heat sink to reactor cannot always be ensured in such a setup due to the poor heat transfer characteristics of the utilized Seebeck elements. As a result, isothermal conditions cannot be achieved if highly reactive compounds are used and formation of local hot spots within the reactor is likely. To overcome the poor thermal conductivity of Seebeck elements, it is desired to control locally the temperature within a reactor by specifically applying increased heat fluxes.

The designed calorimeter described within this work is guided by the abovementioned devices but utilizing the advantages of *3D* printing as well as already existing knowledge of reactor design [93, 8] and microcontroller-based regulation. We present here a novel isothermal heat flow calorimeter which can withstand harsh reaction conditions commonly found in flow chemistry by a combination of two different additive manufacturing techniques and cheap, commercially- available electronics. In addition to its modular and extendable design, the calorimeter's segments are regulated independently from each other and allow to react locally to ongoing reactions. Applicability of the flow calorimeter is shown by studying thermodynamic properties such as reaction enthalpy, heat capacity and molar excess enthalpy, and thus providing necessary data for reactor scale-out as well as safety aspects.

3.3 Experimental

3.3.1 Design of the flow calorimeter

The presented calorimeter features modular and extendable segments with exchangeable elements, as shown in Fig. 3.1 and S3.3. Its elements were designed to utilize advantages of additive manufacturing by accommodating readily available commercial laboratory and electrical components while focusing on reducing standard manufacturing processes. This design for additive manufacturing enables the production of highly complex geometries in a short time with minimal waste.

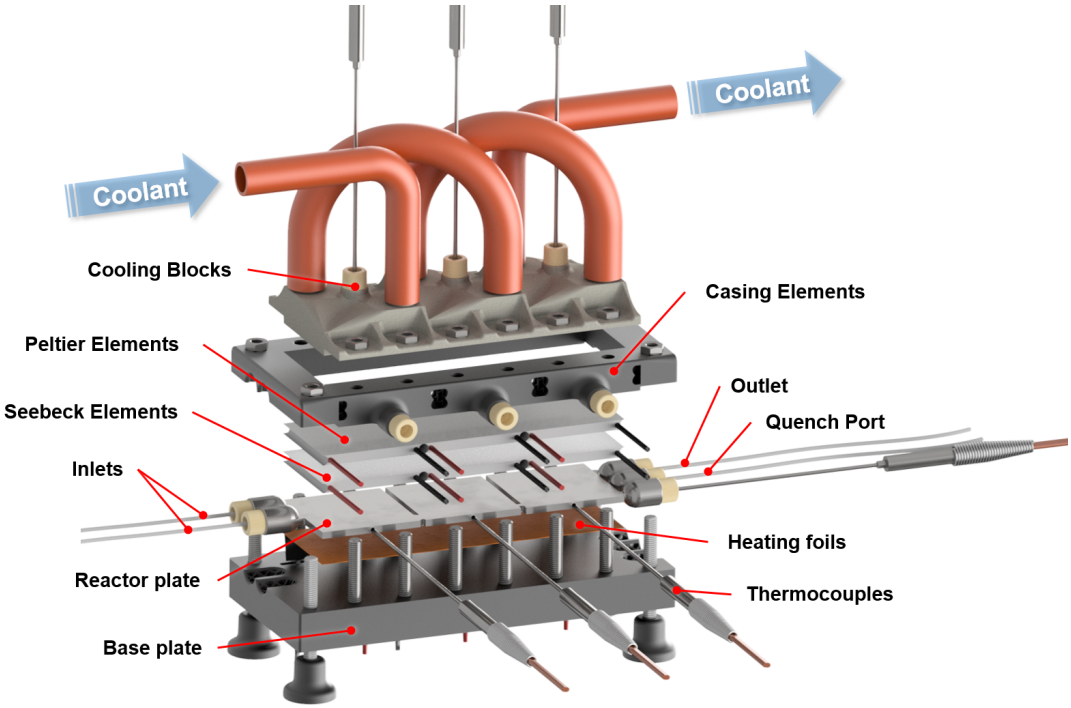

Figure 3.1: Exploded view of the designed calorimeter. Its modular segments were manufactured using additive manufacturing while considering commercial components already during the design phase. Each segment is independently temperature-controlled through the aid of a microcontroller and can be calibrated at prevailing process conditions with integrated heating foils.

Two additive manufacturing techniques were used to manufacture the device, Selective Laser Melting (*SLM*) and Digital Light Processing (*DLP*). Reactor plate and cooling blocks were manufactured by *SLM* of stainless steel to provide high chemical and mechanical stability as well as excellent heat transfer rates, allowing the usage of highly reactive compounds and organic solvents at elevated pressures. The casing of the calorimeter was manufactured by *DLP* of a cheap *UV*-curable resin. This material in combination with an internal support structure showed good thermal insulation against the environment while providing necessary strength to fixate the whole device. Both manufacturing techniques

allow reactor elements to be produced, which can be easily modified to meet a desired configuration of the device in terms of number of reaction segments with different size and mixing geometries.

The calorimeter measures direct heat fluxes using the thermoelectric Seebeck effect with the aid of Seebeck elements contacting the reactor plate. A Seebeck element consists of a series of thermocouples, which themselves are consisting of two dissimilar electrical conductors connected at one end. By applying different temperatures at each end of a thermocouple, it generates an electrical voltage proportional to the temperature difference. By arranging thermocouples in series across two surface areas as within Seebeck elements, it is possible to measure the transferred heat by means of an electrical voltage. Conversely, when a voltage is applied to such a device, a hot and cold side is formed, which allows it to transfer heat. This configuration is described by the Peltier effect and the same electronic components are referred to as Peltier elements within this work.

The generated voltages from the Seebeck elements are measured by a self-made electrical circuit utilizing a microcontroller which is programmed with the Arduino integrated development environment (IDE). To obtain the actual heat flux, a calibration with integrated heating foils has to be made. With these heaters, an exothermic reaction can be simulated and by applying a defined power input, a calibration at prevailing process conditions can be obtained. This calibration already accounts for heat losses of the device operated at a defined temperature. Influences of the heating foils during an actual calorimetric measurement were not investigated and neglected as they are assumed to be very small. Furthermore, ideal heat input of the heating foils was assumed within this work.

In contrast to other designs, [68, 69] this device features a microcontroller-based temperature control of each calorimeter segment. This allows to ensure an operation of each segment independently as close as possible to the desired isothermal set point. The reactor segment's temperature is measured and transmitted to a microcontroller which adjusts the heat flux of a Peltier element through a *PID* based control strategy, see Fig. 3.2.

3.3.2 Reactor control strategy

Isothermal temperatures are ensured in the designed calorimeter through a *PID* control of each reactor segment separately. Here the advantages of additive manufacturing allow accommodation of standard commercial electronic parts, which are used in this temperature regulation. The standard regulation circuit to achieve this constant temperature is shown in Fig. 3.2. This circuit is continuously repeated and started by measuring the temperature of each reactor segment via thermocouples (TJ36-CPSS-116G-4, omega.de) attached in the middle of each reactor segment. The small voltage signal produced by a thermocouple is recognized by an amplifier (MAX31856, adafruit.com) which directly converts this voltage to a readable temperature within the same chip and transfers it to the microcontroller (Arduino Mega 2560). The continuously looping control strategy of the microcontroller is implemented through the Arduino IDE and compares the desired

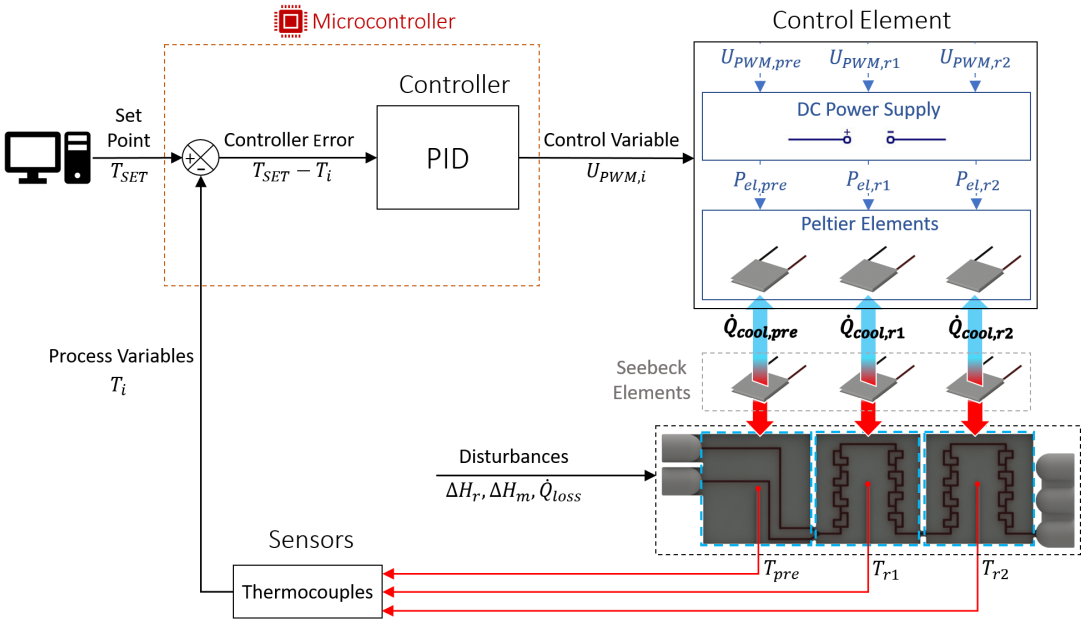

Figure 3.2: Control strategy for the calorimeter. The temperature of each reactor segment is adjusted separately by means of a microcontroller-based temperature control. Peltier elements provide the necessary heat flux to regulate the reactor segments.

temperature set point for each reactor segment to the measured values. The calculated controller errors are passed through a standard *PID* control procedure and lead to specific set values of the current time step. These set values are correlated to electrical voltages between 0 to 5 V through an on board pulse width modulation (PWM) of the microcontroller which gradually opens the gates of metal oxide semiconductor field-effect transistors (MOSFET; IRFZ44N, reichelt.at) to supply a defined amount of current to each cooling Peltier element (QC-127-1.4-6.0MS, quick-cool-shop.de). This defined electrical current to the Peltier element generates a heat sink depending on the operation of each reactor segment. To ensure a steady cooling performance, the hot sides of the Peltier elements are cooled by the custom-designed and *SLM* printed cooling blocks. The cold side of the Peltier elements contacts Seebeck elements of identical construction, which recognise the heat fluxes from the respective reactor segments. Before repeating the control circuit, the measured data is written to a COM port of the microcontroller and is directly processed via an attached PC. Evaluation of the steady state data can be carried out by calculating mean values over a user-defined interval via spreadsheet calculations.

The control strategy presented above only allows the investigation of exothermic measurements. Endothermic measurements can be recognized by the Seebeck elements, since the thermoelectric voltage can change signs. However, the electrical contacts of the Peltier elements would have to be switched to enable a temperature control. This would result in switched cold and hot sides to provide the necessary heating of endothermic events. In

addition, no internal calibration for endothermic events is possible with the implemented heating foils.

3.3.3 PID characteristics

PID parameters influence the time needed to reach a certain set point and account for varying heat fluxes in the system. First estimation of *PID* parameters was done by experimental step response evaluations, based on a known and sudden electrical heat flux applied to the reactor segments through the integrated heating foils, Fig. 3.3. A later fine tuning of parameters led to *PID* values of P = 20, I = 0.52 and D = 0 for cooling at 25 °C. The differential parameter was set to zero since it was not necessary to account its depressing effect for sudden high valued changes in the recorded signals. The parameters depend also on the time needed for each control loop performed on the microcontroller. With these parameters a steady state was reached after approximately 2.5 minutes starting from the sudden change.

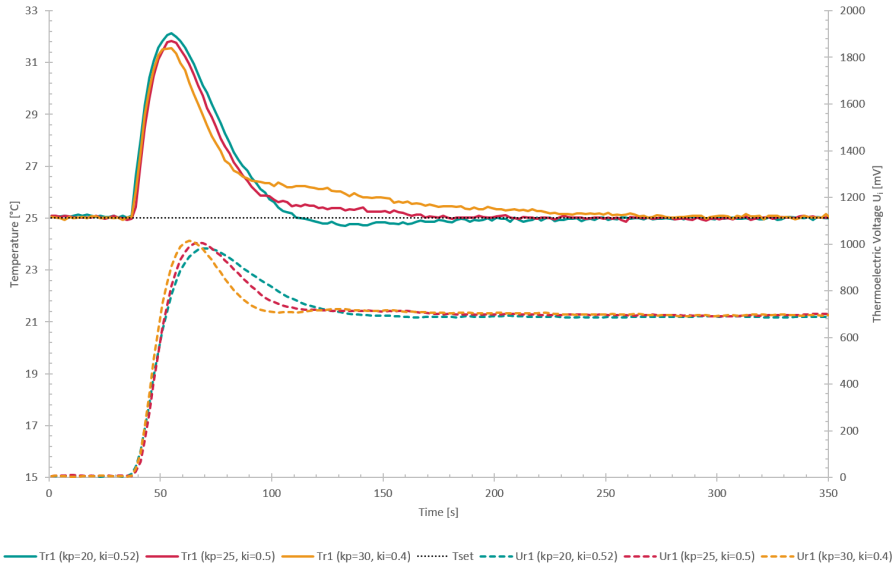

Figure 3.3: Temperature and measured thermoelectric voltage of the Seebeck element during the temperature control of reactor segment r1 with a suddenly applied electrical heating pulse of 6.6 W. Different times to reach a desired stable temperature can be seen by varying the regulation parameters.

3.3.4 Manufacturing – 3D printing

Elements of the calorimeter that require high thermal conductivity, good chemical stability, and mechanical strength were manufactured by *SLM* of stainless steel. One of these elements was the reactor plate with the integrated reaction channel and connector ports. The other parts printed with *SLM* were the cooling blocks. These elements were *3D*

printed according to modified *CAD* models with software-generated support structures to provide the necessary stability and layer-wise connection during the printing procedure. Especially the thin connection points between reactor segments had to be modified to withstand deformation caused by thermal stresses during the manufacturing. Additional material was added to account for such deformations as well as to provide sufficient space for surface modification to allow later an exact contact between the printed parts and electronic components.

The reactor plate was designed with a precooling section and two reaction sections utilizing a split and recombine structure, Fig. 3.2. The internal diameter was set to 0.8 mm, which gives a combined reaction volume of 220 μL for both reaction segments. Due to the modular design, these reaction sections can be duplicated and changed depending on the desired task to reach a defined residence time as well as mixing properties. Reactor sections were separated from each other to reduce heat conduction between them. The additional material mentioned above was removed by laser cutting to separate the sections. Connections of the reactor plate to peripheral tubing can be made with standard flat bottom *HPLC* fittings. Maximum operation pressure of the reactor is therefore limited only by the specifications of the used fittings, in this case 100 bar.

The designed cooling block for heat removal of the Peltier elements needed an internal support structure before printing (see Fig. S3.1). Besides being necessary for fabrication, this structure increases the internal contact area for the heat transfer of the coolant to the metal. If needed, a connector port for temperature measurements close to the Peltier contact area can be implemented as well. This temperature measurement is indicated in Fig. 3.1, but was not used within this work.

Additive manufacturing was then carried out by an *SLM* system from EOS which utilizes an ytterbium fibre laser with 400 Watt maximum power input, scanning through each of the 40 μm high sliced layers. A 316L stainless steel powder bed with a mean particle size of 35.9 μm was used for the calorimeter elements. Post-processing of the stainless steel parts included several cleaning procedures with compressed air, treatments within an ultrasonic bath to free entrapped particles, sandblasting of the outer surfaces, CNC milling and laser cutting to achieve the planned geometries. Accurate contact of the reactor plate and cooling block to the Seebeck and Peltier elements was ensured by the CNC milled surfaces, which have the same roughness properties as standard milled stainless steel parts. Besides removing of excess particles, no further surface treatment of the internal channels was carried out.

Casing elements of the calorimeter were designed to be easily *3D* printable without any additional support structure, see Fig. S3.2. All elements feature prism like internal structures, which connect each layer, give the parts necessary mechanical strength, reduce the amount of material needed during production and provide necessary thermal insulation against the environment. All casing elements were designed to be printed by *DLP* of a *UV*-curable resin. The elements were produced with the Photon from Anycubic and a standard black resin from the same manufacturer. Based on preliminary knowledge of the

printer, a layer height of 50 μm with a normal exposure time of 14 seconds was chosen to produce the casing elements. Due to the small printing area of the device, several printing jobs had to be carried out but the whole production time did not exceed two days. By using this approach of *3D* printed casing, future adaption and extension of the calorimeter can be easily carried out. Post-processing of these parts included only the removal of the parts from the build platform and cleaning with ethanol. The parts could be used directly after printing but a final curing in sunlight until the next day was envisioned.

3.3.5 Reactor setup and external equipment

The experimental setup shown in Fig. 3.4 was used within this work. For continuous measurements, the designed calorimeter needed additional equipment to solve the overall heat balance. To close the heat balance, it was necessary to add additional temperature sensors in both inlet streams. Here, standard T-junctions (*PEEK*, bore 0.020 in, thread 10–32) were modified by drilling a 1.6 mm hole in the middle connector to bring the sensor tips within the flowing liquid stream. Due to fluctuations of room temperature, a heat exchanger was added to bring both inlets to a steady temperature. For this heat exchanger, stainless steel coils (1/16″ *OD*, 0.03″ *ID*, 1 m) were used and heated within a water bath on top of the heating plate of a laboratory magnetic stirrer (IKA® RCT standard). Fluids were pumped into the reactor with *HPLC* pumps (Knauer Azura P4.1S) utilizing Back Pressure Regulator (*BPR*) to achieve a smoother operation of these pumps and a certain backpressure over the reactor. For the mixing characterization, the *HPLC* pumps were exchanged with syringe pumps (Lambda VIT-FIT) due to the pulsing nature of the *HPLC* pumps used, which influences the mixing performance. Within these experiments, no *BPRs* were used. A con- stant operation of the calorimeter segments was envisioned by a continuous coolant supply from a thermostat (Lauda Alpha Ra12) to the cooling blocks.

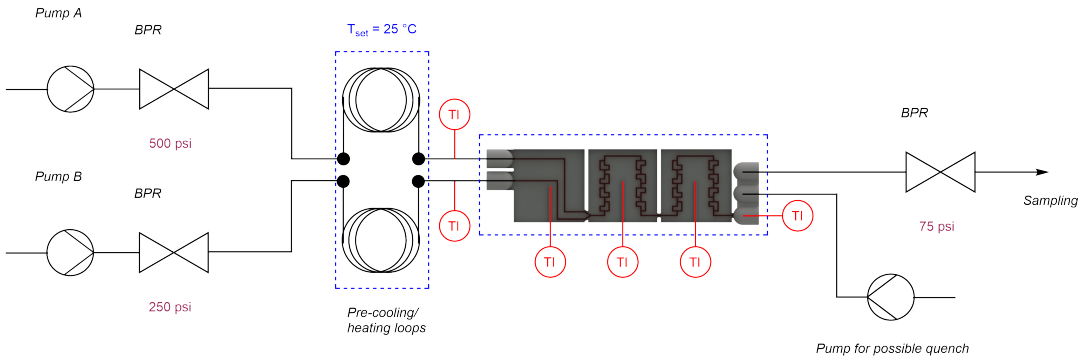

Figure 3.4: Experimental setup used for all measurements. An additional pre-cooling was added directly before the reactor to achieve almost constant input temperatures. A quench pump is indicated in the setup for later applications, but in this work the quench port was plugged with an *HPLC* plug.

3.3.6 Heat balance of the system

A heat balance of the reactor plate is needed in addition to the direct heat flux measurements for the calculation of the produced reaction heat. A general heat balance is depicted in eqn 3.1.

$$\frac{dQ}{dt} = -\dot{Q}_{conv} - \dot{Q}_{tr} + \dot{Q}_{rx} \tag{3.1}$$

The reactive heat flux $\dot{Q}_{rx}$ shown in eqn 3.2 is depending on the total volumetric flow rate $\dot{V}$, initial and limiting concentration c_0, molar reaction enthalpy Δh_R and chemical conversion X regarding the rate limiting substance.

$$\dot{Q}_{rx} = \dot{V} c_0 \Delta h_R X \tag{3.2}$$

Convective heat fluxes $\dot{Q}_{conv}$ of inlet and outlet streams are shown in eqn 3.3, 3.4 and 3.5 with temperature T_i , density ρ_i, molecular mass MM_i, and molar specific heat capacity $c_{P,i}$ of a respective substance or mixture at fluid port A, B or out. In these equations, T_{set} was used as reference temperature and a sign convention was used throughout this work which depicts heat carried out of the system with negative values.

$$\dot{Q}_{out} = \dot{V}_{out} \frac{\rho_{out}}{MM_{out}} c_{P,out} (T_{set} - T_{out}) \tag{3.3}$$

$$\dot{Q}_{in,A} = \dot{V}_A \frac{\rho_A}{MM_A} c_{P,A} (T_{set} - T_{in,A}) \tag{3.4}$$

$$\dot{Q}_{in,B} = \dot{V}_B \frac{\rho_B}{MM_B} c_{P,B} (T_{set} - T_{in,B}) \tag{3.5}$$

Heat fluxes directly measurable through the Seebeck elements, placed at the reactor segments $pre, r1$ and $r2$, are added together to the transmitted heat flux $\dot{Q}_{tr}$ as shown in eqn 3.6.

$$\dot{Q}_{tr} = \dot{Q}_{tr,pre} + \dot{Q}_{tr,r1} + \dot{Q}_{tr,r2} \tag{3.6}$$

Each heat flux from the reactor segments is a function of a measured voltage signal $U_{SE,i}$. In this work, a fit in the form of a second order polynomial was used for eqn 3.7.

$$\dot{Q}_{tr,i} = f_{calibr}(U_{SE,i}) \tag{3.7}$$

No heat losses were added within the calculation due to the internal calibration with heating foils in the device. It was assumed that this calibration already accounts for heat losses to the environment at a specific operation point.

In a steady state operation, the temporal change of energy equals zero in eqn 3.1 and the reaction enthalpy can be calculated as shown in eqn 3.8 whereby convective heat fluxes

of inlet streams need to be subtracted and the heat fluxes of the outlet have to be added.

$$\Delta h_R = \frac{\dot{Q}_{tr} - \dot{Q}_{in,A} - \dot{Q}_{in,B} + \dot{Q}_{out}}{\dot{V} c_0 X} \tag{3.8}$$

3.3.7 Reaction to characterize mixing efficiency

A key parameter to perform homogeneous flow syntheses is mixing performance. Depending on the intrinsic reaction rate of a synthesis, different products and side products can be obtained if mixing of two miscible streams is the rate limiting factor. Therefore, mixing performance of the designed reactor plate was evaluated experimentally. This can be done with mixing-sensitive reactions, *e.g.* a system with consecutive and competitive reactions as described in literature. [1, 34] Despite being well documented, the Villermaux–Dushman system [34] is adapted in various works to customize the redox reaction to the mixing time of the reactor, which complicates a comparison of different reactors. [117, 118] Also, the reaction can be altered by light, heat, and dissolved oxygen. [119]

Because of these limitations, the diazo coupling published by Bourne *et al.* [1] was chosen for mixing evaluations of the designed reactor plate, see Fig. S3.4. In a first step, diazo coupling of 1-naphthol (A) and diazotised sulfanilic acid (B) takes place and gives the monoazo isomers *p*-R and *o*-R. Poor mixing promotes the secondary coupling of *p*-R and *o*-R with B giving the bisazo dye S. Better mixing is indicated by less formation of the secondary coupling product S.

$$A + B \overset{k_{1p}}{\rightarrow} p\text{-}R \tag{3.9}$$

$$A + B \overset{k_{1o}}{\rightarrow} o\text{-}R \tag{3.10}$$

$$p\text{-}R + B \overset{k_{2o}}{\rightarrow} S \tag{3.11}$$

$$o\text{-}R + B \overset{k_{2p}}{\rightarrow} S \tag{3.12}$$

Reaction rates of this coupling are well defined at standard conditions of 25 °C, in a sodium carbonate/bicarbonate buffer (444.4 mM), at a pH of 9.9. [108] Final solutions for the characterization included 1.2 mM of A in an 888.8 mM sodium carbonate/bicarbonate buffer and 1 mM diazotized sulfanilic acid in an aqueous solution.

Solutions were pumped with equal flow rates through the reactor plate at total flow rates of 0.2, 0.5, 1, 2, 4, 6, 8 and 10 ml min^{-1}. Samples were collected after approximately three residence times and stored in a dark container. Before analysis, samples needed to be diluted (1:8) with the 444.4 mM buffer to account for the long path length of 10 mm of the available *UV / VIS* flow cell (Flow Cell-Z-10, Avantes). Spectral data was produced by passing the light from a *UV* light source (AvaLight-DS-DUV) through the flow cell and

to a detector (AvaSpec-ULS2048) with an integration time of 1.05 ms, averaging of 100 samples and saving the obtained data from an interval of 390 to 700 nm in 10 nm steps. Concentrations were calculated by a multi-parameter-linear-regression of the absorption spectra as described in a previous work. [8]

3.3.8 Calorimeter calibration

Direct calibration of the assembled calorimeter is possible through the incorporated heating foils. This calibration method can account for heat losses to the environment already during calibration. To increase the measurement accuracy of the device, a calibration for each temperature set point should be made.

For the calibration of each reactor segment, a known and steady electrical heat flux was supplied to the respective segment simultaneously. This heat flux was delivered by integrated heating foils (TSC0400040gR7.91, pelonistechnologies.com) for each reactor segment separately and recognized by the respective Seebeck element opposite the reactor plate as a thermoelectric voltage $U_{SE,i}$. Heating foils were connected in parallel to a power supply (Manson NRP-3630) which provided a known electrical power input. Each foil's electrical resistance had to be measured to calculate the true applied electrical heat flux for the respective foil. Because of the inaccurate voltage and current display of the power supply, an exact voltage and current measurement was installed with digital multimeters for exact power input characterization. Changes in the electrical resistance of all elements (Fig. S3.5) were seen by varying temperatures with a changing overall resistance of the system. This changing resistance was accounted in the calibration experiments. Calibration data was obtained at steady state conditions with 31 points between zero and 7 W applied to each reactor segment for an operation temperature of 25 °C.

3.3.9 Functionality test of the calorimeter setup

A functionality test of the whole setup was carried out by adding warm deionized water into the calorimeter with the goal to cool it down to 25 °C and measure the transferred heat. In addition to the heat transfer evaluation, it was also planned to see how the calorimeter reacts to unstable inlet conditions. To achieve such an unstable behaviour, the precooling water bath was heated to approximately 40 °C and set to 36 °C in the beginning of the experiment when the pumps were started. The slow cooling of the water bath generated varying inlet temperatures. Together with changing pump rates of 0.5, 1, 2, 3, 4 and 5 ml min^{-1} for the respective pumps, unstable inlet conditions were simulated. All experiments were carried out twice except for the flow rate of 5 ml min^{-1}.

3.3.10 Reaction to generate heat fluxes

To verify performance of the reaction calorimeter, exothermic neutralization of sodium hydroxide ($NaOH$) with acetic acid ($AcOH$) was used. The reaction equation of this

neutralization is depicted in eqn 3.13.

$$CH_3COOH + NaOH \rightarrow H_2O + CH_3COONa \tag{3.13}$$

This neutralization was chosen since it is very well characterized and a standard reaction used in calorimetry. Another advantage is that the reaction products are not depending on mixing while the reaction is quasi instantaneous and leads to full conversion. The starting solutions were prepared by dissolving solid $NaOH$ (sodium hydroxide ≥99%, Carl Roth) in deionized water and dilution of $AcOH$ (acetic acid puriss. p.a., ACS reagent, Sigma Aldrich) with deionized water, both to 1, 2, 3 and 4 mol L^{-1}. For the actual neutralization reactions, the solutions were fed in an equimolar ratio into the calorimeter inlets with 1, 2, 4, 6 and 8 ml min^{-1}. Each operation point was evaluated twice at steady state by calculating mean values over a significant number of samples (more than 100). The correct operation was checked for each measurement point by measuring pH value of the outlet stream after reaching a steady state.

3.3.11 Excess molar enthalpy measurements

Excess molar enthalpy H^E is an essential thermodynamic property for the design of chemical processes, which address the non-linearity of solutions. It can be used to determine the vapour–liquid equilibria by utilizing the Gibbs–Helmholtz equation. [120, 121]

To demonstrate an additional application of the designed calorimeter, measurements of excess molar enthalpy of methanol (CHROMASOLV™ ≥99.9%, Honeywell) and deionized water at 25 °C were carried out. Within the experiments a constant total flow rate of 4 ml min^{-1} was used while different flow rates of the respective pumps were set to obtain mixture data throughout the binary system.

3.3.12 Additional heat capacity measurements

The segment-wise control of each reaction sections makes it possible to set different temperatures and therefore gives another possibility to calculate heat capacities of the pumped liquids if the mass flux is known. For this kind of experiment, the precooling plate was set to 25 °C and both reaction segments were set to 23 °C. A different mode of operation like this requires a new calibration to recognize the heat necessary to decrease the flowing fluids temperature by the calorimeter. To prove this measurement principle, water was pumped through the calorimeter equally with both pumps at total flow rates of 2, 4, 6, 8, 10, 12 and 14 ml min^{-1}. Operating points between 2 and 10 ml min^{-1} were repeated twice.

3.4 Results and discussion

3.4.1 Reactor plate performance evaluation

Applicability of the designed reactor plate for fast reactions was evaluated prior to heat flux measurements. For this evaluation mixing performance of the reactor plate was investigated with a mixing sensitive reaction system proposed by Bourne *et al.* [1] Product formation and therefore decreasing yield of the bisazo dye *S* indicates a high mixing performance. As shown in Fig. 3.5, relatively low yields were obtained at total flow rates above 4 ml min^{-1} for the designed reactor plate. Therefore, the current calorimeter/reactor design should be operated at total flow rates above 4 ml min^{-1} to achieve sufficient mixing performance if the reaction is known to be fast and limited by mixing. Late mixing within the designed calorimeter would influence the product formation of a fast and mixing sensitive reaction but does not influence the heat flux detection. A reaction without mixing sensitivity would proceed to produce heat downstream until the fluid is well mixed and the reaction is completed.

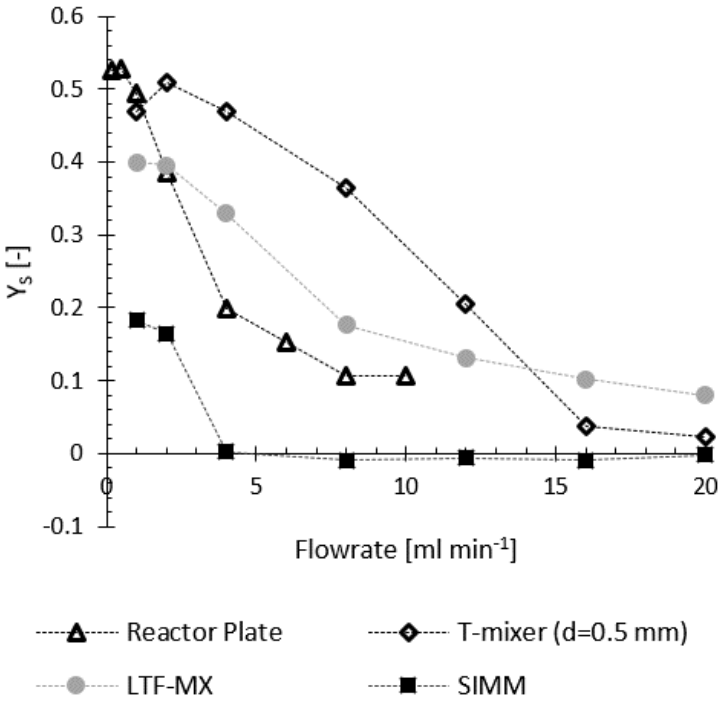

Figure 3.5: Evaluation of the reactor plate's mixing performance. Lower yield of the bisazo dye *S* at higher flow rates indicates increasing mixing performance. The evaluated reactor plate performed well compared to commercial mixers evaluated within literature. [35] It is compared to a standard T-mixer (Upchurch Scientific), an X-mixer (Little Things Factory GmbH, type X) and the Slit interdigital micromixer SIMM-V2-ss (Institut für Mikrotechnik Mainz GmbH).

A comparison of reactor performance with literature is possible with the Bourne re-

action since it was carried out at the proposed standard conditions. [108] Compared to commercial equipment, [35] the designed reactor plate performed very well. It is compared in Fig. 3.5 with a standard T-mixer (Upchurch Scientific), a X-mixer (Little Things Factory GmbH, type X) and the Slit interdigital micromixer SIMM-V2-ss (Institut für Mikrotechnik Mainz GmbH). This comparison is of course still dependent on the chosen pumps; however, both evaluations utilized high-accuracy syringe pumps and similar pumping performance can be assumed.

3.4.2 Calibration with integrated heating foils

Calibration of the calorimeter was carried out with the integrated heating foils for each element. As described above, each reactor segment was calibrated simultaneously by applying a known power input to the respective heating foil. With this direct calibration method, heat losses to the environment were assumed to be accounted for the obtained calibration.

The calibration at 25 °C for each reactor segment is shown in Fig. 3.6. As reported in literature, [69] a correlation of heat flux and thermoelectric voltage $U_{SE,i}$ of the respective Seebeck element was found in the form of a polynomial of second order. This polynomial matches to the theoretical Joule heating by electrical power input P expressed with electrical potential U, when assuming an ideal resistor R, and expressing electrical current with Ohm's law as shown in eqn 3.14.

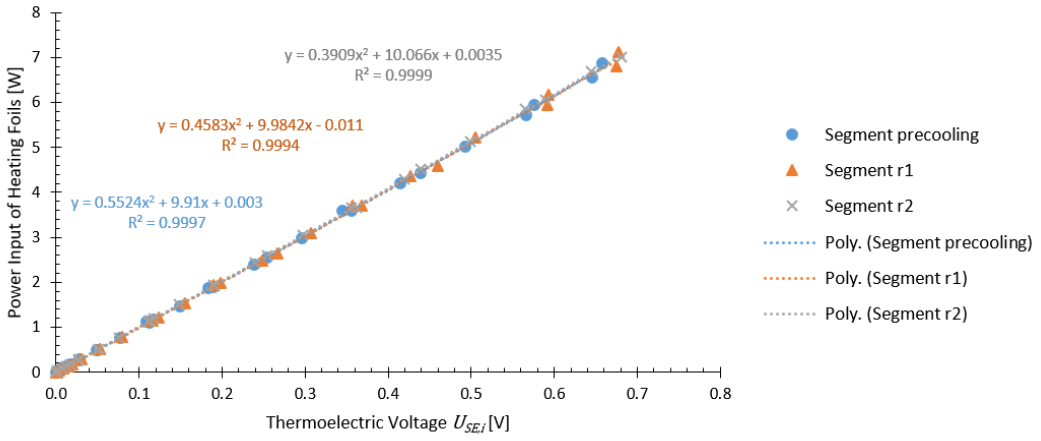

Figure 3.6: Calibration of the reactor segments with known heat fluxes produced by means of electrical energy. This calibration already accounts for the true resistance of each heating foil as well as the change of resistance with applied current.

$$P = U^2 \frac{1}{R} \tag{3.14}$$

Electrical resistance R of the individual element is dependent on temperature and

manufacturing for each element. Therefore, a calibration for each new set point needs to be made if any other operation temperature is needed. A correlation of set point temperature and heat flux calibration was not done within this work.

3.4.3 Functionality test with warm water

After obtaining a calibration for the calorimeter, a general functionality test was done. This experiment was meant to investigate the effects of unstable and varying inlet temperature on the calorimeter performance and to estimate the influence of temperature changes occurring within later operations. Therefore, warm water with changing temperature and different flow rates was pumped into the calorimeter to see how its regulation accounts for these changes. Additionally, with this experiment the outcome of changing inlet conditions on the calculated heat balance was evaluated.

Experimental data of this experiment can be seen in Fig. S3.6 and S3.7. Within this experiment, the necessary heat flux to cool down both feeds was calculated and compared to the heat capacity of water 75.34 J mol^{-1} K^{-1}. [122] A heat capacity of 73.36 J mol^{-1} K^{-1} with a variation of $\pm$2.62 J mol^{-1} K^{-1} was obtained from the measurements. Increasing accuracy of the measurement was seen at higher flow rates above 2 ml min^{-1} total flow rate. At these high flow rates, temperature measurements of in- and outlets can be expected to better represent the true fluid temperature in and out of the device because of heat losses between the sensors and the device. Excluding flow rates below 2 ml min^{-1} leads to a value of 75.74 J mol^{-1} K^{-1} with a variation of $\pm$1.18 J mol^{-1} K^{-1} for the remaining experiments. An accurate function of the device even at changing process conditions could be shown with a deviation of 0.53% of the mean value from the literature value.

3.4.4 Proof of concept AcOH–NaOH neutralization

The neutralization of AcOH with NaOH was chosen to evaluate the calorimeter's applicability for a fast chemical synthesis. The obtained data are depicted in Fig. 3.7 for different mole fluxes of AcOH at changing total flow rates.

From the obtained experimental data, (see Fig. S3.8-S3.10 for a comparison between experiments and Fig. S3.11-S3.18 for time resolved data of the respective measurement) it can be seen that at lower flow rates the reaction finished in the first reactor segment and only remaining heat gets transferred through convection to the second segment. Above flow rates of 6 ml min^{-1} a certain increase of detectable heat flux can be seen on the second segment. Most probably the reaction was shifted downstream at increasing flow rates. The pulsating nature of the *HPLC* pumps at higher flow rates is likely to be the main factor influencing this behaviour. Probably higher and lower concentrated plugs travel through the calorimeter and may experience back mixing to a uniform concentration field after a certain amount of mixing elements. Nevertheless, a constant operation for each measurement point was obtained after approximately 3 minutes.

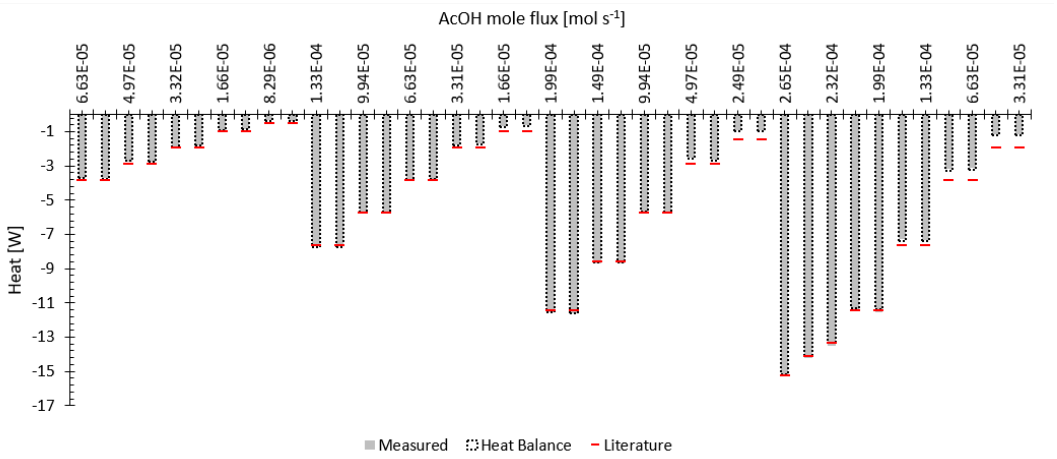

Figure 3.7: Neutralization of *AcOH* with *NaOH* with a comparison to the theoretical heat of neutralization for 1 mol of water. [123] The grey area represents the directly measured heat flux with indication of the energy balance shown by an extending frame.

Measured heat fluxes with contribution of the heat balance were compared to the expected neutralization enthalpy of -57.4 kJ mol^{-1} for the neutralization of *AcOH* with *NaOH*. [123] Within all evaluations, heat capacity of pure water was used for the calculations. All measurements obtained a reaction heat of -52.95 kJ mol^{-1} with a variation of $\pm$6.68 kJ mol^{-1}. As in the previous experiment, low total flow rates of 1 and 2 ml min^{-1} gave dramatically bigger errors compared to higher flow rates. Without these low flow rates, a reaction heat of -57.00 kJ mol^{-1} with a variation of $\pm$1.08 kJ mol^{-1} can be obtained from the measurements. The higher error occurring at lower flow rates was assumed to be caused by ineffective temperature measurements of the inlet stream due to heat losses. In this case, the heat balance was most probably not closed correctly.

3.4.5 Mixing heat of methanol and water

Molar excess enthalpy of methanol and water as a function of the mole fraction of water was chosen as an additional evaluation case. A total flow rate of 4 ml min^{-1} was constantly kept throughout the experiments as lower flow rates showed significantly reduced performances in previous experiments. Experimental data of this measurement can be found in Fig. S3.19 and S3.20.

In Fig. 3.8, the obtained measurements at 25 °C were compared to the literature values presented by Piñeiro *et al.* [114] A slight offset to the reported values from literature can be detected but the general shape of the curve was perfectly mimicked by the obtained measurement data. Apart from the qualitative comparison of the two curves, no further evaluations were carried out with the data at current state.

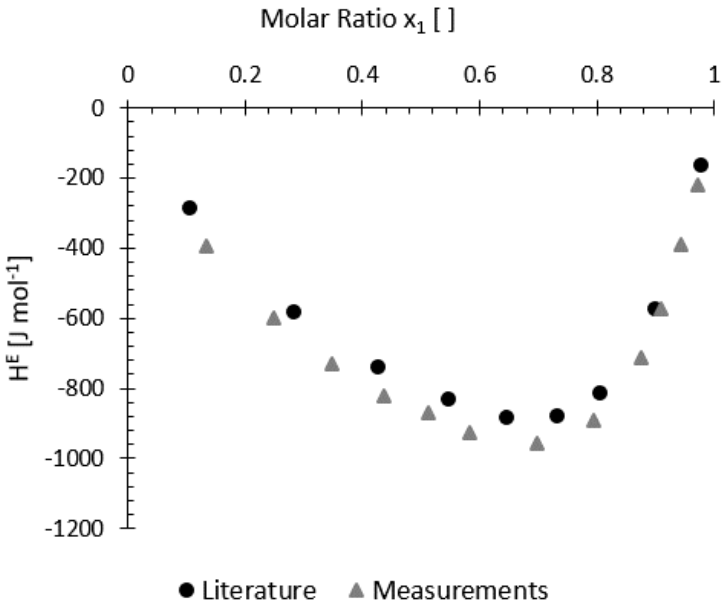

Figure 3.8: Measured molar excess enthalpy H E at 298.15 K for water (1) + methanol (2). With a slight offset, the obtained data nicely resembles measurements from literature. [114]

3.4.6 Additional heat capacity measurements

Heat capacity of water was measured in a different mode of operation by performing a temperature change of 2 °C between the calorimeter segments. This new configuration required a new calibration (see Fig. S3.21).

From all measurements a heat capacity of 80.45 J mol^{-1} K^{-1} with a variation of ±7.51 J mol^{-1} K^{-1} was obtained. In contrast to the other measurements, discarding low flow rates did not shift the obtained value closer to the literature value of 75.34 J mol^{-1} K^{-1} (ref. [122]) but the variance of measurement did improve. Without low flow rates, a heat capacity of 84.01 J mol^{-1} K^{-1} with a variation of ±2.70 J mol^{-1} K^{-1} was measured.

As seen from the experimental data during measurements (see Fig. S3.22 and S3.23), this temperature jump did not produce a high change in recognizable heat flux due to the low temperature difference. Increasing measurement error can be attributed to the small detectable heat flux where reduced measurement efficiency can be expected. This problem could be solved by applying greater temperature jumps between the segments. But accurate heat capacity measurements are generally shown with an experimental setup as reported before within the functionality test with warm water.

3.5 Conclusions

A modular reaction calorimeter is presented for direct and isothermal heat flux measurements intended to be used for highly reactive organic compounds as commonly found in flow chemistry. Its design is based on a combination of commercially available electronics and additive manufacturing. With this combination, elements can be adapted and reassembled easily to fit specific applications. To ensure isothermal operation, calorimeter segments are temperature-regulated independently from each other by means of a microcontroller-based Peltier cooling. Internally-calibrated Seebeck elements measure the transferred heat flux of each calorimeter segment.

The designed calorimeter was validated with a series of experiments which produce a well-known heat flux. Through these experiments, the calorimeter design was proven to be applicable to measure reaction heats of fast reactions, important material properties like specific heat capacities, and system-specific properties as molar excess enthalpies.

Improvements of mixing performance for lower flow rates should still be considered for future models of the reactor plate. Adaptations of the existing calorimeter can be easily made due to its modular design. The reactor plate used can be exchanged to meet the requirements of different flow syntheses for higher or lower flow rates to provide additional mixing performance if required. In addition, additional connector ports can be added to the design if mixing of multiple streams is desired.

Future work will focus on extending the reactor plate to increase internal volume of the device as well as the addition of smaller Seebeck elements for a more locally resolved measurement. Further improvements of the setup will be made by coupling a controllable heat exchanger to both inlets for a precise preconditioning of the streams. Additionally, it is planned to investigate hazardous chemical syntheses with the current device as well as with advanced versions of it.

3.6 Conflicts of interest

There are no conflicts to declare.

3.7 Acknowledgements

The authors would like to thank Stefan Scheer (Technical University Graz) for his support. The CCFLOW project (Austrian Research Promotion Agency FFG No. 862766) is funded through the Austrian COMET Program by the Austrian Federal Ministry of Transport, Innovation and Technology (BMVIT), the Austrian Federal Ministry of Science, Research and Economy (BMWFW) and by the State of Styria (Styrian Funding Agency SFG).

Appendices

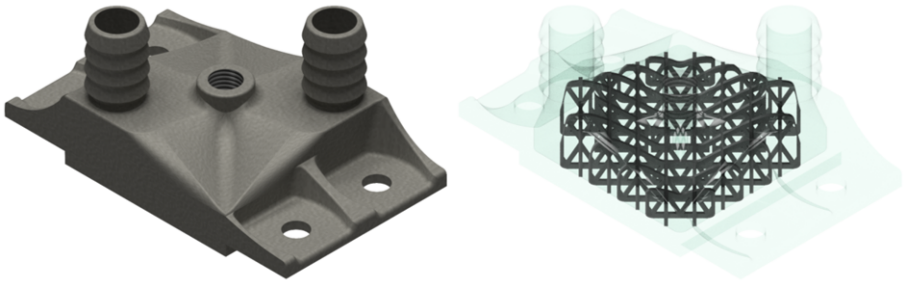

Supporting Information Figure S3.1: *CAD* image of a cooling block with its internal support structure. This support provides necessary connection between layers during fabrication and increases the internal contact area for heat transfer of the coolant to the metal.

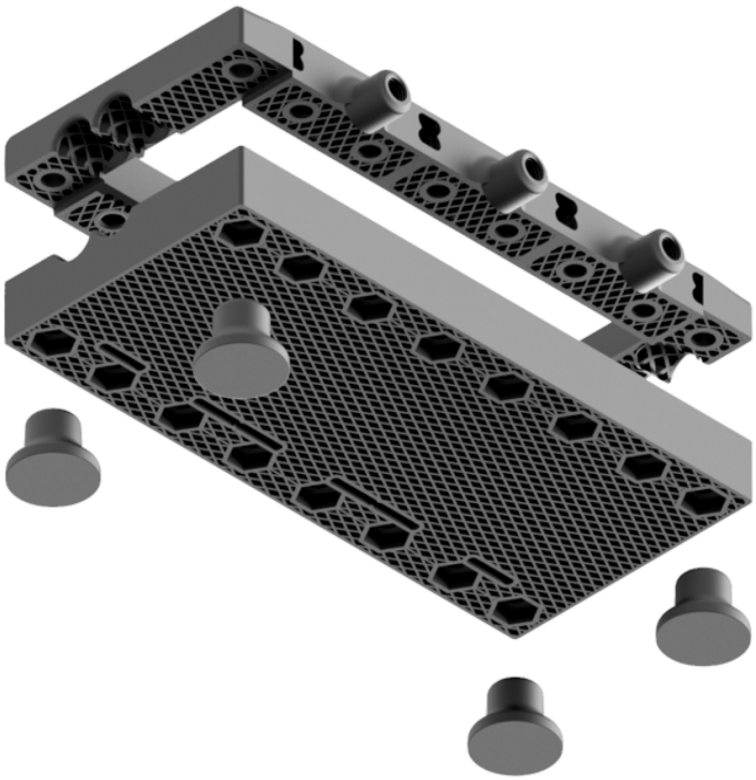

Supporting Information Figure S3.2: *CAD* image of casing elements, base plate, and feet. All parts were manufactured with a *UV*-curable resin printed by a *DLP* printer without additional printing support. Prism like internal structure was added to increase mechanical strength and provide a layer wise connection.

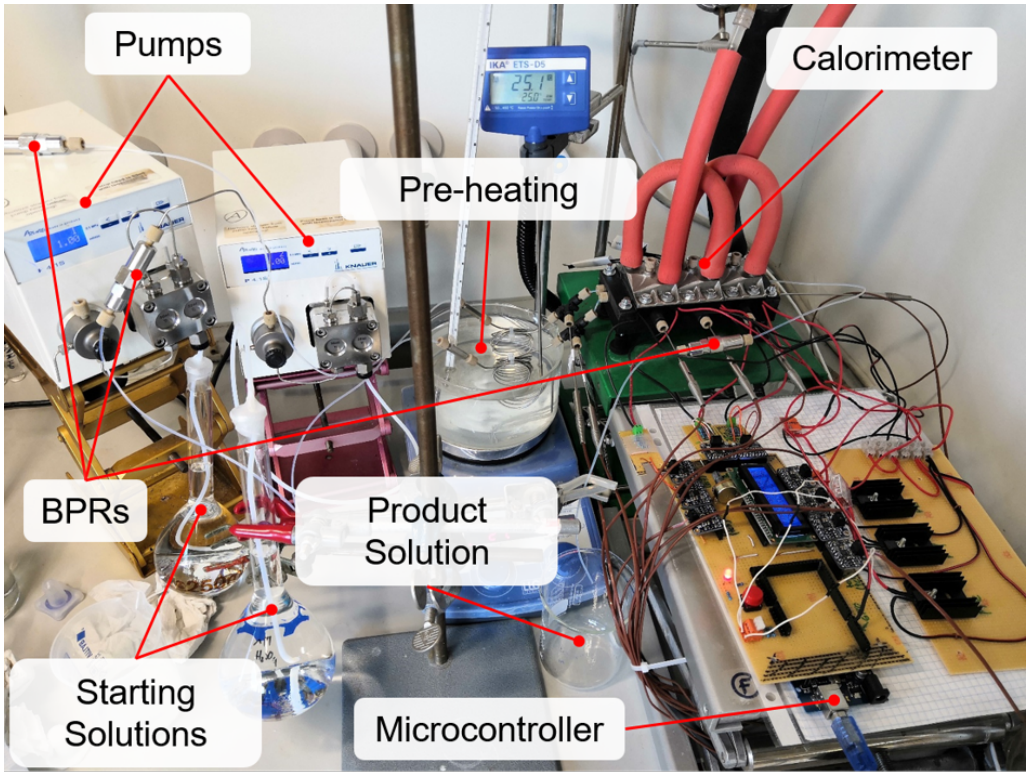

Supporting Information Figure S3.3: Picture of the experimental setup used for the neutralization experiments. The designed calorimeter can be seen in the right corner of the fume hood. In front of it is the control circuit connected to a PC.

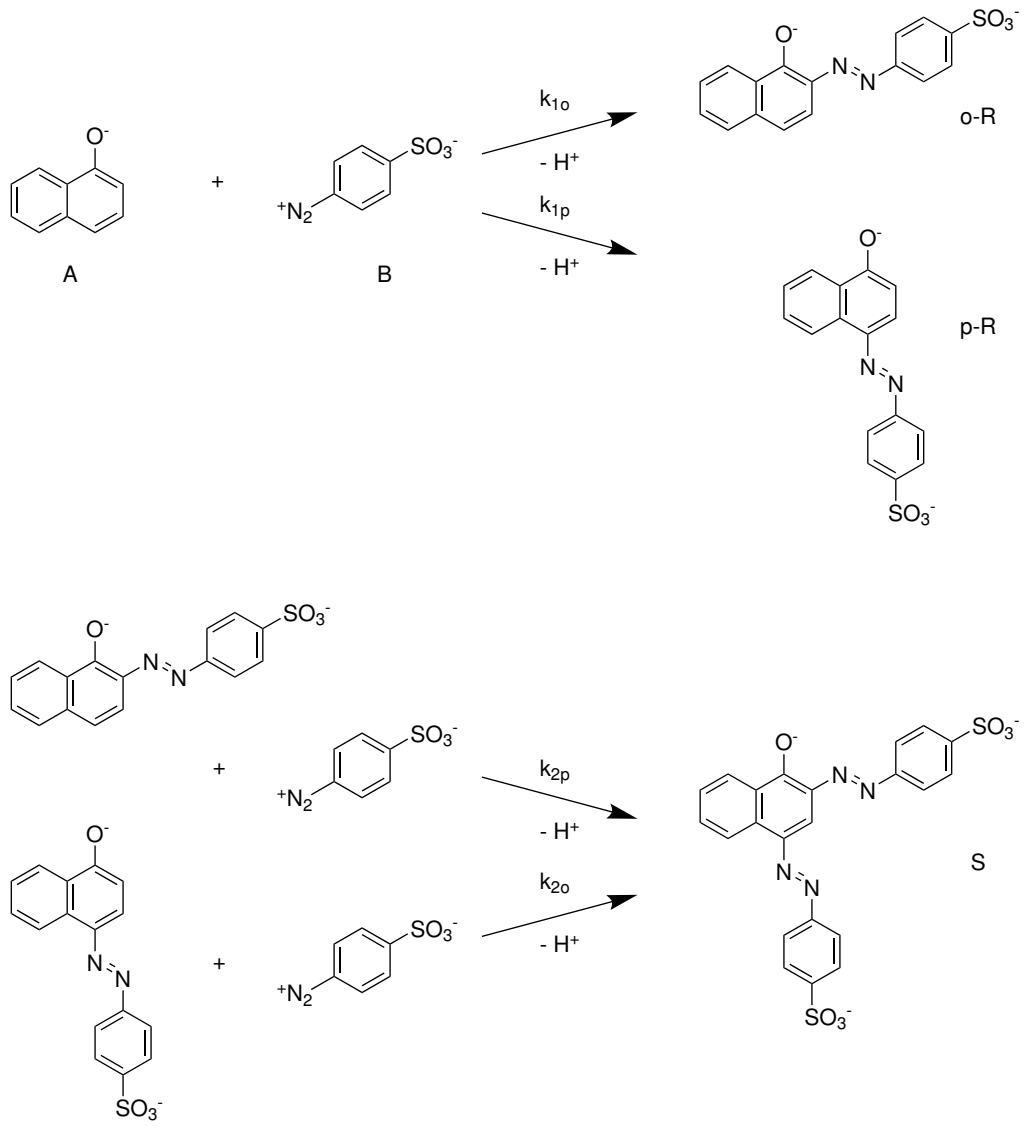

Supporting Information Figure S3.4: Mechanism of the Bourne reaction, as described by J. R. Bourne, O. M. Kut, J. Lenzner and H. Maire, Ind. Eng. Chem. Res., 1990, 29, 1761–1765.

In the next figures, the following temperatures are shown: Set temperature of the regulation, T_set; Temperature of the pre-cooling segment, T_pre; Temperature of the reactor segment r1, T_r1; Temperature of the reactor segment r2, T_r2; Temperature measured at inlet A (used for AcOH during neutralizations), T_A; Temperature measured at inlet B (used for NaOH during neutralizations), T_B; Outlet temperature, T_out. Arrows in the figures indicate total flow rates unless stated otherwise.

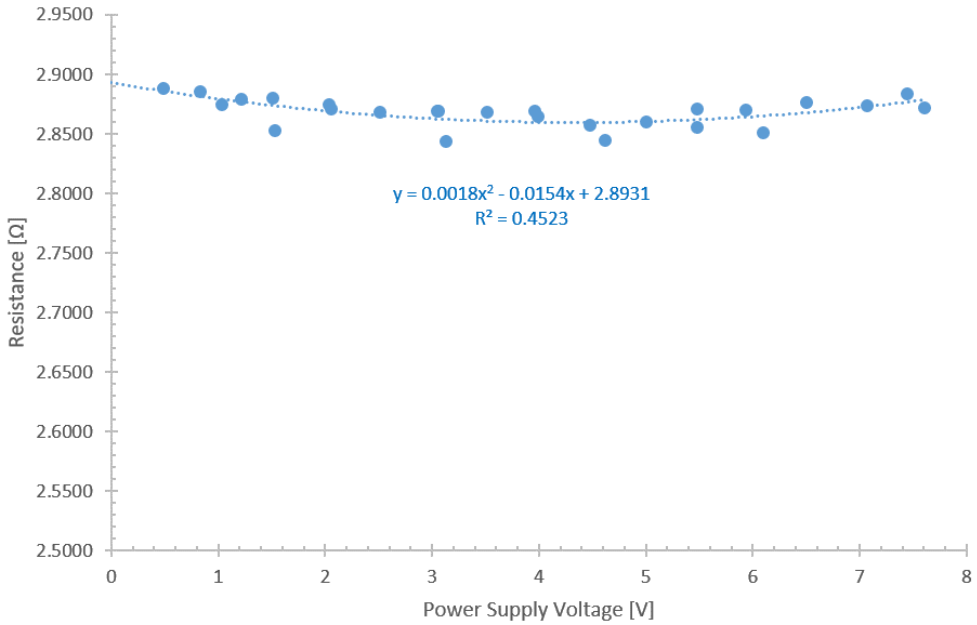

Supporting Information Figure S3.5: Change of heating foil resistance during calibration. This change was accounted within the calibration.

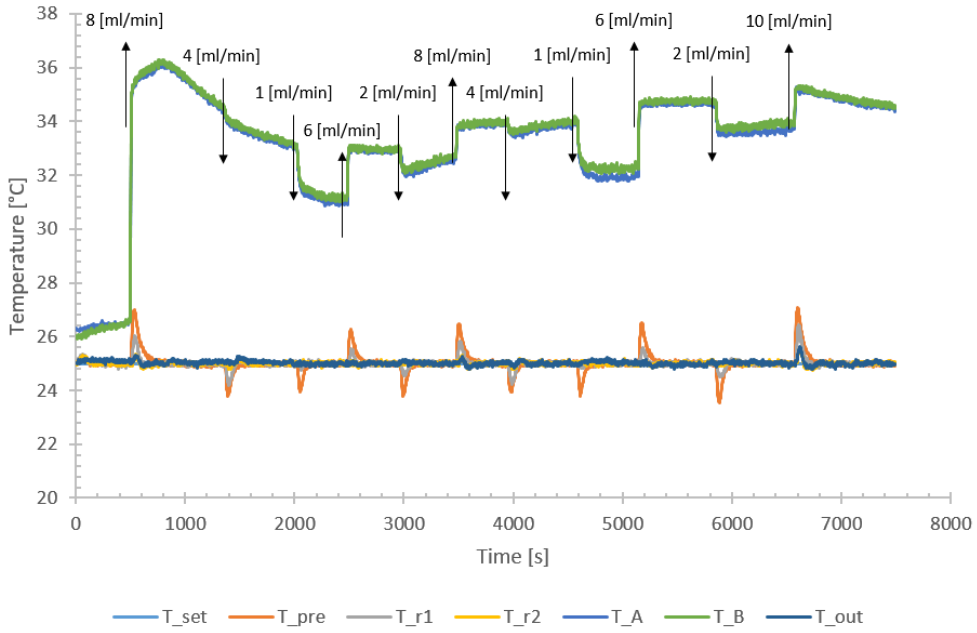

Supporting Information Figure S3.6: Warm water experiment. Shown are the measured temperatures at different positions and at different flow rates (given in ml/min) of the fed water.

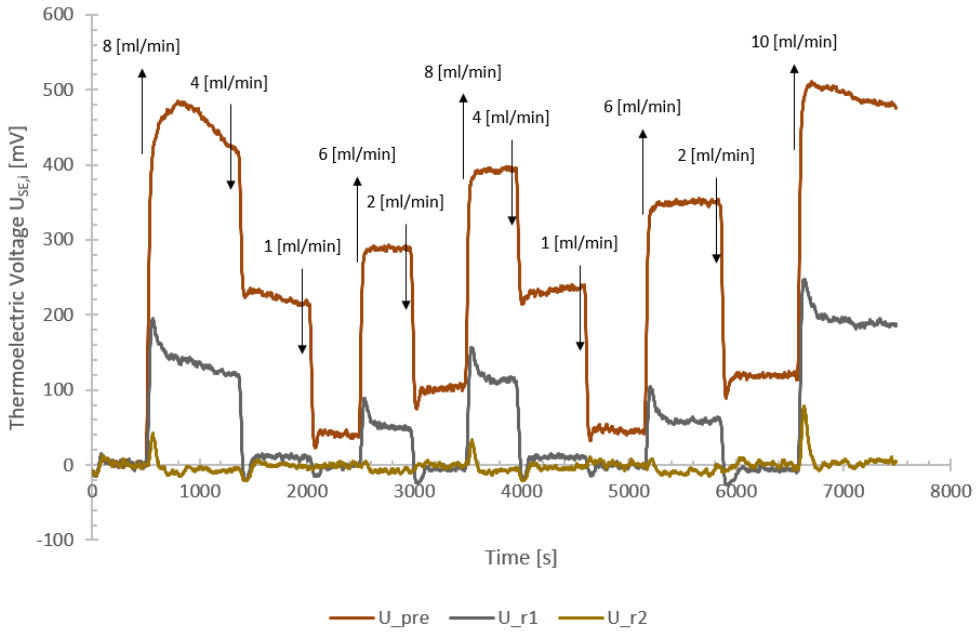

Supporting Information Figure S3.7: Warm water experiment. Shown are the measured voltages at different positions and at different flow rates (given in ml/min) of the fed water.

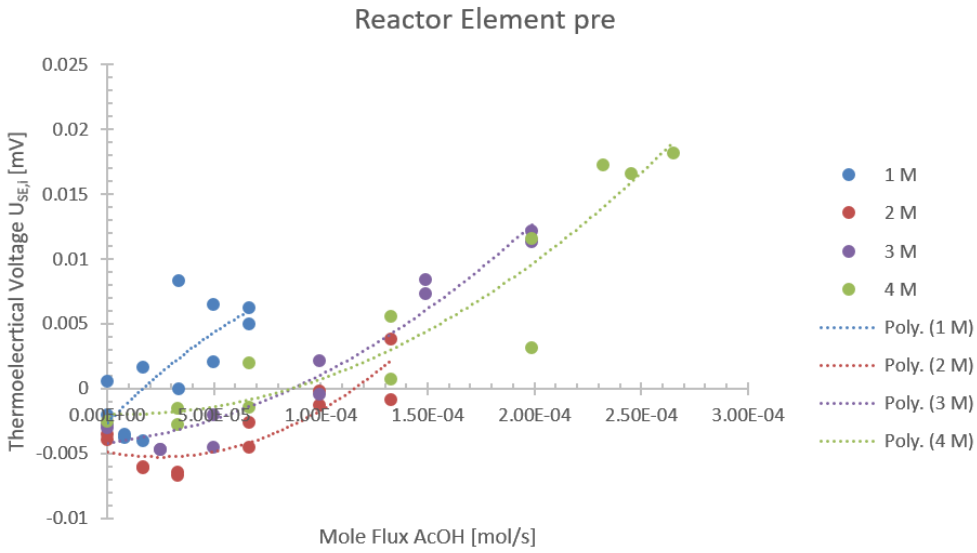

Supporting Information Figure S3.8: Neutralization of acetic acid with sodium hydroxide. Heat flux measured at the precooling element.

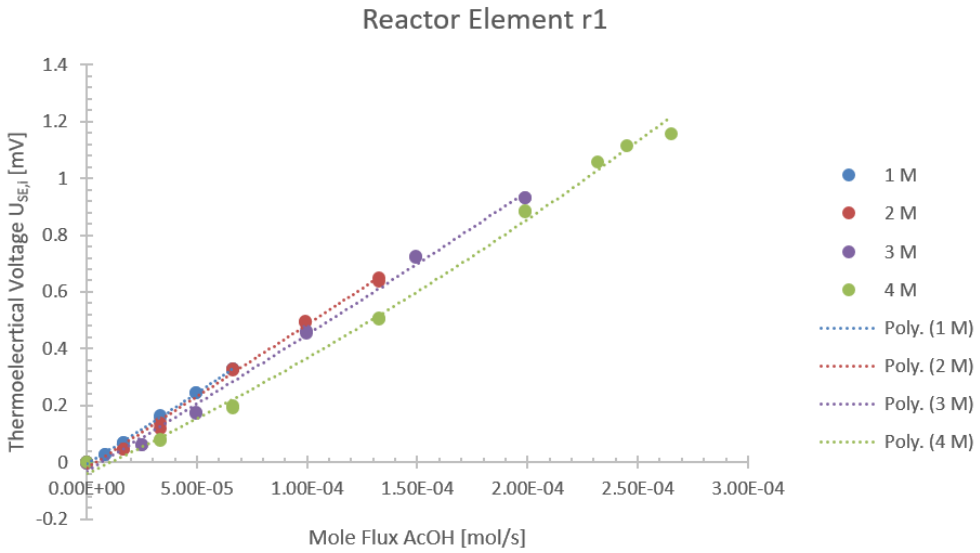

Supporting Information Figure S3.9: Neutralization of acetic acid with sodium hydroxide. Heat flux measured at the reactor element r1.

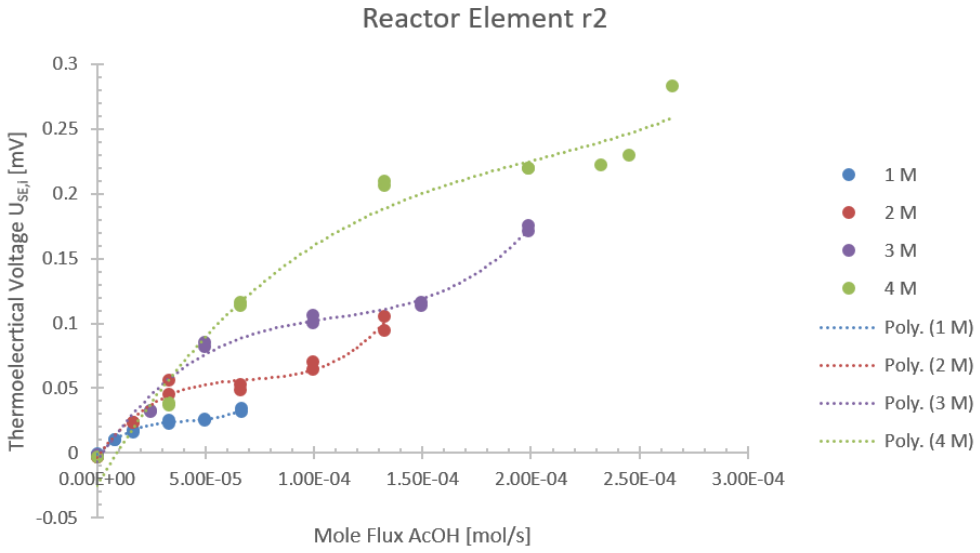

Supporting Information Figure S3.10: Neutralization of acetic acid with sodium hydroxide. Heat flux measured at the reactor element r2.

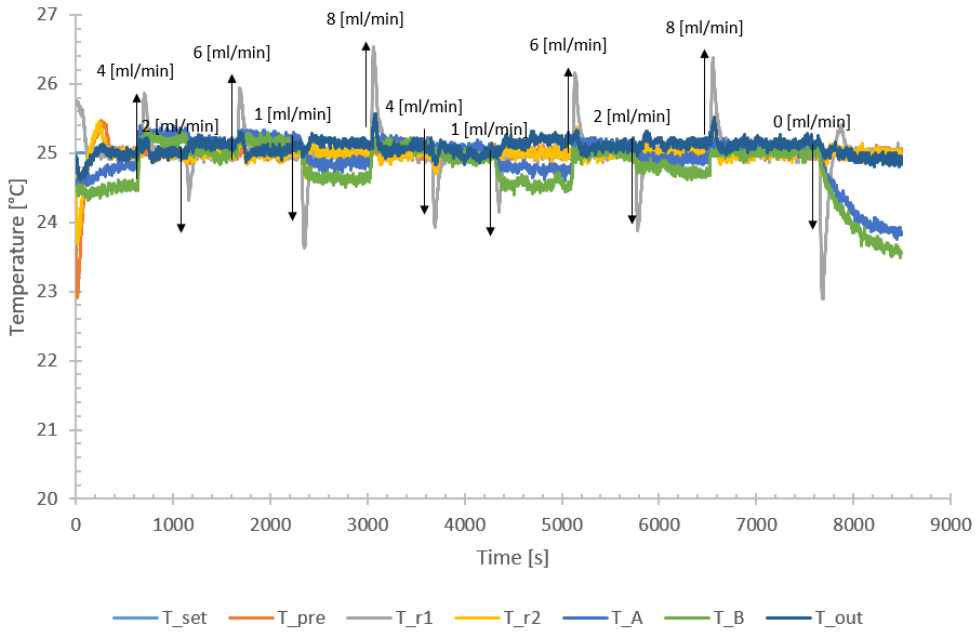

Supporting Information Figure S3.11: Neutralization of 1 M acetic acid with 1 M sodium hydroxide. Temperatures measured at different total flow rates.

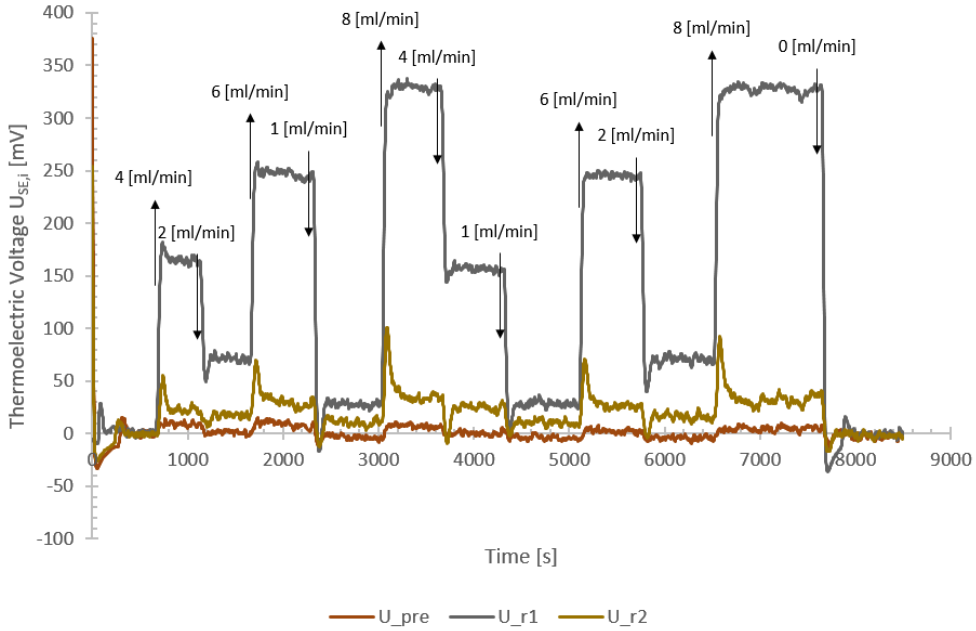

Supporting Information Figure S3.12: Neutralization of 1 M acetic acid with 1 M sodium hydroxide. Voltages measured at different total flow rates.

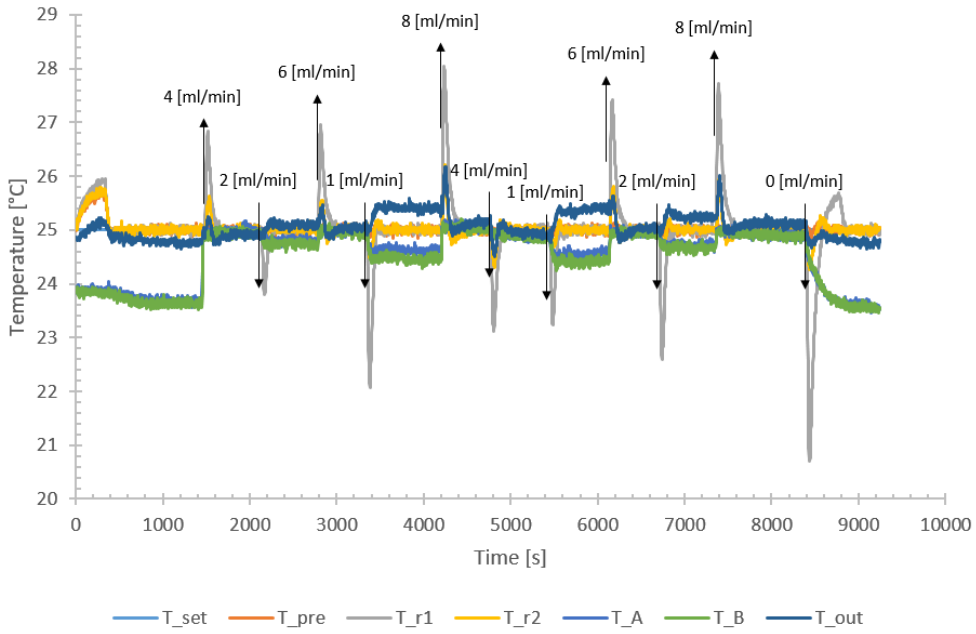

Supporting Information Figure S3.13: Neutralization of 2 M acetic acid with 2 M sodium hydroxide. Temperatures measured at different total flow rates.

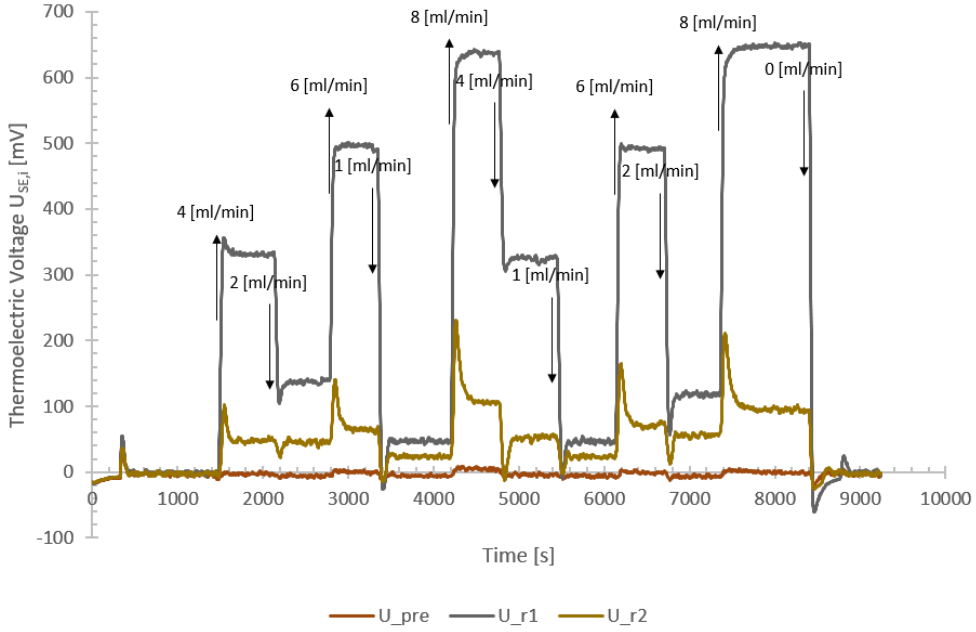

Supporting Information Figure S3.14: Neutralization of 2 M acetic acid with 2 M sodium hydroxide. Voltages measured at different total flow rates.

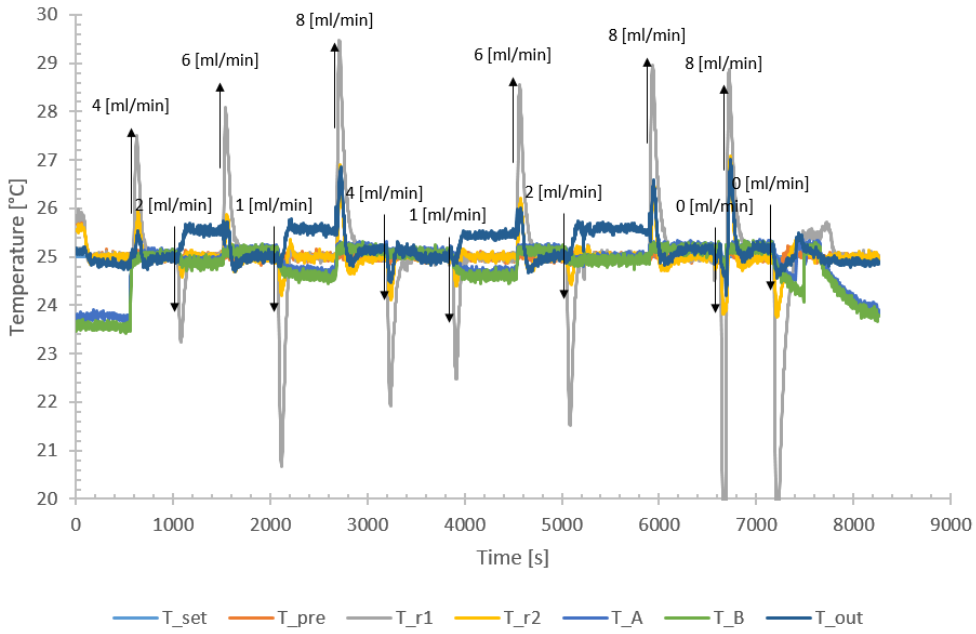

Supporting Information Figure S3.15: Neutralization of 3 M acetic acid with 3 M sodium hydroxide. Temperatures measured at different total flow rates.

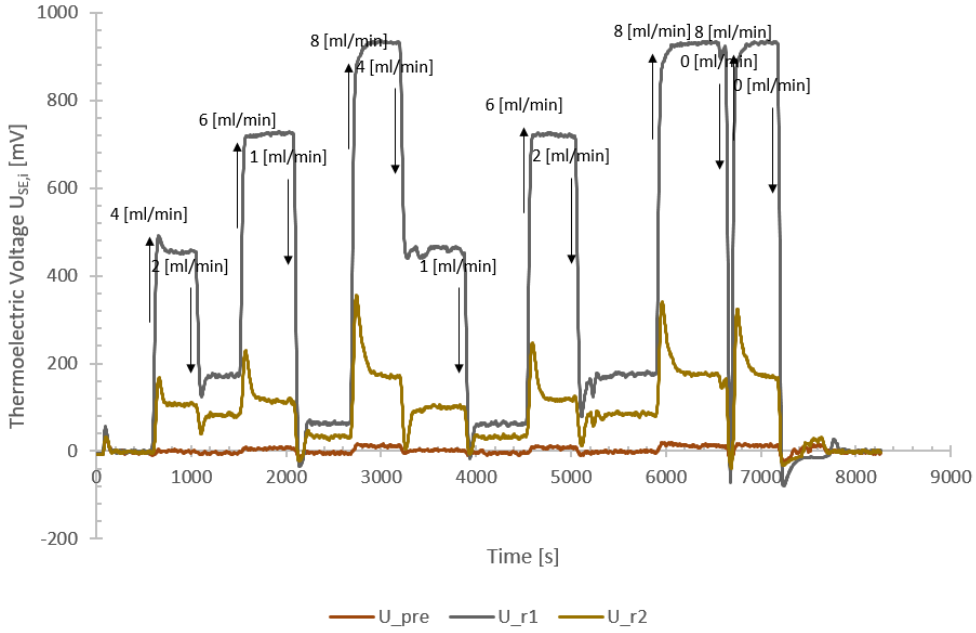

Supporting Information Figure S3.16: Neutralization of 3 M acetic acid with 3 M sodium hydroxide. Voltages measured at different total flow rates.

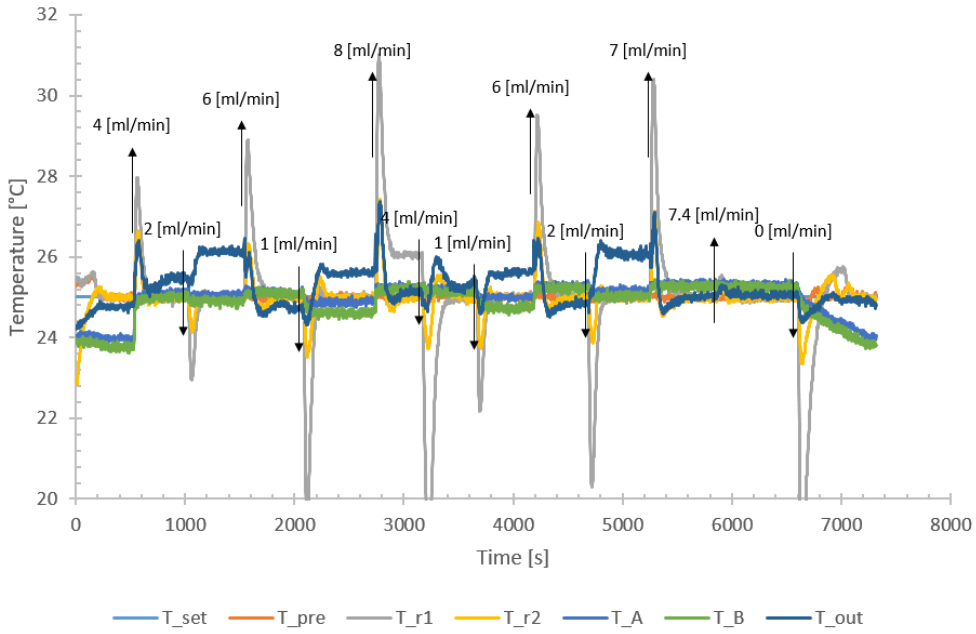

Supporting Information Figure S3.17: Neutralization of 4 M acetic acid with 4 M sodium hydroxide. Temperatures measured at different total flow rates.

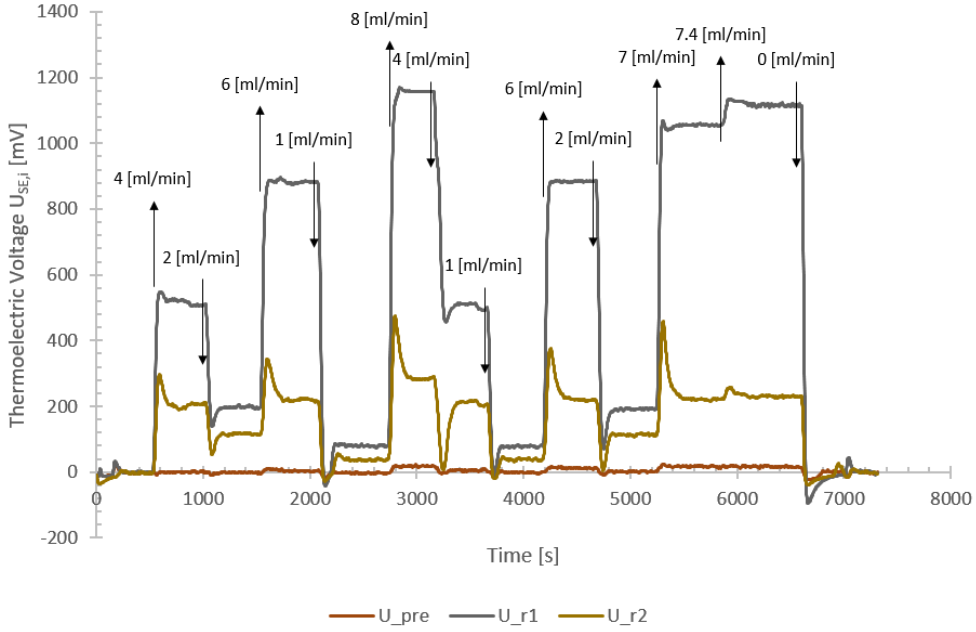

Supporting Information Figure S3.18: Neutralization of 4 M acetic acid with 4 M sodium hydroxide. Voltages measured at different total flow rates.

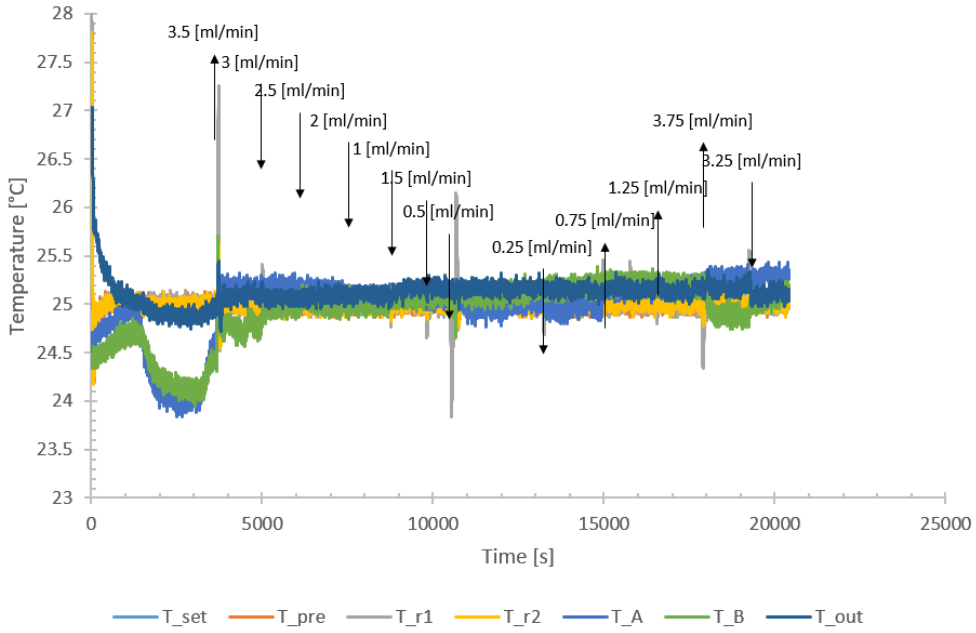

Supporting Information Figure S3.19: Mixing heat of MeOH and water. Temperatures during measurement. Total flow rate was 4 mlmin for all operation points and the shown arrows indicate water flow rate.

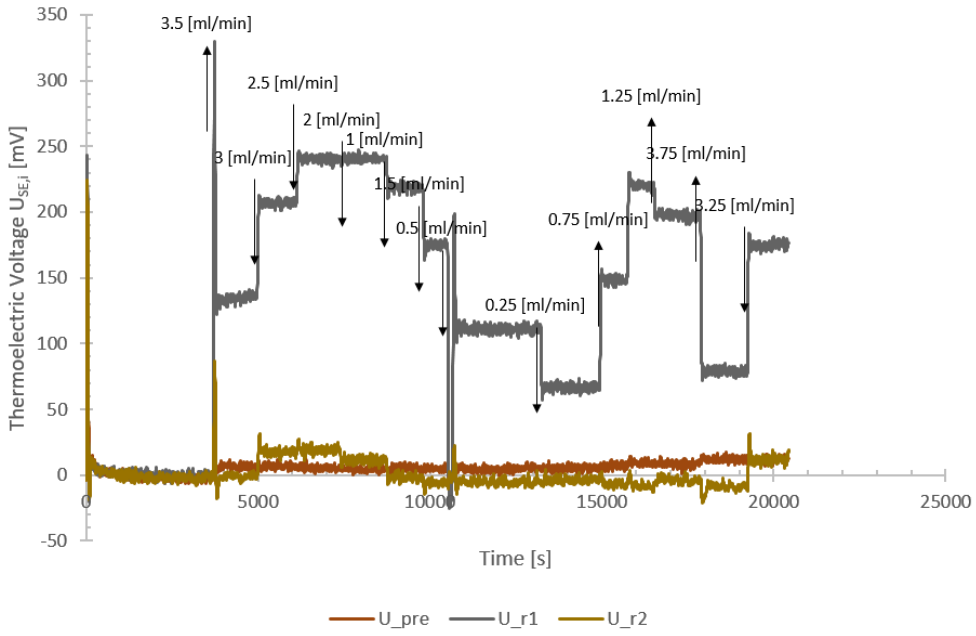

Supporting Information Figure S3.20: Mixing heat of MeOH and water. Voltages during measurement. Total flow rate was 4 mlmin for all operation points and the shown arrows indicate water flow rate.

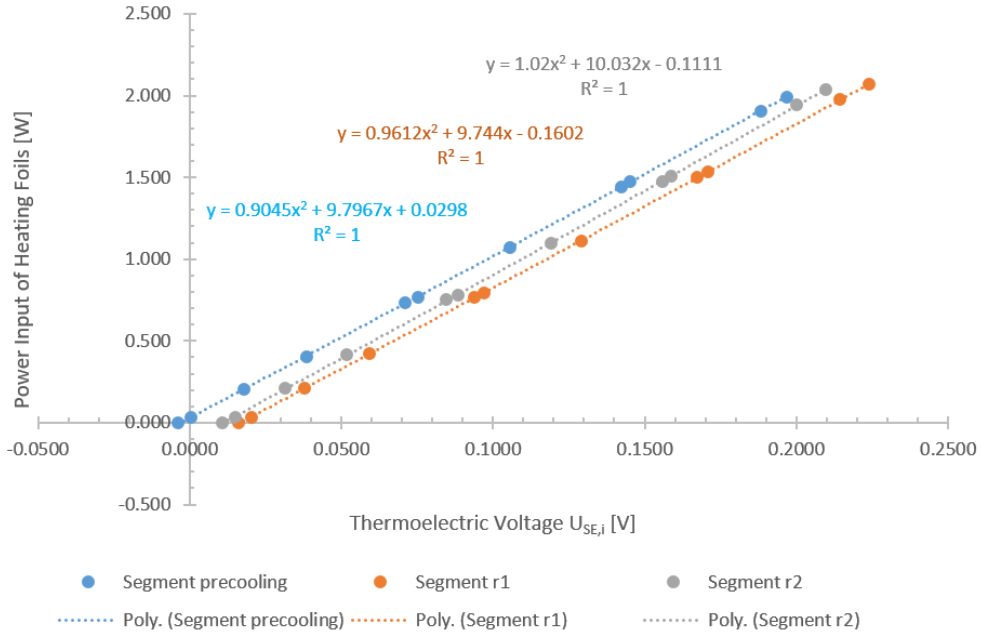

Supporting Information Figure S3.21: New calibration for the heat capacity measurement. This calibration was needed since cooling of the reactor segments to 23 °C also reduced the temperature in the precooling element. Therefore, the thermostat was set to a higher value to provide enough heat for the precooling element to be held at 25 °C.

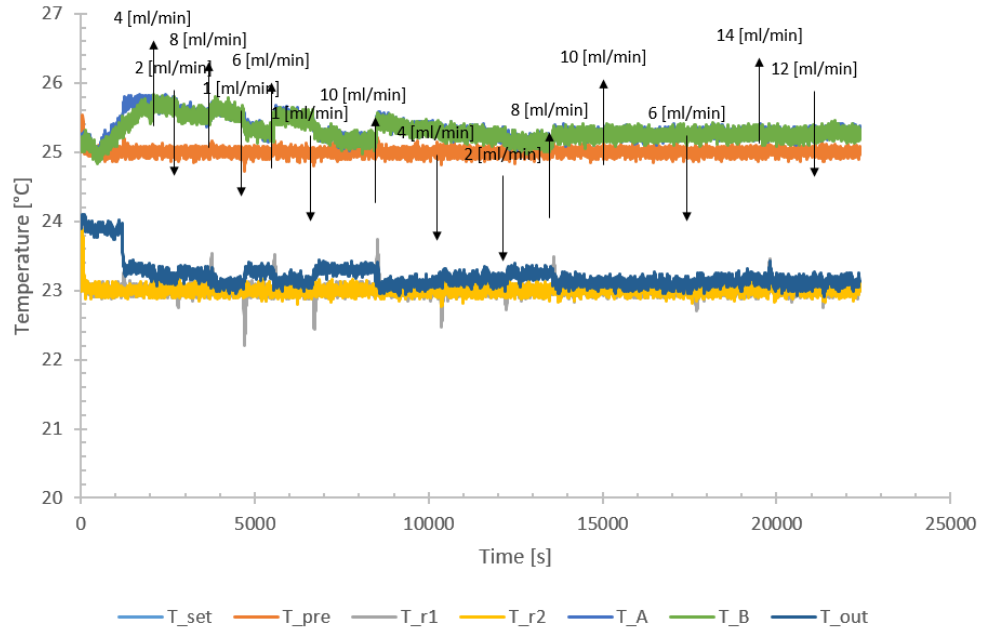

Supporting Information Figure S3.22: Heat capacity measurement of water. Temperatures measured at different total flow rates.

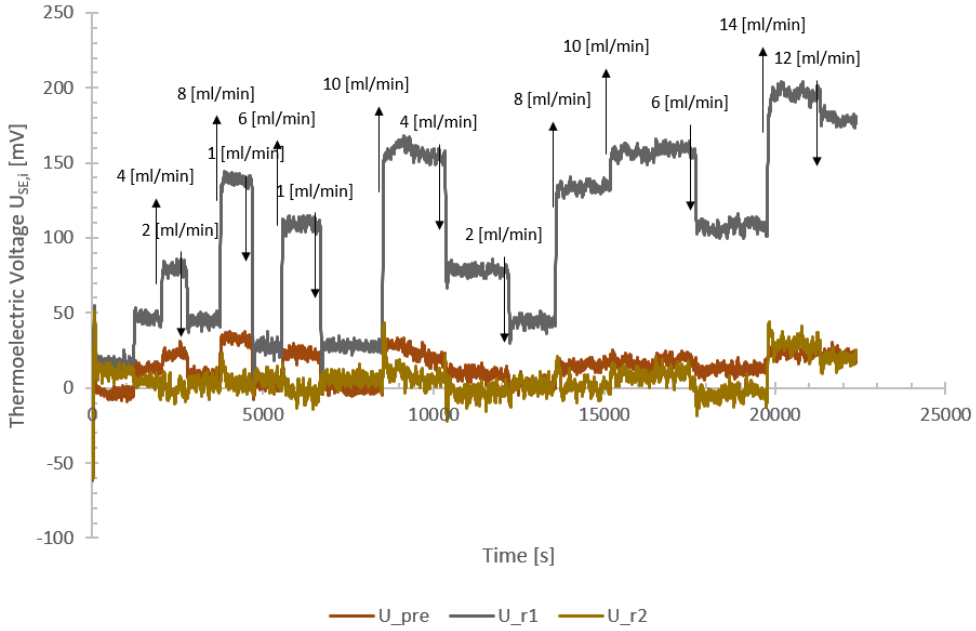

Supporting Information Figure S3.23: Heat capacity measurement of water. Voltages measured at different total flow rates.

Bibliography

[1] John R. Bourne, Oemer M. Kut, Joachim Lenzner, and Horst Maire. "Kinetics of the diazo coupling between 1-naphthol and diazotized sulfanilic acid". In: *Industrial & Engineering Chemistry Research* 29.9 (Sept. 1990), pp. 1761–1765. ISSN: 0888-5885. DOI: 10.1021/ie00105a004. URL: http://pubs.acs.org/doi/abs/10.1021/ie00105a004%20https://pubs.acs.org/doi/abs/10.1021/ie00105a004.

[8] Manuel C. Maier, René Lebl, Philipp Sulzer, Josef Lechner, Torsten Mayr, Matej Zadravec, Eyke Slama, Stefan Pfanner, Christoph Schmölzer, Peter Pöchlauer, C. Oliver Kappe, and Heidrun Gruber-Woelfler. "Development of customized 3D printed stainless steel reactors with inline oxygen sensors for aerobic oxidation of Grignard reagents in continuous flow". In: *Reaction Chemistry and Engineering* 4.2 (2019), pp. 393–401. ISSN: 20589883. DOI: 10.1039/C8RE00278A. URL: http://xlink.rsc.org/?DOI=C8RE00278A.

[16] Matthew B. Plutschack, Bartholomäus Pieber, Kerry Gilmore, and Peter H. Seeberger. "The Hitchhiker's Guide to Flow Chemistry". In: *Chemical Reviews* 117.18 (Sept. 2017), pp. 11796–11893. ISSN: 0009-2665. DOI: 10.1021/acs.chemrev.7b00183. URL: http://pubs.acs.org/doi/10.1021/acs.chemrev.7b00183.

[22] V Hessel, S Hardt, and H Löwe. *Chemical Micro Process Engineering: Fundamentals, Modelling and Reactions*. Weinheim: Wiley-VCH, 2004. ISBN: 9783527307418. DOI: 10.1002/3527603042.

[23] Norbert Kockmann. "Pressure loss and transfer rates in microstructured devices with chemical reactions". In: *Chemical Engineering and Technology* 31.8 (2008), pp. 1188–1195. ISSN: 09307516. DOI: 10.1002/ceat.200800065.

[26] Thomas Westermann and Leslaw Mleczko. "Heat Management in Microreactors for Fast Exothermic Organic Syntheses—First Design Principles". In: *Organic Process Research & Development* 20.2 (Feb. 2016), pp. 487–494. ISSN: 1083-6160. DOI: 10.1021/acs.oprd.5b00205. URL: https://pubs.acs.org/doi/10.1021/acs.oprd.5b00205.

[34] M.-C. Fournier, L. Falk, and J. Villermaux. "A new parallel competing reaction system for assessing micromixing efficiency—Experimental approach". In: *Chemical Engineering Science* 51.22 (Nov. 1996), pp. 5053–5064. ISSN: 00092509. DOI: 10.1016/0009-2509(96)00270-9. URL: https://linkinghub.elsevier.com/retrieve/pii/0009250996002709.

[35] Sebastian Schwolow, Jutta Hollmann, Berthold Schenkel, and Thorsten Röder. "Application-Oriented Analysis of Mixing Performance in Microreactors". In: *Organic Process Research & Development* 16.9 (Sept. 2012), pp. 1513–1522. ISSN: 1083-6160. DOI: 10.1021/op300107z. URL: http://pubs.acs.org/doi/10.1021/op300107z.

[56] Andreas Zogg, Francis Stoessel, Ulrich Fischer, and Konrad Hungerbühler. "Isothermal reaction calorimetry as a tool for kinetic analysis". In: *Thermochimica Acta* 419.1-2 (Sept. 2004), pp. 1–17. ISSN: 00406031. DOI: 10.1016/j.tca.2004.01.015. URL: https://linkinghub.elsevier.com/retrieve/pii/S0040603104000486.

[63] Gabriel Glotz, Donald J. Knoechel, Philip Podmore, Heidrun Gruber-Woelfler, and C. Oliver Kappe. "Reaction Calorimetry in Microreactor Environments - Measuring Heat of Reaction by Isothermal Heat Flux Calorimetry". In: *Organic Process Research and Development* 21.5 (2017), pp. 763–770. ISSN: 1520586X. DOI: 10.1021/acs.oprd.7b00092.

[64] M. A. Schneider and F. Stoessel. "Determination of the kinetic parameters of fast exothermal reactions using a novel microreactor-based calorimeter". In: *Chemical Engineering Journal* 115.1-2 (2005), pp. 73–83. ISSN: 13858947. DOI: 10.1016/j.cej.2005.09.019.

[65] Cindy Hany, Christophe Pradere, Jean Toutain, and Jean-Christophe Batsale. "A millifluidic calorimeter with infrared thermography for the measurement of chemical reaction enthalpy and kinetics". In: *Quantitative InfraRed Thermography Journal* 5.2 (Dec. 2008), pp. 211–229. ISSN: 1768-6733. DOI: 10.3166/qirt.5.211-229. URL: http://www.tandfonline.com/doi/abs/10.3166/qirt.5.211-229.

[66] J.Michael Köhler and Martin Zieren. "Chip reactor for microfluid calorimetry". In: *Thermochimica Acta* 310.1-2 (Feb. 1998), pp. 25–35. ISSN: 00406031. DOI: 10.1016/S0040-6031(97)00381-X. URL: https://linkinghub.elsevier.com/retrieve/pii/S004060319700381X.

[67] Yuyan Zhang and Srinivas Tadigadapa. "Calorimetric biosensors with integrated microfluidic channels". In: *Biosensors and Bioelectronics* 19.12 (July 2004), pp. 1733–1743. ISSN: 09565663. DOI: 10.1016/j.bios.2004.01.009. URL: https://linkinghub.elsevier.com/retrieve/pii/S0956566304000260.

[68] S Loebbecke, J Antes, W Ferstl, D Boskovic, T Tuercke, M Schwarzer, and H Krause. "Microreactors for processing of hazardous and explosible reactions". In: *Institution of Chemical Engineers Symposium Series* 153 (2007), pp. 1–6. URL: https://www.mendeley.com/catalogue/microreactors-processing-hazardous-explosive-reactions/.

[69] Felix Reichmann, Stefan Millhoff, Yannick Jirmann, and Norbert Kockmann. "Reaction Calorimetry for Exothermic Reactions in Plate-Type Microreactors Using Seebeck Elements". In: *Chemical Engineering & Technology* 40.11 (Nov. 2017), pp. 2144–2154. ISSN: 09307516. DOI: 10.1002/ceat.201700419. URL: http://doi.wiley.com/10.1002/ceat.201700419.

[77] M. Movsisyan, E. I. P. Delbeke, J. K. E. T. Berton, C. Battilocchio, S. V. Ley, and C. V. Stevens. "Taming hazardous chemistry by continuous flow technology". In: *Chemical Society Reviews* 45.18 (2016), pp. 4892–4928. ISSN: 0306-0012. DOI: 10.1039/C5CS00902B. URL: http://xlink.rsc.org/?DOI=C5CS00902B.

[79] Norbert Kockmann, Philipp Thenée, Christoph Fleischer-Trebes, Gabriele Laudadio, and Timothy Noël. "Safety assessment in development and operation of modular continuous-flow processes". In: *Reaction Chemistry & Engineering* 2.3 (2017), pp. 258–280. ISSN: 2058-9883. DOI: 10.1039/C7RE00021A. URL: http://xlink.rsc.org/?DOI=C7RE00021A.

[93] Bernhard Gutmann, Manuel Köckinger, Gabriel Glotz, Tania Ciaglia, Eyke Slama, Matej Zadravec, Stefan Pfanner, Manuel C. Maier, Heidrun Gruber-Wölfler, and C. Oliver Kappe. "Design and 3D printing of a stainless steel reactor for continuous difluoromethylations using fluoroform". In: *Reaction Chemistry & Engineering* 2.6 (2017), pp. 919–927. ISSN: 2058-9883. DOI: 10.1039/C7RE00176B. URL: http://xlink.rsc.org/?DOI=C7RE00176B.

[108] J. Bałdyga, J.R. Bourne, and S.J. Hearn. "Interaction between chemical reactions and mixing on various scales". In: *Chemical Engineering Science* 52.4 (Feb. 1997), pp. 457–466. ISSN: 00092509. DOI: 10.1016/S0009-2509(96)00430-7. URL: http://linkinghub.elsevier.com/retrieve/pii/S0009250996004307.

[112] Mettler Toledo. *Reaction Calorimeter RC1*. URL: https://www.mt.com/int/en/home/products/L1_AutochemProducts/Reaction-Calorimeters-RC1-HFCal/RC1mx-Reaction-Calorimeter.html (visited on 11/13/2019).

[113] Andreas Zogg, Ulrich Fischer, and Konrad Hungerbühler. "A new small-scale reaction calorimeter that combines the principles of power compensation and heat balance". In: *Industrial and Engineering Chemistry Research* 42.4 (2003), pp. 767–776. ISSN: 08885885. DOI: 10.1021/ie0201258.

[114] Ángel Piñeiro, Ángeles Olvera, Gonzalo García-Miaja, and Miguel Costas. "Excess Molar Enthalpies of Tetrahydrofuran or Diisopropyl Ether + 1-Alkanols at 298.15 K, Using a Newly Designed Flow Mixing Cell for an Isothermal Microcalorimeter". In: *Journal of Chemical & Engineering Data* 46.5 (Sept. 2001), pp. 1274–1279. ISSN: 0021-9568. DOI: 10.1021/je0100645. URL: https://pubs.acs.org/doi/10.1021/je0100645.

[115] Thermal Hazard technology and Thermal hazard technology. *Micro Reaction Calorimeter - μRC*. URL: http://www.thermalhazardtechnology.com/products/micro+reaction+calorimeter (visited on 11/03/2019).

[116] Agnieszka Ladosz, Andrew R. Teixeira, Baptiste Hardy, Isaac Roes, Jason Moore, and Klavs F. Jensen. "Microscale calorimetry: measuring heat of reaction in flow". In: *Poster pres. at, International Conference on Micro Reaction Technology - IMRET 2018, Karlsruhe* ().

[117] L. Falk and J.-M. M. Commenge. "Performance comparison of micromixers". In: *Chemical Engineering Science* 65.1 (Jan. 2010), pp. 405–411. ISSN: 00092509. DOI: 10.1016/j.ces.2009.05.045. URL: https://linkinghub.elsevier.com/retrieve/pii/S0009250909003819.

[118] John R. Bourne. "Comments on the iodide/iodate method for characterising micromixing". In: *Chemical Engineering Journal* 140.1-3 (July 2008), pp. 638–641. ISSN: 13858947. DOI: 10.1016/j.cej.2008.01.031. URL: https://linkinghub.elsevier.com/retrieve/pii/S1385894708000697.

[119] Jean-Marc Commenge and Laurent Falk. "Villermaux–Dushman protocol for experimental characterization of micromixers". In: *Chemical Engineering and Processing: Process Intensification* 50.10 (Oct. 2011), pp. 979–990. ISSN: 02552701. DOI: 10.1016/j.cep.2011.06.006. URL: https://linkinghub.elsevier.com/retrieve/pii/S0255270111001395.

[120] Richard W. Hanks, Avinash C. Gupta, and James J. Christensen. "Calculation of Isothermal Vapor-Liquid Equilibrium Data for Binary Mixtures from Heats of Mixing". In: *Industrial & Engineering Chemistry Fundamentals* 10.3 (Aug. 1971), pp. 504–509. ISSN: 0196-4313. DOI: 10.1021/i160039a025. URL: https://pubs.acs.org/doi/abs/10.1021/i160039a025.

[121] Richard W. Hanks, Romeo L. Tan, and James J. Christensen. "Limits on the simultaneous correlation of gE and hE data by the NRTL, LEMF and Wilson's equations". In: *Thermochimica Acta* 23.1 (Mar. 1978), pp. 41–55. ISSN: 00406031.

DOI: 10.1016/0040-6031(78)85110-7. URL: https://linkinghub.elsevier.com/retrieve/pii/0040603178851107.

[122] Robert H. Perry, Don W. Green, and James O Maloney. *Perry's Chemical Engineer's Handbook, Eighth Edition*. 2007, Chap. 2 pp. 186–194. ISBN: 0070498415. DOI: 10.1036/0071422943.

[123] Erwin Riedel and Hans-Jürgen Meyer. *Allgemeine und Anorganische Chemie*. Berlin, Boston: De Gruyter, Nov. 2018. ISBN: 9783110583953. DOI: 10.1515/9783110583953. URL: http://www.degruyter.com/view/books/9783110583953/9783110583953/9783110583953.xml.

CHAPTER 4

3D Printed Reactors for Synthesis of Active Pharmaceutical Ingredients in Continuous Flow

The following chapter is taken from the same-titled journal article published in *Organic Process Research & Development* by Maier *et al.*:

Manuel C. Maier[1,2], Alessia Valotta[1,2], Katharina Hiebler[1], Sebastian Soritz[1], Kristian Gavric[1], Bianca Grabner[1], and Heidrun Gruber-Woelfler[1,2]

Organic Process Research & Development, 06/2020, DOI: 10.1021/acs.oprd.0c00228

[1]Institute of Process and Particle Engineering, Graz University of Technology, Graz, Austria

[2]Center for Continuous Flow Synthesis and Processing (CCFLOW), Research Center Pharmaceutical Engineering GmbH (RCPE), Graz, Austria

Contents

4.1 Abstract

Advances in flow chemistry to produce Active Pharmaceutical Ingredients (*APIs*) require performing reactions in tailor-made equipment as complexity of the planned setups increases. To react quickly and with low costs to these demanding reactions, additive manufacturing, also known as *3D* printing, is a preferred way for the production of customized reactors. This work presents three examples of *3D* printed reactors and their application for the synthesis of *API* precursors in continuous flow. The first case deals with an aerobic oxidation of Grignard reagents to the corresponding phenols by molecular oxygen. Here, a design concept was utilized; various stainless steel reactors were tested, and their performances were evaluated in continuous flow. Next, another stainless steel reactor was applied for achieving fast mixing in a cascade, leading to a valsartan precursor. The third and final case employed a Continuous Stirred Tank Reactor (*CSTR*) made of a *UV*-curable resin. It was used for the first step of a multiphase enzymatic decarboxylation followed by a Heck cross-coupling reaction, leading to resveratrol derivatives.

4.2 Introduction

A fast reaction to market demand of Active Pharmaceutical Ingredients (*APIs*) plays a vital role for today's health care as well as the success of a pharmaceutical company. As the production of pharmaceutical products is currently carried out in batch operations at different sites, lead times of up to 12 months need to be considered. [5] As a consequence, knowledge of future demands needs to be estimated to ensure an intact market supply. To overcome this limitation, an increasing interest and motivation led pharmaceutical companies and regulatory bodies to investigate continuous production alternatives. [2, 124, 11]

Due to the high complexity of multistep *API* syntheses in the pharmaceutical industry, plants and reactors need to be flexible in their design as well as cost-effective and quickly producible. Here, *3D* printed reactionware can be seen as a solution to provide such functionalities. [7] While *3D* printing can improve current designs of industrial plants, the fundamental production of *APIs* needs to be changed to a continuous mode. True continuous production of *APIs* can be achieved by flow chemistry as demonstrated in various publications. [125, 126, 78, 77] Here again, the approach to produce tailor-made reactionware by *3D* printing shows a promising way within flow chemistry. [87, 85, 86, 36]

Depending on the applied chemistry, different reactor materials and manufacturing techniques can be chosen. An inexpensive while still chemically stable option is Fused De-

position Modeling (*FDM*) or Fused Filament Fabrication (*FFF*) of polypropylene (*PP*) and polyether ether ketone (*PEEK*). [127, 128] A difficulty of this manufacturing technique is the extrusion-like application of the layers, which could lead to leakage problems if not bound well to the surrounding layers. Stereo Lithography (*SLA*) manufacturing instead chemically binds previous layers; however, the utilized *UV*-resins are brittle, and some age over time upon exposure to light. [129] However, they allow by far the highest geometrical resolution of all additive manufacturing techniques. A more expensive but also the most promising *3D* printing method for thermally demanding reactions is Selective Laser Melting (*SLM*) of various metals. Several examples of the application of *SLM* printed stainless steel reactors in flow chemistry have been reported in the literature. [93, 88]

In this work, we present three examples of tailor-made reactors for flow chemical applications produced via *3D* printing. First, the aerobic oxidation of a Grignard reagent to the corresponding phenol is shown, focusing on the reaction selectivity affected by the use of stainless steel reactors exhibiting different mixing performances. Also, the importance of process stability in terms of a stable oxygen supply is demonstrated. This part is an extension of our previous work. [8] The second example illustrates the use of a *3D* printed reactor for reactions requiring fast mixing in a cascade for the production of a valsartan precursor in three steps, as reported earlier. [130] Again, a stainless steel reactor was successfully used for N-acylation and hydrolysis to achieve the required mixing performance. In the third example, the flexibility of *3D* printing is shown by a novel and custom-designed *CSTR*, made of a *UV*-curable resin, for the synthesis of resveratrol derivatives developed previously in our group. [131] This reaction cascade comprises an enzymatic decarboxylation of phenolic acids by immobilized phenolic acid decarboxylase from *Bacillus subtilis*(*BsPAD*) in alginate beads followed by a heterogeneously catalyzed Heck cross-coupling reaction.

4.3 Case 1: Grignard Oxidation

4.3.1 General and Reactors

The first example of synthesis in our in-house engineered *3D* printed reactors is the aerobic oxidation of Grignard reagents to their corresponding phenols in continuous flow. This application was chosen as a model reaction to demonstrate the benefits of *3D* printing for organic syntheses under harsh conditions. Phenols are compounds of great importance in the pharmaceutical industry, and the usage of molecular oxygen was proposed as a possible green and sustainable path for the production of such compounds. [94] Oxygen is a very interesting reactant due to its low cost and low environmental impact. [78] However, oxidation reactions are dangerous to carry out with common lab equipment due to the explosion hazard derived from using molecular oxygen in the presence of organic mixtures. Efficient heat transfer is a requirement to avoid the formation of hotspots that could

cause the ignition of the flammable solution. [132] Moreover, Grignard reagents are very reactive toward oxygen, and therefore, efficient mixing is required to avoid formation of side products. Microreactors can be an option to safely carry out such types of reactions because they provide an improved heat and mass transfer due to the reduced internal volume and higher surface-to-volume ratio.

Different stainless steel microreactors were designed and demonstrated to show the importance of efficient mixing for aerobic oxidations of Grignard reagents. A *CSTR* cascade (*CSTR* = continuous stirred tank reactor, see Fig. 4.1) was designed based on the obtained knowledge from previous work. [8]

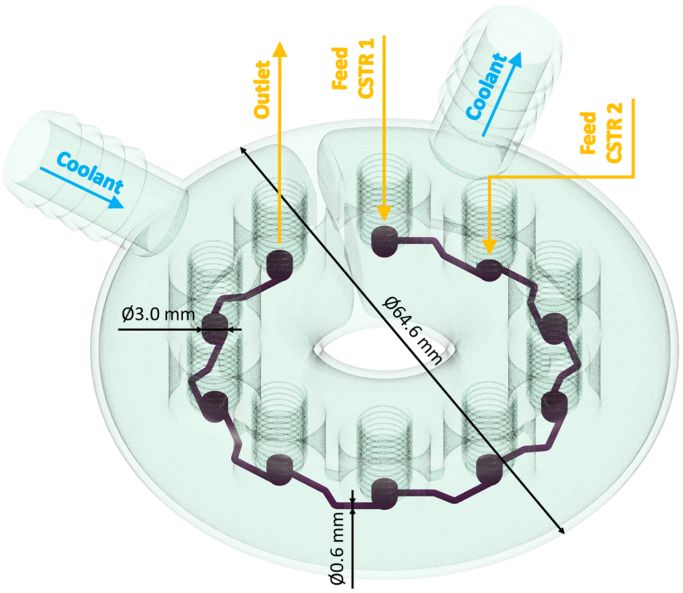

Figure 4.1: *CAD* image of the *CSTR* cascade. It features 10 reaction vessels surrounded by a cooling shell. The vessels have an internal diameter of 3 mm connected by 0.6 mm channels. Each vessel can be equipped with magnetic stirring spheroids of 2.4 mm width and 2.7 mm length.

The *CSTR* cascade features 10 vessels with Inner Diameters (*IDs*) of 3 mm, which are connected via a channel with an *ID* of 0.6 mm. Each vessel can be equipped with microstirrers to actively control the degree of mixing. This is especially important for process development of mixing sensitive reactions, whose product formation depends on the time needed for mixing. Sensor connections to the vessels can be made with flat bottom connectors, which are also used for *HPLC* applications. With the obtained data using this *CSTR* cascade and inline sensors, it is possible to estimate reaction time scales by monitoring decreasing concentrations or temperature profiles between the vessels, as shown earlier. [8]

In addition to this cascade employing active stirring, reactors using passive mixing principles (see Fig. 4.2) were designed using a structure element database developed within this work. This database includes fully scalable reactor sections through parameter-depending Computer Aided Design (*CAD*) files, as reported before. [8] Suitable reactor elements

for the chemical task can be selected and inserted by a click-and-drop procedure within Autodesk Inventor. This allows also non-*CAD* experts to design reactors, as all elements have a defined interface and share the same origin. After selection, they can be scaled arbitrarily by varying only three parameters within a design spreadsheet linked to Autodesk Inventor. These parameters include d, Le, and n, corresponding to the internal diameter, the cubical element length scale, and the number of elements, respectively. They can be calculated and updated in the spreadsheet for a particular design according to several design principles reported in the literature. [23, 26, 22] Due to the possibility to scale these reactors via parameters, we refer to them as parameter reactors. The two designs shown in Fig. 4.2 were generated with the described approach and used for experiments reported within this section. Each reactor was named as AP followed by the number of the design. (Numbers 3 and 4 were used in this work; designs 1 and 2 were presented in a previous work. [8]) AP stands for Anton Paar GmbH, a cooperation partner within the CCFLOW project, [133] who was responsible for printing the reactors. For both reactors 3 and 4, the first point of contact of the two inlet flows is a Y-junction. The difference between the two designs lies in the size and arrangement of the internal channels, which result in different mixing effects. In the AP03 reactor, the channels are arranged according to a helicoidal structure with alternating change of the direction of curvature to induce chaotic flow structures. In the AP04 reactor, after the Y-junction, the main channel splits into three channels. Then, each of them separates again into two more channels, after which they converge again in a main channel. The mixing principle is based on splitting the flow into smaller lamellae to increase the area of contact between the incoming streams.

The presented reactors were manufactured by *SLM* as described in the Sec. 4.B.1. *3D* printing support needs to be generated for the parameter reactors to make them *3D*-printable, whereby the *CSTR* cascade can be printed without any internal support. Internal support can be generated by many different software tools readily available within commercial slicer software. For the stainless steel reactors, the internal support was generated by Materialise's Magics software. This support connects the outer walls of the channels to the cooling shell. It is made by generating a lattice structure inside the cooling shell followed by a Boolean subtraction of a full body reaction channel. The remaining cut was inserted into the final design. Support structures are unchanged in the printed reactors because they also increase internal surface area and lead to increased heat transfer rates.

After printing and postprocessing, the reactors were evaluated for the oxidation of the Grignard reagents in continuous flow. The chosen Grignard reagent was 4-chlorophenylmagnesium bromide, which gives 4-chlorophenol as the main and desired oxidation product, see Fig. 4.3. The reaction was carried out in 2-methyltetrahydrofuran (*2-Me-THF*), as this solvent was determined in previous experiments to be the optimum choice. Although there is a risk of peroxide formation, its generation is slow at room temperature. [134] Due to short residence times within the setup, this risk was considered minimal. However, it was important to ensure that the solvent was properly degassed

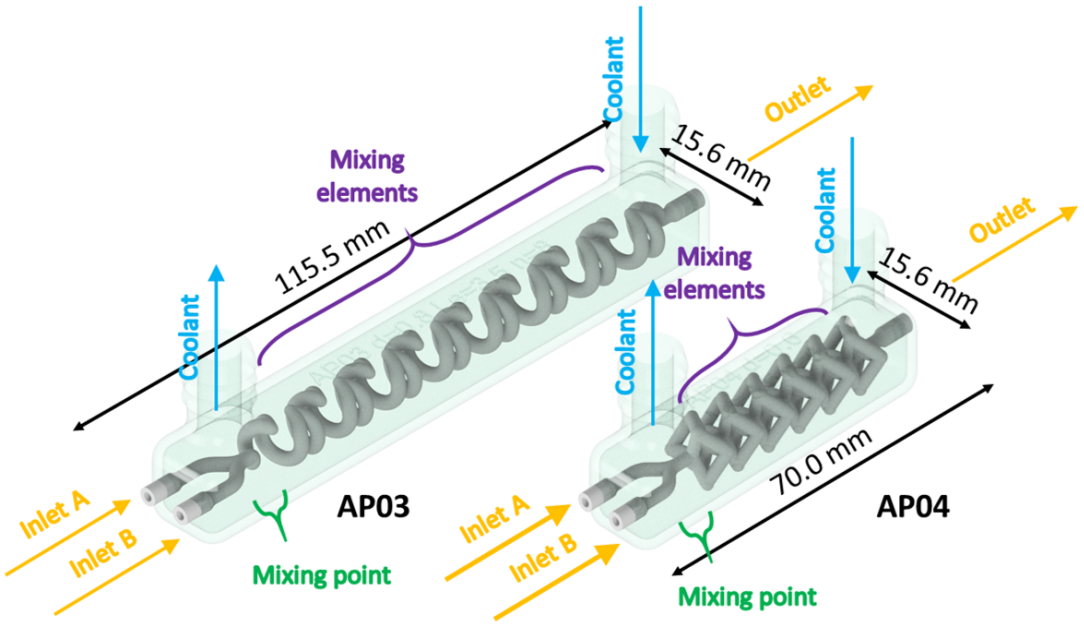

Figure 4.2: *CAD* images of reactors AP03 and AP04. These reactors use passive mixing principles and are assembled from the developed structure element database. Different designs were produced with internal diameters of 0.6, 0.7, and 0.8 mm.

before each run because oxygen contamination could cause the degradation of the Grignard reagent prior to the reaction. Therefore, fresh solvent was always used, which was thoroughly degassed with argon for at least 30 min before each experiment.

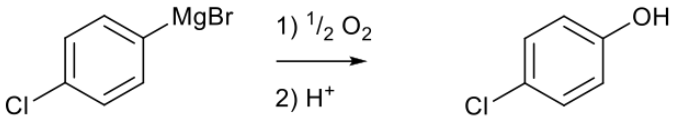

Figure 4.3: Grignard Oxidation Reaction Studied in this Work

In this work, oxygen sensors developed by our collaboration partners within the CCFLOW project [133] were implemented in the final setup to monitor the oxygen concentration in the system. [135] The used optical sensors comprise a fiber-based Near-Infrared (*NIR*) emitting Pt-tetra-(4-fluorophen-yl)-tetrabenzoporphyrine dye immobilized in polyphenylene sulfide and with a CYTOP protection coating and a phase fluorimetry readout system. For a complete description of the sensors' characteristics, see the Sec. 4.C.3.6.

Before testing the reaction in continuous flow, some preliminary experiments had to be carried out. First, the reaction was performed in a batch vessel to obtain benchmark data to compare with the results of flow experiments. The reagent concentration was 0.1 M, and oxygen was supplied via a balloon connected to the vessel, similarly to the setup used by He *et al.*, [94] and the reaction was carried out at 0 °C. The reaction was completed

within 1 h, achieving a yield of 15%, which is in accordance with the results reported in the literature. [94] Second, a stable oxygen supply needs to be provided to obtain comparable results between the reactors. This will be described when the used setup is explained.

4.3.2 Setup

The setup used for the evaluation of the microreactor performance is shown in Fig. 4.4. This setup was developed in resemblance to what was proposed in a previous work; [8] however, some improvements were made to increase the stability of the system. The first feed to the reactor is supplied via a high-pressure syringe pump (Lambda VIT-FIT HP) that pushes degassed *2-Me-THF* into the system. The solvent was loaded into a 20 mL stainless steel syringe via a 6-way valve connected to a sealed solvent bottle. This reduced the possibility of oxygen contamination of the solvent prior to the experiment. Also, syringe pumps were chosen, as they provide a constant flow rate with little pulsation, which is common for *HPLC* pumps and undesirable for our purposes. A Mass Flow Controllers (*MFC*) was used to precisely control the oxygen flow into the system. A Pressure Indicator (*PI*) was mounted on the gas line to check the pressure increase in the startup phase and to track the pressure in the system once steady state was reached. Real time pressure data were collected by connecting an Arduino board to the *PI*, that was programmed to convert the analogue signal into a digital one. Pressure data were sent to the laptop's terminal, to which the board was connected via USB. A check valve was also inserted in the gas line, which was opened when the pressure on the line was the same as in the process (around 7 bar) to avoid backflow to the *MFC*. The liquid and gas lines were brought into contact with a T-mixer, where one phase is sheared into the other to produce a slug or bubbly flow. This biphasic stream enters an absorption unit to completely dissolve the oxygen in the solvent and obtain a stable oxygen supply before reaching the oxygen sensors at the reactor inlet. For the absorption step, both a 4 m long polytetrafluoroethylene (*PTFE*) coil (*OD* 1.58 mm, *ID* 0.8 mm, internal volume 1.75 mL) and a stainless steel *HPLC* column (*ID* 8 mm, height 40 mm) filled with glass beads (Carl Roth GmbH, diameter 0.75-1 mm) were tested as absorption units.

As depicted in Fig. 4.5, the three setups (a-c) were compared at -15 °C. Setup a was already described in a previous work. [8] It features a continuous syringe pump (Asia Syrris) to continuously pump the degassed solvent into the system and an *MFC* to control the incoming oxygen flow rate. Oxygen and solvent flow rates were both set to 1 mL min^{-1} (NmL min^{-1}) in this case. As an absorption unit, the aforementioned coil was used. As visible from the graph below the flowchart, the oxygen supply in this case was very discontinuous and subject to fluctuations. Some improvements were made to reduce these fluctuations: in setup b, a *PI* and a check valve were added to the system to have a controlled startup phase and to connect the liquid with the gas line only when the pressures of both lines were equal. A single syringe pump (Lambda VIT-FIT HP) was used and filled with degassed solvent via a 6-way valve to reduce oxygen contamination.

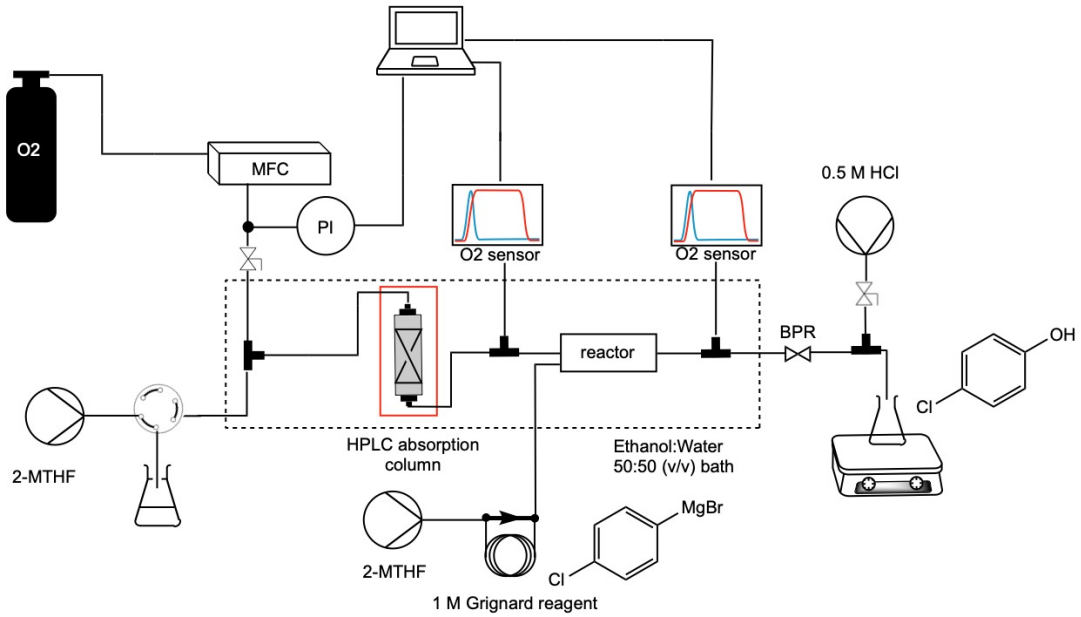

Figure 4.4: Flow Chart for the Experimental Setup Used to Perform the Grignard Reagent Oxidation in Continuous Flow with the Implementation of *3D* Printed Microreactors

For case b, a higher flow rate of oxygen was used (4 NmL min^{-1}) as well as a higher flow rate of solvent (2 mL min^{-1}). The oxygen profile was again fluctuating around a certain state, but this time with random and broader oxygen peaks. This behavior was attributed to varying back pressure of the system. Changing back pressure influences the *MFC* and causes alternating oxygen supply at the T-junction while the set gas flow rate of the *MFC* was still met. To obtain a constant back pressure, it was decided to increase back mixing by switching to an *HPLC* column filled with glass beads, as seen in setup c. For setup c, a solvent and oxygen flow rate of 1.1 mL min^{-1} and 1.5 N mL min^{-1} were used as these flow rates were also used later on in the Grignard reaction experiments. Again, as in all cases, there were fluctuations in oxygen concentration. This can be explained by the presence of gas bubbles that act like springs, causing the oxygen flow rate to vary. The presence of more or less oxygen in the system causes density differences that have to pass parts of the setup during a time corresponding to the residence time, causing oxygen supply variations. Nevertheless, it was possible to obtain a stable oxygen concentration in the case of the *HPLC* column due to the higher surface-to-volume ratio that improves the gas-liquid mixing compared to the simple coil. Moreover, the column has a higher volume than the coil, so changes in oxygen supply are dampened due to higher backmixing. Due to these advantages, the column was chosen as absorber in the final setup. The absorption tests were of great importance because they demonstrated that in the presence of a biphasic slug flow the process is not stable enough to supply a constant amount of oxygen. Therefore, it is important to have an efficient absorption unit to reach stable operating conditions. Because in all of the setups the absorption units were sufficient to completely dissolve the

oxygen in the solvent, it was not deemed reasonable for our purposes to perform slug flow experiments in our setup.

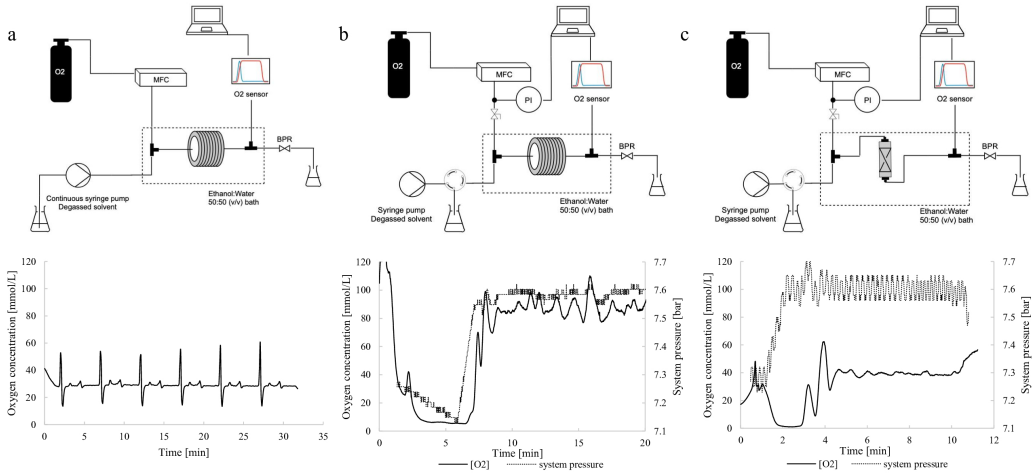

Figure 4.5: Different setups tested during the absorption experiments to compare the oxygen supply provided by different pumps and absorption units.

Before each run, an efficient startup procedure was followed to rapidly reach steady state and perform the experiment successfully. A detailed step-by-step description is reported in the Sec 4.C.2.1. Together with the startup procedure, the conducted oxygen stability tests were crucial to identify flow rates of both the solvent and oxygen that could give a good compromise between experiment time and oxygen solubility. The chosen flow rates for the reaction experiments were 1 mL min^{-1} for the solvent and 1.5 N mL min^{-1} for O_2, which correspond to a molar ratio of 1:3.97 4-chlorophenylmagnesium bromide:O_2. Preliminary tests at all experimental temperatures showed that, by using this molar ratio at the system pressure of 7 bar and setup c, all oxygen was absorbed in the solvent, and no slug flow could be detected at the column outlet. The overall experiment time was around 20 min, limited by the size of the syringes of the pump.

After choosing setup c as an optimal absorption step for the following investigations, a single liquid phase of oxygen-enriched *2-Me-THF* entered the microfluidic device through one inlet. Then, it was mixed with a 1 M reagent solution in *2-Me-THF*, which was pushed into the system through a sample coil connected to a 6-way valve. The flow rate was set by a syringe pump filled with pure solvent, which was also connected to the 6-way valve. The flow rate was set to 0.1 mL min^{-1} to dilute the reagent solution to the process concentration of 0.091 M within the reactor. Utilizing this sample coil setup showed improved startup times while conserving Grignard reagents. The whole reactor and absorption unit were placed in a thermostatic bath filled with an ethanol/water mixture (50 v% ethanol) to

maintain the temperature at the desired level (either 0, -5, or -10 °C, depending on the experiment). Oxygen sensors were positioned before and after the reaction unit as well as within the reactor itself in the case of the *CSTR* cascade, whose vessels can host inline sensors. After the reactor, a Back Pressure Regulator (*BPR*) was used to keep the system pressure at 7 bar. Finally, another syringe pump was used to continuously quench the reaction mixture with 0.1 M *HCl* in a 1.5 molar ratio. Samples at different times were taken and measured with *GC-FID*. Conversion and yield were calculated in comparison to a reference sample, which was directly withdrawn from the reagent bottle and subsequently quenched.

The tested reactors were AP04 with diameter of 0.8 mm and AP03 with diameter of 0.8 and 0.7 mm, respectively. All of the reactions were carried out at three different temperatures (-10, -5, and 0 °C). The results were compared in terms of yield obtained via *GC* measurements and are shown in Fig. 4.6. Also, one reaction at 0 °C was carried out in the Split-and-Recombine Reactor (*SaRR*) depicted in Fig. 4.7 to determine how the new setup performs using the same reactor and conditions tested and published previously. [8] The *SaRR* served as starting point for the design approach featuring the structure element database. It consists of a tangentially shifted T-mixer and split-and-recombine reaction elements. The internal diameter is 0.8 mm, which gives the mixing elements an internal volume of 0.565 mL. In the case of the *CSTR* cascade, some oxygen sensors could be implemented within the reactor vessels, and experiments were carried out at 0 and -5 °C and at different stirring speeds (0 and 1000 *RPM*). The results are compared in Figure 4.6 in terms of *GC* yield, calculated considering the zero sample from the reagent solution, and the final sample taken at the steady state of the reaction. The results obtained can be interpreted as follows, by considering the influence of different process parameters on the outcome of the reaction.

4.3.3 Results and Discussion

Temperature. This is the parameter that generally has the strongest influence on the reaction. It can be noticed that for the parameter reactors the yield increased when lowering the temperature. This can be explained as follows: while the intrinsic reaction rate decreased with decreasing temperature, the mixing time was the same because the same flow rates were used at the different temperatures. The better mixing leads to fewer side reactions and thus to higher yields of the desired product. This trend was not seen in the case of the *CSTR* cascade, where the yield did not change much with varying temperature. Here, it could be either an experimental deviation or, more likely, salt formation influenced the stirring rate within the vessels.

Different Mixing Principles. Concerning the performance of the three parameter reactors, the yield considerably increased when switching from the AP04 to the AP03 reactor, as expected from the results of the characterization process (reported in the Sec. 4.C.1). The yield of the desired product was around 28% for AP04 versus 42% in the

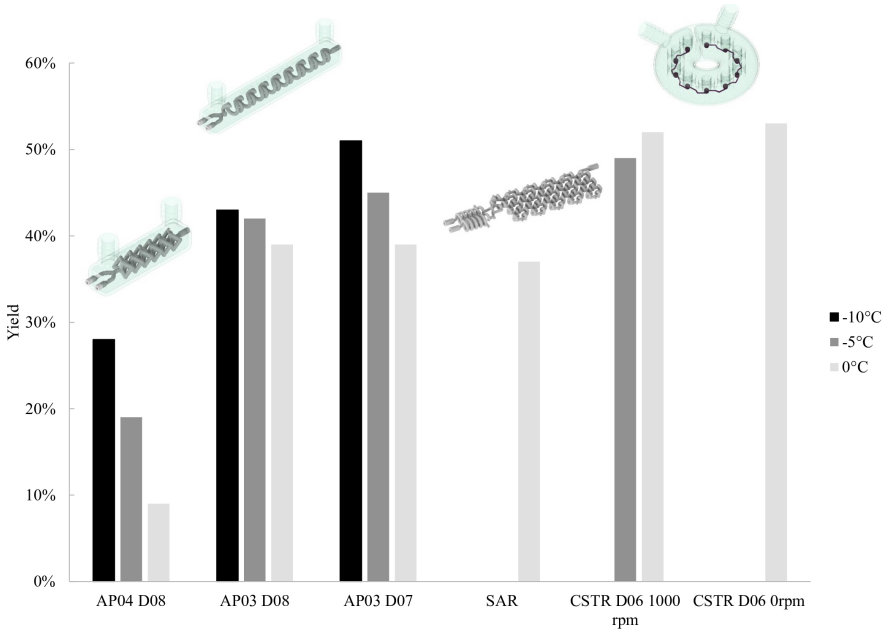

Figure 4.6: Comparison of different reactor types and the effect of temperature on the yield of the desired product in aerobic Grignard oxidation. Yields were determined by *GC* analyses.

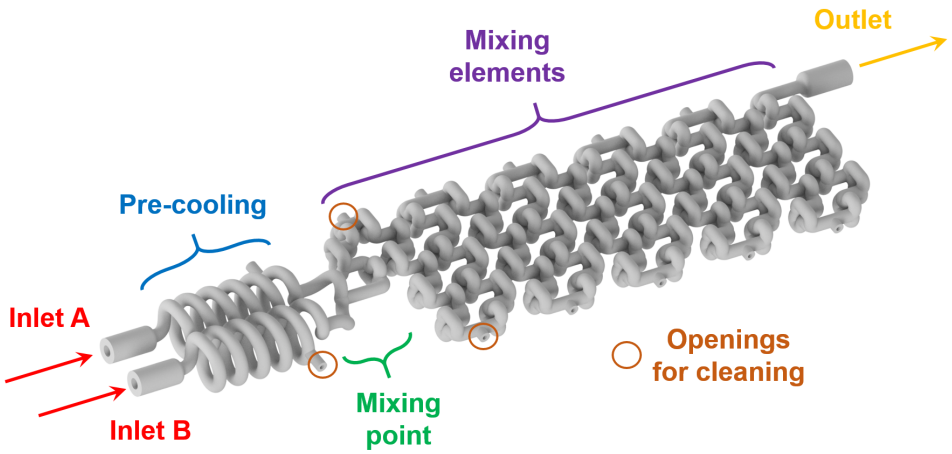

Figure 4.7: *CAD* model of the *SaRR* as published previously. [8] Reproduced with permission from ref [8], published by The Royal Society of Chemistry. Copyright 2019 Royal Society of Chemistry.

AP03. Due to the helicoidal channel structure, the flow is much more chaotic in the AP03 reactor, causing better mixing of the incoming streams. In the AP04 instead, the mixing is realized by continuously splitting the channels while keeping the same internal diameter for both split streams, so the achieved folding of the streams is much lower. The AP03 device also proved to perform slightly better than the *SaRR* at 0 °C for the same reasons as stated above. The *CSTR* cascade was even more efficient with a yield of about 53%, as expected from the results of the micromixing experiments (see Sec. 4.C.1.1). Reactor characterization (shown in the Sec. 4.C.1.2) showed that the cascade does not behave like a series of ideal *CSTRs* as the volume of connecting tubes is not negligible compared to the *CSTR* vessels' volume. Thus, the reactor behaves more like an alternating series of *CSTRs* and tubular reactors. Also, in the case of the *CSTR* cascade, the stream is subjected to a split-and-recombine mixing action: first, the incoming stream flows through a small capillary; then, the section increases when it enters a vessel, and finally, it is squeezed again into a small channel. Considering the size of the inner diameter of the channel connecting each vessel, which is 0.6 mm and smaller than those of the other reactors tested, the fluid velocity is higher in a smaller capillary; therefore, the flow in the system is more chaotic, and better mixing is achieved. However, when looking at the effect of stirring, little difference in yield was observed when using a stirring speed of 0 or 1000 *RPM*. As already stated above, it remains unclear if the stirring rate was affected by the salt formation, but the splitting and recombining of the flowing fluid still remained. Also, the mixing point within the second vessel seems to be improved compared to the other designs as the capillary feeding the Grignard reagent into the second vessel is sheared by a perpendicular stream with oxygen-enriched *2-Me-THF* from vessel one. Considering that the reagent flow rate is very low, the reaction might already take place directly after the tubing that connects the 6-way valve with the second *CSTR* vessel. This means that the reaction might already be over when the reagent reaches the stirrer (which is supported by the sensor data, see Sec. 4.C.2.2). As a result, the reaction is so fast that the earliest point of contact between the two incoming streams has the highest influence on the yield of the reaction. However, not enough data was collected to confirm the effect of the stirring speed on the reaction with certainty.

Internal Diameter. To assess the effect of the internal diameter on the reaction, the two AP03 with internal diameters of 0.8 and 0.7 mm were used. As expected, the reactor with smaller *ID* proved to perform better in terms of yield: 50% versus 42%. Mixing is enhanced because the flow velocity is higher in smaller channels. Therefore, there are higher inertial forces promoting convective mixing and secondary flow structures. Miniaturization of the channel diameter is limited due to solid formation during the reaction. Complex geometries, produced via *3D* printing, improve reactor performance via secondary flow structures, and are able to handle such solids while providing the needed mixing characteristics.

Different Setups. The yields obtained in the *SaRR* performed with setup a shown in Fig. 4.5, and the yields obtained with the parameter reactors as well as the *SaRR* utilizing

setup c in Fig. 4.5 were comparable to the one of the earlier work (around 40-45%) at 0 °C. [8] However, when comparing the results from the *CSTR* cascade, the yield was higher (more than 50%). The major difference between the conducted experiments was that in the previous work the reaction was started in a commercial Y-junction before entering the first *CSTR* vessel. Here again, the importance of the first mixing point is shown. A general assertion that the system benefits from a more stable oxygen supply by switching the reaction setup was not directly seen as cumulative samples were drawn from the reactor outlet over time in both setups. However, it appears reasonable that a more stable supply leads to less product fluctuations. Side products were detected to be <10% of the overall *GC* area. Although no detailed investigation on this topic was carried out in this work, so far no explicit relation between byproduct formation and reactor type could be determined. Nevertheless, it could be shown in accordance with a previous work [8] that all *3D* printed reactors lead to less byproduct formation than a simple *PFA* coil. Moreover, all of the continuous reactors tested gave a much higher yield of the desired product compared to the initial batch setup. While such a comparison with a low pressure batch is not fair, considerably safety efforts would be needed to conduct high pressure batch experiments. Finally, it can be concluded that the production of phenols benefits from implementation of microfluidic devices compared to conventional batch processing and controlled mixing performance with regard to the temperature dependent reactivity.

4.4 Case 2: Valsartan

As reported by the World Health Organization (*WHO*), about one-third of deaths worldwide are caused by cardiovascular diseases. In this respect, elevated blood pressure is one of the early symptoms before developing more severe complaints involving the heart and blood vessels. [136] Therefore, antihypertensive drugs are among the best-selling products on the pharmaceutical market. [137] One potent active pharmaceutical ingredient contained in several medication options for the treatment of hypertension is the nonpeptide angiotensin II receptor blocker valsartan. [138] Its original synthesis route was first patented by Ciba-Geigy in 1991, [139] and since then, a vast amount of research groups (exemplarily refs [140, 141, 142, 143, 144, 145, 146, 147, 148, 149]) aimed to improve the low-yielding process. [150] However, the use of continuous flow technology for that purpose has been reported in only a few cases. [151, 152] Hence, our group targeted the development of a multistep continuous setup for the synthesis of a late-stage valsartan precursor in continuous flow. [130] The envisioned synthetic route comprises N-acylation, Suzuki-Miyaura cross-coupling, as well as basic ester hydrolysis. Whereas the key step of the cascade, Pd-catalyzed C-C bond formation, was achieved in a packed-bed reactor filled with a heterogeneous Pd-Ce-Sn oxide, [153] N-acylation and ester hydrolysis were performed in coil reactors. To obtain high conversions for these transformations using a definite reactor volume, we needed to accomplish fast and efficient mixing of reagent streams. This could be successfully achieved by the utilization of a *3D* printed Split-and-

Recombine Reactor (*SaRR*), shown in Fig. 4.7, which was designed and developed in our group. [8] Although originally intended for the oxidation of Grignard reagents in continuous flow, its design featuring a network of separating and combining channels made it a perfect choice for application as a static mixer. The superior mixing performance of the *SaRR* compared to a standard T- mixer has been reported previously, [8] and thus, we decided to implement two *SaRRs* for mixing purposes (residence times of the individual steps in the *SaRRs* were not optimized) into our final integrated continuous setup for the synthesis of the targeted valsartan precursor. The synthesis of a valsartan precursor in continuous flow was performed as a feasibility study. The single steps of the cascade were optimized in batch (to conserve material) and tested in flow individually before we assembled the different reactor parts to a combined setup. The first step of the reaction cascade, N-acylation, was accomplished in a coil reactor combined with an upstream *SaRR* unit (v = 0.10 mL min^{-1}, $\tau \sim 19.3$ min). Then, the reaction mixture was quenched with a stream of aqueous K_2CO_3 (v = 0.10 mL min^{-1}) and pumped through a fixed-bed of heterogeneous Pd-catalyst $Ce_{0.20}Sn_{0.79}Pd_{0.01}O_{2-\delta}$ for Suzuki-Miyaura cross-coupling (v = 0.20 mL min^{-1}, $\tau \sim 22.3$ min). Finally, aqueous NaOH solution was added to the process stream (v = 0.10 mL min^{-1}) to achieve hydrolysis of the methyl ester ($\tau \sim 17.1$ min). In this way, we successfully synthesized targeted valsartan precursor with up to 96% yield (73% enantiomeric excess) over all three steps (v = 0.30 mL min^{-1}, total $\tau \sim 60$ min, Fig. 4.8).

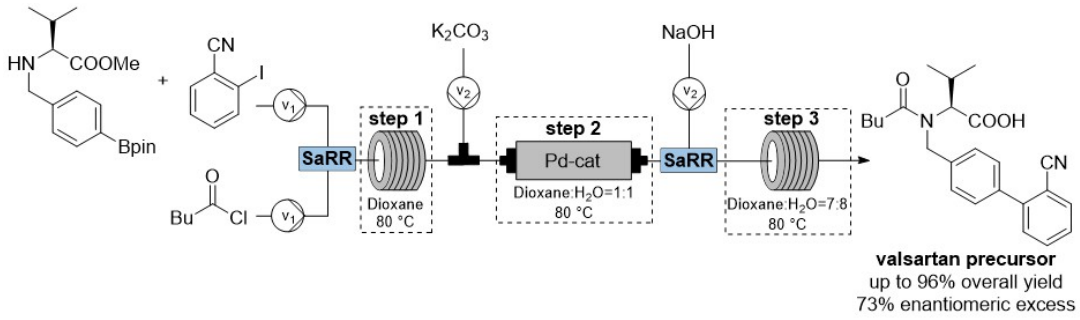

Figure 4.8: Three-Step Continuous Setup for the Synthesis of a Valsartan Precursor. *SaRR*= split-and-recombine reactor, v_1 = 0.05 mL min^{-1}, v_2 = 0.10 mL min^{-1}

4.5 Case 3: Resveratrol Derivatives

Resveratrol is a prominent representative of the stilbene family, which is known for its conjugated double bond system of two benzene rings connected by a C=C double bond. This structure gives the molecule antioxidant, anti-inflammatory, antiaging, and antidiabetic characteristics. [154, 155] Stilbenes are also promising candidates for cancer preventive drugs. [156] A one-pot synthetic route from bio-based resources to stilbenes in a two-step chemo-enzymatic tandem reaction was developed by Gómez Baraibar. [157] Despite

the advantages of the one-pot synthesis, such as reduced process time and elimination of intermediate purification, there is room for improvement. Transferring the batch to a continuous operation mode, the elimination of organic solvents and expansion of the substrate scope of the process from symmetric to asymmetric products make this novel route more sustainable, as well as economically and ecologically favorable. A promising approach for a continuous flow route toward stilbenes was recently published by Peng *et al.* [158] For our target process, we envisioned an integrated two-step flow process, which allows long-term utilization of the expensive catalysts. Further, volatile organic solvents should be eliminated, and resources should originate from renewable feedstock as much as possible. Enzymatic decarboxylation of *para*-coumaric acid via *BsPAD* results in the highly reactive styrol intermediate, which is prone to polymerization. The allyl group of the intermediate serves as substrate for the following Heck reaction with an aryl halide, iodobenzene in our case (Fig. 4.9). A major challenge of the target process was the solubility of *para*-coumaric acid in the first reaction step. Additionally, the compatibility of the solvent of the enzymatic and the chemical step is an obstacle. [159, 160] The hurdle of substrate solubility was tackled by switching from neat buffer to a mixture of Deep Eutectic Solvent (*DES*) and buffer (1:1 v/v). *DES* was prepared from choline chloride (*ChCl*) and glycerol in a ratio of 1:2 (mol/mol). *PAD* proved its activity in the chosen solvent in a previous study. [161] In that study, substrate concentrations up to 300 mM could be achieved and successfully converted to the desired product with excellent yield. We recently reported a two-step chemo-enzymatic tandem synthesis of stilbenes in a series of packed-bed reactors. Due to the substrate's solubility limit of 20 mM, the enzymatic decarboxylation was the bottleneck of this process. [131]To overcome the limitation of substrate solubility, a multiphase process with suspended starting material was desirable. Herein, we present an advanced concept utilizing a *3D* printed continuous stirred tank reactor (*CSTR*; Fig. 4.10). Mild process conditions of enzymatic reactions allow the use of inexpensive reactor material. The *CSTR* and its sealing flange were printed by Digital Light Processing (*DLP*) of a *UV*-curable resin. They were printed simultaneously with the Photon from Anycubic, utilizing a green standard resin from Wanhao. Each slice was cured with an exposure time of 10 s and a layer height of 50 μm. A cleaning step with ethanol was done after removal of the parts from the build platform. The parts could be used directly after removal of support structures, but a final curing in sunlight until the next day was envisioned. The reactor was designed for the purpose of the reaction. A heating shell enabled an operation at the right temperature (30 °C), whereby heat transfer was not characterized as the operation temperature was generally mild and the feeding flow rate low; thus, we assumed a good performance. Baffles improved the mixing pattern, and an integrated sieve in the sealing flange kept the immobilized enzyme in the reactor. Design iterations were made for the whole *CSTR* and its baffles to obtain a good agitating performance. This was evaluated by the naked eye as the polymer was semitransparent.

The starting suspension (45 mM *para*-coumaric acid in buffer-*DES* mixture) was fed into the *CSTR* at a flow rate of 0.05 mL min^{-1} at the bottom fluid port. The desired

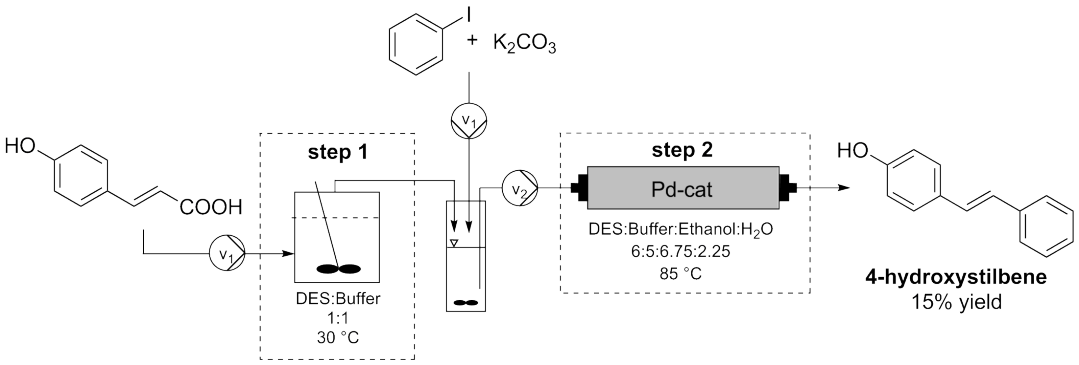

Figure 4.9: Two-Step Chemo-Enzymatic Setup for the Continuous Synthesis of 4-Hydroxystilbene. Step 1: enzymatic decarboxylation of *para*-coumaric acid in the *3D* printed *CSTR*. Step 2: Pd-catalyzed Heck cross-coupling reaction.

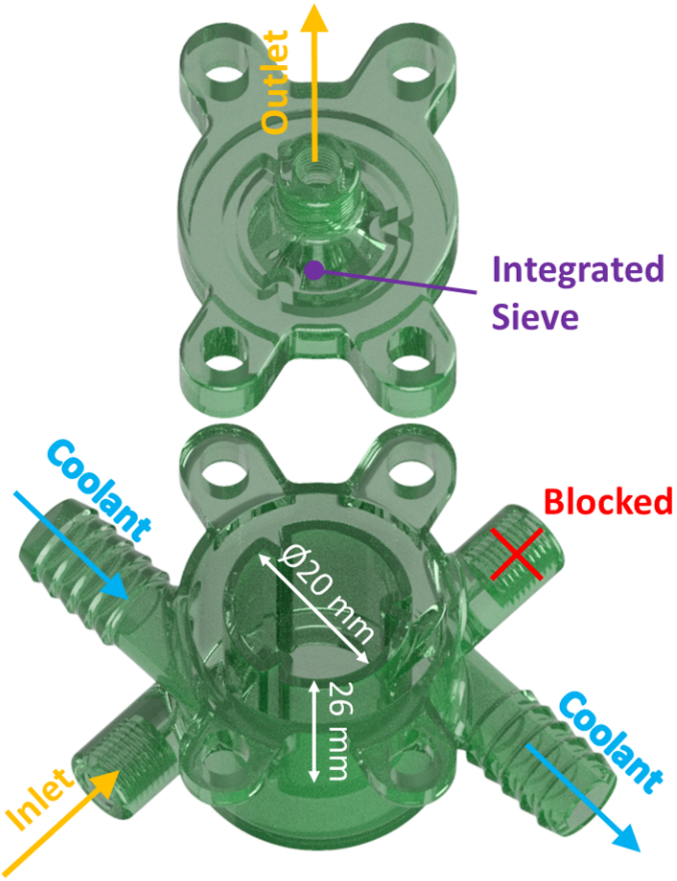

Figure 4.10: *CSTR* designed for the enzymatic decarboxylation of *para*-coumaric acid by phenolic acid decarboxylase. Top: Flange with integrated sieve. Bottom: *CSTR* with integrated baffles.

soluble product, 4-vinylphenol, ejects at the top of the reactor, while alginate beads enclose the enzyme (160 mg freeze-dried cell-free extract from *E. coli*, immobilized in 2% (w/v) calcium alginate beads, details in Sec. 4.E.1) as well as the suspended substrate remain in the reaction. The second connector located at the top of the *CSTR* was not used and plugged in this experiment. It was kept in the design for possible later applications of the *CSTR*. Before entering the second reaction step, the solution was collected in a reservoir, where it was mixed with additional substrates required for the Heck coupling (49.5 mM iodobenzene, 82 mM K_2CO_3, in ethanol:water:*DES* 6.75:2.25:1 v/v/v). The reservoir also helped remove CO_2 from the reaction solution released during decarboxylation. The second step was carried out in a packed-bed reactor (details in the Sec. 4.E.3) filled with a heterogeneous Pd catalyst ($Ce_{0.20}Sn_{0.79}Pd_{0.01}O_{2-\delta}$). [153] The product stream of 0.1 mL min^{-1} was collected and analyzed by means of *HPLC*. For the first step, excellent selectivity (>99%) and a conversion of 70% were detected. The overall yield for (*E*)-4-hydroxystilbene was found to be 15%. Side reactions such as homocoupling of iodobenzene, polymerization of the intermediate, and the formation of the side product of *para*-hydroxy-1,1-diphenylethylene led to reduced selectivity of the Heck reaction. This behavior for the Pd-catalyzed coupling reaction was also observed in batch mode and previous continuous experiments. The space-time yield of the two-step setup was calculated to be 703 mg L^{-1} h^{-1}. In comparison to our earlier results from a process comprising two packed-bed reactors, this is an improvement of 35% in terms of space-time yield. This outcome compensates the longer startup phase of the *CSTR* of 4 h. Overall, the application of the *3D* printed *CSTR* and the alternative solvent (*DES*) allowed us to increase the substrate concentration by a factor of 22 (solubility of *para*-coumaric acid in water: 2 mM).

Case	Microreactor type	Length scale Le (mm)	ID d (mm)	Additive manufacturing technique	Volume (μl)	Ref
1	AP03 (n=8)	4 4	0.8 0.7	*SLM*	256.51 202.4	This work
1	AP04 (n=6)	3.5 3.5	0.8 0.7	*SLM*	221.86 177.6	This work
1	*CSTR* cascade		0.6	*SLM*	349.9	This work
1/2	*SaRR*	3.5	0.8	*SLM*	565	[8]
3	*CSTR*		20	*DLP*	8329.2	This work

Table 4.1: Summary of the characteristics of the microfluidic devices presented in this work. Parameter reactors AP0X are shown with their design parameters: number of elements n, cubical element length scale Le, and internal diameter d.

4.6 Conclusions

Within this article, we demonstrate the high potential of *3D* printing technology for the cost- and time-efficient production of custom-built reactors, applicable for the synthesis of

relevant biologically active molecules in continuous flow. Depending on the requirements of the reactions, two different additive manufacturing techniques were used. Additive manufacturing from stainless steel via *SLM* was used for harsh reaction conditions, while a *UV*-curable resin, processed via *DLP*, was used for milder reaction conditions. An overview of the produced reactors with their specific properties is given in Tab. 4.1. The application of several of the produced reactors are shown by three examples.

The first example shows the continuous aerobic oxidation of a Grignard reagent to the corresponding phenol using different *3D* printed reactor types. After performance evaluation of the reactors by mixing-sensitive reactions and comparison of residence time distributions, influence of different mixing efficiencies and temperatures are shown to affect the formation of the desired phenol. In addition, a focus was held on the stable supply of oxygen into the system by monitoring with optical in-line sensors.

In the second example, two previously reported *3D* printed split-and-recombine reactors were employed in a three-step cascade for the synthesis of a valsartan precursor in continuous flow. While originally designed for the oxidation of the Grignard reagents mentioned above, they were well-suited for the *N*-acylation and hydrolysis reactions due to their efficient mixing properties.

The final example deals with an enzymatic decarboxylation reaction in a multipurpose continuous stirred tank reactor, which led to the formation of resveratrol derivatives after a Pd-catalyzed Heck cross-coupling. Utilization of the developed *CSTR* allowed, in combination with an alternative solvent (*DES*), an increase in substrate concentration by a factor of 22 and therefore an equal increase in productivity.

Overall, we show that by the successful combination of reaction engineering and additive manufacturing, flow chemistry in the tailor-made *3D* printed reactors enabled efficient synthesis of *API* precursors in continuous flow.

4.7 Conflicts of interest

The authors declare no competing financial interest.

4.8 Acknowledgements

The authors kindly acknowledge the funding by the CC FLOW project (Austrian Research Promotion Agency FFG No. 862766), which is funded through the Austrian COMET Program by the Austrian Federal Ministry of Transport, Innovation and Technology (BMVIT), the Austrian Federal Ministry of Science, Research and Economy (BMWFW) and by the State of Styria (Styrian Funding Agency SFG) as well as the H2020FETOPEN-2016-2017 program of the European Commission (Grant 737266-ONE FLOW).

Appendices

4.A General Information

Chemicals and solvents were purchased from commercial suppliers and used as received unless stated otherwise. Analytical thin layer chromatography was performed on pre-coated aluminum plates (Merck, silica gel 60, F_{254}) and spots were visualized with *UV* light (254 nm) and potassium permanganate stain. Column chromatography purifications were carried out using MN silica gel 60 (70-230 mesh). For monitoring of the reaction progress and determination of enantiomeric excess, an Agilent 1100 series *HPLC* system as well as a Perkin Elmer Clarus 500 *GC* system were utilized. *HPLC*-MS measurements were performed on a Waters Acquity H-Class system equipped with a Waters Acquity SQD detector. *NMR*-measurements were recorded using a Bruker Avance III 300 MHz spectrometer (^{1} H: 300 MHz, ^{13}C: 75 MHz).

4.B 3D printing procedures for reactor manufacturing

All the reactors described and implemented in this work were designed using Autodesk®'s *CAD* software Inventor Professional 2019. Parameter reactors were created from a structure element database by a procedure depicted in Fig. S4.1. Reactor elements can be selected and deleted in the standard interface of Inventor (1). Next, a new elements can be selected and new parameters can be set in a Microsoft Excel spread sheet (2), which is connected to the *CAD* program. The new element simply needs to be opened from the database (3) and placed at its origin (4). Autodesk Inventor will indicate that this new component can be updated and by doing so, the new element should fit to the others (5).

4.B.1 SLM printing process

Reactors made of stainless steel (Fig. S4.2) were fabricated via *SLM* at our project partner Anton Paar GmbH, with a procedure presented in previous works [93, 8] and reported in the following. The *3D CAD* model was dissected by the Materialise's Magics software in multiple layers and then printed layer-by-layer by the fusion of a metal powder bed. The sintering of the layers was done by a *SLM* system from EOS utilizing an Ytterbium fiber laser with 400 Watt maximum power input, scanning through a 316L stainless steel powder bed with an average particle size (d50) of 35.9 μm. For the selected layer height of 40 μm, the laser melted the current layer and the prevailing one to generate well-bonded, gas-tight, high density builds. The printing process takes place inside an enclosed chamber filled with nitrogen to avoid oxidation and degradation of the material. After the printing process, the building platform was disassembled from the printer and the unused metal powder was collected for re-use. The inner parts of the freshly printed devices were freed from the powder with compressed air, ultrasound treatment and dried again with compressed

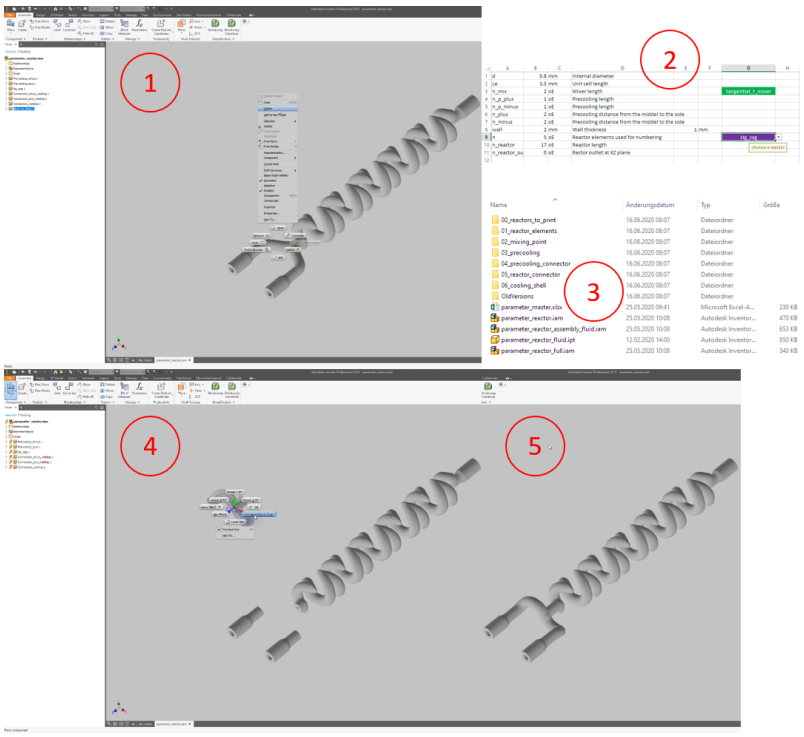

Supporting Information Figure S4.1: Workflow of changing a reactor element from the structure element database.

air. The powder was collected at the cleaning openings of the devices. Afterwards, stress relief annealing of the printed parts was carried out in a vacuum oven. Next, the reactors were cut from the building platform by means of a band saw, and their surface was refined by sandblasting. The cleaning openings were closed by laser welding and the connection to standard equipment was enabled with 1/16" stainless steel capillaries welded to the in- and outlets (only for the parameter reactors). Finally, the prints' surfaces were blasted with micro glass beads and once again, put into the ultrasonic bath followed by drying with compressed air. [8]

4.B.2 DLP printing process

The Continuous Stirred Tank Reactor (*CSTR*) and its sealing flange were printed by Digital Light Processing (*DLP*). Both parts were produced simultaneously within the Photon from Anycubic. A green *UV*-curable resin from Wanhao was used for *3D* printing. The slicing software provided by Anycubic generated the manufacturing sequence for each slice of the *CAD* models, which were cured with an exposure time of 10 seconds and set to a layer height of 50 μm. A support structure was added via the slicing software by using its standard settings and a support density of 50%. The printed parts with partly removed support structures are depicted in Fig. S4.3. Post-processing included a

Supporting Information Figure S4.2: Pictures of the *SLM* printed *CSTR* cascade with inserted *HPLC* flat bottom connectors (left) and various parameter reactors AP03 and AP04 with different length scales and internal diameters (right).

cleaning step with ethanol after removal of the parts from the build platform and refining the pre-printed threads with a 1/4-28" thread cutter. The parts were fully functional after removal of support structures, but a final curing in sunlight until the next day was envisioned. Flange and reactor were sealed by rubber bands, as available in most kitchens, and closed by M5 screws, washers and nuts. This low-cost approach allowed to produce a reactor for under 10 €.

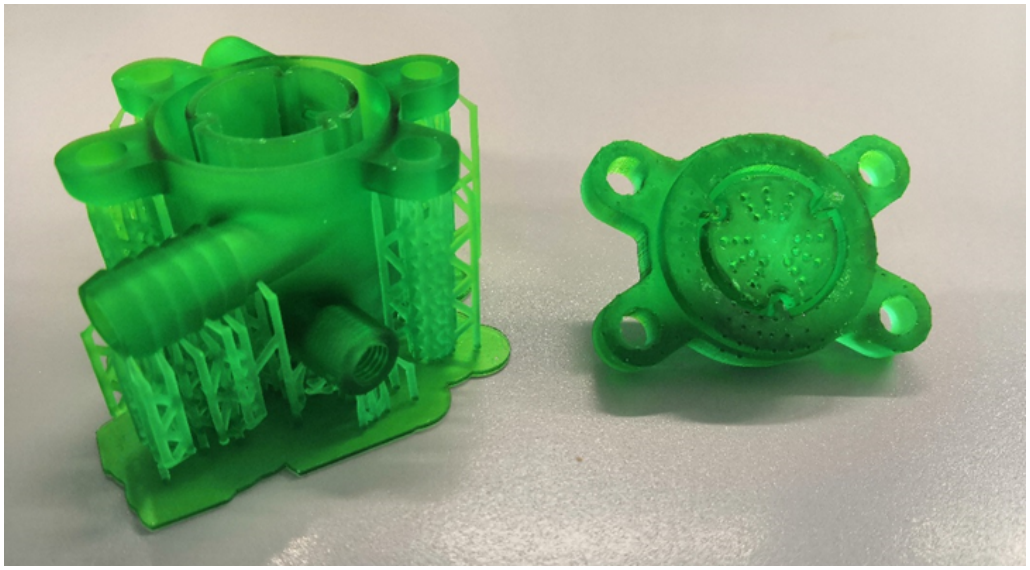

Supporting Information Figure S4.3: Picture of the *CSTR* and flange after *3D* printing. *3D* printing support can still be seen connecting the *CSTR* features to the building surface. The flange on the right hand side shows the integrated sieve to keep the alginate beads within the *CSTR*.

4.C Aerobic oxidation of Grignard reagents in continuous flow

The contents in this section are part of the Master Thesis with the title "Design of *3D*-printed Microreactors for Continuous Flow Synthesis", submitted to Graz University of Technology by Alessia Valotta in September 2019. Parts of the thesis (graphs, equipment) are reproduced here with the authorization of the author.

4.C.1 Reactor characterization of CSTR cascade and parameter reactors

The chosen Grignard oxidation is very fast and requires fast mixing in order to increase the yield of the phenol product and reduce the extent of side reactions. Microfluidic devices are a powerful tool for carrying out this type of reactions: due to the increased surface-to-volume ratio, the effective area for heat and mass transfer is increased. [16] The devices presented in this work were designed based on different mixing principles. Therefore, in order to compare the reactors, it was necessary to evaluate their mixing efficiency. This was necessary not only to classify the reactors according to their performance, but also later on to interpret the results of the Grignard reactions in flow.

The reactor characterization was carried out on two levels. First, the mixing efficiency on the scale of molecular diffusion was investigated by performing mixing sensitive reaction experiments. As the name suggests, the selectivity of these reactions is highly dependent on the mixing time and diffusion path in the device. [35, 162] Many mixing sensitive reactions have been characterized and various protocols are available in literature. [35, 162, 163, 117, 34, 102] Second, mixing on the macro-scale of convection was studied by means of the residence time distribution. This is a well-established method that gives measure of how the flow pattern of the fluid inside of a reactor deviates from the ideal plug-flow or *CSTR* model. [33]

4.C.1.1 Mixing sensitive reactions

In this work, the consecutive competitive diazo coupling of 1-naphthol with diazotised sulfanilic acid, characterized by Bourne *et al.* [1], was chosen to study the micro-mixing efficiency of the designed microreactors. The proposed reaction mechanism is presented in Fig. S4.4. 1-Naphthol (reagent A) reacts with diazotised sulfanilic acid (reagent B) in excess to give two monoazo R-products, where the functional group is either in *ortho* (*o*-R) or *para* (*p*-R) position. The reaction is highly dependent on the mixing efficiency of the reactor. When two entering streams are mixed poorly, there are regions in the reactor with a high concentration of B and the monoazo products, but little or no reagent A is present. Therefore, B reacts with either *o*-R or *p*-R to give the secondary undesired S-product, following the mechanism shown in Fig. S4.4. The amount of S-product formed is quantified by its yield Y_S . If Y_S is low, mixing is fast and the reaction is not mass

transfer limited. This means that the reactor's mixing performance is sufficient to ensure high selectivity even for fast chemical reactions.

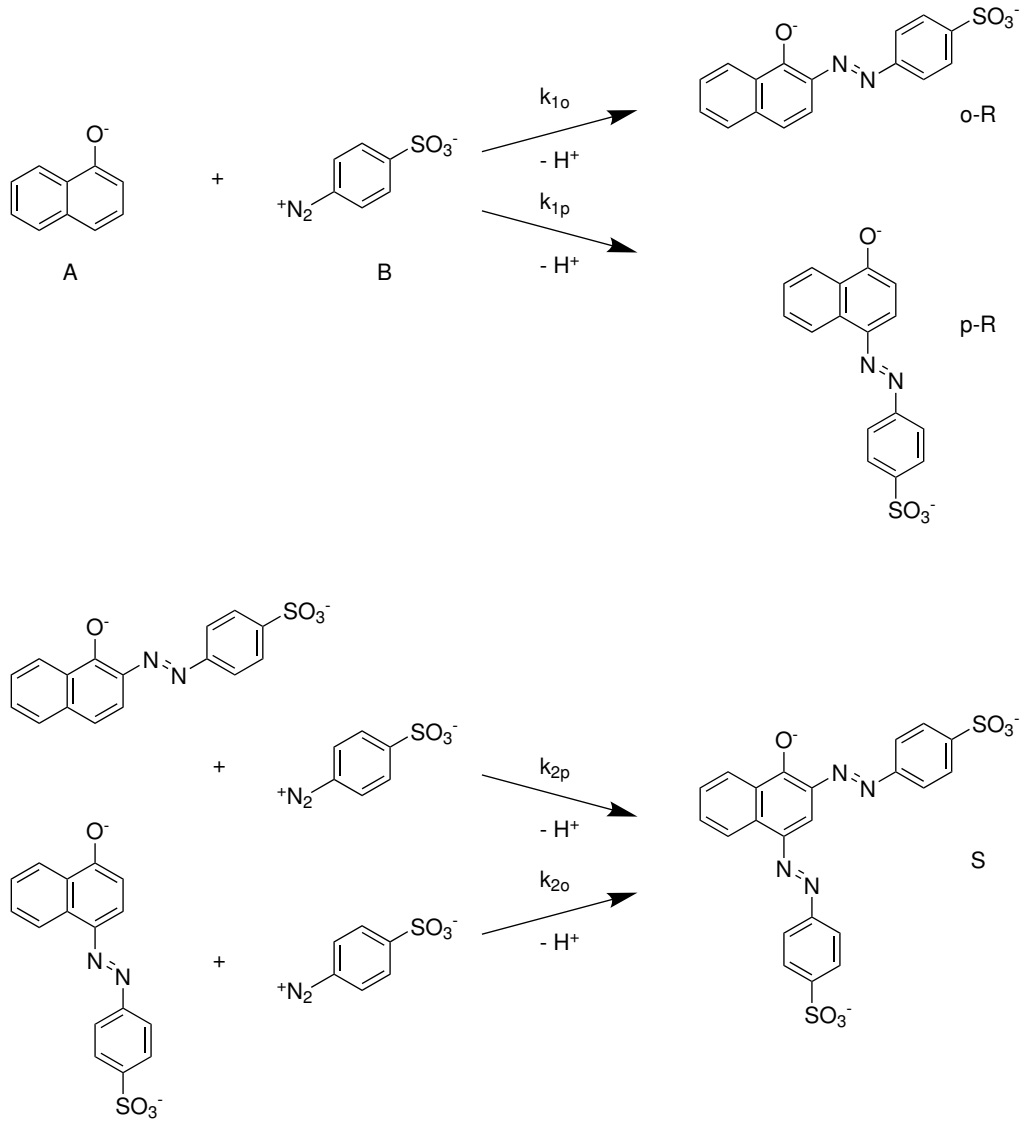

Supporting Information Figure S4.4: Mechanism of the Bourne reaction, as described by Bourne *et al.* [1] Reprinted (adapted) with permission from (Bourne, J. R. *et al.*, Kinetics of the Diazo Coupling between 1-Naphthol and Diazotized Sulfanilic Acid. Ind. Eng. Chem. Res. 1990, 29 (9), 1761–1765.). Copyright (1990) American Chemical Society.

Considering the stoichiometry of the reaction, Y_S is calculated as:

$$Y_S = \frac{2c_S}{c_{p-R} + c_{o-R} + 2c_S} \tag{4.1}$$

The experimental setup is depicted in Fig. S4.5. Mixing reactions were performed with

a 1.2 mM 1-naphthol solution in a carbonate/bicarbonate buffer (pH 9.9, ionic strength 888.8 mM) (reagent A) and a 1 mM solution of diazotised sulfanilic acid (reagent B). Two syringe pumps were used to inject equal volumetric flow rates of both reagents into the microfluidic device. The microfluidic devices were connected to the pump with *PTFE* capillaries (1/16" *OD*, 0.03" *ID*) and standard *HPLC* fittings. At the outlet of the microfluidic devices, 2 mL of the product solution were collected for each operation point. To be sure that the system had reached steady state after the desired flow rate was set and the pumps were turned on, the reactor was flushed for at least three residence times before taking a sample. Each sample was stored in the dark until analysis, since both the reagents and the products are light sensitive. The samples were analyzed within 3 hours from the withdrawal in order to avoid the results being falsified because of product decomposition.

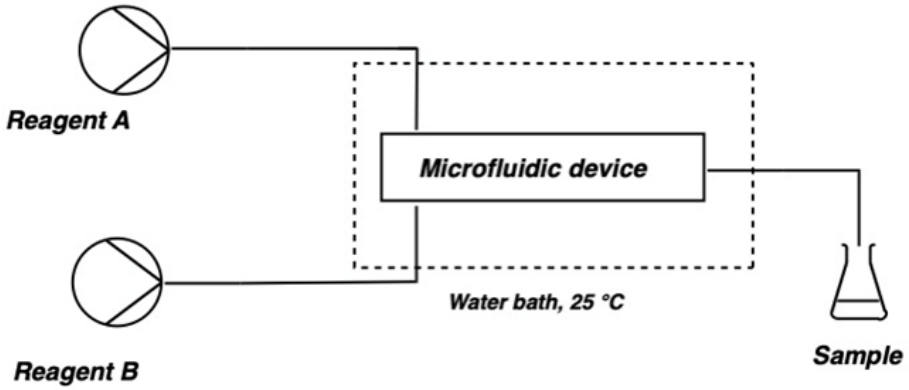

Supporting Information Figure S4.5: Setup used for studying mixing sensitive reactions.

The concentration in each sample was measured by means of *UV*/*VIS* spectroscopy, by flushing the sample through an Avantes flow cell with 10 mm path length. However, it was necessary to dilute the product solution with 5 mL buffer (pH 9.9, ionic strength 444.4 mM) to achieve a concentration in the measurable range of the flow cell, being approximately 0.04 mM. This step was also necessary to ensure that the measured absorbance was between 0.1 and 1, in order to apply the Lambert-Beer law. [164] The measured absorption was exported at wavelengths between 390 nm and 700 nm with intervals of 10 nm into ASCII files. The concentration of each dye was determined by measuring the total absorption of the samples. The total absorption is given by the Lambert-Beer law:

$$A = \epsilon_S c_S l + \epsilon_{oR} c_{oR} l + \epsilon_{pR} c_{pR} l \tag{4.2}$$

where ϵ is the molar extinction coefficient of a dye at a specific wavelength (given in m^2 mol^{-1}), s is the dye concentration (given in mol L^{-1}) and l is the optical path length (given in m). With the extinction coefficients of each component retrieved from Bourne *et al.* [1], it was possible to calculate each concentration using standard-multi-parameter-regression with least square fitting method. This was done by feeding the *UV* spectrum from each

sample to a MATLAB code that evaluated the data and calculated Y_S.

The results obtained are reported in Fig. S4.6. Concerning the parameter reactors, three different reactors were tested: AP04 with inner diameters of 0.8 and 0.7 mm and AP03 with an inner diameter of 0.8 mm, to test both the effect of different passive mixing principles and decreasing channel diameter. The total flow rates used were 0.2 / 0.5 / 1 / 2 / 4 and 6 mL min^{-1}. In order to be able to compare the results obtained for different reactor geometries, the flow rates were converted to Reynolds numbers associated with the hydraulic diameter of each reactor. Looking at the results, the first thing to notice is that for very low flow rates there is no difference among the reactors, as the flow rate is too low and diffusive mixing is dominates over convective mixing. Also, since the reaction is fast, the first contact point is the most relevant one. All of the reactors have the same type of Y-mixer as first contact point, thus no significant difference in yield was observed. However, when slightly increasing the total flow rate from 0.2 to 0.5 mL min^{-1}, it was noticeable that for the device with smaller internal diameter the mixing efficiency increases. In fact, the smaller the diameter, the higher the superficial velocity of the fluid and therefore the higher the Reynolds number, causing chaotic flow structures in the reactor. Also, switching from AP04 to the AP03 reactor results in an improved mixing efficiency. The AP03 reactor has a complex helicoidal structure with an alternate switch in curvatureof the channels. This arrangement increases the chaotic advection and promotes the formation of secondary flow structures inside the reactor. In the AP04 reactor instead, the stream is split into multiple channels of same diameters and then recombined, thus the flow velocity is lower than in the AP03.

Concerning the *CSTR* cascade, in each experiment the first vessel was connected with the 1-naphthol reservoir and the coupling reaction started in the second vessel, where the diazotised sulfanilic acid was added. The mixing sensitive reaction experiments were performed at four different stirring rates (0 / 500 / 1000 and 1500 *RPM*) and seven different total flow rates (0.1 / 0.25 / 0.5 / 1 / 2 / 3 and 4 mL min^{-1}). The greatest effect of stirring on the mixing efficiency was noticed at lower flow rates. Here Y_S decreases when increasing the stirring speed, meaning that the higher the stirring speed, the better the mixing. However, for higher flow rates this is not the case anymore. No significant change in yield was registered for $Re > 150$. Comparing these results with those obtained for the parameter reactors, the *CSTR* cascade always showed higher mixing efficiency, even without stirring. This can be explained by the fact that the inner diameter of the channel connecting each vessel is 0.6 mm, smaller than for the other reactors tested. A smaller diameter is responsible for a more chaotic flow in the system and therefore better mixing. Also, the stream is subject to a split-and-recombine mixing action. First, it travels in a small capillary, then the section increases when it enters a vessel and then it is squeezed again into a small channel.

4.C.1.2 Residence time distributions (RTD)

RTD experiments allow to get an insight into the flow pattern inside the reactor, since this deviates from the ideal models used in reaction engineering due to axial dispersion and backmixing effects. To quantify the extent of these effects, a non-dimensional value is defined, called the Bodenstein number (referred to as *Bo* for simplicity). This number represents the ratio of convective mass transfer over axial dispersion:

$$Bo = \frac{uL_{char}}{D_{ax}} \tag{4.3}$$

where u is the flow velocity, L_{char} is the characteristic length of the device and D_{ax} is the axial dispersion coefficient. The higher *Bo* (above 100), the more the reactor is approaching an ideal PFR behavior. On the other hand, the lower *Bo* (below 100), the higher the backmixing and the more the reactor has a *CSTR* behavior. Different models and correlations are available for calculating *Bo* and have been reported in literature. [33]

The *RTD* experiments were carried out using the step input principle, as reported in literature. [33] The experimental setup is presented in Fig. S4.7. Two syringe pumps were used, one filled with pure solvent and one containing a tracer. The solvent used was a mixture of ethanol (12 wt%) in water and the tracer was a solution of 0.008 v% anisole in the aforementioned solvent. Both lines were connected to a 6-way-valve, which was connected to one of the reactor's inlets. At the outlet of the reactor, the Avantes in-line flow cell with 10 mm path length detected the absorption of anisole between 268-274 nm, a wavelength range where only anisole is measurable. Also, a baseline correction was recorded in the wavelength range of 500-506 nm, where anisole is not detectable. Before each experiment, a dark and light reference sample was taken when the 6-way-valve was set to load and only solvent flowed through the system. The experiment was carried out by generating a step signal when the 6-way-valve was switched to the inject position, so there was a switch from no tracer to constant tracer concentration. After the absorbance

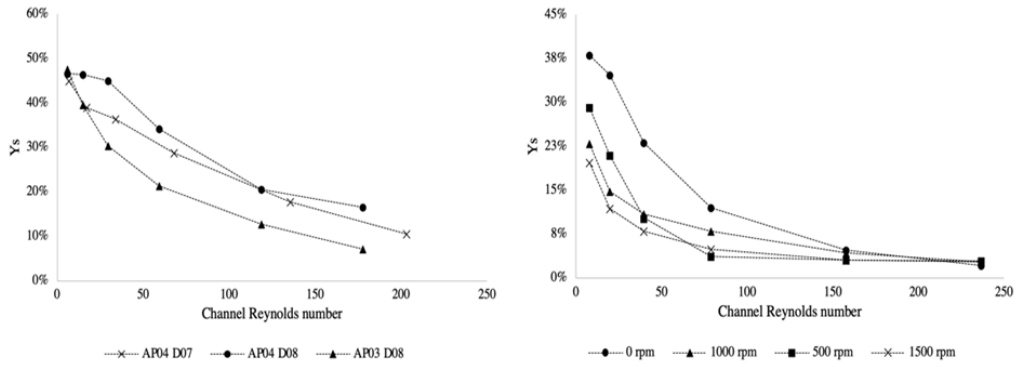

Supporting Information Figure S4.6: Results of the Bourne reaction for parameter reactors (left) and for the *CSTR* cascade (right).

value for the tracer reached a stable value, a step down signal was recorded by switching the valve back to load, so to only solvent and no tracer. The data was recorded by using the Time series function in the Avantes spectrometer software and then exported for evaluation in an Excel file after each run. For each experiment, the Bodenstein number was calculated, according to the open-open model calculations described in literature. [33]

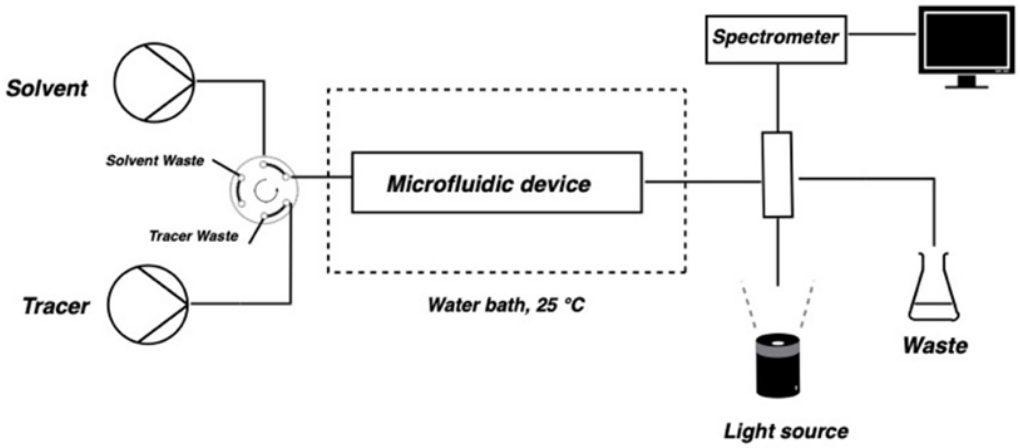

Supporting Information Figure S4.7: Experimental setup for the *RTD* experiments.

The parameter reactors were AP03 with channel diameters of 0.8 and 0.7 mm, respectively, and AP04 with a channel diameter of 0.8 mm. Results for the *RTD* experiments are shown in Fig. S4.8. Seven different flow rates (0.1 / 0.25 / 0.5 / 1 / 2 / 3 and 4 mL min^{-1}) were tested. In the setup, every parameter reactor was connected with one inlet, while the other one was blocked. From the analysis of the results for each reactor, no significant increase in Bodenstein number was recorded with the change of the flow rate. The average in *Bo* was 40.95 for the AP03 reactor with diameter 0.7 mm, 30.23 for the AP03 with diameter 0.8 mm and 9.33 for the AP04 reactor. Overall, it could be noticed that the highest values of averaged *Bo* were obtained for the AP03 d07 reactor. This result was expected because of two factors that improve the mixing efficiency. First, the internal diameter is smaller than the one of the other parameter reactors investigated. As a result, the superficial velocity of the fluid in the channels is higher, therefore the flow is more chaotic and the backmixing effect is lower. Moreover, the AP03 reactor has a helicoidal channel arrangement that causes the flow to bend with high curvature. This promotes the formation of secondary flow structures and increases the chaotic advection effect. The axial dispersion increases when switching to the same reactor with bigger diameter, but its effect is even higher when comparing these results with those obtained with the AP04 reactor. In the AP04 structure, the flow is split into numerous channels, so it is slowed down, therefore less turbulent and subjected to high backmixing. The results, in fact, show that the AP04 reactor tends to an ideal *CSTR* behavior.

For the *CSTR* cascade only the *RTD* of the cascade with 0.6 mm internal diameter was determined. Seven different flow rates (0.1 / 0.25 / 0.5 / 1 / 2 / 3 and 4 mL min^{-1})

and three stirring speeds (0, 500 and 1500 *RPM*) were tested. The 6-port injection valve was connected to the first vessel of the *CSTR* cascade through a flat *HPLC* fitting and a *PTFE* capillary. Looking at the results in Fig. S4.8 (graph to the right), it is noticeable that the Bodenstein number is around 25 for all experiments, indicating the expected *CSTR* behavior and therefore high backmixing and dispersion in the reactor. In contrast to the results of the Bourne experiments, no significant change in the Bodenstein number was noticed when increasing the stirring rate. This means that the backmixing is so high that it is not influenced by the active mixing principle used in this device.

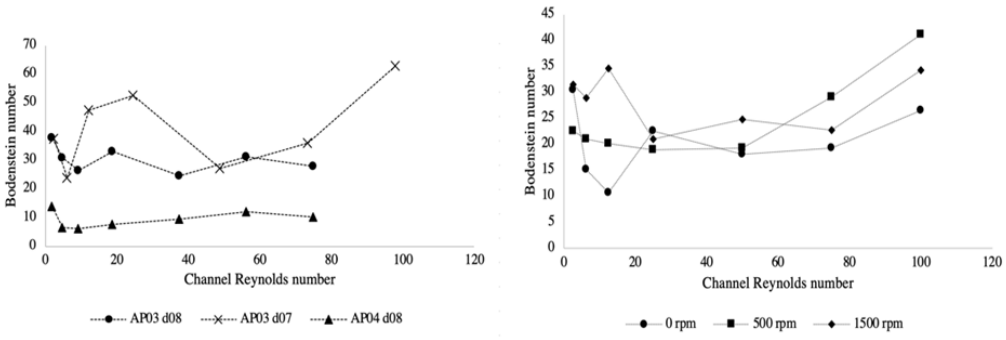

Supporting Information Figure S4.8: Results of *RTD* experiments for parameter reactors (left) and for the *CSTR* cascade (right).

4.C.2 Grignard oxidation experiments

The detailed reaction mechanism for the oxidation of Grignard reagents to their corresponding phenols has been reported in literature, e.g., by He *et al.* [94] The reaction comprises three steps. First, there is an oxidation stage, where free radicals are formed due to a chain sequence that involves an electron transfer between molecular oxygen and the arylmagnesium Grignard species. The radical intermediates further interact to give an organoperoxide intermediate, which reacts in the metathesis stage with another arylmagnesium molecule to give an organoperoxide magnesium salt. The corresponding phenol is obtained in the last step by acidification of the metathesis product. In the experimental setup the last step is achieved by quenching the product stream with 0.5 M *HCl*.

4.C.2.1 Start-up procedure

Before each continuous flow experiment, a precise start-up procedure was followed in order to rapidly reach steady state. First, both syringe pumps were purged with argon, before being filled with degassed solvent. Then, a bottle containing the solvent was connected to the 6-way-valve via a tube going directly into the bottle through a sealed septum. By keeping the valve in the load position, the pump was directly connected to the bottle and using the withdraw function of the pump, the syringe was filled with degassed solvent with

minimum chance of undesirable oxygen contamination. Afterwards, the pumps were set to the desired flow rate and the entire system was flushed with the solvent to remove the oxygen and slowly equilibrate the liquid line to 7 bar. The pumps were then filled again using the same procedure. In the meantime, the oxygen line was turned on while keeping the check valve closed. The flow rate on the line was set to a higher value than in the process (around 10 mL min^{-1}) in order to cause a rapid increase of the pressure on the oxygen line. When the *PI* indicated a pressure slightly above 7 (around 7.2 bar), the flow rate was set to the desired value and the check valve was opened. Once the pressure in the oxygen line and the system reached equilibrium, a stable slug flow left the T-mixer. This procedure was crucial to prevent backflow of the solvent into the *MFC* and avoid possible damage to its electronical parts. After the stable slug flow reached the absorption column, the recording of the data from the oxygen sensors started. Once the signal of the oxygen recorded by the reference sensor placed before the reactor was constant, the second 6-way-valve was opened and the reagent solution was pumped from the sample coil into the reactor. The whole start up procedure lasted around 5 min, giving around 15 min left to perform the experiment, which was enough considering that the reaction is very fast.

4.C.2.2 Sensor data obtained for the CSTR cascade

The *CSTR* cascade presented in this work was designed to host in-line sensors directly in its vessels, by connecting the sensor tips with standard *HPLC* fittings. Oxygen sensors designed within the CC FLOW project [135] were used in the continuous flow setup to keep track of the oxygen supply to the *CSTR* cascade and the oxygen consumption within the reactor itself. Seven sensors were used: one was placed at the outlet of the *HPLC* column and six were placed inside the reactor vessels. The signal measured by the first sensor was taken as a reference value to know the total amount of incoming oxygen and to calculate the percentage of consumed oxygen over time, as shown in Fig. S4.9. For each experiment, after the system had reached steady state, the reagent was pumped into the reactor and the reaction started. However, the small internal channels got clogged during some runs, therefore no significant data could be retrieved from the oxygen sensors, since steady state was never reached. The only exception was the experiment at 0 °C, whose results are reported in Fig. S4.9. From this graph, it is possible to see that the signal for all sensors is constant during the absorption step, stabilizing around the reference value. Then, after 6 minutes, since the oxygen signal was stable enough, the reagent was pumped into the system. At this point the oxygen concentration dropped for all of the sensors with little delay among each of them, indicating that the reaction was already over in the first vessel and no further oxygen consumption was recorded later on. This proved that the reaction is extremely fast. Considering that each vessel has a volume of 85.27 μL, for a flow rate of about 1.1 mL min^{-1} the resulting residence time for each vessel is 4.65 seconds. From the sensors' results it can be assumed that the reaction time is lower than this value. Therefore, it is so fast that it is not possible to determine kinetic parameters with this

setup. Another important factor that can be deduced from the plot in Fig. S4.9 is that the sensors have different sensitivity. For example, sensor 4 was not sensitive enough to track the fluctuations in oxygen concentration visible from the other sensor's readouts. This could be caused by sensor 4 reaching the end of its operating time.

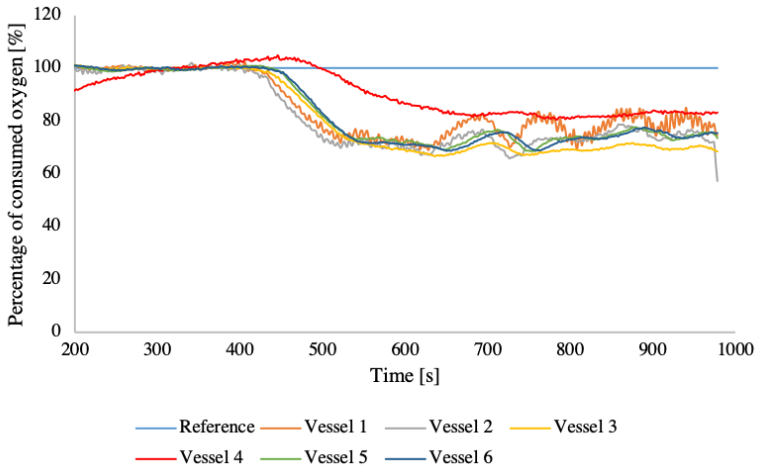

Supporting Information Figure S4.9: Oxygen concentration recorded by the optical oxygens sensors placed before, after and inside the vessels of the *CSTR* cascade reactor. The concentration is calculated as percentage of O_2 consumed compared to the value given by the reference sensor, placed before the reactor inlet.

4.C.3 Analytics & Equipment

4.C.3.1 6-Port injection valve

For injection of *RTD*-tracer and the injection of Grignard reagent during the oxidation experiments, a 6-port medium pressure injection valve V-450 from IDEX Health & Science LLC was used.

4.C.3.2 Back pressure regulator

A Zaiput *BPR*-10 was used in the flow experiments to ensure a constant downstream pressure (higher than ambient). Such device can handle multiphasic systems and can be set up to 20 bar. It can operate until 130 °C and can handle flow rates ranging from 0.05 mL min^{-1} to 20 mL min^{-1}. The *BPR* was connected to the process line via flat bottom *HPLC* fittings.

4.C.3.3 Gas chromatography

Gas chromatography (*GC*) was used to follow the reaction progress in Grignard oxidations. For each sample, 300 μL of reaction mixture were diluted with 700 μL of *2-Me-THF*. *GC*

analysis was performed with a Perkin Elmer Clarus 500 system equipped with an Optima-5 MS capillary column (Machery-Nagel, 30.0 m x 320 μm *ID*, 0.25 μm) with a Flame Ionization Detector (*FID*) with 45 mL min^{-1} H_2 and 450 mL min^{-1} synthetic air. N_2 was used as carrier gas. 1 μL aliquots were injected. The initial temperature was 50 °C, held for 1 min. Afterwards the oven was heated with a rate 25 °C min^{-1} to 300 °C and held for 4 min.

No *NMR* spectra of the products were recorded, as the purpose of the experiments was to compare the *GC* yields of 4-chlorophenol obtained with the different microfluidic devices. The chromatogram obtained for the product samples taken after the reaction (recorded with the *GC* method described above) was crosschecked with the chromatogram of the pure compound, in order to identify the peak for the desired product.

4.C.3.4 Laboratory magnetic stirrer

To set rotational speeds for experiments with the *CSTR* cascade, an IKA RCT standard laboratory magnetic stirrer was used. The *RPM* are digitally displayed and can be set between 0 *RPM* and 1400 *RPM* in steps of 10 *RPM*.

4.C.3.5 Mass flow controller

The oxygen stream for the oxidation experiments was controlled with a Mass Flow Controllers (*MFC*) from Vögtlin instruments, type GSC-A9SA-DD21, with a range from 0 mL min^{-1} to 25 mL min^{-1}.

4.C.3.6 Oxygen sensors

In order to measure the rate of oxygen consumption over time in the flow experiments, in-line optical oxygen sensors were used. These were produced within the CC FLOW project and are based on a phase fluorimetry readout system. [135] They are applicable for pressurized systems in the presence of organic solvents and high oxygen concentrations by utilizing tailored fiber based optical sensors. [8] A *NIR*-emitting Pt-tetra(4-fluorophenyl)tetrabenzoporphyrin (PtTPTBPF) dye was immobilized in polyphenylenesulfide (*PPS*) and coated with a CYTOP® protection coating onto a glass fiber. [8] They were connected to the system via flat bottom *HPLC* fittings. The signals were recorded by a miniaturized USB phase fluorimeter (FirestingO2) and processed by a Python-based software. Since these sensors behave according to the linear Stern-Volmer equation [109, 135], a quick 2-point calibration of oxygen concentration (at 0 and maximum oxygen concentration) was carried out before each run.

4.C.3.7 Pressure logging system

The pressure on the oxygen line during the continuous Grignard oxidation experiments was measured by a digital Pressure Indicator (*PI*) of type Druck DPI 104 produced by GE.

The pressure measured by the indicator was converted internally to an analogous voltage signal in the range of 0-5 V, which is directly proportional to the pressure measured in the system. The *PI* was connected to an Arduino Mega 2560, which was programmed to read the analogue voltage signal from the *PI*, convert it to a pressure value and write it to a serial COM port. The received data was saved on a PC via a terminal logger.

4.C.3.8 Pumps

Two Lambda VIT-FIT syringe pumps equipped with 20 mL Chemyx stainless steel syringes were used for *RTD*, mixing sensitive reactions and continuous flow experiments. The syringes were equipped with special gaskets made of FFKM to withstand *2-Me-THF*.

4.C.3.9 Thermostat

The LAUDA Alpha RA 12 was used as a thermostat for the Grignard reactions. Its operation range is from -25 °C to 100 °C and it has a heating power of 1.5 kW. It is equipped with a bath (volume of 14.5 L) that was filled with a 50:50 solution of water and ethanol in order to reach lower temperatures without causing freezing of the cooling bath.

4.C.3.10 UV-Vis spectrophotometer

An Avantes AvaLight-DS-DUV, equipped with a deuterium lamp, was used as light source for *UV* / *VIS* measurements and an Avantes AvaSpec-ULS2048 was used as detector. They were connected with two optical fibers FC-UV400-1-FIA-SR and a Flow Cell-Z-10 from Avantes with 10 mm optical path length.

4.D Multistep synthesis of a valsartan precursor in continuous flow

The contents are adapted from the Supporting Information of the article "Multistep synthesis of a valsartan precursor in continuous flow" [Hiebler K, Soritz S, Gavric K, Birrer S, Maier MC, Grabner B, Gruber-Woelfler H (2020) J Flow Chem 10:283-294] with the authorization of the authors.

4.D.1 Integrated synthesis of a valsartan precursor in continuous flow

Solution A [containing boronic acid ester (110 mM, 1.1 mol eq.), 2-iodobenzonitrile (100 mM), DIPEA (220 mM, 2.2 mol eq.), anisole (240 mM) as internal standard] and solution B [containing valeryl chloride (220 mM, 2.2 mol eq.)] were prepared in dioxane and degassed via ultrasonic treatment. After equilibration of the reactor system, the two reagent solutions (v= 0.05 mL min^{-1} each) were introduced in a combined *SaRR*/coil reactor unit (*SaRR* + *PEEK* coil L x *OD* x *ID* 3.0 m x 1/16 in. x 0.030 in., v= 0.10 mL

min^{-1}, V total = 1.93 mL, τ= 19.3 min) at 80 °C for N-acylation using high-pressure syringe pumps (VIT-FIT HP, Lambda Instruments). Then, the process stream was quenched with an aqueous K_2CO_3 solution (185 mM, 3.7 mol eq., v= 0.10 mL min^{-1}) by means of an *HPLC* pump (P4.1S, Knauer) using a T-mixing element. Next, the reaction solution was pumped through the Plug & Play reactor [165] equipped with a preparative *HPLC* column (L x I.D. 120 x 8 mm) filled with Pd-catalyst $Ce_{0.20}Sn_{0.79}Pd_{0.01}O_{2-\delta}$ (4.3 g, for synthesis see Sec. 4.E.1.3) at 80 °C for Suzuki-Miyaura cross-coupling (v= 0.20 mL min^{-1}, τ= 22.3 min). Finally, a sodium hydroxide solution (750 mM, 15 mol eq., dioxane:H_2O= 2:3, v= 0.10 mL min^{-1}) was added to the stream using a syringe pump (LA-120, Landgraf) and the resulting mixture was introduced again into a *SaRR*/coil reactor unit at 80 °C for methyl ester hydrolysis (*SaRR* + *PEEK* coil L x *OD* x *ID*. 10.0 m x 1/16 in. x 0.030 in., V total = 5.13 mL, τ= 17.1 min). The outlet flow was collected (residence time of the total system $\tau \sim 1$ h) and after certain time points, an aliquot (50 μL) was quenched with MeOH:H_3PO_4 =55:45 (400 μL) and analyzed by *HPLC*. A graphic representation of yield over time obtained in the multistep continuous process for formation of the valsartan precursor is apparent from Fig. S4.10.

The target compound was extracted from collected outlet flow with ethyl acetate and purified via column chromatography on silica gel (petrol ether:ethyl acetate:acetic acid=69.5:70:0.5, R_f = 0.33).

***HPLC*/MS-ES** (m/z) found 393, calculated for $[M+H]^+$ 393.50

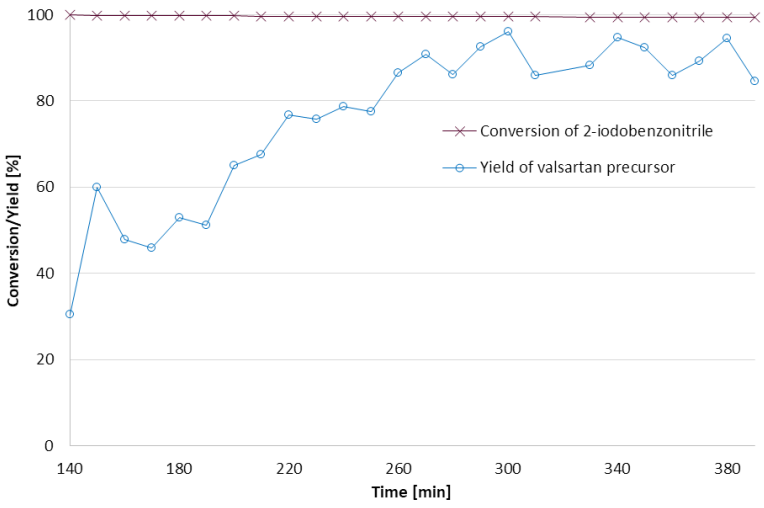

Supporting Information Figure S4.10: Conversion of 2-iodobenzonitrile and yield of targeted valsartan precursor obtained using the multistep continuous setup.

4.D.2 Analytics

4.D.2.1 HPLC analysis

For monitoring of the reaction progress, reaction samples were analyzed using an Agilent 1100 series *HPLC* system equipped with an online degasser, quaternary pump, autosampler, thermostated column compartment and *UV*-visible diode array detector. As mobile phases, MeOH (solvent A) and aq. phosphoric acid (H_2O:H_3PO_4 =300:1 v/v; solvent B) were used. Compounds were separated using a ThermoFischer Scientific Accucore TM C18 reversed phase column (50 x 4.6 mm; 2.6 μm) at 25 °C with a flow rate of 1 mL min^{-1} and detected by *UV*-absorption over the run time of 15 min. Used elution method is summarized in Tab. S4.1.

Supporting Information Table S4.1: *HPLC* method (% A = % MeOH, % B = % H_2O:H_3PO_4 =300:1 v/v) for monitoring of the reaction progress.

Time [*min*]	% A (v/v)	% B (v/v)	Sample diluent	Flow [$mlmin^{-1}$]
0	55	45		
10	80	20	MeOH:H_2O= 55:45	1
12	55	45		

For determination of the enantiomeric excess of the target compound, an Agilent 1100 Series *HPLC* system equipped with a temperature-controlled oven and a *UV* detector was employed. As mobile phase, n-hexane:2-propanol=85:15 (v/v) containing 0.1 v% trifluoroacetic acid (*TFA*) as modifier was used. Compounds were separated using a Daicel Chiralpak® AD-H column (250 x 4.6 mm) with a flow rate of 0.1 mL min^{-1} kept at 30 °C over a time period of 25 min and detected by *UV*-absorption (λ=230 nm).

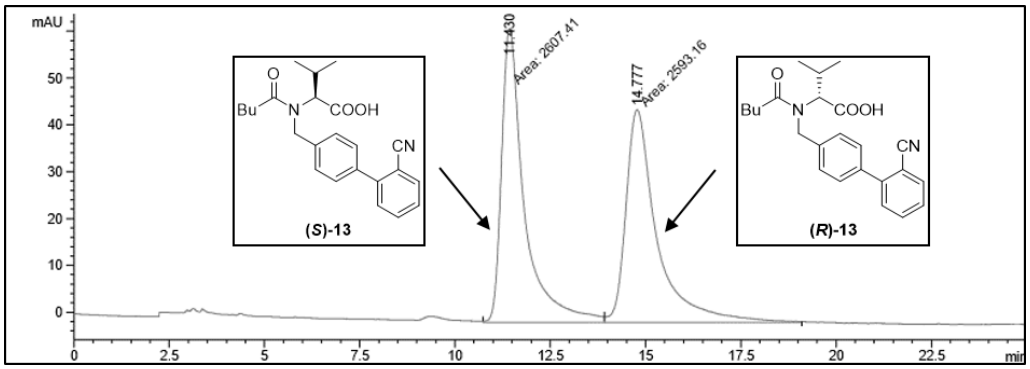

Supporting Information Figure S4.11: Chiral separation of (R)- and (S)-valsartan precursor by *HPLC* (λ= 230 nm).

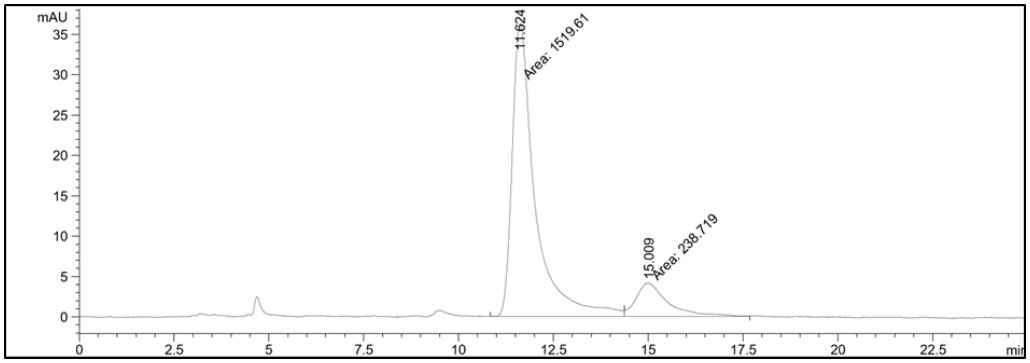

Supporting Information Figure S4.12: Determination of enantiomeric excess of valsartan precursor synthesized in the multistep flow process (λ= 230 nm).

4.D.2.2 NMR

^{1}H- and ^{13}C-*NMR* data (mix of rotamers) are in accordance with literature. [166]

^{1}H-*NMR* Valsartan precursor (300 MHz, $CDCl_3$): δ_H [ppm]= 9.35-8.25 (brs, 1H), 7.72-7.15 (m, 8H), 4.78 (d, J=17.0 Hz, 1H), 4.41 (d, J=17.0 Hz, 1H), 3.99 (d, J= 10.8 Hz, 0.2H), 3.75 (d, J= 10.5 Hz, 0.8H), 2.70-2.17 (m, 3H), 1.72-1.50 (m, 2H), 1.41-1.19 (m, 2H), 0.68-1.03 (m, 9H).

^{13}C-*NMR* Valsartan precursor (75 MHz, $CDCl_3$): δ_C [ppm]= 177.4, 174.8, 172.0, 144.8, 138.1, 136.3, 133.9, 133.7, 133.1, 133.0, 130.2, 130.1, 129.6, 128.6, 128.3, 127.9, 127.5, 127.2, 118.7, 111.3, 71.8, 66.2, 54.3, 46.1, 34.2, 33.6, 27.9, 27.4, 27.3, 22.7, 22.5, 20.0, 19.9, 19.6, 19.0, 14.0, 13.9.

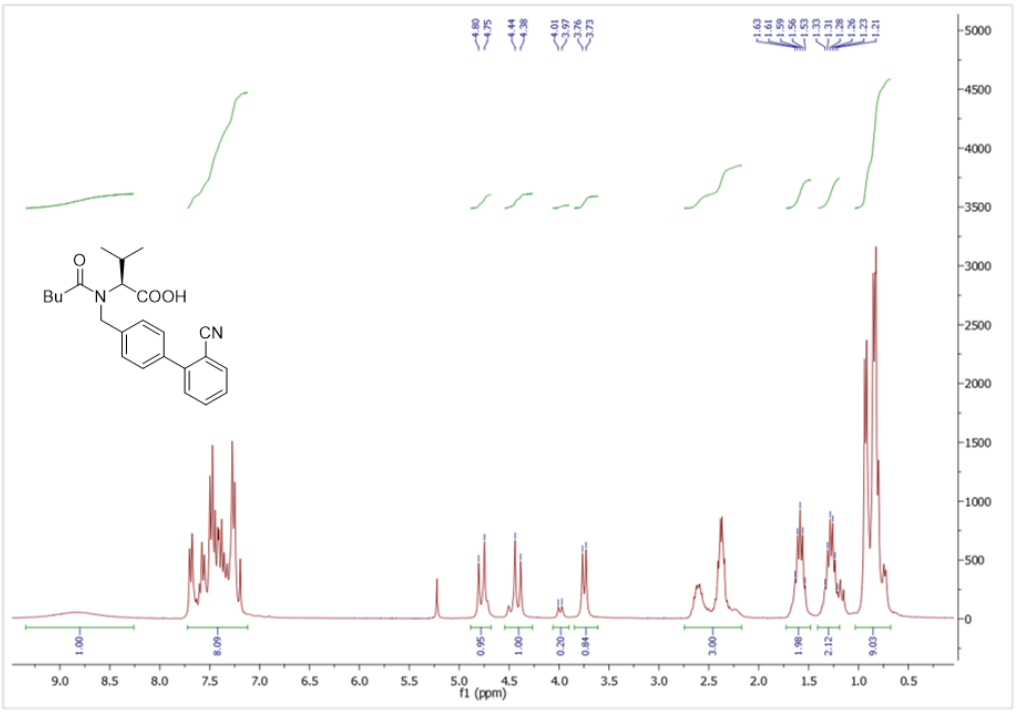

Supporting Information Figure S4.13: ^{1}H-*NMR* of the valsartan precursor in $CDCl_3$.

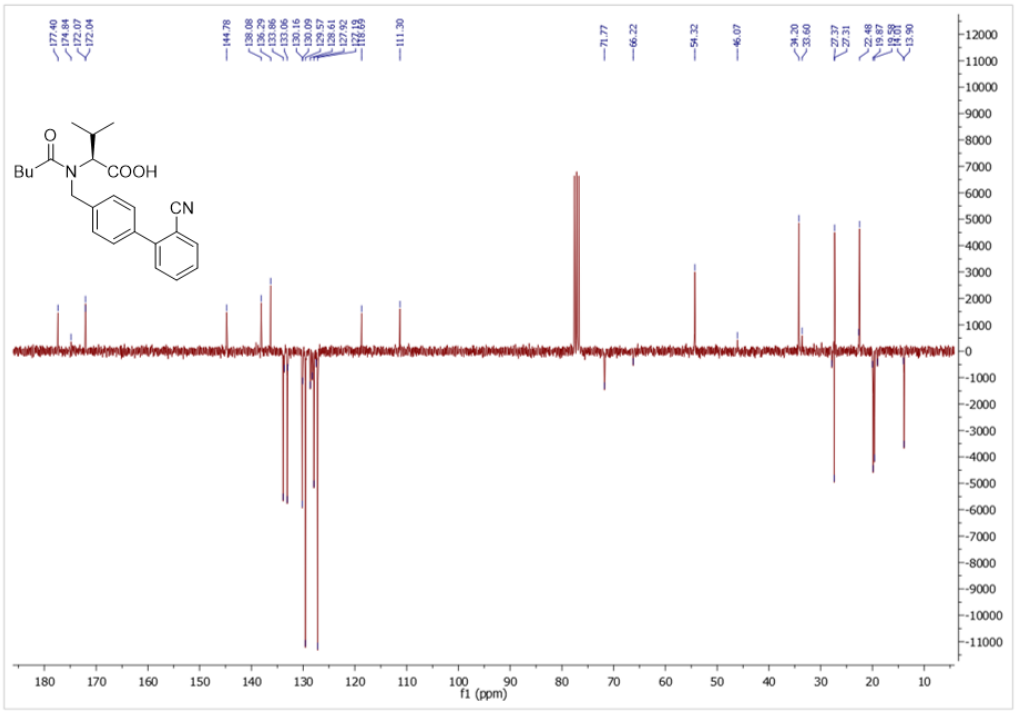

Supporting Information Figure S4.14: ^{13}C-*NMR* of the valsartan precursor in $CDCl_3$.

4.E Chemo-enzymatic tandem reaction for the synthesis of resveratrol derivatives in continuous flow

Parts of this section are adapted from the Supporting Information of the article "A chemo-enzymatic tandem reaction in a mixture of deep eutectic solvent and water in continuous flow" [Grabner B, Schweiger A. K, Gavric K, Kourist R, Gruber-Woelfler H (2020) React. Chem. Eng. 5, 263-269] and the Master Thesis with the title "Development of a Continuous Chemo-Enzymatic Two-Step Synthesis for Resveratrol Derivatives", submitted to Graz University of Technology by Kristian Gavric in January 2020. Parts of these works are reproduced here with the authorization of the authors.

4.E.1 Catalyst preparation

4.E.1.1 Expression of *Bs*PAD, preparation of cell free extract and freeze-drying

The recombinant pET28a expression plasmid, containing the *pad*C gene (Gene ID: 398579 encoding for *PAD* from *Bacillus subtilis*) was constructed as described elsewhere. [157] Both recombinant plasmids pET28a_*BsPAD*_WT were provided by the authors of [157]. Chemo-competent E. *coli* BL21 (DE3) cells were transformed with the expression plasmids and single colonies were used to inoculate overnight cultures (5 mL LB-Kan, 40 μg μL^{-1} kanamycin), which were incubated at 37 °C and 130 *RPM*. The complete overnight culture was used to inoculate 200 mL TB-Kan medium in 1 L baffled flasks. Cultures were incubated at 37 °C and 130 *RPM*, until OD_{600} reached 0.5-0.7 and protein expression was induced by addition of IPTG to a final concentration of 0.1 mM. After incubation at 20 °C and 120 *RPM* for 20-24 h, the cells were harvested by centrifugation (15 min, 4500 *RPM*, 4 °C) and the cell pellet was washed once with 50 mM KPi buffer (pH 6). Cells were either stored at -20 °C or directly used for the preparation of cell-free extract. Cell pellets were resuspended in 50 mM KPi buffer (pH 6) to a concentration of 100 mg_{CWW} mL^{-1} and lysed by sonication (Branson sonifier 250; 5 min, Duty cycle 5, Output control 50 %). The cell-free extract obtained after centrifugation (20 min, 11000 *RPM*, 4 °C) was sterilized by filtration, shock-frozen in liquid nitrogen and directly used for freeze-drying (AdVantage Pro Lyophilizer, SP Scientific). The lyophilized cell-free extract was stored at -20 °C until further use.

4.E.1.2 Enzyme immobilization

Cell-free extract (CFE) was dissolved in 2 % (w/v) sodium alginate solution in 50 mM potassium phosphate buffer (pH 6.0) in a concentration of 38.8 mg mL^{-1}. The mixture was then added dropwise to a 2 % (w/v) $BaCl_2$-solution in purified water using a syringe and a needle (0.8 mm *ID*) in order to form uniform beads of approximately 2-3 mm diameter. The beads were gently stirred in $BaCl_2$-solution for 1 h to solidify and turned from almost

clear to opaque. The beads were washed with 0.9 % (w/v) NaCl-solution and dried in ambient conditions for 30 min in order to solidify the surface of the beads and make them more resistant to shear forces.

4.E.1.3 Synthesis of the Pd-catalyst

The catalyst synthesis was adopted from the procedure described by Lichtenegger *et al.* parenciteLichtenegger2017 All the starting materials ($(NH_4)_2Ce(NO_3)_6$ (2.124 g), SnC_2O_4 (3.162 g), $PdCl_2$ (0.034 g) and glycine (3.345 g) were weighed out in a mortar and mixed with a pestle. The mixture was then dispersed in 3 mL of water in a 600 mL beaker. The dispersion was treated with ultrasound until a homogeneous solution was obtained. The redox mixture was heated to 350 °C in a furnace, where a self-propagating combustion reaction took place. The product, a light yellow-brown porous solid, was ground and again heated in the furnace to 350 °C for another 5 h. The obtained yellow-brown powder was used as catalyst without further treatment.

4.E.2 Preparation of deep eutectic solvent

For the preparation of the Deep Eutectic Solvent (*DES*), the components choline chloride (*ChCl*) and glycerol were weighed out in a ratio of 1:2 (mol/mol) and mixed together. The mixture was heated to 80 °C and stirred for 1 h. After cooling down, the prepared clear viscous liquid could be used as reaction solvent.

4.E.3 Continuous synthesis of resveratrol derivatives in continuous flow

Two stock solutions were prepared. Stock A served as feed for the enzymatic decarboxylation consisting of *DES*:potassium phosphate buffer (50 mM, pH 6.0) in a ratio of 1:1 (v/v) and *para*-coumaric acid (45 mM) Stock B was the feed for the Heck coupling and was mixed with the outlet of the decarboxylation before entering the Pd-packed column. Stock B contained 49.5 mM iodobenzene and 82 mM K_2O_3 dissolved in *DES*:ethanol:water in a ratio of 1:6.75:2.25. The used capillaries, fittings and syringe adapters were standard *HPLC* equipment (1/16 inch *OD*. x 0.03 inch *ID*, *PEEK*). A 5 mL vial was used to mix the product stream of the first reactor with the substrate feed for the second reactor. The reactors were heated to 30 °C for the decarboxylation (160 mg *PAD* immobilized in alginate bead of a total volume of 4 mL were flushed with solvent with 50 μL min^{-1} overnight to remove loosely bound enzyme and non-linked alginate) and 85 °C for the Heck reaction (6 g of catalyst powder in a stainless steel column 120 mm x 8 mm *ID*). After flushing the system with solvent for 1 h, the feed was switched to the stock solutions (stock A: peristaltic pump ISMATEC REGLO Digital Ms-4/8 ISM 834C, flow rate: 50 μL min^{-1}; stock B: Lambda VIT-FIT, Syringe pump equipped with 20 mL stainless steel syringe, Lambda Instruments, flow rate: 50 μL min^{-1}; feed for second step: *HPLC* pump P4.1S Knauer AZURA® Compact, flow rate: 0.1 mL min^{-1}). The pressure for the packed-bed reactor

was kept at 5 bar (IDEX *BPR* Cartridge 75 psi Gold Coat). Samples were collected at the outlet in 15 min intervals. From the product stream 50 μL were diluted with 500 μL of HLPC solvent (methanol: *HPLC* buffer 7:3, *HPLC* buffer = water:H_3PO_4 300:1).

4.E.4 Analytics

4.E.4.1 HPLC analysis

The samples were analyzed by reversed phase high performance liquid chromatography (RP-*HPLC*) using an Agilent Instrument 1100 Series equipped with a ThermoFischer Scientific Accucore^{TM} C18 reversed phase column (50 x 4.6 mm *ID*; 2.6 μm). 2.0 μL of the sample was injected. Eluent: 0-1 min 60 % H_2O:H_3PO_4 300:1, 40 % methanol; 1-12 min gradient to 10 % H_2O:H_3PO_4 300:1, 90 % methanol; 12-14 min gradient to 60 % H_2O:H_3PO_4 300:1, 40 % methanol. Sample analysis lasted 16 min. Flow rate: 1 mL min^{-1}. Column temperature: 25 °C. For detection of the analytes, a *UV* detector was used. Retention times: *para*-coumaric acid 1.1 min (282.4 nm), 4-vinylphenol 3.4 min (237.4 nm), iodobenzene 8.7 min (237.4 nm), para-hydroxy-1,1-diphenylethylene 8.9 min (237.4 nm), 4-hydroxystilbene 9.1 min (282.4 nm).

4.E.4.2 NMR

^{1}H-*NMR* data of para-hydroxystilbene are in accordance with literature. [167]

^{1}H-*NMR* *para*-hydroxystilbene (300 MHz, $CDCl_3$): δ_H [ppm]= 7.50 – 7-48 (d, 2H, Ar-H), 7.43 - 7.40 (d, 2H, Ar-H), 7.37 - 7.32 (t, 2H, Ar-H), 7.26 - 7.22 (t, 1H, Ar-H), 7.09 - 6.94 (dd, 2H, H-C=C-H), 6.85 – 6.82 (d, 2H, Ar-H), 4.77 (s, 1H, O-H).

^{1}H-*NMR* *para*-hydroxy-1,1-diphenylethylene (300 MHz, $CDCl_3$): δ_H [ppm]= 7.31 – 7.28 (m, 5H, Ar-H), 7.25 - 7.20 (d, 2H, Ar-H), 6.81 - 6.78 (d, 2H, Ar-H), 5.39 (s, 1H, C=C-H), 5.35 (s, 1H, C=C-H), 4.74 (s, 1H, O-H).

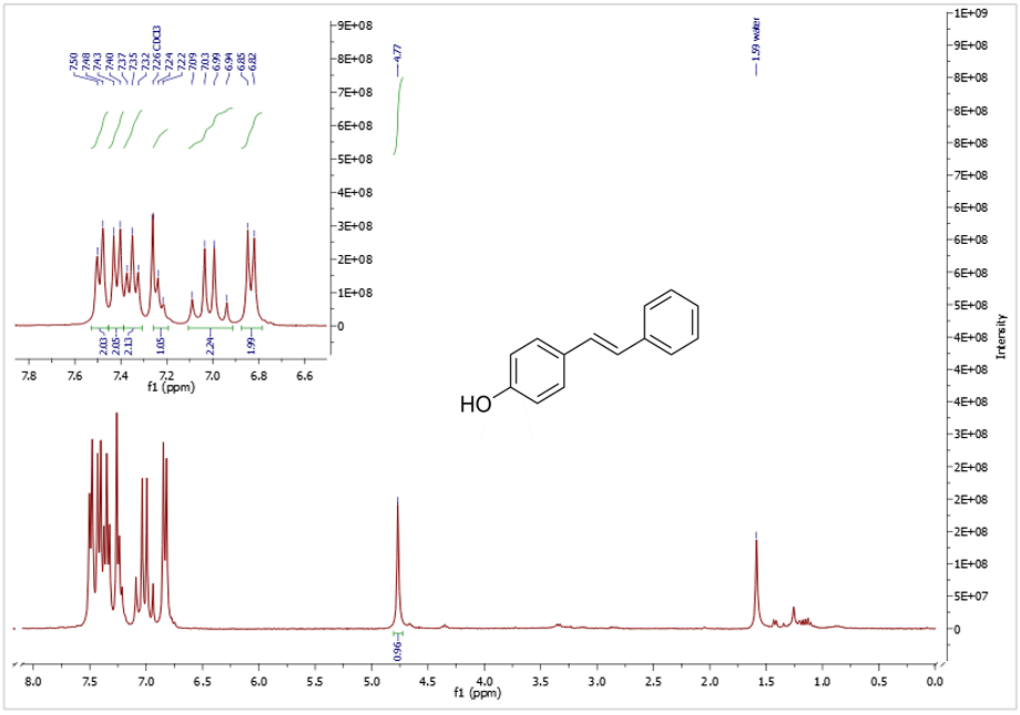

Supporting Information Figure S4.15: ^{1}H-*NMR* of *para*-hydroxystilbene in $CDCl_3$.

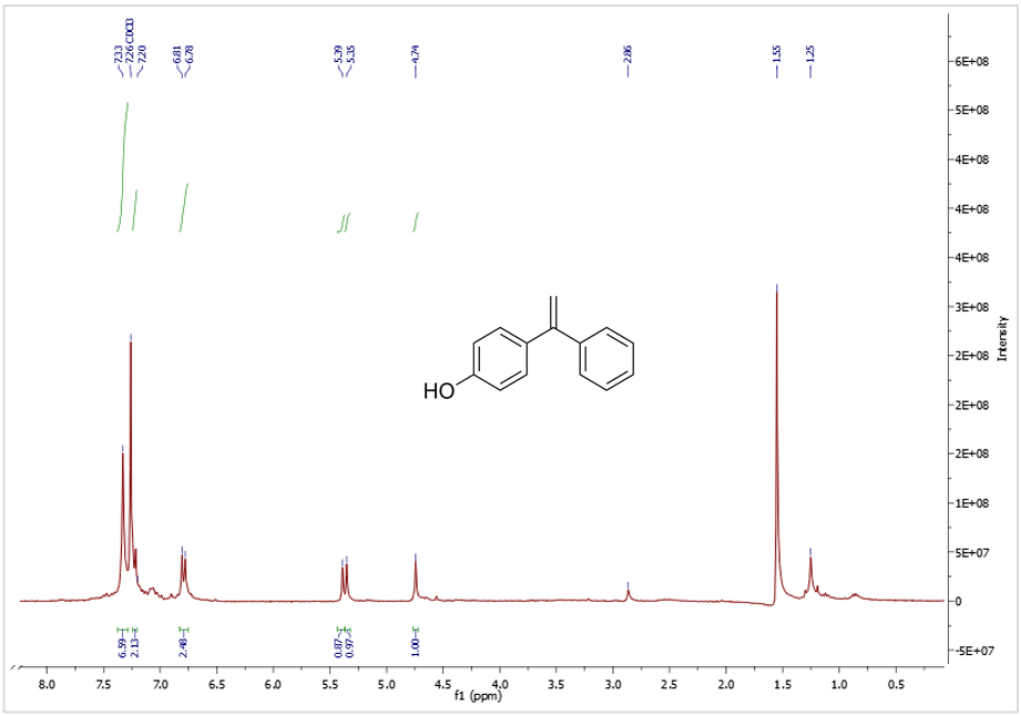

Supporting Information Figure S4.16: ^{1}H-*NMR* of *para*-hydroxy-1,1-diphenylethylene in $CDCl_3$.

Bibliography

[1] John R. Bourne, Oemer M. Kut, Joachim Lenzner, and Horst Maire. "Kinetics of the diazo coupling between 1-naphthol and diazotized sulfanilic acid". In: *Industrial & Engineering Chemistry Research* 29.9 (Sept. 1990), pp. 1761–1765. ISSN: 0888-5885. DOI: 10.1021/ie00105a004. URL: http://pubs.acs.org/doi/abs/10.1021/ie00105a004%20https://pubs.acs.org/doi/abs/10.1021/ie00105a004.

[2] Peter Poechlauer, Julie Manley, Rinus Broxterman, Björn Gregertsen, and Mats Ridemark. "Continuous processing in the manufacture of active pharmaceutical ingredients and finished dosage forms: An industry perspective". In: *Organic Process Research and Development* (2012). ISSN: 10836160. DOI: 10.1021/op300159y.

[5] David J. am Ende and Mary T. am Ende. *Chemical Engineering in the Pharmaceutical Industry*. Ed. by David J. Ende and Mary T. Ende. Second Edi. John Wiley & Sons, Inc., Mar. 2019. ISBN: 9781119285496. DOI: 10.1002/9781119600800. URL: https://onlinelibrary.wiley.com/doi/book/10.1002/9781119600800.

[7] Philip J. Kitson, Guillaume Marie, Jean-Patrick Francoia, Sergey S. Zalesskiy, Ralph C. Sigerson, Jennifer S. Mathieson, and Leroy Cronin. "Digitization of multistep organic synthesis in reactionware for on-demand pharmaceuticals". In: *Science* 359.6373 (Jan. 2018), pp. 314–319. ISSN: 0036-8075. DOI: 10.1126/science.aao3466. URL: http://www.sciencemag.org/lookup/doi/10.1126/science.aao3466%20http://www.ncbi.nlm.nih.gov/pubmed/29348235%20https://www.sciencemag.org/lookup/doi/10.1126/science.aao3466.

[8] Manuel C. Maier, René Lebl, Philipp Sulzer, Josef Lechner, Torsten Mayr, Matej Zadravec, Eyke Slama, Stefan Pfanner, Christoph Schmölzer, Peter Pöchlauer, C. Oliver Kappe, and Heidrun Gruber-Woelfler. "Development of customized 3D printed stainless steel reactors with inline oxygen sensors for aerobic oxidation of Grignard reagents in continuous flow". In: *Reaction Chemistry and*

Engineering 4.2 (2019), pp. 393–401. ISSN: 20589883. DOI: 10.1039/C8RE00278A. URL: http://xlink.rsc.org/?DOI=C8RE00278A.

[11] Sau L. Lee, Thomas F. O'Connor, Xiaochuan Yang, Celia N. Cruz, Sharmista Chatterjee, Rapti D. Madurawe, Christine M. V. Moore, Lawrence X. Yu, and Janet Woodcock. "Modernizing Pharmaceutical Manufacturing: from Batch to Continuous Production". In: *Journal of Pharmaceutical Innovation* 10.3 (Sept. 2015), pp. 191–199. ISSN: 1872-5120. DOI: 10.1007/s12247-015-9215-8. URL: http://link.springer.com/10.1007/s12247-015-9215-8.

[16] Matthew B. Plutschack, Bartholomäus Pieber, Kerry Gilmore, and Peter H. Seeberger. "The Hitchhiker's Guide to Flow Chemistry". In: *Chemical Reviews* 117.18 (Sept. 2017), pp. 11796–11893. ISSN: 0009-2665. DOI: 10.1021/acs.chemrev.7b00183. URL: http://pubs.acs.org/doi/10.1021/acs.chemrev.7b00183.

[22] V Hessel, S Hardt, and H Löwe. *Chemical Micro Process Engineering: Fundamentals, Modelling and Reactions*. Weinheim: Wiley-VCH, 2004. ISBN: 9783527307418. DOI: 10.1002/3527603042.

[23] Norbert Kockmann. "Pressure loss and transfer rates in microstructured devices with chemical reactions". In: *Chemical Engineering and Technology* 31.8 (2008), pp. 1188–1195. ISSN: 09307516. DOI: 10.1002/ceat.200800065.

[26] Thomas Westermann and Leslaw Mleczko. "Heat Management in Microreactors for Fast Exothermic Organic Syntheses—First Design Principles". In: *Organic Process Research & Development* 20.2 (Feb. 2016), pp. 487–494. ISSN: 1083-6160. DOI: 10.1021/acs.oprd.5b00205. URL: https://pubs.acs.org/doi/10.1021/acs.oprd.5b00205.

[33] Octave Levenspiel. *Chemical Reaction Engineering*. 3rd Ed. New York: Wiley, 1999, pp. 293–320. ISBN: 0-471-25424-X.

[34] M.-C. Fournier, L. Falk, and J. Villermaux. "A new parallel competing reaction system for assessing micromixing efficiency—Experimental approach". In: *Chemical Engineering Science* 51.22 (Nov. 1996), pp. 5053–5064. ISSN: 00092509. DOI: 10.1016/0009-2509(96)00270-9. URL: https://linkinghub.elsevier.com/retrieve/pii/0009250996002709.

[35] Sebastian Schwolow, Jutta Hollmann, Berthold Schenkel, and Thorsten Röder. "Application-Oriented Analysis of Mixing Performance in Microreactors". In: *Organic Process Research & Development* 16.9 (Sept. 2012), pp. 1513–1522. ISSN: 1083-6160. DOI: 10.1021/op300107z. URL: http://pubs.acs.org/doi/10.1021/op300107z.

[36] Nirveek Bhattacharjee, Arturo Urrios, Shawn Kang, and Albert Folch. "The upcoming 3D-printing revolution in microfluidics". In: *Lab on a Chip* 16.10 (2016), pp. 1720–1742. ISSN: 1473-0197. DOI: 10.1039/C6LC00163G. arXiv: 15334406. URL: http://xlink.rsc.org/?DOI=C6LC00163G%20http://www.ncbi.nlm.nih.gov/pubmed/27101171%20http://www.pubmedcentral.nih.gov/articlerender.fcgi?artid=PMC4862901.

[77] M. Movsisyan, E. I. P. Delbeke, J. K. E. T. Berton, C. Battilocchio, S. V. Ley, and C. V. Stevens. "Taming hazardous chemistry by continuous flow technology". In: *Chemical Society Reviews* 45.18 (2016), pp. 4892–4928. ISSN: 0306-0012. DOI: 10.1039/C5CS00902B. URL: http://xlink.rsc.org/?DOI=C5CS00902B.

[78] Bernhard Gutmann, David Cantillo, and C. Oliver Kappe. "Continuous-flow technology—a tool for the safe manufacturing of active pharmaceutical ingredients." In: *Angewandte Chemie (International ed. in English)* 54.23 (June 2015), pp. 6688–6728. ISSN: 1521-3773. DOI: 10.1002/anie.201409318. URL: http://doi.wiley.com/10.1002/anie.201409318%20http://www.ncbi.nlm.nih.gov/pubmed/25989203.

[85] Cesar Parra-Cabrera, Clement Achille, Simon Kuhn, and Rob Ameloot. "3D printing in chemical engineering and catalytic technology: structured catalysts, mixers and reactors." In: *Chemical Society reviews* 47.1 (Jan. 2018), pp. 209–230. ISSN: 1460-4744. DOI: 10.1039/c7cs00631d. URL: http://xlink.rsc.org/?DOI=C7CS00631D%20http://www.ncbi.nlm.nih.gov/pubmed/29131228.

[86] Philip J. Kitson, Stefan Glatzel, Wei Chen, Chang-Gen Lin, Yu-Fei Song, and Leroy Cronin. "3D printing of versatile reactionware for chemical synthesis". In: *Nature Protocols* 11.5 (May 2016), pp. 920–936. ISSN: 1754-2189. DOI: 10.1038/nprot.2016.041. URL: http://www.nature.com/articles/nprot.2016.041%20http://www.ncbi.nlm.nih.gov/pubmed/27077333.

[87] Andrew J. Capel, Rowan P. Rimington, Mark P. Lewis, and Steven D. R. Christie. "3D printing for chemical, pharmaceutical and biological applications". In: *Nature Reviews Chemistry* (Nov. 2018), pp. 2397–3358. ISSN: 2397-3358. DOI: 10.1038/s41570-018-0058-y. URL: http://www.nature.com/articles/s41570-018-0058-y.

[88] Raf Reintjens, David J. Ager, and Andr?? H M Andr?? H M André H.M. De Vries. "Flow chemistry, how to bring it to industrial scale?" In: *Chimica Oggi/Chemistry Today* 33.4 (2015), pp. 21–24. ISSN: 19738250. URL: https://www.teknoscienze.com/Contents/Riviste/PDF/CO4_2015_LOW_23-27.pdf.

[93] Bernhard Gutmann, Manuel Köckinger, Gabriel Glotz, Tania Ciaglia, Eyke Slama, Matej Zadravec, Stefan Pfanner, Manuel C. Maier, Heidrun Gruber-Wölfler, and C. Oliver Kappe. "Design and 3D printing of a stainless steel reactor for continuous difluoromethylations using fluoroform". In: *Reaction Chemistry &*

Engineering 2.6 (2017), pp. 919–927. ISSN: 2058-9883. DOI: 10.1039/C7RE00176B. URL: http://xlink.rsc.org/?DOI=C7RE00176B.

[94] Zhi He and Timothy F. Jamison. "Continuous-Flow Synthesis of Functionalized Phenols by Aerobic Oxidation of Grignard Reagents". In: *Angewandte Chemie International Edition* 53.13 (Mar. 2014), pp. 3353–3357. ISSN: 14337851. DOI: 10.1002/anie.201310572. URL: http://doi.wiley.com/10.1002/anie.201310572%20http://www.ncbi.nlm.nih.gov/pubmed/24554581.

[102] Magdalena Jasińska. "Test Reactions to Study Efficiency of Mixing". In: *Chemical and Process Engineering* 36.2 (June 2015), pp. 171–208. ISSN: 2300-1925. DOI: 10.1515/cpe-2015-0013. URL: http://content.sciendo.com/view/journals/cpe/36/2/article-p171.xml.

[109] Xu-dong Wang and Otto S. Wolfbeis. "Optical methods for sensing and imaging oxygen: materials, spectroscopies and applications". In: *Chem. Soc. Rev.* 43.10 (May 2014), pp. 3666–3761. ISSN: 0306-0012. DOI: 10.1039/C4CS00039K. URL: http://xlink.rsc.org/?DOI=C4CS00039K%20http://www.ncbi.nlm.nih.gov/pubmed/24638858.

[117] L. Falk and J.-M. M. Commenge. "Performance comparison of micromixers". In: *Chemical Engineering Science* 65.1 (Jan. 2010), pp. 405–411. ISSN: 00092509. DOI: 10.1016/j.ces.2009.05.045. URL: https://linkinghub.elsevier.com/retrieve/pii/S0009250909003819.

[124] FDA. *Pharmaceutical CGMPs for the 21s Century - A risk-based approach*. Tech. rep. 2004.

[125] Joshua Britton and Colin L. Raston. "Multi-step continuous-flow synthesis". In: *Chemical Society Reviews* 46.5 (2017), pp. 1250–1271. ISSN: 14604744. DOI: 10.1039/c6cs00830e.

[126] Damien Webb and Timothy F. Jamison. "Continuous flow multi-step organic synthesis". In: *Chemical Science* 1.6 (2010), pp. 675–680. ISSN: 20416520. DOI: 10.1039/c0sc00381f. arXiv: {_}barataMaterialsandTechniquesofpolychromewoodensculpture.

[127] Vincenza Dragone, Victor Sans, Mali H. Rosnes, Philip J. Kitson, and Leroy Cronin. "3D-printed devices for continuous-flow organic chemistry". In: *Beilstein Journal of Organic Chemistry* 9 (May 2013), pp. 951–959. ISSN: 1860-5397. DOI: 10.3762/bjoc.9.109. URL: https://www.beilstein-journals.org/bjoc/articles/9/109.

[128] Matthew J Harding, Sarah Brady, Heather O'Connor, Rafael Lopez-Rodriguez, Matthew D Edwards, Saoirse Tracy, Denis Dowling, Geoff Gibson, Kevin P Girard, and Steven Ferguson. "3D printing of PEEK reactors for flow chemistry and continuous chemical processing". In: *Reaction Chemistry & Engineering* 5.4

(2020), pp. 728–735. ISSN: 2058-9883. DOI: 10.1039/C9RE00408D. URL: http://dx.doi.org/10.1039/C9RE00408D%20http://xlink.rsc.org/?DOI=C9RE00408D.

[129] F. Marc Michel, J. Donald Rimstidt, and Karel Kletetschka. "3D printed mixed flow reactor for geochemical rate measurements". In: *Applied Geochemistry* 89.November 2017 (Feb. 2018), pp. 86–91. ISSN: 08832927. DOI: 10.1016/j.apgeochem.2017.11.008. URL: https://doi.org/10.1016/j.apgeochem.2017.11.008%20https://linkinghub.elsevier.com/retrieve/pii/S0883292717303554.

[130] Katharina Hiebler, Sebastian Soritz, Kristian Gavric, Sam Birrer, Manuel C. Maier, Bianca Grabner, and Heidrun Gruber-Woelfler. "Multistep synthesis of a valsartan precursor in continuous flow". In: *Journal of Flow Chemistry* 10.1 (2020), pp. 283–294. ISSN: 20630212. DOI: 10.1007/s41981-019-00044-x.

[131] Bianca Grabner, Anna K. Schweiger, Kristian Gavric, Robert Kourist, and Heidrun Gruber-Woelfler. "A chemo-enzymatic tandem reaction in a mixture of deep eutectic solvent and water in continuous flow". In: *Reaction Chemistry & Engineering* 5.2 (2020), pp. 263–269. ISSN: 2058-9883. DOI: 10.1039/C9RE00467J. URL: http://xlink.rsc.org/?DOI=C9RE00467J.

[132] Christopher A. Hone and C. Oliver Kappe. "The Use of Molecular Oxygen for Liquid Phase Aerobic Oxidations in Continuous Flow". In: *Topics in Current Chemistry* 377.1 (Feb. 2019), p. 2. ISSN: 2365-0869. DOI: 10.1007/s41061-018-0226-z. URL: http://link.springer.com/10.1007/s41061-018-0226-z.

[133] *CC Flow Project*. URL: http://goflow.at/cc-flow (visited on 02/20/2020).

[134] PubChem. *2-Methyltetrahydrofuran - Compound Summary*. URL: https://pubchem.ncbi.nlm.nih.gov/compound/2-Methyltetrahydrofuran%7B%5C#%7Dsection=Peroxide-Forming-Chemical (visited on 04/18/2020).

[135] Philipp Sulzer, René Lebl, C. Oliver Kappe, and Torsten Mayr. "Oxygen sensors for flow reactors – measuring dissolved oxygen in organic solvents". In: *Reaction Chemistry & Engineering* 4.12 (2019), pp. 2081–2087. ISSN: 2058-9883. DOI: 10.1039/C9RE00253G. URL: http://xlink.rsc.org/?DOI=C9RE00253G.

[136] *Cardiovascular diseases (2017) World Health Organization*. URL: http://www.who.int/news-room/fact-sheets/detail/cardiovascular-diseases-(cvds) (visited on 09/04/2018).

[137] *EvaluatePharma, 2018. World Preview 2018, Outlook to 2024. EvaluatePharma, online available at*. URL: https://info.evaluate.com/rs/607-YGS-364/images/EvaluatePharma_World_Preview_2019.pdf (visited on 03/31/2020).

[138] Suzanne Oparil and Roland E. Schmieder. "New Approaches in the Treatment of Hypertension". In: *Circulation Research* 116.6 (2015), pp. 1074–1095. ISSN: 15244571. DOI: 10.1161/CIRCRESAHA.116.303603.

[139] P. Bühlmayer, F. Ostermayer, and T. Schmidlin. *Acyl compounds.*

[140] G Verardo, P Geatti, G Castaldi, N Toniutti, and P Allegrini. *A process for the preparation of valsartan and intermediates thereof.*

[141] G Sedelmeier. *Process for the preparation of tetrazole derivatives from organo boron and organo aluminium azides.*

[142] M Villa, P Allegrini, K Arrighi, and M Paiocchi. *Ortho-metalation process for the synthesis of 2-substituted-1-(tetrazol-5-yl)benzenes.*

[143] Chen Xi Zhang, Guo Jun Zheng, Fu Qiang Bi, and Yu Lin Li. "A simple and efficient synthesis of the valsartan". In: *Chinese Chemical Letters* 19.7 (2008), pp. 759–761. ISSN: 10018417. DOI: 10.1016/j.cclet.2008.04.032.

[144] Chen Zhang, Guojun Zheng, Lijing Fang, and Yulin Li. "Efficient synthesis of valsartan, a nonpeptide angiotensin II receptor antagonist". In: *Synlett* 9.3 (2006), pp. 475–477. ISSN: 09365214. DOI: 10.1055/s-2006-926234.

[145] E Tsiperman, S Fine, S Yurkovsky, and V Braude. *Process for preparing valsartan.*

[146] Masahiko Seki and Masaki Nagahama. "Synthesis of angiotensin II receptor blockers by means of a catalytic system for C-H Activation". In: *Journal of Organic Chemistry* 76.24 (2011), pp. 10198–10206. ISSN: 00223263. DOI: 10.1021/jo202041e.

[147] Samir Ghosh, A. Sanjeev Kumar, and G. N. Mehta. "A short and efficient synthesis of valsartan via a Negishi reaction". In: *Beilstein Journal of Organic Chemistry* 6 (2010), pp. 4–7. ISSN: 18605397. DOI: 10.3762/bjoc.6.27.

[148] Nicola Galaffu, Siud Pui Man, Robin D. Wilkes, and John R.H. H Wilson. "Highly functionalised sulfur-based silica scavengers for the efficient removal of palladium species from active pharmaceutical ingredients". In: *Organic Process Research and Development* 11.3 (2007), pp. 406–413. ISSN: 10836160. DOI: 10.1021/op7000172.

[149] Belmunt J Bessa, Clotet J Huguet, Andres JA A Perez, and Barjoan P Dalmases. *Process for the preparation of valsartan and precursors thereof.*

[150] C Lamberth and J Dinges. *Bioactive Carboxylic Compound Classes: Pharmaceuticals and Agrochemicals.* Ed. by Clemens Lamberth and Jürgen Dinges. Weinheim, Germany: Wiley-VCH Verlag GmbH & Co. KGaA, Aug. 2016. ISBN: 9783527339471. DOI: 10.1002/9783527693931. URL: http://doi.wiley.com/10.1002/9783527693931.

[151] Valerica Pandarus, Geneviève Gingras, François Béland, Rosaria Ciriminna, and Mario Pagliaro. "Process intensification of the Suzuki-Miyaura reaction over sol-gel entrapped catalyst silia cat DPP-Pd under conditions of continuous flow". In: *Organic Process Research and Development* 18.11 (2014), pp. 1550–1555. ISSN: 1520586X. DOI: 10.1021/op4003449.

[152] Aiichiro Nagaki, Katsuyuki Hirose, Osamu Tonomura, Satoshi Taniguchi, Toshiki Taga, Shinji Hasebe, Norio Ishizuka, and Jun Ichi Yoshida. "Design of a Numbering-up System of Monolithic Microreactors and Its Application to Synthesis of a Key Intermediate of Valsartan". In: *Organic Process Research and Development* 20.3 (2016), pp. 687–691. ISSN: 1520586X. DOI: 10.1021/acs.oprd.5b00414.

[153] G.J. Lichtenegger, M. Maier, M. Hackl, J.G. Khinast, W. Gössler, T. Griesser, V.S.Phani Kumar, H. Gruber-Woelfler, and P.A. Deshpande. "Suzuki-Miyaura coupling reactions using novel metal oxide supported ionic palladium catalysts". In: *Journal of Molecular Catalysis A: Chemical* 426 (Jan. 2017), pp. 39–51. ISSN: 13811169. DOI: 10.1016/j.molcata.2016.10.033. URL: https://linkinghub.elsevier.com/retrieve/pii/S1381116916304563.

[154] Waqas Nawaz, Zhongqin Zhou, Sa Deng, Xiaodong Ma, Xiaochi Ma, Chuangang Li, and Xiaohong Shu. "Therapeutic Versatility of Resveratrol Derivatives". In: *Nutrients* 9.11 (Oct. 2017), p. 1188. ISSN: 2072-6643. DOI: 10.3390/nu9111188. URL: http://www.mdpi.com/2072-6643/9/11/1188.

[155] Hui-Yun Tsai, Chi-Tang Ho, and Yu-Kuo Chen. "Biological actions and molecular effects of resveratrol, pterostilbene, and 3'-hydroxypterostilbene". In: *Journal of Food and Drug Analysis* 25.1 (Jan. 2017), pp. 134–147. ISSN: 10219498. DOI: 10.1016/j.jfda.2016.07.004. URL: https://linkinghub.elsevier.com/retrieve/pii/S1021949816300965.

[156] Monica Savio, Daniela Ferraro, Cristina Maccario, Rita Vaccarone, Lasse D. Jensen, Federica Corana, Barbara Mannucci, Livia Bianchi, Yihai Cao, and Lucia Anna Stivala. "Resveratrol analogue 4,4'-dihydroxy-trans-stilbene potently inhibits cancer invasion and metastasis". In: *Scientific Reports* 6.1 (Apr. 2016), p. 19973. ISSN: 2045-2322. DOI: 10.1038/srep19973. URL: http://www.nature.com/articles/srep19973.

[157] Álvaro Gómez Baraibar, Dennis Reichert, Carolin Mügge, Svenja Seger, Harald Gröger, and Robert Kourist. "A One-Pot Cascade Reaction Combining an Encapsulated Decarboxylase with a Metathesis Catalyst for the Synthesis of Bio-Based Antioxidants". In: *Angewandte Chemie International Edition* 55.47 (Nov. 2016), pp. 14823–14827. ISSN: 14337851. DOI: 10.1002/anie.201607777. URL: http://doi.wiley.com/10.1002/anie.201607777.

[158] Martin Peng, Esther Mittmann, Lukas Wenger, Jürgen Hubbuch, Martin K. M. Engqvist, Christof M. Niemeyer, and Kersten S. Rabe. "3D-Printed Phenacrylate Decarboxylase Flow Reactors for the Chemoenzymatic Synthesis of 4-Hydroxystilbene". In: *Chemistry – A European Journal* 25.70 (Dec. 2019), pp. 15998–16001. ISSN: 0947-6539. DOI: 10.1002/chem.201904206. URL: https://onlinelibrary.wiley.com/doi/abs/10.1002/chem.201904206.

[159] Sandy Schmidt, Kathrin Castiglione, and Robert Kourist. "Overcoming the Incompatibility Challenge in Chemoenzymatic and Multi-Catalytic Cascade Reactions". In: *Chemistry - A European Journal* 24.8 (Feb. 2018), pp. 1755–1768. ISSN: 15213765. DOI: 10.1002/chem.201703353. URL: http://doi.wiley.com/10.1002/chem.201703353.

[160] Josef M. Sperl, Jörg M. Carsten, Jan-Karl Guterl, Petra Lommes, and Volker Sieber. "Reaction Design for the Compartmented Combination of Heterogeneous and Enzyme Catalysis". In: *ACS Catalysis* 6.10 (Oct. 2016), pp. 6329–6334. ISSN: 2155-5435. DOI: 10.1021/acscatal.6b01276. URL: https://pubs.acs.org/doi/10.1021/acscatal.6b01276.

[161] Anna K. Schweiger, Nicolás Ríos-Lombardía, Christoph K. Winkler, Sandy Schmidt, Francisco Morís, Wolfgang Kroutil, Javier González-Sabín, and Robert Kourist. "Using Deep Eutectic Solvents to Overcome Limited Substrate Solubility in the Enzymatic Decarboxylation of Bio-Based Phenolic Acids". In: *ACS Sustainable Chemistry & Engineering* 7.19 (Oct. 2019), pp. 16364–16370. ISSN: 2168-0485. DOI: 10.1021/acssuschemeng.9b03455. URL: https://pubs.acs.org/doi/10.1021/acssuschemeng.9b03455.

[162] Sven R L Gobert, Simon Kuhn, Leen Braeken, and Leen C J Thomassen. "Characterization of Milli- and Microflow Reactors: Mixing Efficiency and Residence Time Distribution". In: *Organic Process Research & Development* 21.4 (Apr. 2017), pp. 531–542. ISSN: 1083-6160. DOI: 10.1021/acs.oprd.6b00359. URL: https://pubs.acs.org/doi/10.1021/acs.oprd.6b00359.

[163] John R Bourne. "Mixing and the Selectivity of Chemical Reactions". In: *Organic Process Research & Development* 7.4 (July 2003), pp. 471–508. ISSN: 1083-6160. DOI: 10.1021/op020074q. URL: https://pubs.acs.org/doi/10.1021/op020074q.

[164] Karol Malecha, Leszek J Golonka, Jerzy Bałdyga, Magdalena Jasińska, and Paweł Sobieszuk. "Serpentine microfluidic mixer made in LTCC". In: *Sensors and Actuators B: Chemical* 143.1 (Dec. 2009), pp. 400–413. ISSN: 09254005. DOI: 10.1016/j.snb.2009.08.010. URL: https://linkinghub.elsevier.com/retrieve/pii/S0925400509006285.

[165] Georg J. Lichtenegger, Vitan Tursic, Hannes Kitzler, Klemens Obermaier, Johannes G. Khinast, and Heidrun Gruber-Wölfler. "The Plug & Play Reactor: A Highly Flexible Device for Heterogeneous Reactions in Continuous Flow". In: *Chemie Ingenieur Technik* 88.10 (Oct. 2016), pp. 1518–1523. ISSN: 0009286X. DOI: 10.1002/cite.201600013. URL: http://doi.wiley.com/10.1002/cite.201600013.

[166] Y Wang, G Zheng, G Cai, B Chen, and H Li. *Process for preparation of valsartan.*

[167] José F. Cívicos, Diego A. Alonso, and Carmen Nájera. "Oxime Palladacycle-Catalyzed Suzuki-Miyaura Alkenylation of Aryl, Heteroaryl, Benzyl, and Allyl Chlorides under Microwave Irradiation Conditions". In: *Advanced Synthesis & Catalysis* 353.10 (July 2011), pp. 1683–1687. ISSN: 16154150. DOI: 10.1002/adsc.201100019. URL: http://doi.wiley.com/10.1002/adsc.201100019.

CHAPTER 5

Conclusion and Outlook

The presented work is part of the *C2P* approach described in Sec. 1.5 and carried out within the CCFlow project. Its aim is to design and implement additive manufactured reactors for a given chemical task. The interdisciplinary *C2P* work flow aims to provide a chemical plant within a few months compared to the currently needed one to two years. By using continuous flow technology and additive manufacturing, this work contributed to the development of the *C2P* work flow.

Starting point for the *C2P* work flow was the aerobic oxidation of 4-chlorophenylmagnesium bromide in continuous flow, shown in Chap. 2. Additive manufacturing of *3D* printed stainless steel reactors showed to be a promising way to produce custom-made reactors with the possibility to add in-line oxygen sensors. The shown sensors can be easily implemented using standard *HPLC* equipment and allowed to track the reaction progress in a *CSTR* cascade at various operation conditions. The gained insight into the reaction was used to design a static mixing *SaRR*, adapted to the needed process conditions. With this reactor, the basis of a parameter dependent structure element database was made. It aimed to provide reactor elements which can be adapted by a user in a simple click-and-drop like manner. The micro- and macro mixing characterized elements from the design database can be assembled virtually as *CAD* files and scaled by only three design parameters. One of the advantages of additive manufacturing is that the virtual reactor file is already available and its performance can be investigated by *CFD* simulations at process conditions. The following additive manufacturing of the reactor is saving resources during manufacturing since only energy and the material for the geometry generation are consumed. The printing and post-processing of additive manufactured parts only requires days until the first prototype reactor is manufactured, and thus perfectly fits to the *C2P* approach. After

an investigation at reaction conditions of the first prototype, adaptions can be made to it if desired.

Design tools developed within this work provide the needed chemical investigation prior to the first prototype. The concept of a *CSTR* cascade with integrated process analytics showed to be a promising tool to investigate novel flow reactions. Such a cascade allows to manipulate flow conditions by actively influencing mixing properties. The implemented analytic sensors give further information about chemical conversion and may allow in future works a feedback control strategy for operation. Such an approach allows not only to optimize a reaction but fully screen the chemical space and obtain reaction models over a broad operation range.

This is similarly applicable to the developed flow calorimeter shown in Chap. 3. As an assisting tool during the process design, it allows reactions at harsh conditions currently not accessible by batch calorimetry and the possibility to screen a continuous steady state operation. Its design is based on the combination of commercially available electronics and additive manufacturing. Its independent temperature control of each reactor segment allows a controlled and isothermal operation. The measurement principle is based on a direct heat flux measurement utilizing internally calibrated Seebeck elements. The calorimeter design was validated with several experiments which produce a well-known heat flux and shown to be applicable for organic synthesis. Future work with the calorimeter should focus on reactions at elevated pressures and temperatures. Especially a focus should be held on improving the design with respect to heat losses to the environment. A temperature controlled casing could improve the measurement accuracy at high or low temperatures.

The work presented in Chap. 4 shows further development of the parameter depending design approach of 3D printed reactors. Different manufactured reactors were experimentally evaluated by mixing-sensitive reactions and a comparison of their residence time distributions was made. The results showed influences of different mixing efficiencies of a respective reactor geometry and temperatures on the formation of a desired phenol during an aerobic oxidation of 4-chlorophenylmagnesium bromide. An additional focus was held on process stability of the supplied oxygen content to the reactor by in-line monitoring with the previously developed optical sensors. The usage of an adsorption column positively influenced the process stability. Furthermore, this chapter showed two other applications of *3D* printed reactors. The previously designed *SaRR* was re-used for the *N*-acylation and hydrolysis in a three-step cascade for the synthesis of a valsartan precursor. Here its good mixing performance was a good addition to the process. The next example deals with an enzymatic decarboxylation in a multipurpose *CSTR*, which led to the formation of reservatrol derivates after a Pd-catalyzed Heck cross-coupling. This reactor was made from a low cost *UV*-curable resin and showed to be applicable at the used mild reaction conditions. With this reactor and an alternative *DES* solvent, it was possible to increase substrate concentration by a factor of 22, leading to an equal increase in productivity.

The possibility to select materials depending on the desired chemical task, while using the same design files, makes *3D* printing a valuable tool for the production of reactors.

Further studies with different printing techniques and their unique features and limitations should be focused on. Especially the usage of multi-compound materials in a reactor is a promising way to obtain integrated functional parts such as valves or the possibility to have reactors adapting their geometry to a chemical reaction during operation.

A reactor for a desired plant can be manufactured on-demand by the above presented work flow and simply requires an adequate *3D* printer, design files, printing parameters and given post-processing steps. Creating an application database, for a desired chemical task, with designed reactor files and the corresponding process conditions for operation, could improve significantly the on-demand *API* production. Future work should focus on providing a modular concept for peripheral equipment and process control strategies. A reactor system for *API* production with such modular interconnections and the possibility to provide exchangeable reactors can be highly valuable for the on-demand production.

APPENDIX A

List of Acronyms

BsPAD	phenolic acid decarboxylase from *Bacillus subtilis*
2-Me-THF	2-methyltetrahydrofuran
2D	Two-dimensional
3D	Three-dimensional
ABS	acrylonitrile butadiene styrene
API	Active Pharmaceutical Ingredient
APIs	Active Pharmaceutical Ingredients
BPR	Back Pressure Regulator
BPRs	Back Pressure Regulators
C2P	Chemistry to Plant
CAD	Computer Aided Design
CFD	Computational Fluid Dynamics
ChCl	choline chloride
COC	cyclic olefin copolymer
CSTR	Continuous Stirred Tank Reactor
CSTRs	Continuous Stirred Tank Reactors
DES	Deep Eutectic Solvent
DLP	Digital Light Processing
DMP	2,2-dimethoxypropane
FDM	Fused Deposition Modeling
FFF	Fused Filament Fabrication
FID	Flame Ionization Detector
GC	Gas chromatography
HCl	hydrochloric acid

HPLC	High Pressure Liquid Chromatography
ID	Inner Diameter
IDs	Inner Diameters
LCD	Liquid Crystal Display
MFC	Mass Flow Controllers
MRS	Micro- and Milli Reactor Systems
MS	Mass Spectrometry
MW	Molecular Weight
NIR	Near-Infrared
NMR	Nuclear Magnetic Resonance
NPW	Novel Process Window
OD	Outer Diameter
PAD	phenolic acid decarboxylase
PAT	Process Analytical Technology
PC	polycarbonate
PDMS	poly-dimethylsiloxane
PEEK	polyether ether ketone
PFA	perfluoroalkoxy alkane
PI	Pressure Indicator
PID	proportional–integral–derivative
PLA	polylactic acid
PP	polypropylene
PPS	polyphenylenesulfide
PTFE	polytetrafluoroethylene
RPM	Revolutions Per Minute
RPMs	Revolutions Per Minutes
RTD	Residence Time Distribution
SaRR	Split-and-Recombine Reactor
SaRRs	Split-and-Recombine Reactors
SLA	Stereo Lithography
SLM	Selective Laser Melting
SLS	Selective Laser Sintering
STL	Standard Triangle Language
TFA	trifluoroacetic acid
THF	tetrahydrofuran
UV	Ultraviolet
VIS	visible
WHO	World Health Organization

Bibliography

[1] John R. Bourne, Oemer M. Kut, Joachim Lenzner, and Horst Maire. "Kinetics of the diazo coupling between 1-naphthol and diazotized sulfanilic acid". In: *Industrial & Engineering Chemistry Research* 29.9 (Sept. 1990), pp. 1761–1765. ISSN: 0888-5885. DOI: 10.1021/ie00105a004. URL: http://pubs.acs.org/doi/abs/10.1021/ie00105a004%20https://pubs.acs.org/doi/abs/10.1021/ie00105a004.

[2] Peter Poechlauer, Julie Manley, Rinus Broxterman, Björn Gregertsen, and Mats Ridemark. "Continuous processing in the manufacture of active pharmaceutical ingredients and finished dosage forms: An industry perspective". In: *Organic Process Research and Development* (2012). ISSN: 10836160. DOI: 10.1021/op300159y.

[3] Peter Poechlauer, Juan Colberg, Elizabeth Fisher, Michael Jansen, Martin D. Johnson, Stefan G. Koenig, Michael Lawler, Thomas Laporte, Julie Manley, Benjamin Martin, and Anne O'Kearney-Mcmullan. "Pharmaceutical Roundtable Study Demonstrates the Value of Continuous Manufacturing in the Design of Greener Processes". In: *Organic Process Research and Development* 17.12 (2013), pp. 1472–1478. ISSN: 10836160. DOI: 10.1021/op400245s.

[4] Stephen G. Newman and Klavs F. Jensen. "The role of flow in green chemistry and engineering". In: *Green Chemistry* 15.6 (2013), pp. 1456–1472. ISSN: 14639270. DOI: 10.1039/c3gc40374b. URL: http://dx.doi.org/10.1039/C3GC40374B.

[5] David J. am Ende and Mary T. am Ende. *Chemical Engineering in the Pharmaceutical Industry*. Ed. by David J. Ende and Mary T. Ende. Second Edi. John Wiley & Sons, Inc., Mar. 2019. ISBN: 9781119285496. DOI: 10.1002/9781119600800. URL: https://onlinelibrary.wiley.com/doi/book/10.1002/9781119600800.

[6] Gerard Capellades, Clemence Neurohr, Naomi Briggs, Kersten Rapp, Gregory Hammersmith, David Brancazio, Bridget Derksen, and Allan S. Myerson. " On-Demand Continuous Manufacturing of Ciprofloxacin in Portable Plug-and-Play Factories: Implementation and In Situ Control of Downstream Production ". In: *Organic Process Research & Development* (2021). ISSN: 1083-6160. DOI: 10.1021/acs.oprd.1c00117.

[7] Philip J. Kitson, Guillaume Marie, Jean-Patrick Francoia, Sergey S. Zalesskiy, Ralph C. Sigerson, Jennifer S. Mathieson, and Leroy Cronin. "Digitization of multistep organic synthesis in reactionware for on-demand pharmaceuticals". In: *Science* 359.6373 (Jan. 2018), pp. 314–319. ISSN: 0036-8075. DOI: 10.1126/science.aao3466. URL: http://www.sciencemag.org/lookup/doi/10.1126/science.aao3466%20http://www.ncbi.nlm.nih.gov/pubmed/29348235%20https://www.sciencemag.org/lookup/doi/10.1126/science.aao3466.

[8] Manuel C. Maier, René Lebl, Philipp Sulzer, Josef Lechner, Torsten Mayr, Matej Zadravec, Eyke Slama, Stefan Pfanner, Christoph Schmölzer, Peter Pöchlauer, C. Oliver Kappe, and Heidrun Gruber-Woelfler. "Development of customized 3D printed stainless steel reactors with inline oxygen sensors for aerobic oxidation of Grignard reagents in continuous flow". In: *Reaction Chemistry and Engineering* 4.2 (2019), pp. 393–401. ISSN: 20589883. DOI: 10.1039/C8RE00278A. URL: http://xlink.rsc.org/?DOI=C8RE00278A.

[9] Manuel C. Maier, Michael Leitner, C. Oliver Kappe, and Heidrun Gruber-Woelfler. "A modular 3D printed isothermal heat flow calorimeter for reaction calorimetry in continuous flow". In: *Reaction Chemistry and Engineering* 5.8 (2020), pp. 1410–1420. ISSN: 20589883. DOI: 10.1039/d0re00122h. URL: http://xlink.rsc.org/?DOI=D0RE00122H.

[10] Manuel C. Maier, Alessia Valotta, Katharina Hiebler, Sebastian Soritz, Kristian Gavric, Bianca Grabner, and Heidrun Gruber-Woelfler. "3D Printed Reactors for Synthesis of Active Pharmaceutical Ingredients in Continuous Flow". In: *Organic Process Research and Development* (2020). ISSN: 1520586X. DOI: 10.1021/acs.oprd.0c00228.

[11] Sau L. Lee, Thomas F. O'Connor, Xiaochuan Yang, Celia N. Cruz, Sharmista Chatterjee, Rapti D. Madurawe, Christine M. V. Moore, Lawrence X. Yu, and Janet Woodcock. "Modernizing Pharmaceutical Manufacturing: from Batch to Continuous Production". In: *Journal of Pharmaceutical Innovation* 10.3 (Sept. 2015), pp. 191–199. ISSN: 1872-5120. DOI: 10.1007/s12247-015-9215-8. URL: http://link.springer.com/10.1007/s12247-015-9215-8.

[12] Hans Leuenberger. "New trends in the production of pharmaceutical granules: batch versus continuous processing". In: *European Journal of Pharmaceutics and Biopharmaceutics* 52.3 (Nov. 2001), pp. 289–296. ISSN: 09396411. DOI: 10.1016/

S0939-6411(01)00199-0. URL: https://www.sciencedirect.com/science/article/pii/S0939641101001990%20https://linkinghub.elsevier.com/retrieve/pii/S0939641101001990.

[13] Lawrence X. Yu. "Pharmaceutical Quality by Design: Product and Process Development, Understanding, and Control". In: *Pharmaceutical Research* 25.4 (Apr. 2008), pp. 781–791. ISSN: 0724-8741. DOI: 10.1007/s11095-007-9511-1. URL: https://doi.org/10.1007/s11095-007-9511-1%20http://link.springer.com/10.1007/s11095-007-9511-1.

[14] Dominique M. Roberge, Laurent Ducry, Nikolaus Bieler, Philippe Cretton, and Bertin Zimmermann. "Microreactor technology: A revolution for the fine chemical and pharmaceutical industries?" In: *Chemical Engineering and Technology* 28.3 (2005), pp. 318–323. ISSN: 09307516. DOI: 10.1002/ceat.200407128. URL: https://onlinelibrary.wiley.com/doi/abs/10.1002/ceat.200407128.

[15] Norbert Kockmann. *Process Engineering Methods and Microsystem Technology*. Vol. 5. 2008, pp. 1–45. ISBN: 9783527616749. DOI: 10.1002/9783527616749.ch1. URL: http://dx.doi.org/10.1002/9783527616749.ch1.

[16] Matthew B. Plutschack, Bartholomäus Pieber, Kerry Gilmore, and Peter H. Seeberger. "The Hitchhiker's Guide to Flow Chemistry". In: *Chemical Reviews* 117.18 (Sept. 2017), pp. 11796–11893. ISSN: 0009-2665. DOI: 10.1021/acs.chemrev.7b00183. URL: http://pubs.acs.org/doi/10.1021/acs.chemrev.7b00183.

[17] Charlotte Wiles and Paul Watts. "Continuous flow reactors: a perspective". In: *Green Chem.* 14.1 (2012), pp. 38–54. ISSN: 1463-9262. DOI: 10.1039/C1GC16022B. URL: http://dx.doi.org/10.1039/C1GC16022B%20http://xlink.rsc.org/?DOI=C1GC16022B.

[18] Volker Hessel, Dana Kralisch, Norbert Kockmann, Timothy Noël, and Qi Wang. "Novel Process Windows for Enabling, Accelerating, and Uplifting Flow Chemistry". In: *ChemSusChem* 6.5 (May 2013), pp. 746–789. ISSN: 18645631. DOI: 10.1002/cssc.201200766. URL: https://chemistry-europe.onlinelibrary.wiley.com/doi/abs/10.1002/cssc.201200766%20https://onlinelibrary.wiley.com/doi/10.1002/cssc.201200766.

[19] Volker Hessel, Dana Kralisch, and Norbert Kockmann. *Novel Process Windows*. Ed. by Volker Hessel, Dana Kralisch, and Norbert Kockmann. Weinheim, Germany: Wiley-VCH Verlag GmbH & Co. KGaA, Nov. 2014, pp. 1–314. ISBN: 9783527654826. DOI: 10.1002/9783527654826. URL: http://doi.wiley.com/10.1002/9783527654826.

[20] Volker Hessel, Dana Kralisch, and Norbert Kockmann. "Novel Process Windows". In: *Novel Process Windows*. Weinheim, Germany: Wiley-VCH Verlag GmbH & Co. KGaA, Jan. 2015, pp. 15–24. ISBN: 9783527654840. DOI: 10.1002/9783527654826.ch2.

[21] Dominique M. Roberge. "An integrated approach combining reaction engineering and design of experiments for optimizing reactions". In: *Organic Process Research and Development* 8.6 (2004), pp. 1049–1053. ISSN: 10836160. DOI: 10.1021/op0400160.

[22] V Hessel, S Hardt, and H Löwe. *Chemical Micro Process Engineering: Fundamentals, Modelling and Reactions*. Weinheim: Wiley-VCH, 2004. ISBN: 9783527307418. DOI: 10.1002/3527603042.

[23] Norbert Kockmann. "Pressure loss and transfer rates in microstructured devices with chemical reactions". In: *Chemical Engineering and Technology* 31.8 (2008), pp. 1188–1195. ISSN: 09307516. DOI: 10.1002/ceat.200800065.

[24] Norbert Kockmann, Michael Gottsponer, Bertin Zimmermann, and Dominique M. Roberge. "Enabling continuous-flow chemistry in microstructured devices for pharmaceutical and fine-chemical production". In: *Chemistry - A European Journal* 14.25 (2008), pp. 7470–7477. ISSN: 09476539. DOI: 10.1002/chem.200800707.

[25] Norbert Kockmann, Michael Gottsponer, and Dominique M. Roberge. "Scale-up concept of single-channel microreactors from process development to industrial production". In: *Chemical Engineering Journal* 167.2-3 (2011), pp. 718–726. ISSN: 13858947. DOI: 10.1016/j.cej.2010.08.089. URL: http://dx.doi.org/10.1016/j.cej.2010.08.089.

[26] Thomas Westermann and Leslaw Mleczko. "Heat Management in Microreactors for Fast Exothermic Organic Syntheses—First Design Principles". In: *Organic Process Research & Development* 20.2 (Feb. 2016), pp. 487–494. ISSN: 1083-6160. DOI: 10.1021/acs.oprd.5b00205. URL: https://pubs.acs.org/doi/10.1021/acs.oprd.5b00205.

[27] Albert Renken and Lioubov Kiwi-Minsker. "Chemical Reactions in Continuous –flow Microstructured Reactors". In: Feb. 2006, pp. 173–201. DOI: 10.1002/9783527616749.ch6. URL: https://onlinelibrary.wiley.com/doi/abs/10.1002/9783527616749.ch6.

[28] Frank P Incropera and David P DeWitt. *Fundamentals of Heat and Mass Transfer*. John Wiley & Sons, 1996, p. 890. ISBN: 0471304603. DOI: 10.1016/j.applthermaleng.2011.03.022. arXiv: 1105-.

[29] Jens Weitkamp and Roger Gläser. "Chemische Technik: Prozesse und Produkte". In: *Wiley-VCH: Weinheim.* (2004), 645 ff.

[30] Stephen A. Solovitz and Jeffrey Mainka. "Manifold Design for Micro-Channel Cooling With Uniform Flow Distribution". In: *Journal of Fluids Engineering* 133.5 (May 2011). ISSN: 0098-2202. DOI: 10.1115/1.4004089. URL: https://asmedigitalcollection.asme.org/fluidsengineering/article/doi/10.1115/1.4004089/450502/Manifold-Design-for-MicroChannel-Cooling-With.

[31] V.A. Antonets, M.A. Antonets, and I.A. Shereshevsky. "The statistical cluster dynamics in the dendroid transfer sys- tems". In: *Fractals in the Fundamental and Applied Sciences* (1991), pp. 59–71.

[32] Yongping Chen and Ping Cheng. "Heat transfer and pressure drop in fractal tree-like microchannel nets". In: *International Journal of Heat and Mass Transfer* 45.13 (2002), pp. 2643–2648. ISSN: 00179310. DOI: 10.1016/S0017-9310(02)00013-3.

[33] Octave Levenspiel. *Chemical Reaction Engineering*. 3rd Ed. New York: Wiley, 1999, pp. 293–320. ISBN: 0-471-25424-X.

[34] M.-C. Fournier, L. Falk, and J. Villermaux. "A new parallel competing reaction system for assessing micromixing efficiency—Experimental approach". In: *Chemical Engineering Science* 51.22 (Nov. 1996), pp. 5053–5064. ISSN: 00092509. DOI: 10.1016/0009-2509(96)00270-9. URL: https://linkinghub.elsevier.com/retrieve/pii/0009250996002709.

[35] Sebastian Schwolow, Jutta Hollmann, Berthold Schenkel, and Thorsten Röder. "Application-Oriented Analysis of Mixing Performance in Microreactors". In: *Organic Process Research & Development* 16.9 (Sept. 2012), pp. 1513–1522. ISSN: 1083-6160. DOI: 10.1021/op300107z. URL: http://pubs.acs.org/doi/10.1021/op300107z.

[36] Nirveek Bhattacharjee, Arturo Urrios, Shawn Kang, and Albert Folch. "The upcoming 3D-printing revolution in microfluidics". In: *Lab on a Chip* 16.10 (2016), pp. 1720–1742. ISSN: 1473-0197. DOI: 10.1039/C6LC00163G. arXiv: 15334406. URL: http://xlink.rsc.org/?DOI=C6LC00163G%20http://www.ncbi.nlm.nih.gov/pubmed/27101171%20http://www.pubmedcentral.nih.gov/articlerender.fcgi?artid=PMC4862901.

[37] Anthony K. Au, Wilson Huynh, Lisa F. Horowitz, and Albert Folch. "3D-Printed Microfluidics". In: *Angewandte Chemie International Edition* 55.12 (Mar. 2016), pp. 3862–3881. ISSN: 14337851. DOI: 10.1002/anie.201504382. URL: http://doi.wiley.com/10.1002/anie.201504382%20http://www.ncbi.nlm.nih.gov/pubmed/26854878%20https://onlinelibrary.wiley.com/doi/10.1002/anie.201504382.

[38] Andrew J. Capel, Andrew Wright, Matthew J. Harding, George W. Weaver, Yuqi Li, Russell A. Harris, Steve Edmondson, Ruth D. Goodridge, and Steven D.R. R Christie. "3D printed fluidics with embedded analytic functionality for automated reaction optimisation". In: *Beilstein Journal of Organic Chemistry*

13 (Jan. 2017), pp. 111–119. ISSN: 18605397. DOI: 10.3762/bjoc.13.14. URL: http://www.beilstein-journals.org/bjoc/content/13/1/14.

[39] Sergio Rossi, Alessandra Puglisi, and Maurizio Benaglia. "Additive Manufacturing Technologies: 3D Printing in Organic Synthesis". In: *ChemCatChem* 10.7 (Apr. 2018), pp. 1512–1525. ISSN: 18673880. DOI: 10.1002/cctc.201701619. URL: https://onlinelibrary.wiley.com/doi/10.1002/cctc.201701619%20https://chemistry-europe.onlinelibrary.wiley.com/doi/abs/10.1002/cctc.201701619%20http://doi.wiley.com/10.1002/cctc.201701619.

[40] Jan Holmström, Jouni Partanen, Jukka Tuomi, and Manfred Walter. "Rapid manufacturing in the spare parts supply chain: Alternative approaches to capacity deployment". In: *Journal of Manufacturing Technology Management* 21.6 (2010), pp. 687–697. ISSN: 1741038X. DOI: 10.1108/17410381011063996.

[41] Ian Gibson, David W Rosen, and Brent Stucker. "Design for Additive Manufacturing". In: *Additive Manufacturing Technologies*. Boston, MA: Springer US, 2010, pp. 299–332. ISBN: 978-1-4419-1120-9. DOI: 10.1007/978-1-4419-1120-9_11. URL: https://doi.org/10.1007/978-1-4419-1120-9_11%20http://link.springer.com/10.1007/978-1-4419-1120-9_11.

[42] André De Vries. "3D-Printed Metal Flow Reactors and Mixers". In: *RSC Symposium Chemspec*. München, Germany, 2017. URL: https://www.chemspeceurope.com/2019/assets/CSE18_RSCArchive_2017_7b.pdf.

[43] Ben Vandenbroucke and Jean Pierre Kruth. "Selective laser melting of biocompatible metals for rapid manufacturing of medical parts". In: *Rapid Prototyping Journal* 13.4 (Jan. 2007), pp. 196–203. ISSN: 13552546. DOI: 10.1108/13552540710776142. URL: https://doi.org/10.1108/13552540710776142.

[44] Vojislav Petrovic, Juan Vicente Haro Gonzalez, Olga Jordá Ferrando, Javier Delgado Gordillo, Jose Ramón Blasco Puchades, and Luis Portolés Griñan. "Additive layered manufacturing: sectors of industrial application shown through case studies". In: *International Journal of Production Research* 49.4 (Feb. 2011), pp. 1061–1079. ISSN: 0020-7543. DOI: 10.1080/00207540903479786. URL: https://doi.org/10.1080/00207540903479786%20https://www.tandfonline.com/doi/full/10.1080/00207540903479786.

[45] J.-P. Kruth, G Levy, F Klocke, and T.H.C. Childs. "Consolidation phenomena in laser and powder-bed based layered manufacturing". In: *CIRP Annals* 56.2 (2007), pp. 730–759. ISSN: 00078506. DOI: 10.1016/j.cirp.2007.10.004. URL: https://www.sciencedirect.com/science/article/pii/S0007850607001540%20https://linkinghub.elsevier.com/retrieve/pii/S0007850607001540.

[46] Eleftherios Louvis, Peter Fox, and Christopher J. Sutcliffe. "Selective laser melting of aluminium components". In: *Journal of Materials Processing Technology* 211.2 (Feb. 2011), pp. 275–284. ISSN: 09240136. DOI: 10.1016/j.jmatprotec.2010.09.019. URL: https://www.sciencedirect.com/science/article/pii/S0924013610003018%20https://linkinghub.elsevier.com/retrieve/pii/S0924013610003018.

[47] A. Bertsch, S. Zissi, J. Y. Jézéquel, S. Corbel, and J. C. André. "Microstereophotolithography using a liquid crystal display as dynamic mask-generator". In: *Microsystem Technologies* 3.2 (Feb. 1997), pp. 42–47. ISSN: 0946-7076. DOI: 10.1007/s005420050053. URL: https://doi.org/10.1007/s005420050053%20http://link.springer.com/10.1007/s005420050053.

[48] Ferry P.W. Melchels, Jan Feijen, and Dirk W. Grijpma. "A review on stereolithography and its applications in biomedical engineering". In: *Biomaterials* 31.24 (Aug. 2010), pp. 6121–6130. ISSN: 01429612. DOI: 10.1016/j.biomaterials.2010.04.050. URL: https://www.sciencedirect.com/science/article/pii/S0142961210005661%20https://linkinghub.elsevier.com/retrieve/pii/S0142961210005661.

[49] R. Gygax. "Chemical reaction engineering for safety". In: *Chemical Engineering Science* 43.8 (1988), pp. 1759–1771. ISSN: 00092509. DOI: 10.1016/0009-2509(88)87040-4. URL: https://linkinghub.elsevier.com/retrieve/pii/0009250988870404.

[50] Zogg Andreas. *Calorimetry Kinetic and Approach using IR-ATR Spectroscopy Reaction Parameters for the Determination of Thermodynamic*. 15086. ETH Zurich, 2003, pp. 30–35. ISBN: 3906734331.

[51] Vinicius Kartnaller, Danielly C.O. Mariano, and João Cajaiba. "Application of In-Line Mid-Infrared (MIR) Spectroscopy Coupled with Calorimetry for the Determination of the Molar Enthalpy of Reaction between Ammonium Chloride and Sodium Nitrite". In: *Applied Spectroscopy* 70.3 (2016), pp. 531–538. ISSN: 19433530. DOI: 10.1177/0003702815626682. URL: https://doi.org/10.1177/0003702815626682.

[52] Agnieszka Ładosz, Christina Kuhnle, and Klavs F. Jensen. "Characterization of reaction enthalpy and kinetics in a microscale flow platform". In: *Reaction Chemistry and Engineering* 5.11 (2020), pp. 2115–2122. ISSN: 20589883. DOI: 10.1039/d0re00304b. URL: http://xlink.rsc.org/?DOI=D0RE00304B.

[53] Francis Stoessel. *Thermal Safety of Chemical Processes: Risk Assessment and Process Design*. Wiley, Feb. 2008, pp. 1–374. ISBN: 9783527317127. DOI: 10.1002/9783527621606. URL: https://onlinelibrary.wiley.com/doi/book/10.1002/9783527621606.

[54] Andreas Keller, Daniel Stark, Hans Fierz, Elmar Heinzle, and Konrad Hungerbühler. "Estimation of the time to maximum rate using dynamic DSC experiments". In: *Journal of Loss Prevention in the Process Industries* 10.1 (1997), pp. 31–41. ISSN: 09504230. DOI: 10.1016/S0950-4230(96)00037-X.

[55] D. I. Townsend and J. C. Tou. "Thermal hazard evaluation by an accelerating rate calorimeter". In: *Thermochimica Acta* 37.1 (1980), pp. 1–30. ISSN: 00406031. DOI: 10.1016/0040-6031(80)85001-5.

[56] Andreas Zogg, Francis Stoessel, Ulrich Fischer, and Konrad Hungerbühler. "Isothermal reaction calorimetry as a tool for kinetic analysis". In: *Thermochimica Acta* 419.1-2 (Sept. 2004), pp. 1–17. ISSN: 00406031. DOI: 10.1016/j.tca.2004.01.015. URL: https://linkinghub.elsevier.com/retrieve/pii/S0040603104000486.

[57] W. Regenass. "Thermoanalytische Methoden in der Chemischen Verfahrenentwicklung". In: *Thermochim. Acta*. Vol. 20. 1. Elsevier, 1976, pp. 65–79.

[58] Hans Martin. *Waermefiusskalorimetrie unter praeparativen Bedingungen und ihre Anwendung zur Verfolgung der Isomerisierungskinetik von Trimethylphosphit*. Basel: Ph.D. Thesis, University of Basel, 1975.

[59] H M Andersen. "Isothermal kinetic calorimeter applied to emulsion polymerization". In: *Journal of Polymer Science Part A-1: Polymer Chemistry* 4.4 (1966), pp. 783–791.

[60] M R Meeks. "An analog computer study of polymerization rates in vinyl chloride suspensions". In: *Polymer Engineering & Science* 9.2 (1969), pp. 141–151.

[61] F Becker. "Thermokinetische Messmethoden". In: *Chemie Ingenieur Technik* 40.19 (1968), pp. 933–947.

[62] Martin Zogg. *Einführung in die mechanische Verfahrenstechnik mit 29 Tabellen und 32 Berechnungsbeispielen*. Teubner, 1993. ISBN: 3519163195.

[63] Gabriel Glotz, Donald J. Knoechel, Philip Podmore, Heidrun Gruber-Woelfler, and C. Oliver Kappe. "Reaction Calorimetry in Microreactor Environments - Measuring Heat of Reaction by Isothermal Heat Flux Calorimetry". In: *Organic Process Research and Development* 21.5 (2017), pp. 763–770. ISSN: 1520586X. DOI: 10.1021/acs.oprd.7b00092.

[64] M. A. Schneider and F. Stoessel. "Determination of the kinetic parameters of fast exothermal reactions using a novel microreactor-based calorimeter". In: *Chemical Engineering Journal* 115.1-2 (2005), pp. 73–83. ISSN: 13858947. DOI: 10.1016/j.cej.2005.09.019.

[65] Cindy Hany, Christophe Pradere, Jean Toutain, and Jean-Christophe Batsale. "A millifluidic calorimeter with infrared thermography for the measurement of chemical reaction enthalpy and kinetics". In: *Quantitative InfraRed Thermography Journal* 5.2 (Dec. 2008), pp. 211–229. ISSN: 1768-6733. DOI: 10.3166/qirt.5.211-229. URL: http://www.tandfonline.com/doi/abs/10.3166/qirt.5.211-229.

[66] J.Michael Köhler and Martin Zieren. "Chip reactor for microfluid calorimetry". In: *Thermochimica Acta* 310.1-2 (Feb. 1998), pp. 25–35. ISSN: 00406031. DOI: 10.1016/S0040-6031(97)00381-X. URL: https://linkinghub.elsevier.com/retrieve/pii/S004060319700381X.

[67] Yuyan Zhang and Srinivas Tadigadapa. "Calorimetric biosensors with integrated microfluidic channels". In: *Biosensors and Bioelectronics* 19.12 (July 2004), pp. 1733–1743. ISSN: 09565663. DOI: 10.1016/j.bios.2004.01.009. URL: https://linkinghub.elsevier.com/retrieve/pii/S0956566304000260.

[68] S Loebbecke, J Antes, W Ferstl, D Boskovic, T Tuercke, M Schwarzer, and H Krause. "Microreactors for processing of hazardous and explosible reactions". In: *Institution of Chemical Engineers Symposium Series* 153 (2007), pp. 1–6. URL: https://www.mendeley.com/catalogue/microreactors-processing-hazardous-explosive-reactions/.

[69] Felix Reichmann, Stefan Millhoff, Yannick Jirmann, and Norbert Kockmann. "Reaction Calorimetry for Exothermic Reactions in Plate-Type Microreactors Using Seebeck Elements". In: *Chemical Engineering & Technology* 40.11 (Nov. 2017), pp. 2144–2154. ISSN: 09307516. DOI: 10.1002/ceat.201700419. URL: http://doi.wiley.com/10.1002/ceat.201700419.

[70] Timothy Aljoscha Frede, Marlene Dietz, and Norbert Kockmann. "Software-guided microscale flow calorimeter for efficient acquisition of thermokinetic data". In: *Journal of Flow Chemistry* (2021). ISSN: 20630212. DOI: 10.1007/s41981-021-00145-6.

[71] Frederik Mortzfeld, Jutta Polenk, Bertrand Guelat, Francesco Venturoni, Berthold Schenkel, and Paolo Filipponi. "Reaction Calorimetry in Continuous Flow Mode: A New Approach for the Thermal Characterization of High Energetic and Fast Reactions". In: *Organic Process Research and Development* 24.10 (Oct. 2020), pp. 2004–2016. ISSN: 1520586X. DOI: 10.1021/acs.oprd.0c00117. URL: https://doi.org/10.1021/acs.oprd.0c00117%20https://pubs.acs.org/doi/10.1021/acs.oprd.0c00117.

[72] Jürgen Antes. *Fraunhofer Institute for Chemical Technology Ict Reaction Calorimetry in Microreactors*. URL: https://www.ict.fraunhofer.de/content/dam/ict/en/documents/media/em/EM_Reaktionskalorimetrie_V05_en.pdf (visited on 06/22/2021).

[73] Andrew J. Capel, Steve Edmondson, Steven D.R. R. R Christie, Ruth D. Goodridge, Richard J. Bibb, and Matthew Thurstans. "Design and additive manufacture for flow chemistry." In: *Lab on a chip* 13.23 (Dec. 2013), pp. 4583–4590. ISSN: 1473-0189. DOI: 10.1039/c3lc50844g. URL: http://xlink.rsc.org/?DOI=c3lc50844g%20http://www.ncbi.nlm.nih.gov/pubmed/24100659.

[74] Ian Gibson, David Rosen, and Brent Stucker. *Additive manufacturing technologies: 3D printing, rapid prototyping, and direct digital manufacturing, second edition*. 2015, pp. 1–498. ISBN: 9781493921133. DOI: 10.1007/978-1-4939-2113-3. URL: http://www.scopus.com/inward/record.url?eid=2-s2.0-84944216444%7B%5C&%7DpartnerID=40%7B%5C&%7Dmd5=5823d88f66cd6827200a60b798005d95.

[75] Axel Günther and Klavs F. Jensen. "Multiphase microfluidics: from flow characteristics to chemical and materials synthesis". In: *Lab Chip* 6.12 (Dec. 2006), pp. 1487–1503. ISSN: 1473-0197. DOI: 10.1039/B609851G. URL: http://xlink.rsc.org/?DOI=B609851G%20http://www.ncbi.nlm.nih.gov/pubmed/17203152.

[76] Madhvanand N. Kashid, Albert Renken, and Lioubov Kiwi-Minsker. "Gas-liquid and liquid-liquid mass transfer in microstructured reactors". In: *Chemical Engineering Science* 66.17 (2011), pp. 3876–3897. ISSN: 00092509. DOI: 10.1016/j.ces.2011.05.015. URL: http://dx.doi.org/10.1016/j.ces.2011.05.015.

[77] M. Movsisyan, E. I. P. Delbeke, J. K. E. T. Berton, C. Battilocchio, S. V. Ley, and C. V. Stevens. "Taming hazardous chemistry by continuous flow technology". In: *Chemical Society Reviews* 45.18 (2016), pp. 4892–4928. ISSN: 0306-0012. DOI: 10.1039/C5CS00902B. URL: http://xlink.rsc.org/?DOI=C5CS00902B.

[78] Bernhard Gutmann, David Cantillo, and C. Oliver Kappe. "Continuous-flow technology—a tool for the safe manufacturing of active pharmaceutical ingredients." In: *Angewandte Chemie (International ed. in English)* 54.23 (June 2015), pp. 6688–6728. ISSN: 1521-3773. DOI: 10.1002/anie.201409318. URL: http://doi.wiley.com/10.1002/anie.201409318%20http://www.ncbi.nlm.nih.gov/pubmed/25989203.

[79] Norbert Kockmann, Philipp Thenée, Christoph Fleischer-Trebes, Gabriele Laudadio, and Timothy Noël. "Safety assessment in development and operation of modular continuous-flow processes". In: *Reaction Chemistry & Engineering* 2.3 (2017), pp. 258–280. ISSN: 2058-9883. DOI: 10.1039/C7RE00021A. URL: http://xlink.rsc.org/?DOI=C7RE00021A.

[80] Joseph M. Reckamp, Ashira Bindels, Sophie Duffield, Yangmu Chloe Liu, Eric Bradford, Eric Ricci, Flavien Susanne, and Andrew Rutter. "Mixing Performance Evaluation for Commercially Available Micromixers Using Villermaux–Dushman Reaction Scheme with the Interaction by Exchange with the Mean Model". In: *Organic Process Research & Development* 21.6 (June 2017), pp. 816–

820. ISSN: 1083-6160. DOI: 10.1021/acs.oprd.6b00332. URL: http://pubs.acs.org/doi/10.1021/acs.oprd.6b00332.

[81] Reza Amin, Stephanie Knowlton, Alexander Hart, Bekir Yenilmez, Fariba Ghaderinezhad, Sara Katebifar, Michael Messina, Ali Khademhosseini, and Savas Tasoglu. "3D-printed microfluidic devices". In: *Biofabrication* 8.2 (June 2016), p. 022001. ISSN: 1758-5090. DOI: 10.1088/1758-5090/8/2/022001. URL: http://stacks.iop.org/1758-5090/8/i=2/a=022001?key=crossref.42b00d58e7924bfe38fd579dcd1cb84e%20http://www.ncbi.nlm.nih.gov/pubmed/27321137%20https://iopscience.iop.org/article/10.1088/1758-5090/8/2/022001.

[82] Bethany C. Gross, Jayda L. Erkal, Sarah Y. Lockwood, Chengpeng Chen, and Dana M. Spence. "Evaluation of 3D Printing and Its Potential Impact on Biotechnology and the Chemical Sciences". In: *Analytical Chemistry* 86.7 (Apr. 2014), pp. 3240–3253. ISSN: 0003-2700. DOI: 10.1021/ac403397r. URL: http://pubs.acs.org/doi/10.1021/ac403397r%20http://www.ncbi.nlm.nih.gov/pubmed/24432804.

[83] Yong He, Yan Wu, Jian-zhong Fu, Qing Gao, and Jing-jiang Qiu. "Developments of 3D Printing Microfluidics and Applications in Chemistry and Biology: a Review". In: *Electroanalysis* 28.8 (Aug. 2016), pp. 1658–1678. ISSN: 10400397. DOI: 10.1002/elan.201600043. URL: http://doi.wiley.com/10.1002/elan.201600043.

[84] Bethany Gross, Sarah Y. Lockwood, and Dana M. Spence. "Recent Advances in Analytical Chemistry by 3D Printing." In: *Analytical chemistry* 89.1 (Jan. 2017), pp. 57–70. ISSN: 1520-6882. DOI: 10.1021/acs.analchem.6b04344. URL: http://pubs.acs.org/doi/10.1021/acs.analchem.6b04344%20http://www.ncbi.nlm.nih.gov/pubmed/28105825.

[85] Cesar Parra-Cabrera, Clement Achille, Simon Kuhn, and Rob Ameloot. "3D printing in chemical engineering and catalytic technology: structured catalysts, mixers and reactors." In: *Chemical Society reviews* 47.1 (Jan. 2018), pp. 209–230. ISSN: 1460-4744. DOI: 10.1039/c7cs00631d. URL: http://xlink.rsc.org/?DOI=C7CS00631D%20http://www.ncbi.nlm.nih.gov/pubmed/29131228.

[86] Philip J. Kitson, Stefan Glatzel, Wei Chen, Chang-Gen Lin, Yu-Fei Song, and Leroy Cronin. "3D printing of versatile reactionware for chemical synthesis". In: *Nature Protocols* 11.5 (May 2016), pp. 920–936. ISSN: 1754-2189. DOI: 10.1038/nprot.2016.041. URL: http://www.nature.com/articles/nprot.2016.041%20http://www.ncbi.nlm.nih.gov/pubmed/27077333.

[87] Andrew J. Capel, Rowan P. Rimington, Mark P. Lewis, and Steven D. R. Christie. "3D printing for chemical, pharmaceutical and biological applications". In: *Nature Reviews Chemistry* (Nov. 2018), pp. 2397–3358. ISSN: 2397-3358. DOI:

10.1038/s41570-018-0058-y. URL: http://www.nature.com/articles/s41570-018-0058-y.

[88] Raf Reintjens, David J. Ager, and Andr?? H M Andr?? H M André H.M. De Vries. "Flow chemistry, how to bring it to industrial scale?" In: *Chimica Oggi/Chemistry Today* 33.4 (2015), pp. 21–24. ISSN: 19738250. URL: https://www.teknoscienze.com/Contents/Riviste/PDF/CO4_2015_LOW_23-27.pdf.

[89] Gianmario Scotti, Ville Matilainen, Petri Kanninen, Heidi Piili, Antti Salminen, Tanja Kallio, and Sami Franssila. "Laser additive manufacturing of stainless steel micro fuel cells". In: *Journal of Power Sources* 272 (Dec. 2014), pp. 356–361. ISSN: 03787753. DOI: 10.1016/j.jpowsour.2014.08.096. URL: http://dx.doi.org/10.1016/j.jpowsour.2014.08.096%20https://linkinghub.elsevier.com/retrieve/pii/S0378775314013615.

[90] Gianmario Scotti, Petri Kanninen, Ville-Pekka Matilainen, Antti Salminen, and Tanja Kallio. "Stainless steel micro fuel cells with enclosed channels by laser additive manufacturing". In: *Energy* 106 (July 2016), pp. 475–481. ISSN: 03605442. DOI: 10.1016/j.energy.2016.03.086. URL: http://dx.doi.org/10.1016/j.energy.2016.03.086%20https://linkinghub.elsevier.com/retrieve/pii/S0360544216303309.

[91] S. Sandron, B. Heery, V. Gupta, D. A. Collins, E P Nesterenko, P. N. Nesterenko, M. Talebi, S. Beirne, F. Thompson, G. G. Wallace, D. Brabazon, F. Regan, and B. Paull. "3D printed metal columns for capillary liquid chromatography." In: *The Analyst* 139.24 (Dec. 2014), pp. 6343–6347. ISSN: 1364-5528. DOI: 10.1039/c4an01476f. URL: http://xlink.rsc.org/?DOI=C4AN01476F%20http://www.ncbi.nlm.nih.gov/pubmed/25285334.

[92] Vipul Gupta, Mohammad Talebi, Jeremy Deverell, Sara Sandron, Pavel N. Nesterenko, Brendan Heery, Fletcher Thompson, Stephen Beirne, Gordon G. Wallace, and Brett Paull. "3D printed titanium micro-bore columns containing polymer monoliths for reversed-phase liquid chromatography." In: *Analytica chimica acta* 910 (Mar. 2016), pp. 84–94. ISSN: 1873-4324. DOI: 10.1016/j.aca.2016.01.012. URL: http://dx.doi.org/10.1016/j.aca.2016.01.012%20https://linkinghub.elsevier.com/retrieve/pii/S0003267016300617%20http://www.ncbi.nlm.nih.gov/pubmed/26873472.

[93] Bernhard Gutmann, Manuel Köckinger, Gabriel Glotz, Tania Ciaglia, Eyke Slama, Matej Zadravec, Stefan Pfanner, Manuel C. Maier, Heidrun Gruber-Wölfler, and C. Oliver Kappe. "Design and 3D printing of a stainless steel reactor for continuous difluoromethylations using fluoroform". In: *Reaction Chemistry & Engineering* 2.6 (2017), pp. 919–927. ISSN: 2058-9883. DOI: 10.1039/C7RE00176B. URL: http://xlink.rsc.org/?DOI=C7RE00176B.

[94] Zhi He and Timothy F. Jamison. "Continuous-Flow Synthesis of Functionalized Phenols by Aerobic Oxidation of Grignard Reagents". In: *Angewandte Chemie International Edition* 53.13 (Mar. 2014), pp. 3353–3357. ISSN: 14337851. DOI: 10.1002/anie.201310572. URL: http://doi.wiley.com/10.1002/anie.201310572%20http://www.ncbi.nlm.nih.gov/pubmed/24554581.

[95] C. A. Fyfe. *The Hydroxyl Group (1971)*. Ed. by Saul Patai. Chichester, UK: John Wiley & Sons, Ltd., Jan. 1971, pp. 83–127. ISBN: 9780470771259. DOI: 10.1002/9780470771259. URL: http://doi.wiley.com/10.1002/9780470771259.

[96] D. G. Hall. *Boronic Acids*. Ed. by Dennis G. Hall. Weinheim, Germany: Wiley-VCH Verlag GmbH & Co. KGaA, Oct. 2011. ISBN: 9783527639328. DOI: 10.1002/9783527639328. URL: http://doi.wiley.com/10.1002/9783527639328.

[97] Stephan Enthaler and Anna Company. "Palladium-catalysed hydroxylation and alkoxylation." In: *Chemical Society reviews* 40.10 (Oct. 2011), pp. 4912–4924. ISSN: 1460-4744. DOI: 10.1039/c1cs15085e. URL: http://xlink.rsc.org/?DOI=c1cs15085e%20http://www.ncbi.nlm.nih.gov/pubmed/21643619.

[98] Wladimir Reschetilowski, ed. *Microreactors in Preparative Chemistry*. Weinheim, Germany: Wiley-VCH Verlag GmbH & Co. KGaA, Aug. 2013. ISBN: 9783527652891. DOI: 10.1002/9783527652891. URL: http://doi.wiley.com/10.1002/9783527652891.

[99] Ivana Dencic, Volker Hessel, and Wladimir Reschetilowski. *Microreactors in Organic Chemistry and Catalysis*. Ed. by Thomas Wirth. Weinheim, Germany: Wiley-VCH Verlag GmbH & Co. KGaA, Apr. 2013, pp. 373–446. ISBN: 9783527659722. DOI: 10.1002/9783527659722. URL: http://doi.wiley.com/10.1002/9783527659722%20https://doi.org/10.1002/9783527659722.ch11.

[100] Bartholomäus Pieber and C. Oliver Kappe. *Aerobic Oxidations in Continuous Flow*. Vol. 57. Springer, 2015, pp. 97–136. ISBN: 978-3-642-04728-2. DOI: 10.1007/3418_2015_133. URL: http://link.springer.com/10.1007/3418_2015_133.

[101] John F. Garst, Calvin D. Smith, and Alice Chandler Farrar. "Radical intermediates in the oxygenation of phenylmagnesium bromide. Evidence from aromatic phenylation". In: *Journal of the American Chemical Society* 94.22 (Nov. 1972), pp. 7707–7710. ISSN: 0002-7863. DOI: 10.1021/ja00777a016. URL: http://pubs.acs.org/doi/abs/10.1021/ja00777a016.

[102] Magdalena Jasińska. "Test Reactions to Study Efficiency of Mixing". In: *Chemical and Process Engineering* 36.2 (June 2015), pp. 171–208. ISSN: 2300-1925. DOI: 10.1515/cpe-2015-0013. URL: http://content.sciendo.com/view/journals/cpe/36/2/article-p171.xml.

[103] Alex Povitsky. "Three-dimensional flow with elevated helicity in driven cavity by parallel walls moving in perpendicular directions". In: *Physics of Fluids* 29.8 (Aug. 2017), p. 083601. ISSN: 1070-6631. DOI: 10.1063/1.4996179. URL: http://aip.scitation.org/doi/10.1063/1.4996179.

[104] Boštjan Rajh, Chungen Yin, Niko Samec, Matjaž Hriberšek, Filip Kokalj, and Matej Zadravec. "Advanced CFD modelling of air and recycled flue gas staging in a waste wood-fired grate boiler for higher combustion efficiency and greater environmental benefits". In: *Journal of Environmental Management* 218 (July 2018), pp. 200–208. ISSN: 03014797. DOI: 10.1016/j.jenvman.2018.04.030. URL: https://linkinghub.elsevier.com/retrieve/pii/S0301479718304122.

[105] Chia-Yen Lee, Chin-Lung Chang, Yao-Nan Wang, and Lung-Ming Fu. "Microfluidic Mixing: A Review". In: *International Journal of Molecular Sciences* 12.5 (May 2011), pp. 3263–3287. ISSN: 1422-0067. DOI: 10.3390/ijms12053263. URL: https://www.mdpi.com/1422-0067/12/5/3263%20http://www.mdpi.com/1422-0067/12/5/3263.

[106] Edward L. Paul, Victor A. Atiemo-Obeng, and Suzanne M. Kresta. *Handbook of Industrial Mixing*. Ed. by Edward L Paul, Victor A Atiemo-Obeng, and Suzanne M Kresta. Hoboken, NJ, USA: John Wiley & Sons, Inc., Nov. 2003, pp. 1140–1149. ISBN: 0471269190. URL: http://doi.wiley.com/10.1002/0471451452.

[107] Kevin Ward and Z. Hugh Fan. "Mixing in microfluidic devices and enhancement methods". In: *Journal of Micromechanics and Microengineering* 25.9 (Sept. 2015), p. 094001. ISSN: 0960-1317. DOI: 10.1088/0960-1317/25/9/094001. URL: http://stacks.iop.org/0960-1317/25/i=9/a=094001?key=crossref.76c24b2dae65e0dfc89a9f04c8d4462b%20http://www.ncbi.nlm.nih.gov/pubmed/26549938%20http://www.pubmedcentral.nih.gov/articlerender.fcgi?artid=PMC4634658.

[108] J. Bałdyga, J.R. Bourne, and S.J. Hearn. "Interaction between chemical reactions and mixing on various scales". In: *Chemical Engineering Science* 52.4 (Feb. 1997), pp. 457–466. ISSN: 00092509. DOI: 10.1016/S0009-2509(96)00430-7. URL: http://linkinghub.elsevier.com/retrieve/pii/S0009250996004307.

[109] Xu-dong Wang and Otto S. Wolfbeis. "Optical methods for sensing and imaging oxygen: materials, spectroscopies and applications". In: *Chem. Soc. Rev.* 43.10 (May 2014), pp. 3666–3761. ISSN: 0306-0012. DOI: 10.1039/C4CS00039K. URL: http://xlink.rsc.org/?DOI=C4CS00039K%20http://www.ncbi.nlm.nih.gov/pubmed/24638858.

[110] S.M. M Borisov, G. Nuss, W. Haas, R. Saf, M. Schmuck, and I. Klimant. "New NIR-emitting complexes of platinum(II) and palladium(II) with fluorinated benzoporphyrins". In: *Journal of Photochemistry and Photobiology A: Chemistry* 201.2-3 (Jan. 2009), pp. 128–135. ISSN: 10106030. DOI: 10.1016/j.

jphotochem.2008.10.003. URL: http://linkinghub.elsevier.com/retrieve/pii/S1010603008004292.

[111] Chris D Geddes and Joseph R Lakowicz. *Reviews in fluorescence 2006*. Springer, 2005. URL: https://scholar.google.at/scholar?hl=de%7B%5C&%7Das_sdt=0%7B%5C%%7D2C5%7B%5C&%7Dq=Reviews+in+fluorescence+2006+geddes%7B%5C&%7DbtnG=.

[112] Mettler Toledo. *Reaction Calorimeter RC1*. URL: https://www.mt.com/int/en/home/products/L1_AutochemProducts/Reaction-Calorimeters-RC1-HFCal/RC1mx-Reaction-Calorimeter.html (visited on 11/13/2019).

[113] Andreas Zogg, Ulrich Fischer, and Konrad Hungerbühler. "A new small-scale reaction calorimeter that combines the principles of power compensation and heat balance". In: *Industrial and Engineering Chemistry Research* 42.4 (2003), pp. 767–776. ISSN: 08885885. DOI: 10.1021/ie0201258.

[114] Ángel Piñeiro, Ángeles Olvera, Gonzalo García-Miaja, and Miguel Costas. "Excess Molar Enthalpies of Tetrahydrofuran or Diisopropyl Ether + 1-Alkanols at 298.15 K, Using a Newly Designed Flow Mixing Cell for an Isothermal Microcalorimeter". In: *Journal of Chemical & Engineering Data* 46.5 (Sept. 2001), pp. 1274–1279. ISSN: 0021-9568. DOI: 10.1021/je0100645. URL: https://pubs.acs.org/doi/10.1021/je0100645.

[115] Thermal Hazard technology and Thermal hazard technology. *Micro Reaction Calorimeter - μRC*. URL: http://www.thermalhazardtechnology.com/products/micro+reaction+calorimeter (visited on 11/03/2019).

[116] Agnieszka Ladosz, Andrew R. Teixeira, Baptiste Hardy, Isaac Roes, Jason Moore, and Klavs F. Jensen. "Microscale calorimetry: measuring heat of reaction in flow". In: *Poster pres. at, International Conference on Micro Reaction Technology - IMRET 2018, Karlsruhe* ().

[117] L. Falk and J.-M. M. Commenge. "Performance comparison of micromixers". In: *Chemical Engineering Science* 65.1 (Jan. 2010), pp. 405–411. ISSN: 00092509. DOI: 10.1016/j.ces.2009.05.045. URL: https://linkinghub.elsevier.com/retrieve/pii/S0009250909003819.

[118] John R. Bourne. "Comments on the iodide/iodate method for characterising micromixing". In: *Chemical Engineering Journal* 140.1-3 (July 2008), pp. 638–641. ISSN: 13858947. DOI: 10.1016/j.cej.2008.01.031. URL: https://linkinghub.elsevier.com/retrieve/pii/S1385894708000697.

[119] Jean-Marc Commenge and Laurent Falk. "Villermaux–Dushman protocol for experimental characterization of micromixers". In: *Chemical Engineering and Processing: Process Intensification* 50.10 (Oct. 2011), pp. 979–990. ISSN: 02552701. DOI: 10.1016/j.cep.2011.06.006. URL: https://linkinghub.elsevier.com/retrieve/pii/S0255270111001395.

[120] Richard W. Hanks, Avinash C. Gupta, and James J. Christensen. "Calculation of Isothermal Vapor-Liquid Equilibrium Data for Binary Mixtures from Heats of Mixing". In: *Industrial & Engineering Chemistry Fundamentals* 10.3 (Aug. 1971), pp. 504–509. ISSN: 0196-4313. DOI: 10.1021/i160039a025. URL: https://pubs.acs.org/doi/abs/10.1021/i160039a025.

[121] Richard W. Hanks, Romeo L. Tan, and James J. Christensen. "Limits on the simultaneous correlation of gE and hE data by the NRTL, LEMF and Wilson's equations". In: *Thermochimica Acta* 23.1 (Mar. 1978), pp. 41–55. ISSN: 00406031. DOI: 10.1016/0040-6031(78)85110-7. URL: https://linkinghub.elsevier.com/retrieve/pii/0040603178851107.

[122] Robert H. Perry, Don W. Green, and James O Maloney. *Perry's Chemical Engineer's Handbook, Eighth Edition*. 2007, Chap. 2 pp. 186–194. ISBN: 0070498415. DOI: 10.1036/0071422943.

[123] Erwin Riedel and Hans-Jürgen Meyer. *Allgemeine und Anorganische Chemie*. Berlin, Boston: De Gruyter, Nov. 2018. ISBN: 9783110583953. DOI: 10.1515/9783110583953. URL: http://www.degruyter.com/view/books/9783110583953/9783110583953/9783110583953.xml.

[124] FDA. *Pharmaceutical CGMPs for the 21s Century - A risk-based approach*. Tech. rep. 2004.

[125] Joshua Britton and Colin L. Raston. "Multi-step continuous-flow synthesis". In: *Chemical Society Reviews* 46.5 (2017), pp. 1250–1271. ISSN: 14604744. DOI: 10.1039/c6cs00830e.

[126] Damien Webb and Timothy F. Jamison. "Continuous flow multi-step organic synthesis". In: *Chemical Science* 1.6 (2010), pp. 675–680. ISSN: 20416520. DOI: 10.1039/c0sc00381f. arXiv: {_}barataMaterialsandTechniquesofpolychromewoodensculpture.

[127] Vincenza Dragone, Victor Sans, Mali H. Rosnes, Philip J. Kitson, and Leroy Cronin. "3D-printed devices for continuous-flow organic chemistry". In: *Beilstein Journal of Organic Chemistry* 9 (May 2013), pp. 951–959. ISSN: 1860-5397. DOI: 10.3762/bjoc.9.109. URL: https://www.beilstein-journals.org/bjoc/articles/9/109.

[128] Matthew J Harding, Sarah Brady, Heather O'Connor, Rafael Lopez-Rodriguez, Matthew D Edwards, Saoirse Tracy, Denis Dowling, Geoff Gibson, Kevin P Girard, and Steven Ferguson. "3D printing of PEEK reactors for flow chemistry and continuous chemical processing". In: *Reaction Chemistry & Engineering* 5.4 (2020), pp. 728–735. ISSN: 2058-9883. DOI: 10.1039/C9RE00408D. URL: http://dx.doi.org/10.1039/C9RE00408D%20http://xlink.rsc.org/?DOI=C9RE00408D.

[129] F. Marc Michel, J. Donald Rimstidt, and Karel Kletetschka. "3D printed mixed flow reactor for geochemical rate measurements". In: *Applied Geochemistry* 89.November 2017 (Feb. 2018), pp. 86–91. ISSN: 08832927. DOI: 10.1016/j.apgeochem.2017.11.008. URL: https://doi.org/10.1016/j.apgeochem.2017.11.008%20https://linkinghub.elsevier.com/retrieve/pii/S0883292717303554.

[130] Katharina Hiebler, Sebastian Soritz, Kristian Gavric, Sam Birrer, Manuel C. Maier, Bianca Grabner, and Heidrun Gruber-Woelfler. "Multistep synthesis of a valsartan precursor in continuous flow". In: *Journal of Flow Chemistry* 10.1 (2020), pp. 283–294. ISSN: 20630212. DOI: 10.1007/s41981-019-00044-x.

[131] Bianca Grabner, Anna K. Schweiger, Kristian Gavric, Robert Kourist, and Heidrun Gruber-Woelfler. "A chemo-enzymatic tandem reaction in a mixture of deep eutectic solvent and water in continuous flow". In: *Reaction Chemistry & Engineering* 5.2 (2020), pp. 263–269. ISSN: 2058-9883. DOI: 10.1039/C9RE00467J. URL: http://xlink.rsc.org/?DOI=C9RE00467J.

[132] Christopher A. Hone and C. Oliver Kappe. "The Use of Molecular Oxygen for Liquid Phase Aerobic Oxidations in Continuous Flow". In: *Topics in Current Chemistry* 377.1 (Feb. 2019), p. 2. ISSN: 2365-0869. DOI: 10.1007/s41061-018-0226-z. URL: http://link.springer.com/10.1007/s41061-018-0226-z.

[133] *CC Flow Project*. URL: http://goflow.at/cc-flow (visited on 02/20/2020).

[134] PubChem. *2-Methyltetrahydrofuran - Compound Summary*. URL: https://pubchem.ncbi.nlm.nih.gov/compound/2-Methyltetrahydrofuran%7B%5C#%7Dsection=Peroxide-Forming-Chemical (visited on 04/18/2020).

[135] Philipp Sulzer, René Lebl, C. Oliver Kappe, and Torsten Mayr. "Oxygen sensors for flow reactors – measuring dissolved oxygen in organic solvents". In: *Reaction Chemistry & Engineering* 4.12 (2019), pp. 2081–2087. ISSN: 2058-9883. DOI: 10.1039/C9RE00253G. URL: http://xlink.rsc.org/?DOI=C9RE00253G.

[136] *Cardiovascular diseases (2017) World Health Organization*. URL: http://www.who.int/news-room/fact-sheets/detail/cardiovascular-diseases-(cvds) (visited on 09/04/2018).

[137] *EvaluatePharma, 2018. World Preview 2018, Outlook to 2024. EvaluatePharma, online available at*. URL: https://info.evaluate.com/rs/607-YGS-364/images/EvaluatePharma_World_Preview_2019.pdf (visited on 03/31/2020).

[138] Suzanne Oparil and Roland E. Schmieder. "New Approaches in the Treatment of Hypertension". In: *Circulation Research* 116.6 (2015), pp. 1074–1095. ISSN: 15244571. DOI: 10.1161/CIRCRESAHA.116.303603.

[139] P. Bühlmayer, F. Ostermayer, and T. Schmidlin. *Acyl compounds*.

[140] G Verardo, P Geatti, G Castaldi, N Toniutti, and P Allegrini. *A process for the preparation of valsartan and intermediates thereof.*

[141] G Sedelmeier. *Process for the preparation of tetrazole derivatives from organo boron and organo aluminium azides.*

[142] M Villa, P Allegrini, K Arrighi, and M Paiocchi. *Ortho-metalation process for the synthesis of 2-substituted-1-(tetrazol-5-yl)benzenes.*

[143] Chen Xi Zhang, Guo Jun Zheng, Fu Qiang Bi, and Yu Lin Li. "A simple and efficient synthesis of the valsartan". In: *Chinese Chemical Letters* 19.7 (2008), pp. 759–761. ISSN: 10018417. DOI: 10.1016/j.cclet.2008.04.032.

[144] Chen Zhang, Guojun Zheng, Lijing Fang, and Yulin Li. "Efficient synthesis of valsartan, a nonpeptide angiotensin II receptor antagonist". In: *Synlett* 9.3 (2006), pp. 475–477. ISSN: 09365214. DOI: 10.1055/s-2006-926234.

[145] E Tsiperman, S Fine, S Yurkovsky, and V Braude. *Process for preparing valsartan.*

[146] Masahiko Seki and Masaki Nagahama. "Synthesis of angiotensin II receptor blockers by means of a catalytic system for C-H Activation". In: *Journal of Organic Chemistry* 76.24 (2011), pp. 10198–10206. ISSN: 00223263. DOI: 10.1021/jo202041e.

[147] Samir Ghosh, A. Sanjeev Kumar, and G. N. Mehta. "A short and efficient synthesis of valsartan via a Negishi reaction". In: *Beilstein Journal of Organic Chemistry* 6 (2010), pp. 4–7. ISSN: 18605397. DOI: 10.3762/bjoc.6.27.

[148] Nicola Galaffu, Siud Pui Man, Robin D. Wilkes, and John R.H. H Wilson. "Highly functionalised sulfur-based silica scavengers for the efficient removal of palladium species from active pharmaceutical ingredients". In: *Organic Process Research and Development* 11.3 (2007), pp. 406–413. ISSN: 10836160. DOI: 10.1021/op7000172.

[149] Belmunt J Bessa, Clotet J Huguet, Andres JA A Perez, and Barjoan P Dalmases. *Process for the preparation of valsartan and precursors thereof.*

[150] C Lamberth and J Dinges. *Bioactive Carboxylic Compound Classes: Pharmaceuticals and Agrochemicals.* Ed. by Clemens Lamberth and Jürgen Dinges. Weinheim, Germany: Wiley-VCH Verlag GmbH & Co. KGaA, Aug. 2016. ISBN: 9783527339471. DOI: 10.1002/9783527693931. URL: http://doi.wiley.com/10.1002/9783527693931.

[151] Valerica Pandarus, Geneviève Gingras, François Béland, Rosaria Ciriminna, and Mario Pagliaro. "Process intensification of the Suzuki-Miyaura reaction over sol-gel entrapped catalyst silia cat DPP-Pd under conditions of continuous flow". In: *Organic Process Research and Development* 18.11 (2014), pp. 1550–1555. ISSN: 1520586X. DOI: 10.1021/op4003449.

[152] Aiichiro Nagaki, Katsuyuki Hirose, Osamu Tonomura, Satoshi Taniguchi, Toshiki Taga, Shinji Hasebe, Norio Ishizuka, and Jun Ichi Yoshida. "Design of a Numbering-up System of Monolithic Microreactors and Its Application to Synthesis of a Key Intermediate of Valsartan". In: *Organic Process Research and Development* 20.3 (2016), pp. 687–691. ISSN: 1520586X. DOI: 10.1021/acs.oprd.5b00414.

[153] G.J. Lichtenegger, M. Maier, M. Hackl, J.G. Khinast, W. Gössler, T. Griesser, V.S.Phani Kumar, H. Gruber-Woelfler, and P.A. Deshpande. "Suzuki-Miyaura coupling reactions using novel metal oxide supported ionic palladium catalysts". In: *Journal of Molecular Catalysis A: Chemical* 426 (Jan. 2017), pp. 39–51. ISSN: 13811169. DOI: 10.1016/j.molcata.2016.10.033. URL: https://linkinghub.elsevier.com/retrieve/pii/S1381116916304563.

[154] Waqas Nawaz, Zhongqin Zhou, Sa Deng, Xiaodong Ma, Xiaochi Ma, Chuangang Li, and Xiaohong Shu. "Therapeutic Versatility of Resveratrol Derivatives". In: *Nutrients* 9.11 (Oct. 2017), p. 1188. ISSN: 2072-6643. DOI: 10.3390/nu9111188. URL: http://www.mdpi.com/2072-6643/9/11/1188.

[155] Hui-Yun Tsai, Chi-Tang Ho, and Yu-Kuo Chen. "Biological actions and molecular effects of resveratrol, pterostilbene, and 3'-hydroxypterostilbene". In: *Journal of Food and Drug Analysis* 25.1 (Jan. 2017), pp. 134–147. ISSN: 10219498. DOI: 10.1016/j.jfda.2016.07.004. URL: https://linkinghub.elsevier.com/retrieve/pii/S1021949816300965.

[156] Monica Savio, Daniela Ferraro, Cristina Maccario, Rita Vaccarone, Lasse D. Jensen, Federica Corana, Barbara Mannucci, Livia Bianchi, Yihai Cao, and Lucia Anna Stivala. "Resveratrol analogue 4,4'-dihydroxy-trans-stilbene potently inhibits cancer invasion and metastasis". In: *Scientific Reports* 6.1 (Apr. 2016), p. 19973. ISSN: 2045-2322. DOI: 10.1038/srep19973. URL: http://www.nature.com/articles/srep19973.

[157] Álvaro Gómez Baraibar, Dennis Reichert, Carolin Mügge, Svenja Seger, Harald Gröger, and Robert Kourist. "A One-Pot Cascade Reaction Combining an Encapsulated Decarboxylase with a Metathesis Catalyst for the Synthesis of Bio-Based Antioxidants". In: *Angewandte Chemie International Edition* 55.47 (Nov. 2016), pp. 14823–14827. ISSN: 14337851. DOI: 10.1002/anie.201607777. URL: http://doi.wiley.com/10.1002/anie.201607777.

[158] Martin Peng, Esther Mittmann, Lukas Wenger, Jürgen Hubbuch, Martin K. M. Engqvist, Christof M. Niemeyer, and Kersten S. Rabe. "3D-Printed Phenacrylate Decarboxylase Flow Reactors for the Chemoenzymatic Synthesis of 4-Hydroxystilbene". In: *Chemistry – A European Journal* 25.70 (Dec. 2019), pp. 15998–16001. ISSN: 0947-6539. DOI: 10.1002/chem.201904206. URL: https://onlinelibrary.wiley.com/doi/abs/10.1002/chem.201904206.

[159] Sandy Schmidt, Kathrin Castiglione, and Robert Kourist. "Overcoming the Incompatibility Challenge in Chemoenzymatic and Multi-Catalytic Cascade Reactions". In: *Chemistry - A European Journal* 24.8 (Feb. 2018), pp. 1755–1768. ISSN: 15213765. DOI: 10.1002/chem.201703353. URL: http://doi.wiley.com/10.1002/chem.201703353.

[160] Josef M. Sperl, Jörg M. Carsten, Jan-Karl Guterl, Petra Lommes, and Volker Sieber. "Reaction Design for the Compartmented Combination of Heterogeneous and Enzyme Catalysis". In: *ACS Catalysis* 6.10 (Oct. 2016), pp. 6329–6334. ISSN: 2155-5435. DOI: 10.1021/acscatal.6b01276. URL: https://pubs.acs.org/doi/10.1021/acscatal.6b01276.

[161] Anna K. Schweiger, Nicolás Ríos-Lombardía, Christoph K. Winkler, Sandy Schmidt, Francisco Morís, Wolfgang Kroutil, Javier González-Sabín, and Robert Kourist. "Using Deep Eutectic Solvents to Overcome Limited Substrate Solubility in the Enzymatic Decarboxylation of Bio-Based Phenolic Acids". In: *ACS Sustainable Chemistry & Engineering* 7.19 (Oct. 2019), pp. 16364–16370. ISSN: 2168-0485. DOI: 10.1021/acssuschemeng.9b03455. URL: https://pubs.acs.org/doi/10.1021/acssuschemeng.9b03455.

[162] Sven R L Gobert, Simon Kuhn, Leen Braeken, and Leen C J Thomassen. "Characterization of Milli- and Microflow Reactors: Mixing Efficiency and Residence Time Distribution". In: *Organic Process Research & Development* 21.4 (Apr. 2017), pp. 531–542. ISSN: 1083-6160. DOI: 10.1021/acs.oprd.6b00359. URL: https://pubs.acs.org/doi/10.1021/acs.oprd.6b00359.

[163] John R Bourne. "Mixing and the Selectivity of Chemical Reactions". In: *Organic Process Research & Development* 7.4 (July 2003), pp. 471–508. ISSN: 1083-6160. DOI: 10.1021/op020074q. URL: https://pubs.acs.org/doi/10.1021/op020074q.

[164] Karol Malecha, Leszek J Golonka, Jerzy Bałdyga, Magdalena Jasińska, and Paweł Sobieszuk. "Serpentine microfluidic mixer made in LTCC". In: *Sensors and Actuators B: Chemical* 143.1 (Dec. 2009), pp. 400–413. ISSN: 09254005. DOI: 10.1016/j.snb.2009.08.010. URL: https://linkinghub.elsevier.com/retrieve/pii/S0925400509006285.

[165] Georg J. Lichtenegger, Vitan Tursic, Hannes Kitzler, Klemens Obermaier, Johannes G. Khinast, and Heidrun Gruber-Wölfler. "The Plug & Play Reactor: A Highly Flexible Device for Heterogeneous Reactions in Continuous Flow". In: *Chemie Ingenieur Technik* 88.10 (Oct. 2016), pp. 1518–1523. ISSN: 0009286X. DOI: 10.1002/cite.201600013. URL: http://doi.wiley.com/10.1002/cite.201600013.

[166] Y Wang, G Zheng, G Cai, B Chen, and H Li. *Process for preparation of valsartan.*

[167] José F. Cívicos, Diego A. Alonso, and Carmen Nájera. "Oxime Palladacycle-Catalyzed Suzuki-Miyaura Alkenylation of Aryl, Heteroaryl, Benzyl, and Allyl Chlorides under Microwave Irradiation Conditions". In: *Advanced Synthesis & Catalysis* 353.10 (July 2011), pp. 1683–1687. ISSN: 16154150. DOI: 10.1002/adsc.201100019. URL: http://doi.wiley.com/10.1002/adsc.201100019.